

DOTTORATO DI RICERCA IN
Biologia Molecolare e Cellulare
Ciclo XXX

Settore Concorsuale di afferenza: 05/I2

Settore Scientifico disciplinare: BIO/19 Microbiologia

**Chemotaxis, respiratory oxidases and stringent response
to carbon sources of the polychlorinated-biphenyl degrader
Pseudomonas pseudoalcaligenes KF707**

Presentata da:
Federica Sandri

Supervisore:
Prof. Davide Zannoni
Co-supervisore:
Dott. Stefano Fedi

Coordinatore dottorato:
Prof. Giovanni Capranico

Abstract

Bacteria are important for the so called “environmental bioremediation procedures” that can be defined as *the use of microorganisms to degrade or transform toxic compounds*, an approach particularly important for the recovery/reuse of polluted sites. In this respect, *Pseudomonas pseudoalcaligenes* KF707, a soil Gram negative Proteobacterium isolated near a biphenyl manufacturing plant in Japan [Furukawa and Myazaki, 1986], it is known as one of the most effective polychlorinated-biphenyls (PCBs) degraders. The KF707 genome analysis [Triscari-barberi et al., 2012], has highlighted the potential capacity of this bacterium to use as carbon and energy sources an extraordinary wide spectrum of aromatic compounds. The latter feature makes KF707 a promising microbial-cell tool to be utilized in environmental remediation procedures.

In this present PhD work, several aspects of KF707 metabolism have been studied for the first time. In particular we have analyzed:

- *The role of cheA genes in swarming and swimming motility.* Indeed, although the genome of KF707 contains three *cheA* gene clusters, we found that only the *cheA1* gene is involved in swimming motility. Conversely, the swarming motility is strongly dependent on the presence of *cheA2* and *cheA1* genes while the *cheA3* gene deletion has a negative effect on this type of bacterial movement.
- *The modulation of the terminal respiratory oxidases in the presence of biphenyl.* In the genome of KF707 five terminal oxidases were identified: two *caa3*-type oxidases (*Caa3* and *Ccaa3*), two *ccb3*-type (*Cbb31* and *Cbb32*) and one cyanide-insensitive quinol oxidase CIO. Here, we demonstrated that not only biphenyl modulates the expression and function of the respiratory oxidases (in particular the *Caa3* and *Cbb32* enzymes), but we also provided biochemical and structural evidence that KF707 overproduces a *Caa3* oxidase in cells grown with biphenyl. This is the first time that a *caa3*-type oxidase has been structurally characterized in a *Pseudomonas* spp.
- *The role of relA and spoT genes in KF707 stringent response mechanism.* KF707 owns two proteins, RelA and SpoT, which are necessary for the stringent response mechanism. Notably, deletion of these two genes affects: i) KF707 growth in the presence of sugars and aromatic compounds, ii) the swarming motility with an increase of the swarming area, and iii) the expression of the terminal cytochrome oxidases, that is fully disconnected from the cell growth phase and carbon source.

The results gave rise to an important set of biochemical and molecular clues useful for the KF707 application in environmental technologies.

Table of contents

General Introduction	1
Characteristics of <i>Pseudomonas</i> genus	1
<i>Pseudomonas pseudoalcaligenes</i> KF707	3
Aromatic catabolic pathways in KF70	6
Analysis of biphenyl gene cluster	6
Phenol, benzoate, catechol and <i>p</i> -hydroxybenzoate gene clusters	10
General Materials and Methods	17
Media and growth conditions	17
Extraction of genomic DNA from KF707	18
DNA manipulation and genetic techniques	19
DNA sequencing and sequence analysis	19
KF707 deletion mutant strains	20
Gene deletion constructs by using “Gene SOEing” method	20
Construction of recombinant plasmid containing deletion fragments	22
Conjugation	23
Chapter 1: The role of <i>cheA</i> genes in swarming and swimming motility of <i>Pseudomonas pseudoalcaligenes</i> KF707	25
Background: Bacterial chemotaxis	25
The chemotaxis signaling in <i>E. coli</i>	27
1.1 Introduction	31
1.2 Materials and Methods	37
1.2.1 Bacterial strains and plasmids	37
1.2.2 KF707 deletion mutant and complemented strains for <i>cheA</i> genes	38
1.2.3 Motility assay	40
1.3 Results	41
1.3.1 KF707 <i>cheA</i> genes complemented strains	41
1.3.2 Swimming motility assay	43
1.3.3 Swarming motility assay	44
1.4 Discussion	47

Chapter 2: Biphenyl modulates the expression and function of respiratory oxidases in the polychlorinated-biphenyls degrader <i>Pseudomonas pseudoalcaligenes</i> KF707	49
Background: The microbial aerobic respiration	49
The aerobic respiration in bacteria	50
The electron transport chain	52
The terminal oxidase enzymes	54
The haem-copper oxidases (HCO)	55
<i>bd</i> -type terminal oxidases	59
2.1 Introduction	60
2.2 Materials and Methods	65
2.2.1 Bacterial strains and plasmids	65
2.2.2 KF707 deletion mutant strains	67
2.2.3 NADI assay	68
2.2.4 Growth curves	69
2.2.5 KF707 <i>lacZ</i> translational fusion strains	69
Amplification and cloning of promoter fragments for translational fusion strains	71
Construction of KF707 translational fusion strains	72
2.2.6 β -galactosidase assay	74
2.2.7 Preparation of membrane fragments	76
2.2.8 Spectroscopic analysis and Respiratory activities	77
2.3 Results	78
2.3.1 Putative genes for terminal oxidases	78
The <i>caa</i> ₃ -type cytochrome oxidases	79
The <i>cbb</i> ₃ -type cytochrome oxidases	80
The <i>bd</i> -type oxidase	81
2.3.2 KF707 terminal oxidases mutant strains	84
2.3.3 Phenotype analysis of KF707 mutant strains	87
2.3.4 KF707 <i>lacZ</i> translational fusion strains and oxidases expression	90
2.3.5 Spectroscopic analysis and Respiratory activities	94
2.3.6 The cyanide-insensitive oxidase (CIO) overexpression	99
2.4 Discussion	102
2.4.1 The branched respiratory chain of KF707 terminal cytochrome oxidases	102

2.4.2 Effect of the carbon source on the arrangement of KF707 respiratory chain	104
Chapter 3: Biochemical and structural evidence that <i>Pseudomonas pseudoalcaligenes</i> KF707 expresses a <i>caa3</i>-type cytochrome <i>c</i> oxidase	107
3.1 Introduction	107
3.2 Materials and Methods	112
3.2.1 Bacterial strains and plasmids	112
3.2.2 KF707 deletion mutant and <i>lacZ</i> translational fusion strains	113
3.2.3 Preparation of membrane fragments	113
3.2.4 SDS-PAGE and <i>c</i> -type haem staining	114
3.2.5 Nano LC-MS/MS analysis and database searching	114
3.2.6 Membrane protein modeling	115
3.2.7 Other analyses	116
3.3 Results	117
3.3.1 Cytochrome <i>c</i> profile and Nano LC-MS/MS analysis of KF707 W.T. and oxidase mutant strains	117
3.3.2 <i>Caa3</i> protein modeling	123
3.3.3 Cytochrome <i>c</i> oxidases electron donor	129
3.4 Discussion	135
Chapter 4: The role of the genes <i>relA</i> and <i>spoT</i> coding for stringent response in <i>Pseudomonas pseudoalcaligenes</i> KF707	141
Background: The bacterial stringent response	141
The RelA/SpoT Homologue (RSHs protein)	142
The role of (p)ppGpp in bacterial cells	146
Regulation of transcription	146
Effects on bacterial physiology	147
4.1 Introduction	150
4.2 Materials and Methods	154
4.2.1 Bacterial strains and plasmids	154
4.2.2 KF707 deletion mutant and complemented strains for <i>relA</i> and <i>spoT</i> genes	155
4.2.3 Growth of KF707 mutant strains with different carbon sources	156
4.2.4 Growth of KF707 W.T. and mutant strains in the presence of stringent response inducer	157

4.2.5 (p)ppGpp detection analysis	157
4.2.6 KF707 W.T. and KF Δ relA/spoT mutant strain 2-DE analysis	158
Bacterial proteins extraction	158
2-DE and image analysis	158
Samples preparation for mass spectrometry	159
Mass spectrometry analysis	160
Proteins identification	161
4.2.7 Other analysis	161
4.3 Results	162
4.3.1 KF707 <i>relA</i> and <i>spoT</i> deletion mutant and complemented strains	162
4.3.2 KF707 W.T. and mutant strains growth on different carbon sources	162
4.3.3 Growth in the presence of stringent response inducer	166
4.3.4 (p)ppGpp detection analysis	167
4.3.5 KF707 W.T. and KF Δ relA/spoT mutant strain 2-DE analysis	170
4.3.6 Additional experiments	176
Stringent response and swarming motility in KF707	176
Stringent response and terminal oxidase promoters expression	178
4.4 Discussion	181
General Conclusions	185
Bibliography	189

Abbreviations

°C	Celsius degree
2-DE	Two-dimension gel Electrophoresis
A	Adenine
aa	amino acids
AB	<i>Agrobacterium</i> medium
ACN	Acetonitrile
ADP	Adenosine-Diphosphate
Ala	Alanine
Amp	Ampicillin
AMP	Adenosine-Monophosphate
ANOVA	Analysis of Variance
AOX	Alternative Oxidase
Arg	Arginine
Asp	Aspartate
ATP	Adenosine-Triphosphate
ben	benzoate
BLAST	Basic Local Alignment Search Tool
bp	base pairs
bph	biphenyl
BSA	Bovine Serum Albumine
C	Cytosine
cat	catechol
CHAPS	3-(3-cholamidopropyl) dimethylammonio)-1-ropanesulfonate
Cm	Chloramphenicol
CN-	Sodium Cyanide
CTD	carboxy-terminal domain
Cys	Cysteine
cyt	cytochrome
DMPD	N,N-dimethyl-p-phenylenediamine
DNA	Deoxyribonucleic acid
DNase	Deoxyribonuclease
dNTP	Deoxy Nucleoside Triphosphate
DTT	1,4-dithio-DL-threitol
e.g.	for example (abbreviation of Latin: <i>exempli gratia</i>)
EDTA	Ethylenediamine tetraacetate
et al.	and others (abbreviation of Latin: <i>et alteri</i>)

ETC	Electron Transport Chain
ETS	Electron Transport System
FAD(H)	Flavin Adenine Dinucleotide
FOR	primer Forward
G	Guanine
GDP	Guanosine-Diphosphate
Gln	Glutamine
Glu	Glutamic Acid
Gm	Gentamycin
GMP	Guanosine-Monophosphate
GTP	Guanosine-Triphosphate
HAP	Histidine-Aspartate Phosphorelay system
HCO	Heme-Copper Oxidase
His	Histidine
hrs	hours
HSP	Heat Shock Proteins
i.e.	that is (abbreviation of Latin: <i>id est</i>)
IC50	Inhibitory Concentration
ID	Identity
IEF	Isoelectric Focusing
IPG	Immobilized pH Gradient
Kb	Kilo base pairs
kDa	kilo Dalton
KF707	<i>Pseudomonas pseudoalcaligenes</i> KF707
Km	Kanamycin
kV	kiloVolts
<i>lacZ</i>	Bacterial β -galactosidase gene
LB	Luria Bertani medium
LC-MS/MS	Liquid Chromatography - quadrupole Mass Spectrometry
Lys	Lysine
M	molar
m/z	mass-to-charge ratio
mA	milliAmpere
Mb	Mega base pairs
MCPs	Methyl-accepting Chemotaxis Proteins
MCS	Multiple Cloning Site
Met	Methionine
mg	milligrams
min	minutes
mL	milliliters

mM	millimolar
mRNA	Messenger RNA
MSM	Minimal Salt Medium
N ₃ -	Azide
NAD(H)	Nicotinamide Adenine Dinucleotide
NCBI	National Center for Biotechnology Information
ng	nanograms
nm	nanometers
NTD	amino-terminal domain
OD	Optical Density
ONPG	Ortho-Nitrophenyl- β -galactoside
PCBs	Polychlorinated-biphenyls
PCR	Polymerase Chain Reaction
PDB	Protein Data Bank
pH	negative decade logarithm of the proton concentration
Phe	Phenylalanine
pI	Isoelectric point
ppGpp	Guanosine tetraphosphate
pppGpp	Guanosine pentaphosphate
Pro	Proline
Q	Quinol
RAST	Rapid Annotation based on Subsystem Technology
REV	primer Reverse
RNA	Ribonucleic acid
RNAP	RNA Polymerase
RNase	Ribonuclease
rpm	rotations per minute
rRNA	ribosomal RNA
RSH	RelA/SpoT Homologue
SDS	Sodium Dodecyl Sulfate
SDS-PAGE	Sodium Dodecyl Sulfate Polyacrilamide Gel Electrophoresis
Ser	Serine
SHX	DL-serine-hydroxamate
spp	species
SU	Subunits
T	Thymine
Tc	Tetracyclin
TE	Tris-EDTA buffer
Thr	Threonine
TLC	Thin-layer Chromatography

TMBZ	3,3',5,5'-tetramethylbenzidine
TMPD	N,N,N',N'-tetramethyl-p-phenylenediamine
Tris	Tris(hydroxymethyl) aminomethane
tRNA	Transfer RNA
Trp	Tryptophan
Tyr	Tyrosine
UQ	Ubiquinol
UV	Ultraviolet ray
V	Volts
v/v	volume per volume
W.T.	Wild Type
w/v	weight per volume
X-gal	5-bromo-4-chloro-3-indolyl- β -D-galactoside
λ	Wavelength
μ A	microAmpere
μ Ci	microCurie
μ F	microFarad
μ g	microgramms
μ L	microliters
μ m	micrometers
μ M	micromolar
Ω	Ohm

General Introduction

Characteristics of *Pseudomonas* genus

The microorganisms belonging to *Pseudomonas* genus were classified in the Proteobacteria phylum, and comprise a heterogeneous group with a great physiological flexibility. While some *Pseudomonas*, such as *Pseudomonas (P.) aeruginosa*, are pathogenic and cause, for example, urinary and respiratory infections to humans [Madigan et al., 2015], many of these microorganisms are ecologically important for soils and waters and are the main agents of the aerobic degradation of numerous soluble compounds, resulting from the decomposition of animal and plant materials. A few *Pseudomonas* species are able to degrade xenobiotics (such as pesticides) which are structurally related to natural compounds; these toxic chemicals can be slowly metabolized by specific enzymes evolved for the degradation of defined molecules. Interestingly, part of these xenobiotics are partially or totally degraded in the presence of other organic compounds, used as the main carbon source, in a peculiar process called co-metabolism [Nelson et al., 2002].

The genus *Pseudomonas* includes organisms with simple nutritional requirements, which grow in a chemoorganotrophic way, at neutral pH and mesophilic temperature. Many of these bacteria are strictly aerobes and use, for growth, a respiratory metabolism in which oxygen is the final electron acceptor; however, in some cases nitrate can also be used as the final electron acceptor, being reduced to N_2O or N_2 [Madigan et al., 2015].

Several pseudomonads grow in minimal media containing phosphate, ammonium, magnesium, iron and a single specific carbon source, that can be chosen from a wide range of organic molecules such as hydrocarbons (like aromatic hydrocarbons, aliphatic with straight or branched chains, or alicyclic), amines, amino acids, aromatic compounds, alcohols or carbohydrates [Spiers et al., 2000]. These latter compounds cannot be metabolized in all *Pseudomonas* species; in fact some of these bacteria grow slowly if they have only sugars in the growth medium. However, in general, *Pseudomonas* spp. have the ability to exploit more than 100 different organic compounds [Bergey's manual]. Species belonging to the *Pseudomonas* genus are about 128 and they can be subdivided into seven

different clusters based on the rRNA 16S sequencing analysis [Anzai et al., 2000]. These are Gram-negative, non-spore-forming bacteria, which exhibit polar flagellum (single or multiple); they usually have a *bacillus*-like structure, straight or curved, and their size is comprised between 0.5-1.0 µm for the diameter and 1.5-4.0 µm for the length. The main characteristics for the identification of *Pseudomonas*, are the absence of gas production in the presence of glucose and positive oxidase test results. The great metabolic versatility that characterizes this genus, attributable to the presence of numerous inducible operons, which code for specific enzymes, makes *Pseudomonas* bacteria an efficient tool for biotechnological applications, particularly in the field of bioremediation [Madigan et al., 2015] (Figure 1).

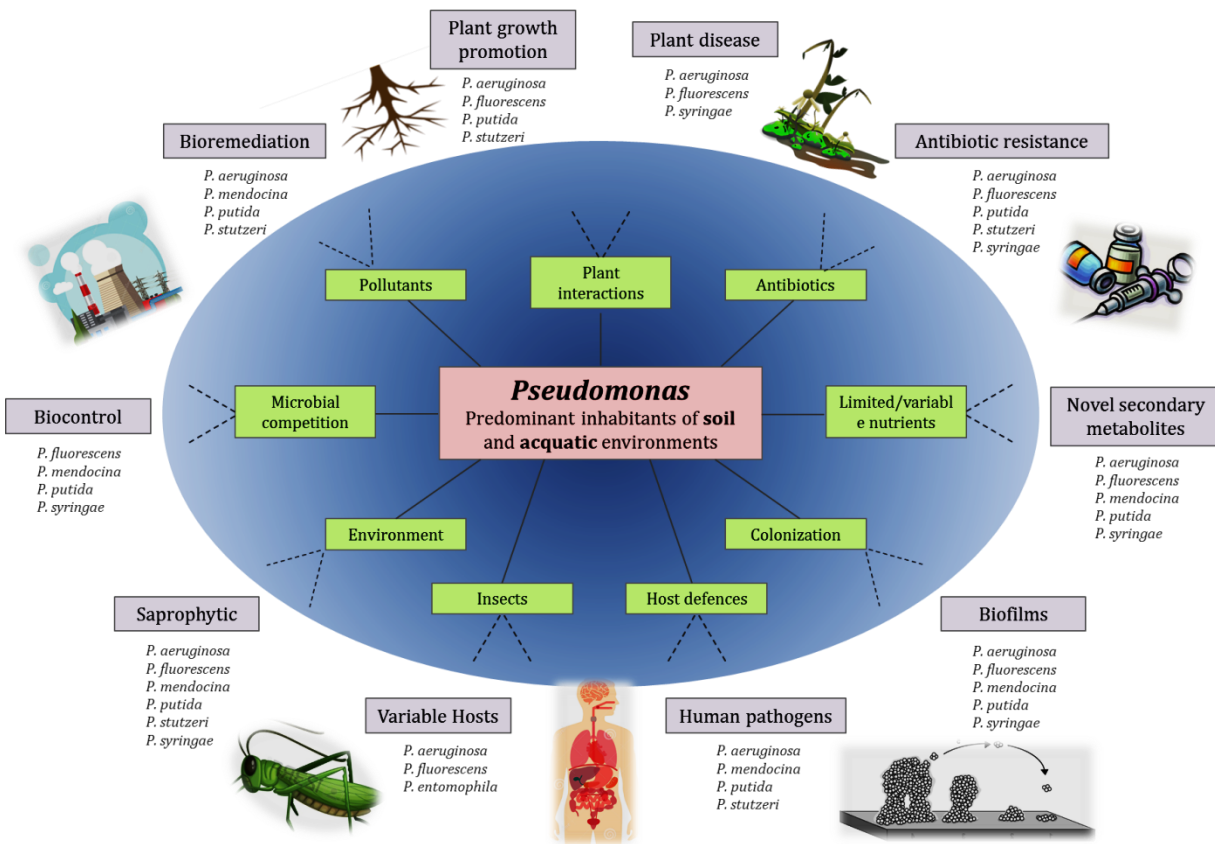


Figure 1: The functional environmental range of *Pseudomonas* spp. The *Pseudomonas* common ancestor encountered a wide range of abiotic and biotic environments that led to the evolution of a multitude of traits and lifestyles with significant overlap among species [Kahlon, 2016].

***Pseudomonas pseudoalcaligenes* KF707**

The bacterium *Pseudomonas pseudoalcaligenes* KF707 (hereafter named KF707), isolated near a biphenyl manufacturing plant in Japan [Furukawa and Myazaki, 1986], is known as one of the most effective polychlorinated-biphenyls (PCBs) degraders [Fedi et al., 2001], a particular class of toxic and aromatic compounds.

As many other *Pseudomonas* strains, KF707 is provided with only one flagellum (Figure 2A); this feature is essential since KF707 is able to grow suspended in a water column (planktonic growth) or as a biofilm attached to a solid surface [Tremaroli et al., 2008] in the presence of various toxic metals and metalloids [Di Tomaso et al., 2002; Tremaroli et al., 2010]. This latter property is of particular interest as the efficiency of microorganisms to degrade organic pollutants is strongly improved by their ability to tolerate both toxic intermediate metabolites and co-contaminants such as metal(loid)s. KF707 not only degrades toxic pollutants such as biphenyls and PCB [Furukawa and Miyazaki, 1986], but is also attracted by them [Tremaroli et al., 2008]. This is an important clue, and the presence of the flagellum, that supports the bacterial chemotaxis to pollutants, is needed to successfully set up a strategy for KF707 bioremediation. Unfortunately, the low bioavailability of organic contaminants is a limitation for the microbial remediation of contaminated sites, as toxic hydrophobic chemicals are often adsorbed in a non-aqueous liquid phase. In this last case, microorganisms may have access to a polluted surface through biofilm development, so that chemotaxis is a key factor in biofilm formation [O'Toole and Kolter, 1998].

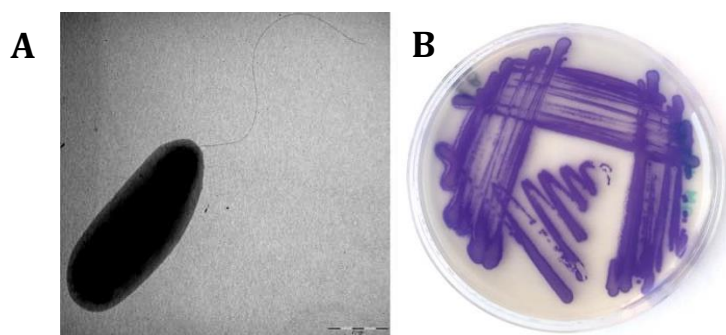


Figure 2: A) Electron micrographs [Tremaroli et al., 2011] and B) Cytochrome oxidases test of KF707.

The genome of KF707 was completely sequenced in 2012 [Triscari-Barberi et al., 2012] and the presence of different gene clusters, involved in the degradation of xenobiotic compounds, was confirmed. The genome has a total length of 5.95 Mb with 64.24% of GC content; there are 6.620 genes, 6.512 are coding sequences, 81 tRNA (for the 20 amino acids) and 27 rRNA.

Among the coding sequences (Figure 3), 22 are implicated in biphenyl and PCB degradation while 54 in benzoate pathway; 118 of them are involved in flagellum motility and chemotaxis (in particular three *cheA* genes, organized in different clusters, were found) while 55 are necessary for heavy metals (such as cobalt, zinc, cadmium, arsenic and tellurite) survival [Triscari-Barberi et al., 2012]. Like other *Pseudomonas* strains, KF707 contains in its genome multiple clusters that code for five different terminal oxidases; usually the presence of multiple enzymes of this type is related to the ability of the bacterium to adapt its survival to specific environmental changes in the growth medium, such as oxygen levels variations, pH or nutrient deficiency.

In addition, the annotation of KF707 genome (by Rapid Annotation based on Subsystem Technology RAST) led to the identification of 142 coding sequences associated with the peripheral pathways for the catabolism of aromatic compounds such as *p*-hydroxybenzoate, *n*-phenylalkanoate, quinate and phenol. Furthermore, 192 coding sequences were identified as putative genes involved in the central metabolism of aromatic compounds like gentisate and cresols, or in the degradation of intermediates including catechol, protocatechuate, salicylate and homogentisate. Taken together, genes coding for components of both central and peripheral degradation pathways represent a significant portion, around 5%, of KF707 genome [Triscari-Barberi, 2013].

As for other environmental bacteria [Bratlie et al., 2010], the KF707 genomic analysis displayed the existence of many paralogous genes that are likely to be involved in the aerobic degradation of aromatic compounds (i.e. *bph* cluster, *ben* clusters and *catA* genes). A high redundancy level might explain the ability of KF707 to grow on different aromatic carbon sources as it is believed that gene redundancy can facilitate genetic adaptation or create novel biochemical functions [Andersson and Hughes, 2009]. It also allows bacteria to relieve the metabolic competition generated by concomitant expression of the different *meta* and *ortho* aromatic pathways [Jiménez et al., 2002]. A high level of paralogous genes

may also have a role in the genetic regulation and modulation of the different aromatic pathways [Andersson and Hughes, 2009].

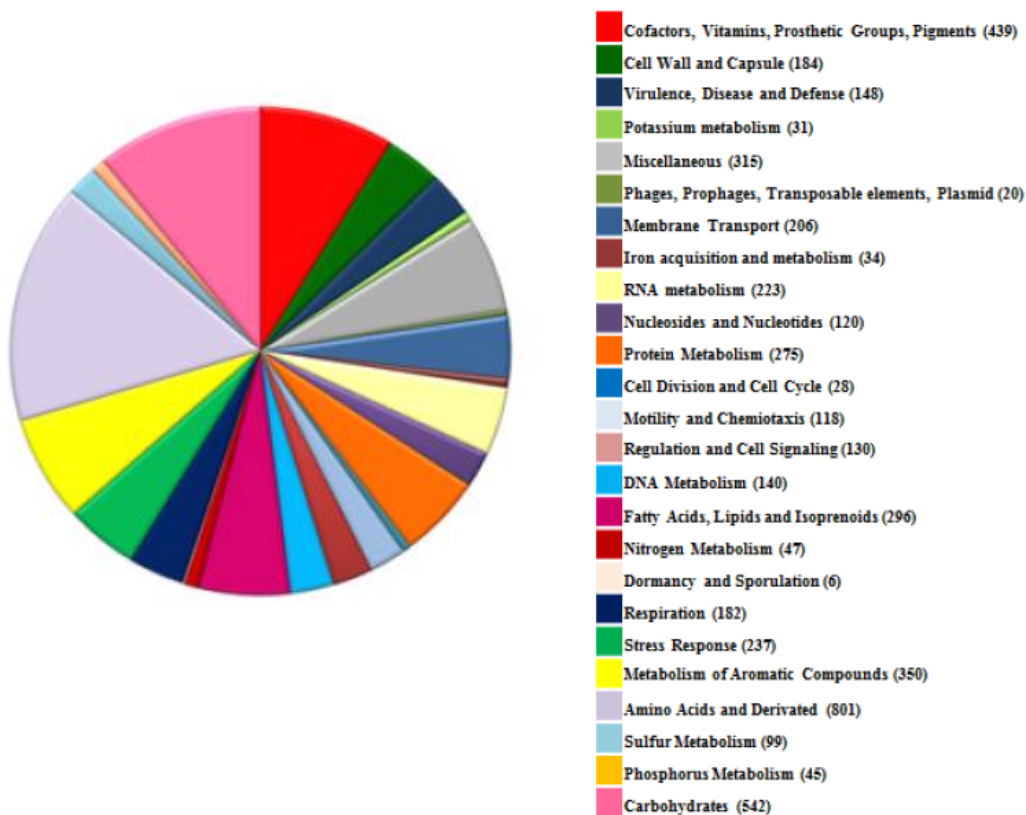


Figure 3: RAST annotation of KF707 DNA coding sequences found after complete genome sequencing analysis [Triscari-Barberi et al., 2012].

Aromatic catabolic pathways in KF707

KF707 is known for its ability to degrade biphenyl and its derivatives; the enzymes involved in this degradation pathway have been genetically and biochemically characterized in the past [Pieper, 2005; Furukawa and Fujihara, 2008]. After the completion of the KF707 genome analysis, additional information on the gene clusters for the catabolism of aromatic compounds, were discovered. Further, the presence and structure of gene clusters for the degradation of biphenyl and other aromatic compounds, were confirmed [Triscari-Barberi et al., 2012].

Analysis of biphenyl gene cluster

As previously mentioned, KF707 is known for its ability to co-metabolize PCBs by using the metabolic pathway of biphenyl degradation. PCBs are synthetic xenobiotic compounds, synthesized from the late 1800s by Monsanto USA company, used on an industrial scale from 1930 and declared toxic to both animals and humans and the environment between 1980 and 1990 [Borja et al., 2005].

PCBs are a class of organic-chlorinated molecules whose general form is $C_{12}H_xCl_y$, where x is a number between 0 and 9, whereas y is equal to $10-x$; depending on the position of the chlorine atoms, in the ring of the biphenyl molecule, more than 209 different congeners can be obtained, which also corresponds to differences in chemical and biological behavior. These chemical compounds are very stable, resistant to acids and alkalis, they cannot be oxidized, they are not soluble in water but are soluble in organic solvents or in oil, they are volatile and non-flammable; all these characteristics make these molecules poorly biodegradable. The PCBs toxicity is comparable to that of dioxin, so they have been renamed "*dioxin like compounds*" [Borja et al., 2005]. Most PCBs dispersed in the biosphere are contained in the soil, sediments and waters near the sites of their initial production and/or application [Mackova et al., 2007], but it seems that traces of these substances are now distributed across the planet, including remote areas like Antarctica [Abraham et al., 2002].

The metabolic network for the transformation of PCBs is strictly dependent on both the environmental factors and the chemical-physical properties of these molecules (position of chlorine substitutes and their number). The presence of chlorine as a substitute alters the

resonance properties of aromatic molecules and causes stereochemical effects on the affinity between the degrading enzymes and their substrates [Sylvestre and Sandossi 1994].

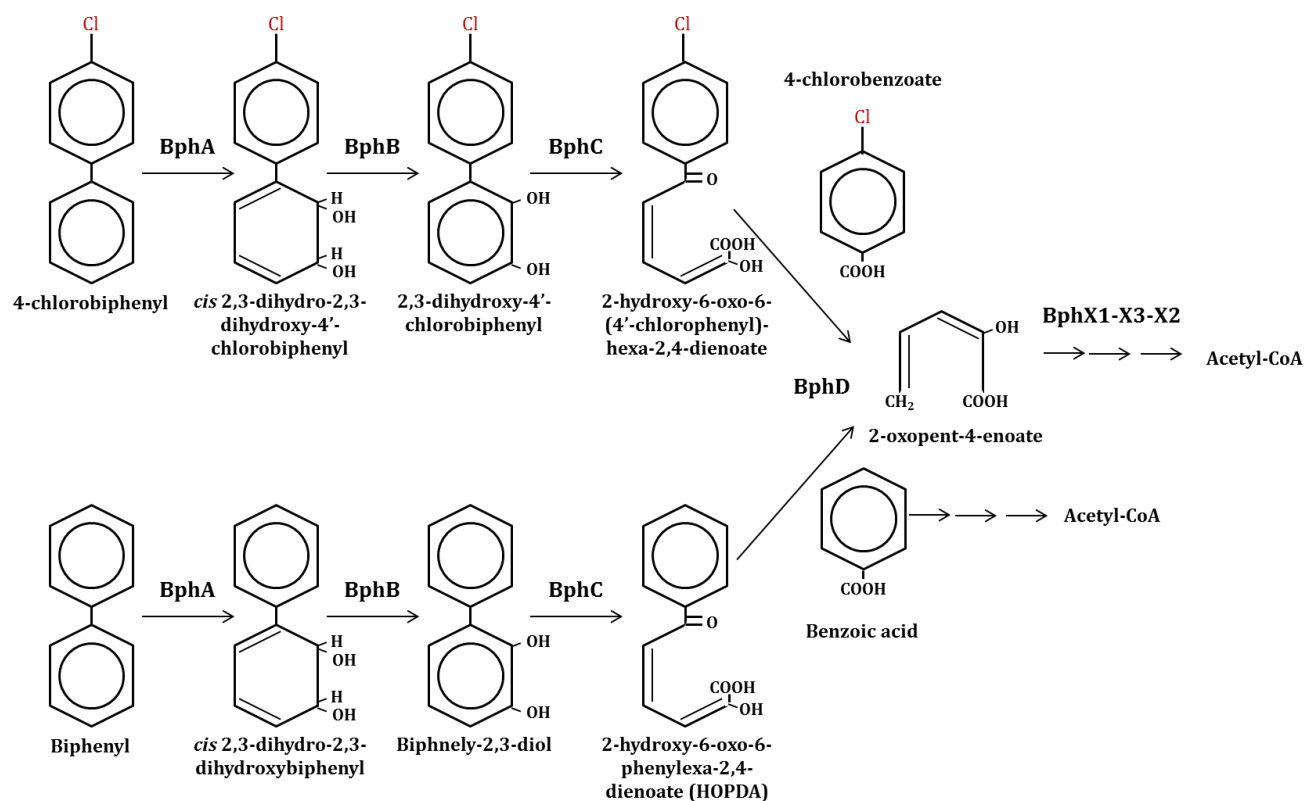


Figure 4: KF707 PCB and Biphenyl degradation *Upper Pathway*. The enzymes encoded by *bph* operon are used for both of these pathways, and the final product, obtained at the end of *Lower Pathway* (details not shown) is Acetyl-CoA. Abbreviations: BphA – Biphenyl dioxygenase; BphB – Dihydrodiol dioxygenase; BphC – 2,3-dihydroxybiphenyl dioxygenase; BphD – 2-hydroxy-6-oxo-6-phenylhexa-2,4-dienoic acid hydrolase.

The degradation of PCBs can be analyzed under two main aspects: dechlorination by anaerobic microorganisms and oxidative degradation by aerobic bacteria [Furukawa and Fujihara, 2008]. This latter growth condition is performed by *Pseudomonas* spp. such as KF707 which is able to use biphenyl as the sole source of carbon and energy, and it co-metabolizes PCBs using the biphenyl metabolic enzymes [Furukawa and Fujihara, 2008] (Figure 4).

Usually only congeners with a lower degree of chlorination are degraded in the presence of oxygen, but whereas aerobic microorganisms grow with a higher growth rate they can support higher biodegradation rates than anaerobic bacteria [Fain and Haddock, 2001] and

can therefore contribute to the development of new technologies for environmental bioremediation.

The aerobic co-metabolism using **bph** genes (Table 1; Figures 4 and 5) consists in the oxidation of the aromatic ring, containing less chlorine atoms, to obtain acetyl-CoA molecules, necessary for the Krebs cycle. The degradation occurs by means of enzymes located in a single operon of 11.8 Kb and consists in the following steps:

- ✓ BphA, 2,3-biphenyl-dioxygenase: it catalyzes the hydroxylation of the aromatic ring by the formation of dihydrodiol compound; this enzyme introduces an oxygen molecule in 2,3 position of the non-chlorinated (or less chlorinated) biphenyl ring [Furukawa and Fujihara, 2008].
- ✓ BphB, 2,3-dihydrodiol-dehydrogenase: this molecule promotes dehydrogenation of dihydrodiol compound in 2,3-dihydroxybiphenyl, a molecule that is subsequently oxidized. There are different forms of this enzyme in bacteria and all of them belong to the SDR (dehydrogenase/reductase) proteins family [Khan et al., 1997].
- ✓ BphC, 2,3-dihydroxybiphenyl-dioxygenase: it determines the *meta*-cleavage at the 1,2 position of the aromatic ring, with the formation of 2-hydroxy-6-oxo-6-phenyl-hexa-2,4-dienoic-acid (HODPA). If there are six chlorine atoms on both biphenyl rings in the starting PCB compound, the HODPA will also be chlorinated in its aliphatic branched form [Hofer et al., 1993].
- ✓ BphD, hydrolase: finally, this enzyme cleaves HODPA in chlorobenzoic acid and 2-hydroxypenta-2,4-dienoate; these two molecules proceed in a different way. Chlorobenzoic acid is generally not metabolized directly from KF707, but from other degrading bacteria present in the environment (it is a waste product), while in the absence of chlorine atoms (like in normal metabolism of biphenyl), benzoate is converted, by a specific series of enzymes in Acetyl-CoA [Fava et al., 2002; Rodrigues et al., 2006]. 2-hydroxypenta-2,4-dienoate is converted into pyruvate and acetaldehyde by two other enzymes of the gene cluster, BphX1 and BphX2, and finally the last enzyme BphX2 acetaldehyde-dehydrogenase leads to the formation of Acetyl-CoA [Watanabe et al., 2000].

The first part of biphenyl degradation is usually called *Upper Pathway* and it is mediated by the initial four enzymes while the second part, leading to the formation of Acetyl-CoA, is named *Lower Pathway*.

The biphenyl pathway is generally under the control of the two transcriptional regulators BphR1 and BphR2 belonging to GntR and LysR family, respectively [Watanabe et al., 2000; Watanabe et al., 2003]. Although the role of both these regulators in *bph* genes regulation has been described, only the location of *bphR1* gene was defined just upstream of *bphA1* gene. The genome sequencing analysis reported that *bphR2* gene is located approximately 6.500 bp downstream the *bph* operon and that, unlike *bphR1*, *bphR2* is transcribed in the opposite direction compared to *bph* operon [Triscari-Barberi et al., 2012].

In addition, immediately downstream of the *bph* gene cluster, a gene was found coding for a long-chain fatty acid transport protein putatively involved in the catabolism of aromatic compounds. Furthermore, the genomic analysis reveals that the region including the *bph* operon is flanked by mobile elements. Genes coding for integrases and transposons were also found in the flanking regions of *bph* operons from other bacterial strains [Ohtsubo et al., 2012]. Notably, KF707 genome contains additional copies of predicted *bph* genes that do not appear to be organized in operons; some of these genes (*e.g.* two copies of *bphX2*) are clustered together with genes involved in *n*-phenylalkanoic acids, benzoates and catechol catabolism belonging to the biphenyl *Lower Pathways*.

Phenol, benzoate, catechol and *p*-hydroxybenzoate gene clusters

The gene clusters for additional aromatic compounds degradation were found after the KF707 genome sequencing and annotation analysis [Triscari-Barberi et al., 2012] (Table 1; Figures 5 and 6).

Table 1: Key pathways of aromatic compounds degradation in KF707.

Genes involved in:	Pathway name	Number of CDSs	Main genes
Peripheral pathways for catabolism of aromatic compounds	Phenol hydroxylase	7	<i>dmpP, dmpO, dmpN, dmpM, dmpL, dmpK, dmpR</i>
	Biphenyl degradation	22	<i>bphA1, bphA2, bphA3, bphA4, bphB, bphC, bphX0, bphX1, bphX2, bphX3, bphD</i>
	Quinate degradation	2	<i>quiB</i>
	n-phenyl-alcanoic acid degradation	58	<i>fadA, fadB, fadD, phaJ1</i>
	Benzoate degradation	36	<i>benA, benB, benC, benD, benK, benE2, benF</i>
	<i>p</i> -hydroxybenzoate degradation	4	<i>pobA</i>
	Chloroaromatics degradation	13	<i>catJ, catI, catF, catD</i>
Metabolism of central aromatic intermediates	Catechol branch of β -keto adipate pathway	20	<i>catA, catC, catB, catD, catEA, catEB</i>
	Proto-catechuate branch of β -keto adipate pathway	32	<i>pcaH, pcaG, pcaQ, pcaI, pcaJ, pcaF, pcaB, pcaD, pcaC, pcaI2, pcaJ2, pcaK</i>
	4-hydroxyphenylacetic acid catabolic pathway	12	<i>hpaI, hpaH, hpaF, hpaD, hpaE, hpaG, hpaA, hpaC, hpaR</i>
	Salicilate and gentisate metabolism	20	<i>sala, salD</i>
	Homogentisate pathway	20	<i>hmgR</i>
	Central meta-cleavage pathway	48	<i>dmpP, dmpM, dmpL, dmpK, dmpR</i>
	N-heterocyclic aromatic compounds degradation	3	<i>iqoA, iqoB</i>
Additional pathways of aromatic compounds metabolism	Aromatic amines metabolism	11	<i>feaB, maoC</i>
	Cresol degradation	8	<i>pchA, pchC, pchF</i>

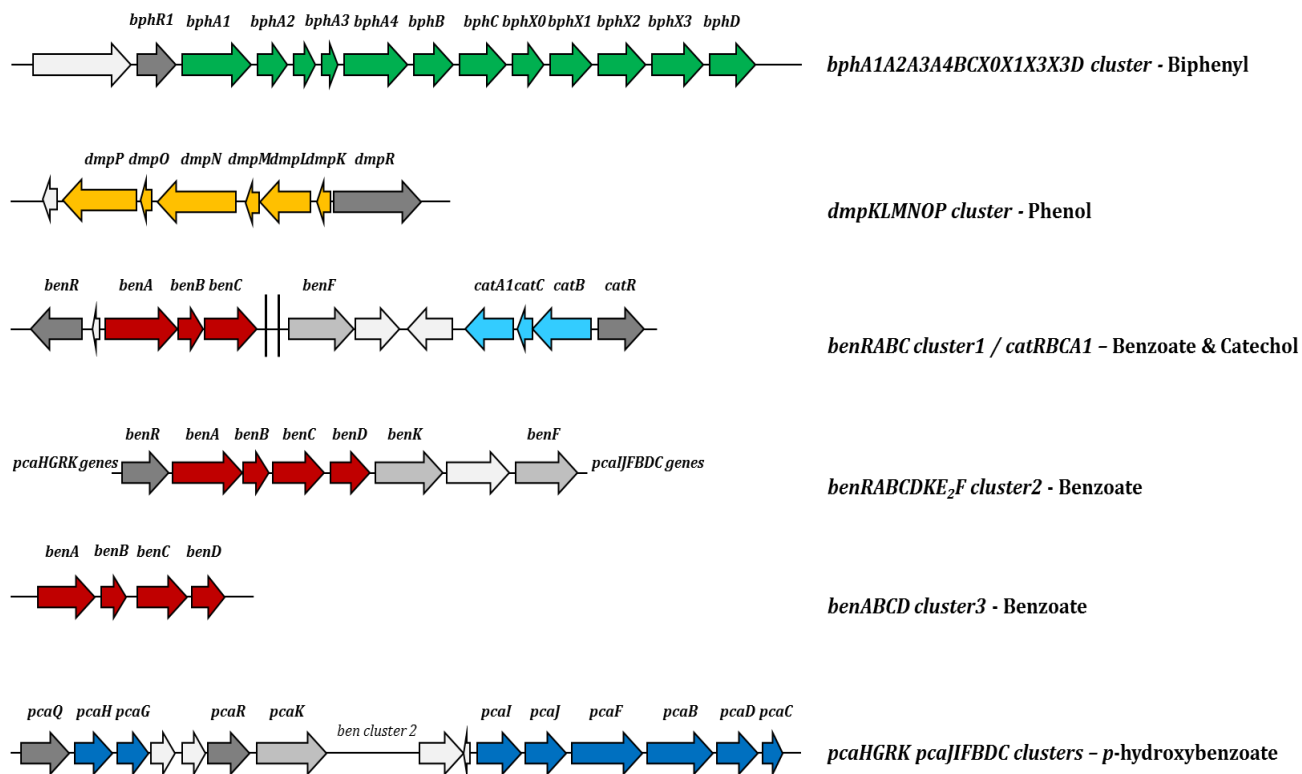


Figure 5: Organization of the *bph*, *dmp*, *ben* and *pca* gene clusters and the corresponding flanking regions from KF707. Genes (listed in Table 1) are represented by arrows; two vertical lines mean that the genes are not adjacent in the genome. About the color: full color – genes encoding catabolic enzymes involved in the metabolic pathways described in the text; dark gray – regulatory genes; medium gray – transport genes; light gray – genes of unknown function.

The degradation of phenolic compounds requires an initial hydroxylation of the phenolic ring, commonly mediated by a multicomponent phenol hydroxylase, and a subsequent *meta*-cleavage pathway [Shingler et al., 1992]. The ***dmpKLMNOP*** gene cluster (Table 1; Figures 5 and 6), found in KF707 genome [Triscari-Barberi et al., 2012], is predicted to encode all the enzymes required for phenol catabolism and the organization of the locus is maintained among *Pseudomonas* spp. [Nordlund et al., 1993]. The *dmp* operon is transcribed in the opposite direction of the *dmpR* gene; this latter coding for the DmpR protein, which belongs to the NtrC class of positive transcriptional activators, that regulate genes involved in a variety of physiological processes in response to different environmental signals [Leedj r v et al., 2006]. It shows 65% of similarity with homologous protein of *Pseudomonas* sp. CF600 where the *dmp* operon organization and regulation was

firstly described [Shingler et al., 1992]. These data, taken together, suggest the capacity of KF707 cells to grow also on phenol as sole carbon and energy source.

Moreover, the KF707 genome analysis reported the presence, location and organization of three *ben* gene clusters (Table 1; Figures 5 and 6) that might be involved in benzoate degradation.

- ✓ The *ben1* cluster (*benRABC-benF*) includes: the coding sequences for the benzoate 1,2-dioxygenase α , β subunits and the ferredoxin reductase component (*benABC*, respectively), the *benR* gene for a transcriptional regulator and the *benF* gene coding for a benzoate specific porin.
- ✓ The *ben2* cluster (*benRABCDKE2F*) is composed by *benABC* and *benR* that code for the same proteins described in *ben1* but, in addition, this cluster contains genes encoding benzoate transporters and specific porins (*benKE2F*). In this second case, the gene cluster is flanked by the *pcaBCDIJF* genes which encode products also involved in the degradation of benzoate.
- ✓ The *ben3* cluster (*benABCD*), which lacks the regulatory component and the genes encoding benzoate transporters, is flanked by transposases and mobile protein elements. Amino acid sequence of *ben3* cluster products showed a very high level of similarity (91%-96%) to XylXYZL of *P. putida* pWW0 (NC_003350) involved in toluene degradation.

In KF707, there are genes responsible for catechol oxidation that are organized in the *catRBCA1* operon (Table 1; Figures 5 and 6) with a *catR* gene located upstream of a *catB* gene and transcribed in opposite orientation. KF707 CatA1 amino acid sequence shares identities of 90% with the CatA1 of *P. resinovorans* NBRC 106553 and 70% with the CatA1 of *P. putida* KT2440. The gene organization and the transcriptional orientation of *catR* and *catBCA1* cluster genes in KF707 are maintained in *P. putida* and *P. aeruginosa* [Udaondo et al., 2013]. Moreover, similarly to these bacteria, KF707 *catRBCA1* genes localize in a region including *benRABC* genes (*ben1* cluster), although in KF707 these *cat* and *ben* clusters are transcribed in opposite direction.

Finally, the degradation of *p-hydroxybenzoate* is also possible in KF707; the 4-hydroxybenzoate 3-monooxygenase (PobA), along with the protocatechuate dioxygenase (PcaGHB), transform *p-hydroxybenzoate* to β -keto adipate enol-lactone. The lower part of the pathway is catalyzed by the *pcaDIJF* gene products (Table 1; Figures 5 and 6), which are also involved in the degradation of benzoate and phenol. In KF707, *pobA* gene co-localizes with its regulator *pobR* coding gene. This type of organization, as well as the opposite transcriptional orientation of *pobA* and *pobR* is maintained among *Pseudomonas* spp. [Paliwal et al., 2014]. The *pcaGH* genes are also grouped together with the gene encoding the PcaQ regulator. The *ben2* cluster separates the *pcaQ* sequence from the *pcaIJBDC* genes. Like KF707, the *pca* genes are arranged in a single cluster, in *P. fluorescens* Pf-5, while in other *Pseudomonas* strains such as *P. putida* CSV86 they are segregated in different regions of the genome.

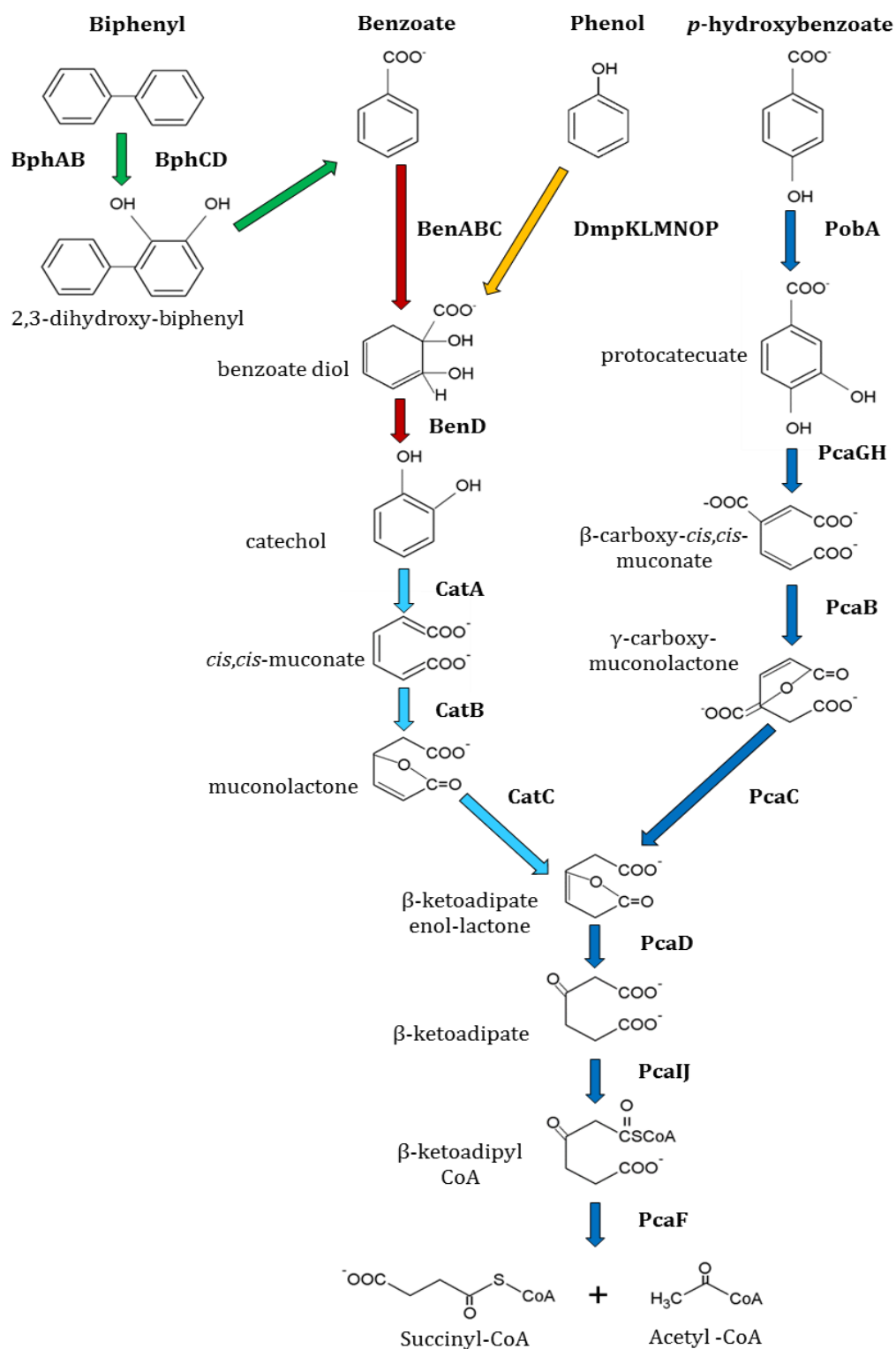


Figure 6: Predicted biochemical pathways for the catabolism of aromatic compounds in KF707. The names of the metabolites are shown; the enzymes involved in each reaction are in bold and are represented by arrows, and all of them have the same color of the gene clusters showed in Figure 5.

The KF707 genome analysis, obtained after its complete sequencing, has highlighted the ability of this bacterium to use, as carbon and energy source, a wide spectrum of aromatic compounds normally considered to be toxic and contaminants. KF707 can therefore be considered a promising “microbial-cell tool” for environmental bioremediation although in order to take advantage of these abilities, it is necessary to know and understand all the various metabolic and genetic aspects making this microorganism versatile.

In this work, three main aspects which are related to the ability of KF707 to adapt its growth in the presence of xenobiotic compounds, will be analyzed:

- ✓ **Motility and chemotaxis** – that is the function of the three *che* gene clusters involved in swimming and swarming KF707 motility;
- ✓ Functional analysis of the different **terminal oxidases** – that is the characterization of five different oxidase gene clusters and analysis of the different enzyme’s expression in response to the carbon source used in the growth medium;
- ✓ The role of *relA* and *spoT* genes – that is their role in the so call cell “**stringent response**” and cell growth in the presence of aromatic compounds.

General Materials and Methods

Media and growth conditions

Table 1: Media composition.

Media	Composition	Concentration
Luria Bertani (LB) pH 7-7.2	Tryptone	10 g/L
	NaCl	10 g/L
	Yeast Extract	5 g/L
Minimal Sal Medium (MSM) pH 7	K ₂ HPO ₄	4.4 g/L
	KH ₂ HPO ₄	1.7 g/L
	(NH ₄) ₂ SO ₄	2.6 g/L
	MgSO ₄ *	0.4 g/L
	CaSO ₄ *	0.00031 g/L
	MnSO ₄ *	0.5 g/L
	FeSO ₄ *	0.1 g/L
	Yeast Extract*	0.001 g/L
Carbon source*	6 mM	
AB glucose pH 7	K ₂ HPO ₄	3 g/L
	KH ₂ PO ₄	1.2 g/L
	20X Salt mix solution*	
	NH ₄ Cl	20 g/L
	MgSO ₄	2.9 g/L
	KCl	3 g/L
	CaCl ₂	0.2 g/L
FeSO ₄ + 7 H ₂ O	0.05 g/L	

Liquid cultures of all bacterial strains were grown in agitation at 130-150 rpm at their optimal temperatures: 37°C for *Escherichia coli* and 30°C for KF707. In the table, the asterisk (*) indicates medium components which were prepared as concentrated stock solutions, autoclaved separately and then added to the medium at the final concentration of 1 X. For growth on solid media, agar was added at the final concentration of 15 g/L.

The X-gal stock solution, necessary in the case of bacteria transformation, was prepared at the final concentration of 40 mg/mL in NN-dimethylformamide and stored in 1 mL aliquots, protected from light, at -20°C.

Antibiotics stock solutions were prepared in MilliQ sterile water as reported in Table 2 and stored at -20°C in 1 mL aliquots until use.

Table 2: Antibiotics stock solutions.

Antibiotic stock solution	Final concentration	
	<i>E. coli</i>	<i>P. pseudoalcaligenes</i> KF707
Ampicillin 50 mg/mL, in water solution	50 µg/mL	100 µg/mL
Kanamycin 50 mg/mL, in water solution	50 µg/mL	50 µg/mL
Gentamicin 30 mg/ml, in water solution	20 µg/mL	10 µg/mL

Extraction of genomic DNA from KF707

KF707's DNA was isolated from cells according to the following protocol. A 10 mL culture, grown on LB media overnight, was centrifuged at 5.000 rpm at 4°C for 15 minutes and washed twice with 10 mL of TES solution ([50 mM] Tris-HCl, [20 mM] EDTA, [50 mM] NaCl, pH 8.0). At the end of this step the cell pellet was suspended in 5 mL of TE buffer ([50 mM] Tris-HCl, [20 mM] EDTA, pH 8.0), with the addition of lysozyme solution (final concentration of 20 mg/mL in TE buffer). Next cells were incubated at 37°C for 30 minutes, mixing them by inversion every 10 minutes. At the end of incubation, 500 µL of a 10% SDS solution and Proteinase K [10 mg/mL] were added and left to act at 37°C for 1 hour; then the reaction was stopped by adding a solution of EDTA [10 mM] and sodium acetate [3 mM]. The lysate was incubated with RNase at 37°C for 1 hour after which an iso-volume of a phenol-chlorophorm-isoamyl alcohol 25:24:1 v/v mixture was added and the sample was mixed by inversion at room temperature for 15 minutes. The water phase containing the genomic DNA was separated from the organic phase and cell debris by centrifugation at 5.000 rpm at 4°C for 15 minutes. The extraction was repeated three times and phenol traces were removed by adding an iso-volume of a 24:1 v/v mixture of chlorophorm-isoamyl alcohol. The water phase was recovered after centrifugation at 5.000 rpm at 4°C for 15 minutes in a clean beaker. 1.5 volumes of cold absolute ethanol were added to the extracted

water phase and the genomic DNA was collected using a clean glass stick. The DNA was washed by immersing the glass stick in a cold 70% ethanol solution and then air-dried. After this, the stick with DNA was immersed in a small volume of sterile nuclease free water and left at 4°C over-night to allow DNA suspension. The suspended genomic DNA preparation was quantified with Nanodrop and stored at -20°C.

DNA manipulations and genetic techniques

All restriction digests, ligations, cloning and DNA electrophoresis were performed using standard techniques [Sambrook et al., 1989]. Taq polymerase, restriction endonucleases and T4 DNA ligase were used as specified by the vendors (Roche, Biolabs, or Thermo Scientific). The StrataClone cloning vector (Agilent technologies) was routinely used and recombinant plasmids were introduced into StrataClone SoloPack Competent Cells by thermal shock mediated transformation. For cloning into pG19II or pSEVA vectors, the plasmid was introduced into *E. coli* DH5α host by transformation of chemically competent cells, prepared according to the CaCl₂ method [Sambrook et al., 1989]. To detect the presence of insert DNA, X-gal was added to agar media at a final concentration of 40 µg/mL. Kits for plasmid mini- and midi-preps, PCR purification and DNA gel extraction were purchased from QIAGEN or SIGMA and used according to the manufacturer's instructions.

DNA sequencing and sequence analysis

Genomic DNA fragments of interest, cloned in the StrataClone cloning vector (Agilent technologies) or in pG19II or in pSEVA vectors, were sent to the BMR-genomics service of the University of Padova (Padova, Italy) or to the NAPCore Facility (The Children's Hospital of Philadelphia, Philadelphia, PA, USA) for sequencing.

Samples were prepared according to the recommended procedures (www.bmr-genomics.it, www.napcore.research.chop.edu). M13 Forward and Reverse primers were used for sequencing the ends of DNA fragments cloned into the vectors from the M13 promoter. Sequence identities were determined by DNA homology searches using the BLAST program to search both NCBI and ClustalW software [Thompson et al., 1994]. As regards membrane-spanning helices for all the proteins they were searched for using the program TMpred.

KF707 deletion mutant strains

Gene deletion constructs by using “Gene SOEing” method

KF707 deletion constructs (Δ), for single or multiple genes, were obtained by Gene SOEing (Splicing Overlap Extension) PCR [Izumi et al., 2007], a PCR based approach which allows site-specific mutagenesis. These constructs lack the coding region but they have the flanking regions of the wild type genes, in order to carry out an homologous recombination. Amplifications of DNA fragments flanking the target genes were performed from KF707 wild type (W.T.) strain genomic DNA, which was extracted according to the protocol previously described. Here the approach is described as a general procedure in order to allow the reader to understand. This procedure consists of three essential steps (Figure 1): primers design, PCR reactions to amplify regions flanking the target gene and, finally, an overlap PCR reaction to join the fragments.

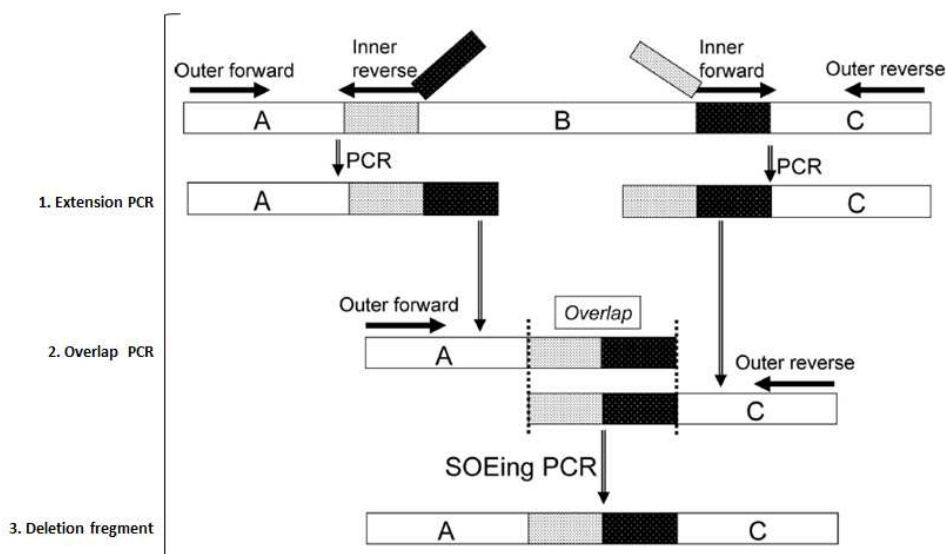


Figure 1: Schematic diagram of Gene SOEing PCR. Two regions (A, C) flanking the region to be deleted (B) were fused by overlap PCR. The fusion is mediated by an overlap of the two strands of PCR products that were created with the use of the following primers: outer forward primer, inner reverse primer, inner forward primer and outer reverse primer. 5'-region of inner reverse primer used in the amplification of region A is complementary to the segment of region C. 5'-region of inner forward primer used in the amplification of region C is complementary to the segment of region A. A recombinant product is formed when this overlap is extended in a subsequent reaction, and this recombined product is amplified with outer primers [Izumi et al., 2007].

Primers design. According to the Gene SOEing method, two pairs of primers were used to amplify the upstream and downstream flanking regions of each target gene. The reverse primer for the upstream region flanking the target gene, owns an oligonucleotide linker (at the 5'-OH end) which overlaps with that of the forward primer for the downstream flanking region. Moreover, the outer primers, specifically the forward for the upstream region and the reverse for the downstream one, own a sequence for restriction enzymes.

Extension PCR. Two separated PCR reactions were performed in order to obtain the two fragments, flanking the gene to delete, named UP and DOWN. Reaction mixtures, 50 μ L, were prepared according to the data sheet of Taq DNA Polymerase, recombinant (5 U/ μ L) (Thermo Fisher Scientific). Amplifications were performed in a Life-Pro™ Gradient Thermo Cycler (Bioer Technology). Optimal conditions of denaturation, annealing and extension were used for each pair of primers. In general, the following parameters were applied: initial denaturation at 95°C for 3 minutes, followed by 30 cycles consisting of denaturation at 95°C for 1 minute, annealing at the optimal temperature for each primers pair for 45 seconds, elongation at 72°C for 1 min/Kb and a final extension step at 72°C for 10 minutes. PCR products were separated by electrophoresis on 0.7% (w/v) agarose gel, and after staining in a Gel-Red solution, they were visualized under UV-light: when clear and clean bands were observed, the PCR reactions were cleaned-up using QIAGEN PCR purification kit; otherwise, if no specific products were observed, the correct bands were cut from gel and cleaned-up using the QIAGEN gel extraction kit.

Overlap PCR. Purified PCR products from the two separated reactions were quantified by NanoDrop ND-1000 UV-Vis Spectrophotometer, and 50 ng of each were used as templates in the “overlap step”: for each target gene, only the two outer primers were used in the reaction, since the overlapping linkers have the 3'-OH extremity to allow extension by Taq polymerase; the fragments formed an eteroduplex intermediate mediated by the overlapping linkers. Subsequent extension of the eteroduplex led to the formation of the recombinant molecules.

Purification of deletion constructs. PCR overlap products were separated by electrophoresis on 0.7% (w/v) agarose gel and after staining in Gel-Red solution they were visualized under UV-light; bands were cut from gel and cleaned-up using the QIAGEN gel extraction kit, according to the manufacturer's guide. The purified joined amplicons were stored at -20°C until use for subsequent experiments.

Construction of recombinant plasmids containing deletion fragments

Cloning in StrataClone vector. Deletion fragments (Δ), obtained from Gene SOEing method, were double digested with the appropriate restriction enzymes and cloned into StrataClone cloning vector (Agilent technologies). Plasmids were inserted into StrataClone SoloPack Competent Cells by thermal shock mediated transformation, and clones were selected *via* white/blue screening on LB kanamycin agar containing X-gal at the final concentration of 40 $\mu\text{g}/\text{mL}$. In order to assess the presence of the insert, plasmid mini-preps were performed from white clones cultures and double digested with restriction enzymes; after electrophoresis on 0.7% (w/v) agarose gel and staining in Gel-Red solution, digestions were visualized under UV-light. For further validation, white clones were selected for colony PCR reactions: inserts were amplified using universal M13 forward and reverse primers and purified PCR products were sequenced to confirm the insertion of the DNA fragments.

Cloning in pG19II. Subsequently, each fragment was cloned into the conjugative plasmid pG19II [Maseda et al., 2004] double digested with restriction enzymes. pG19II is a pK19mobsacB derived conjugative plasmid, which carries its own origin of replication, the *oriV*, and an origin of transfer, named *oriT*. Moreover, this plasmid harbors two selection markers: Gm^{R} gene, which confers resistance to the antibiotic gentamicin and *sacB* gene, codifying for the secreted enzyme levansucrase which causes sensitivity to sucrose [Maseda et al., 2004]. Recombinant plasmids were inserted into *E. coli* DH5 α host by transformation of chemically competent cells and transformant clones were selected for gentamicin resistance and *via* white/blue screening. Mini-preps were performed from cultures of positive clones and all the recombinant plasmids were sent for sequencing in order to verify the presence of the insert.

Conjugation

pG19II recombinant plasmids carrying the constructs were transferred by conjugation to KF707 W.T. strain.

Day I. Donor (*E. coli* DH5 α with pG19II+deletion fragment), receiver (KF707) and helper (*E. coli* HB101 pRK2013) strains were streaked on LB agar plates with the appropriate antibiotics. LB plates were incubated overnight at 37°C and at 30°C for *E. coli* and KF707 optimal growth temperature respectively. *E. coli* HB101 strain carrying the mobilization plasmid pRK2013, was commonly used as helper strain for tri-parental mating.

Day II. Donor, receiver and helper strains were inoculated in 10 mL of LB medium from single colonies grown on the agar plates; the appropriate antibiotics were added in order to maintain selection. LB liquid cultures were grown overnight at the appropriate temperature under agitation at 150 rpm.

Day III. After overnight growth, 1 mL aliquot from each culture was collected in a sterile tube and washed twice with 1 mL LB medium. Cells were suspended in 1 mL of fresh LB and then used for the preparation of conjugation mix by adding equal volumes (100 μ L) of donor, receiver and helper suspensions to a sterile tube. The conjugation mix was incubated at 30°C for 45 minutes and a 100 μ L spot was plated onto well dry LB agar plates without selection.

Day IV. The bacterial biomass was collected with a sterile loop and suspended in 1 mL of fresh LB and serial dilutions were performed using phosphate buffer. 100 μ L of the dilutions between 10⁻¹ to 10⁻⁴ were plated on AB glucose agar plates containing gentamicin; this medium was used to counter-select *E. coli* donor and helper strains, given that this medium does not support *E. coli* growth, thus resulting selective for KF707. Plates were incubated at 30°C for 48 hours.

Day V-VI. Transconjugants were *tooth-picked* in fresh AB glucose plus gentamicin agar medium and incubated at 30°C until growth was clearly visible. This selection step was repeated at least twice, in order to obtain a pure culture and remove both donor and helper strain backgrounds.

Day VII. Once a pure colony of KF707 was obtained, this was inoculated in modified LB broth without NaCl, in order to force a double cross-over between the recombinant plasmid

and the homologous genomic DNA sequence. Cells were grown for 48 hours at 150 rpm at 30°C.

Day VIII. After 48 hours growth, serial dilutions were performed with phosphate buffer and 100 μ L of dilutions between 10^{-2} to 10^{-5} were plated on LB media + 10% of sucrose. Since pG19II harbors the *sacB* gene which codifies for the levansucrase, an enzyme that doesn't allow growth on sucrose, this carbon source was added at high concentration to stimulate the expulsion of the plasmid. Plates were incubated at 30°C for 48 hours.

Day IX. After incubation, grown clones were *tooth-picked* onto both LB agar 10% sucrose and LB agar with gentamicin. Plates were incubated at 30°C overnight.

Day X. After over-night incubation, the growth of the selected clones in the two types of media was compared: double cross-over clones were those able to grow only on 10% sucrose plates and not on gentamicin plates. They were selected as probable double cross-over mutants and this was subsequently confirmed by performing colony PCR reaction using two pairs of primers: the outer primers for the flanking regions of each deleted gene and new primers necessary to amplify a fragment inside the deleted gene. The clones that only showed the first amplified but not the second were chosen as mutants and sequenced.

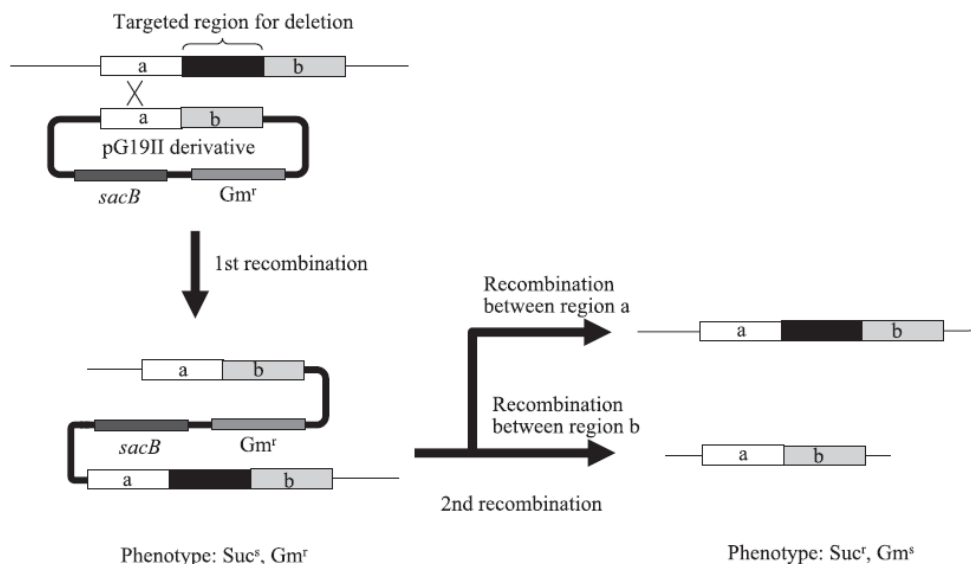


Figure 2: Scheme of unmarked deletion mutation. Here it is shown what happens during the conjugation protocol at the genomic DNA level, the two recombination events and the possible results are shown [Kita et al., 2009].

Chapter 1

The role of *cheA* genes in swarming and swimming motility of *Pseudomonas pseudoalcaligenes* KF707

This chapter is based on:

S. Fedi, T. Triscari-Barberi, M.R. Nappi, F. Sandri, S. Booth, R.J. Turner, M. Attimonelli, M. Cappelletti and D. Zannoni. Microbes and Environments. Vol. 31, No. 2, 169-172 (2016).

Background: Bacterial chemotaxis

In a constantly evolving environment, it is essential for microorganisms to be able to respond, appropriately and rapidly, to changes. Possible responses to these phenomena include variations in gene expression and/or movement toward or away from a local environment. In Prokaryotes, the most common system involved in these kind of responses, is the histidine-aspartate phosphorelay system (HAP). These systems have two components: a dimeric histidine kinase protein and a response regulator [West and Stock, 2001]. Bacteria can receive signals depending on a wide range of environmental changes such as the concentration of nutrients and toxic substances present in a soil or a water body, the levels of oxygen, pH, osmolarity, and light-wavelength intensity [Wadhams and Armitage, 2004]. The sequencing of different bacterial species genomes has identified over 600 HAP systems and, in particular, some bacteria own more than 130 systems. These systems are involved in the regulation of gene expression, but one of the most well-understood pathway regulated by HAP is the motile behavior. In bacteria, chemotaxis is a complex network of signals that are balanced to produce a physiological response of adaptation to a specific habitat. It is a process allowing the migration of microorganisms under the influence of a chemical gradient, leading the bacterium to find a chemically favorable niche to grow and survive in unfavorable environments. Most bacteria, in fact, are mobile, since they own a structure called flagellum, and chemiotactic behavior is obtained by integrating signals received through receptors that detect the properties of the surrounding environment. In nature, there are several examples where chemotaxis plays an essential role such as colonization by bacteria of sites contaminated by xenobiotic compounds, biofilm formation and invasion and pathogenic colonization of hosts [Grimm

and Harwood, 1997; Pittman et al., 2001; Parales and Harwood, 2002; Stoodley, 2002]. In particular, bacteria can respond to stimuli with different motility strategies, and the most common are:

- ✓ **Swarming:** (Figure 1.1) it consists of an organized translocation of cells on a solid surface and it is usually associated with the presence of a type IV pili and cell-cell communication. In this phenomenon the bacteria that are outside the colony can expand and move outward, leaving, an empty space, in the center of the colony, in which new cells start to grow or to move; in these cases the bacterial colonies form a dendritic pattern on the surface [Kearns, 2010].
- ✓ **Swimming:** (Figure 1.1) it is the most common bacterial strategy in a fluid environment, it is the result of flagellar rotation which exerts a propulsion or repulsion force that moves the bacterium; in this case the motility depends on the number of flagella and on their position in the cell [Mattik, 2002].

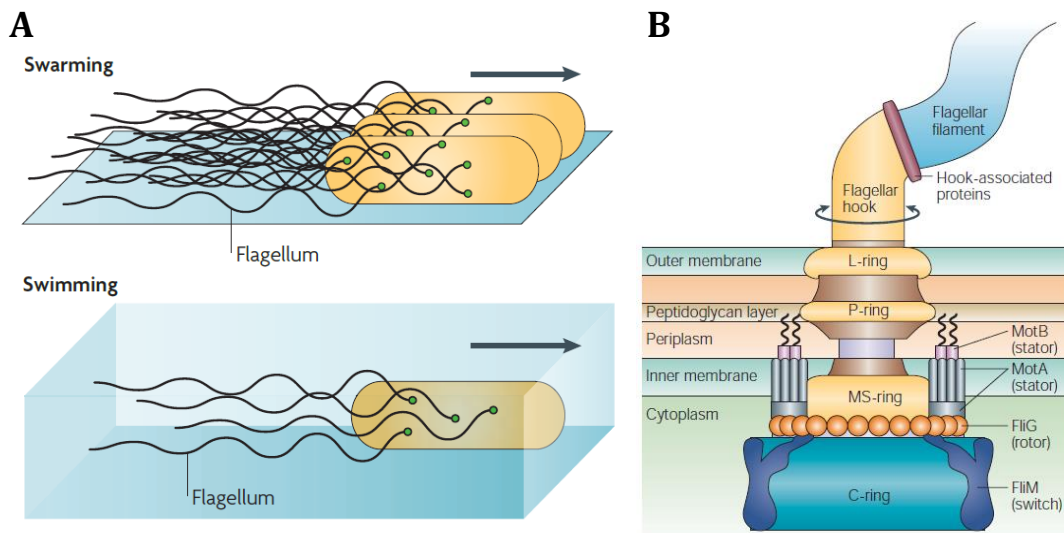


Figure 1.1: **A)** Swarming is the multicellular movement of bacteria across a surface and it is powered by rotating helical flagella. Swimming is the movement of an individual bacterium in liquid, also powered by rotating flagella [Kearns, 2010]. **B)** Schematic representation of bacterial flagellum this system consists of three major parts: the filament, the hook and the basal body that is inside the membrane. There are many differences between bacterial species concerning flagella, but the main structures are common to all [Wadhams and Hermitage, 2004].

The chemotaxis signaling in *E. coli*

One of the most studied chemotaxis network is that of *E. coli*, which is in fact considered a simple model for explaining these mechanisms [Berg, 1975; Adler, 1975].

Bacteria, like *E. coli*, have two types of swimming motility: a straight line called *run* and an overturning motion called *tumble*. In the absence of stimuli, when the concentration of nutritional compounds in the environment is uniform, the cells *run* for about a second and then *tumble* for about 10 seconds by changing orientation and then move towards a new direction. This causes the bacterial cells to walk randomly without having a pre-defined motion direction. The *run* is the consequence of a counter-clockwise rotation while the *tumble* is the consequence of a clockwise rotation of flagella [Sourjik and Wingreen, 2012]. When a cell detects the increase of a carbon source concentration, the *tumble* occurs less often and there is a clear movement towards the attracting source. Cells are able to immediately compare the concentrations of the chemo-effectors and establish the direction of movement. Conversely, negative stimuli increase the probability of a clockwise rotation and cells *tumble* much more frequently [Tsang et al., 1973].

In *E. coli* as in many bacterial species, the chemotaxis molecular mechanism depends on two different types of molecules: the membrane receptors and the chemotactic proteins Che. Usually the chemotactic proteins Che are anchored to the inner membrane through the receptors which are necessary for the transmission of the signal between periplasm and cytoplasm (Figure 1.2).

- ✓ In *E. coli* there are five different chemoreceptors (Figure 1.2A) called Tsr, Tar, Tap, Tgr and Aer; these proteins are commonly known as Methyl-accepting Chemotaxis Proteins (MCPs), because they are substrates for methylation or demethylation. Their function is closely related to their structure and they are classified according to a series of properties such as: cellular localization (in the membrane or cytoplasmic), their abundance, their size and the ligand-binding region (extra-cellular or cytosolic) [Wadhams and Armitage, 2004; Baker et al., 2006]. The different chemoreceptors respond in a specific way according to different stimuli. For example, the Tar molecule of *E. coli*, is the specific receptor for the detection of aspartate or maltose; in this case

aspartate binds directly the periplasmic domain, while maltose binds the periplasmic maltose binding protein associated to Tar [Yeh et al., 1996].

- ✓ In *E. coli* there are six different Che proteins:
 - ❖ **CheA** is a member of the kinase histidine family and catalyzes the transfer of a phosphoric group from ATP to an aspartate residue present on a stimulation response regulator. Its structure consists of five specific domains, and it is the largest and most complex protein in the chemotaxis system [Baker et al., 2006].
 - ❖ **CheW** is a soluble monomeric protein; it adapts and forms a complex with CheA, and its function is to anchor the kinase histidine to chemoreceptor molecules. Its structure is very similar to one of the CheA domain [Griswold et al., 2002].
 - ❖ **CheY** is a response regulator located downstream of the CheA-CheW complex and interacts directly with the FliM protein situated at the base of the flagellar motor, determining a rotational change of the flagellum [Bren et al., 1998]. It is a highly conserved monomeric protein.
 - ❖ **CheR** and **CheB** proteins are response regulators involved in methylation and demethylation of the cytoplasmic domain of chemoreceptors. CheR is an S-adenosyl-methionine-dependent methyl-transferase, which methylates specific glutathione residues, while CheB is an esterase that hydrolyzes methyl ester produced by CheR [Okomura et al., 1998; Levit and Stock, 2002].
 - ❖ **CheZ** is a phosphatase that closes and completes stimulus mechanism [Wang and Matsumura, 1996].

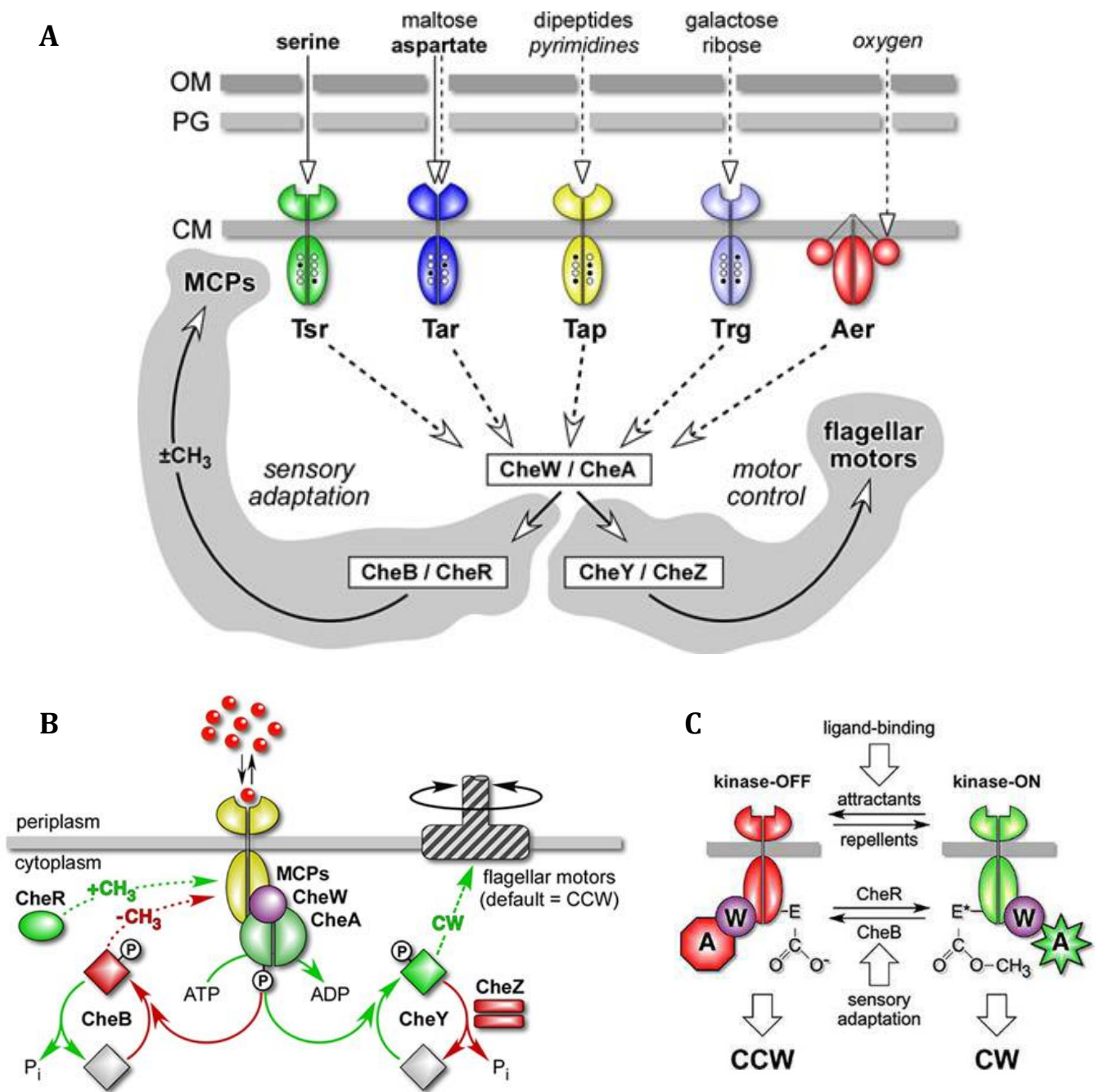


Figure 1.2: Chemotaxis signaling and components in *E. coli*. **A)** *E. coli* chemoreceptors and Che proteins involved in the signaling. **B)** Phosphorelay signaling the spinning of flagellar motor, reactions and components that augment CW rotation are in green, those that augment the CCW rotation are in red. **C)** Two state model of receptor signaling; receptor ternary complexes in kinase-active (on) and kinase-inactive (off) signaling states. Abbreviations: OM, outer membrane; PG, peptidoglycan layer of cell wall; CM, cytoplasmic membrane; CW, clockwise; CCW, counterclockwise [Parkinson et al., 2015].

The chemotactic signaling starts when a chemo-repellent molecule (Figure 1.2C) binds one of the transmembrane receptors; this activates and together with the CheW adapter stimulates the autophosphorylation of CheA. CheA phosphorylation also determines that of CheY; CheY-P spreads to the flagellar motor [Li et al., 1995; Sourjik and Berg, 2002] where it acts as an allosteric regulator for FliM protein, changing the direction of rotation by clockwise to counter-clockwise and, consequently, *tumble* occurs [Alon et al., 1998]. The signaling ends with the phosphatase CheZ, which dephosphorylates CheY [Stock, A.M and Stock, J.B., 1987; Wang and Matsumura, 1996].

If the ligand is a chemo-attractive agent (Figure 1.2C), its binding to chemoreceptors does not result in conformational change, and the CheA autophosphorylation is inhibited, causing the decrease of the CheY-P levels; in this way swimming motility is reduced and the counterclockwise rotation is also decreased. As already reported, the result is a prolonged *run* with rare moments of *tumble*.

The cascade of the chemotaxis signal is characterized by a specific activation time, which guarantees an effective response and allows the recovery of the initial state of the chemoreceptor. The time control of the signaling mechanism of the cell response is critical and depends on the dephosphorylation of CheY-P protein. This response regulator can catalyze dephosphorylation itself, but this happens too slowly; for this reason, the reaction requires a phosphatase enzyme, and in the case of *E. coli* this protein is the CheZ phosphatase [Zhu et al., 2000; Gao and Stock, 2009; Kenney, 2010]. This enzyme is composed of two symmetrical monomers, each containing a binding site for CheY-P. Previous studies have demonstrated that the link between CheZ and CheY-P proteins shows positive co-operation [Blat et al., 1998; Silversmith et al., 2008]; this means that CheZ activity is suppressed when CheY-P concentration is low, in this way it is possible to maintain the correct CheY-P levels necessary for the *steady-state* of the receptor. The decrease in CheY-P levels in the cell cytoplasm determines the signal attenuation [Wadhams and Armitage, 2004].

1.1 Introduction

Bacterial chemotaxis, as noticed above, is the ability of bacteria to move from or to a particular substance, it can therefore be considered a prerequisite for the survival of the bacterial population when it is necessary need to adapt its metabolism to a particular environment or when bacteria interact with new ecological niches [Lauffenburger, 1991].

In particular, for some bacterial species, such as for example KF707, chemotaxis is regarded as a selective advantage for the colonization of environments contaminated by xenobiotic compounds [Parales et al., 2002]. As described in the main introduction section, KF707 is known for its ability to co-metabolize PCBs through the expression of genes products involved in the biphenyl degradation pathway; unfortunately, these chemicals are less bioavailable due to their hydrophobicity and as a consequence the bioremediation of contaminated sites through bacteria is a more complex process than initially thought [Stelmack et al., 1999]. Specifically, in the case of KF707, the ability to form biofilm is essential for the colonization of contaminated sites and chemotaxis plays a crucial role in this mechanism [O'Toole and Kolter, 1998; Tremaroli et al., 2010; Tremaroli et al., 2011].

Usually, Gram negative bacteria possess multiple chemotactic pathways, and not all of them are involved in motility and/or in chemotaxis, but sometimes they are responsible for other physiological functions. Many bacterial species, belonging to genera *Pseudomonas*, *Vibrio* or *Rhodobacter*, contain genomes with different gene clusters involved in chemiotaxis-like signaling pathways. For example, in *P. aeruginosa* PAO1, whose genome has different homologies with that of KF707, there are four operons involved in chemotaxis, named *Che*, *Che2*, *Pil-Chp* and *Wsp*, and some components are necessary for biofilm formation and for the control of cyclic-di-GMP production [Kato et al., 2008]. The genome of *Rhodobacter sphaeroides*, a Gram negative facultative photosynthetic bacterium, codifies three different operons involved in its chemotactic system: *CheOP1*, *CheOP2* and *CheOP3*. This specific case is an important example since, it is known that the first two operons are both necessary for chemotaxis [Porter et al., 2002] while the function of the third is unknown, as *CheOP3* is not expressed in laboratory conditions [Poggio et al., 2007].

In the KF707 genome, that was completely sequenced in 2012 [Triscari-Barberi et al., 2012], three gene clusters (***che1***, ***che2*** and ***che3***) predicted to be involved in the chemotaxis pathway (Table 1.1; Figure 1.3), were identified and annotated. The *cheA* gene, the most

important gene of each cluster, is known to encode for a protein, a histidine kinase ATPase, which is part of an additional two-component signal transduction system, necessary for regulation of flagellar activity [Stock and Levit, 2000] in response to environmental stimuli. The *che1* gene cluster was investigated in an early study [Tremaroli et al., 2011] through the analysis of a mutant impaired in its swimming motility, which was obtained from a KF707 mini-Tn5 insertion library. In this case the CheA1 protein was interrupted by the transposon insertion, and the phenotype of this strain showed that this gene, *cheA1*, was not only involved in flagellum-driven motility but also in the regulation of biofilm development. The nucleotide sequence of *cheA1* gene showed a high homology (between 81% and 95%) with the *cheA* genes of other *Pseudomonads* and in particular it displayed the maximum identity with the histidine kinase gene of *P. mendocina* NK-01. As regarding *cheA2*, also in this case, the maximum coverage (84%) was found with the nucleotide sequence of *P. mendocina* NK-01 signal transduction histidine kinase moreover, the CheA2 protein had a 72% similarity with *P. aeruginosa* PAO1 ChpA protein, encoded by *pil-chp* gene cluster. In this latter case the regions flanking the *cheA2* gene, code for two methyltransferase proteins, CheB and CheR; this arrangement is similar to the one found in *P. aeruginosa* PAO1 *pil-chp* gene cluster, known to be involved in type IV pili biogenesis and motility [Alm and Mattick, 1995; Whitchurch et al., 2004]. Finally, the nucleotide sequence of *cheA3*, showed a high identity with *P. aeruginosa* UCBPP-PA14 (83%) gene, while its amino acids sequence displayed maximum identity (72%) with a *P. aeruginosa* PA7 sensor, being in both cases two-component sensor proteins. The KF707 *che3* gene cluster contains two ORFs coding for a Methyl-accepting Chemotaxis Proteins (MCP), a chemotaxis regulator protein, CheA3 protein (histidine kinase) and other proteins usually involved in the motility pathways.

Table 1.1: The KF707 *che* gene clusters. compared to other *Pseudomonas* strains. Names of the genes from which are encoded, lengths of the products in amino acids and the Gene Bank accession number (KF707 = NBRC 110670 – Nov. 2016), are reported. For each gene the Gene Bank accession number resulting as best hit from BLASTP against other *Pseudomonas* genome is reported with the related amino acids % of identity (aa % ID).

Gene	Gene product (aa)	Gene Bank KF707	aa % ID	Organism	Gene Bank
che1 cluster					
<i>cheY1</i>	128	BAU75677	100%	<i>P. aeruginosa</i> PAO1/P1	EHS34928
<i>cheZ1</i>	262	BAU75676	90%	<i>P. resinovorans</i> NBRC_106553	BAN49711
<i>cheA1</i>	753	BAU75675	95%	<i>P. resinovorans</i> NBRC_106553	BAN49710
<i>cheB1</i>	367	BAU75674	92%	<i>P. resinovorans</i> NBRC_106553	BAN49709
<i>motA</i>	246	BAU75673	92%	<i>P. resinovorans</i> NBRC_106553	BAN49708
<i>motB</i>	297	BAU75672	87%	<i>P. resinovorans</i> NBRC_106553	BAN49707
<i>cheW1.2</i>	285	BAU75670	78%	<i>P. resinovorans</i> NBRC_106553	BAN49705
<i>cheW1</i>	159	BAU75669	99%	<i>P. resinovorans</i> NBRC_106553	BAN49704
che2 cluster					
<i>pilG</i>	135	BAU71994	99%	<i>P. alcaligenes</i> OT.69	EQM7052
<i>pilH</i>	121	BAU71995	98%	<i>P. resinovorans</i> NBRC_106553	BAN46075
<i>pilI</i>	178	BAU71996	92%	<i>P. resinovorans</i> NBRC_106553	BAN46076
<i>pilJ</i>	682	BAU71997	96%	<i>P. resinovorans</i> NBRC_106553	BAN46077
<i>cheR2</i>	286	BAU71998	87%	<i>P. resinovorans</i> NBRC_106553	BAN46078
<i>cheA2</i>	2528	BAU71999	78%	<i>P. resinovorans</i> NBRC_106553	BAN46079
<i>cheB2</i>	343	BAU72000	89%	<i>P. resinovorans</i> NBRC_106553	BAN46080
<i>cheW2</i>	156	BAU72001	83%	<i>P. resinovorans</i> NBRC_106553	BAN46081
che3 cluster					
<i>cheY3</i>	121	BAU75960	97%	<i>P. resinovorans</i> NBRC_106553	BAN47123
<i>cheA3</i>	588	BAU75961	87%	<i>P. resinovorans</i> NBRC_106553	BAN47122
<i>cheW3</i>	161	BAU75962	96%	<i>P. resinovorans</i> NBRC_106553	BAN47121
<i>aer</i>	668	BAU75963	86%	<i>P. resinovorans</i> NBRC_106553	BAN47120
<i>cheR3</i>	281	BAU75964	78%	<i>P. resinovorans</i> NBRC_106553	BAN47119
<i>cheD3</i>	203	BAU75965	89%	<i>P. resinovorans</i> NBRC_106553	BAN47118
<i>cheB3</i>	349	BAU75966	91%	<i>P. resinovorans</i> NBRC_106553	BAN47117

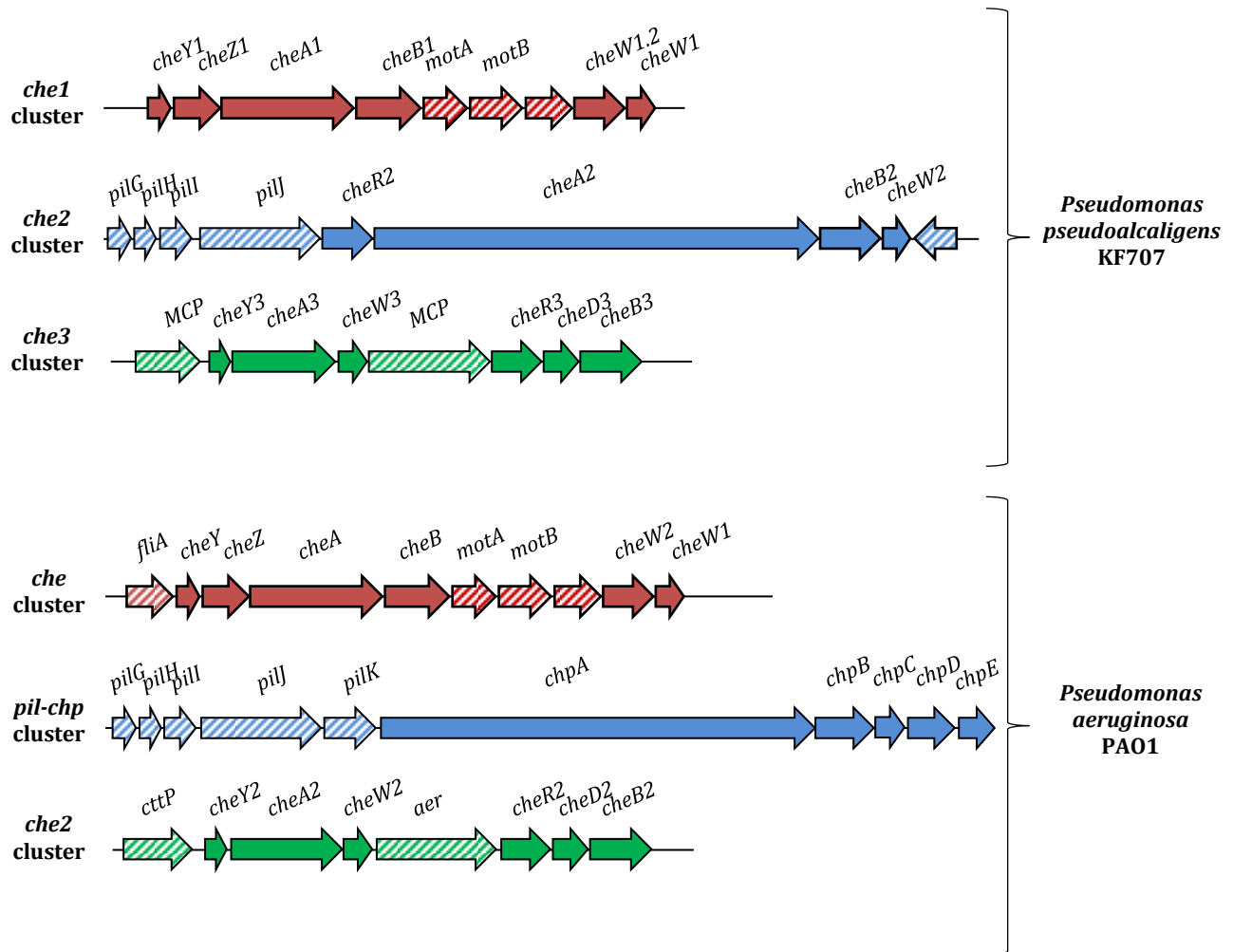


Figure 1.3: Genetic organization of three chemotactic systems of KF707 (*che1*, *che2* and *che3*) relative to those of *P. aeruginosa* PAO1. Gene clusters shown in full colors, accessory genes in dashed stripes.

The three main genes of the KF707's clusters, *cheA1*, *cheA2* and *cheA3* do not show high similarity among them. As reported in Table 1.1, the three proteins encoded (CheA1, CheA2 and CheA3) have different amino acids-size, but, analyzing the amino acid sequence, the presence of conserved domains has been found.

In particular, as reported in Figure 1.4, they contain five conserved domains, connected by linkers, named P1-P5 from N- to C-terminus. Four of them are present in all of these three proteins:

- ✓ **P1:** histidine-phosphotransfer domain; this domain transfers a phosphoryl group between ATP and the phosphor-accepting aspartate side chain.
- ✓ **P3:** histidine kinase homodimeric domain that is a helical domain situated at the interface of signal transducing histidine kinase family.
- ✓ **P4:** histidine kinase-like ATPase domain; this is part of a family including several ATP-binding proteins like DNA gyrase type B, DNA mismatch proteins, heat shock protein HSP90 and histidine kinase.
- ✓ **P5:** CheA regulatory domain belonging to the CheW-like proteins, it seems to be involved in the interaction with the kinase regulator CheW.

Finally, the **P2** signal receiver domain was found only in CheA2 protein in which multiple P1 domains are also present.

In addition to the main *cheA* genes, inside the clusters there are other important genes involved in motility and chemotaxis. Multiple CheW proteins are encoded by all three clusters; CheW could be involved in chemoreceptors arrays organization, they can anchor the CheA dimers to the methyl-accepting chemotaxis proteins, transmitting the “piston-like movement” to the histidine kinase CheA. The *cheY* genes, found in *che1* and *che3* clusters are involved in response regulation; usually multiple copies of these genes are present in bacteria lacking *cheZ*, but this is not the case of KF707; here, the additional CheY protein could help CheZ activity, which is involved in signal termination and it is present only in *che1* cluster. All the others proteins found in multiple copies, in all the gene clusters, such as CheB and/or CheR, may be involved in adaptation mechanisms.

The presence of different gene clusters for the chemo-sensory pathway suggests that this pathway is rather complex in KF707 and it may be possible that the different clusters play a role in different cellular functions such as biofilm formation and gene expression regulation, as well as being involved in the bacterium motility. To better analyze the role of these genes in swimming and swarming motility and in chemotaxis, KF707 deletion and transconjugant complementation mutant strains for *cheA1*, *cheA2* and *cheA3* genes, were obtained.

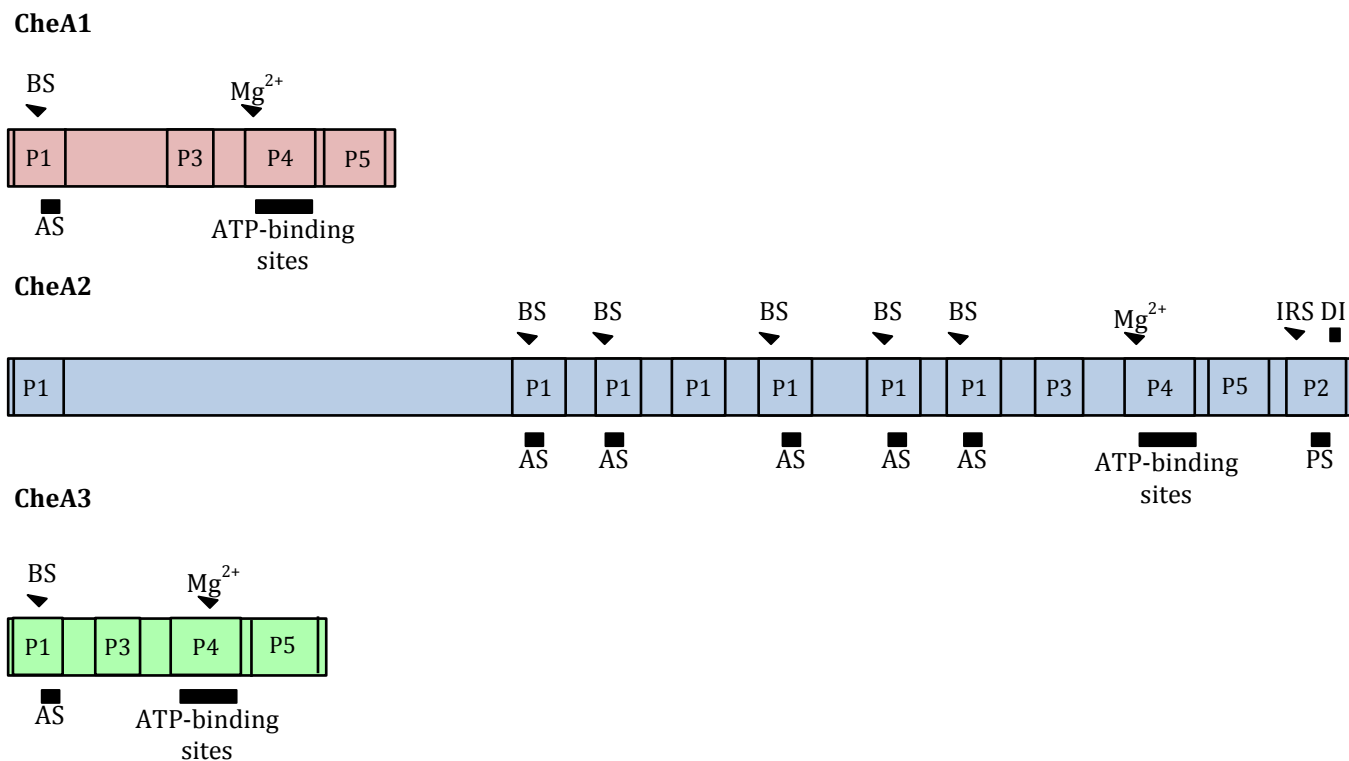


Figure 1.4: Schematic representation of the CheA histidine kinase (CheA1, CheA2 and CheA3) of KF707 based on amino acids sequences analysis. Relevant domains and features of the CheA proteins are indicated as follows: P1 domain = histidine-phosphotransfer domain; P2 domain = signal receiver domain; P3 domain = histidine kinase homodimeric domain; P4 domain = histidine kinase-like ATPase domain; P5 domain = cheA regulatory domain; BS = putative binding surface; AS = putative active site; Mg^{2+} = Mg^{2+} binding site; DI = dimerization interface; IRS = intermolecular recognition site; PS = phosphorylation site. Active or binding sites composed by more than one conserved amino acid residue are shown as black rectangles while features constituted by one conserved residue are indicated by black triangles.

1.2 Materials and Methods

1.2.1 Bacterial strains and plasmids

All strains and plasmids, used in this chapter, are listed in Table 1.2.

Table 1.2: Bacterial strains and plasmids.

Bacterial Strains	Relevant Genotype	Reference
<i>P. pseudoalcaligenes</i> KF707		
Wild type (W.T.)	Amp ^r	Furukawa and Miyazaki, 1986
KFcheA1::Km	Insertion of mini-Tn5 transposon inside <i>cheA1</i> gene, Km ^r , Amp ^r	Tremaroli et al., 2011
KFΔ <i>cheA2</i>	Deletion of <i>cheA2</i> , Amp ^r	Triscari-Barberi, 2013
KFΔ <i>cheA3</i>	Deletion of <i>cheA3</i> , Amp ^r	Triscari-Barberi, 2013
KFcheA1::Km/Δ <i>cheA2</i>	Insertion of mini-Tn5 transposon inside <i>cheA1</i> gene, deletion of <i>cheA2</i> , Km ^r , Amp ^r	Triscari-Barberi, 2013
KFcheA1::Km/Δ <i>cheA3</i>	Insertion of mini-Tn5 transposon inside <i>cheA1</i> gene, deletion of <i>cheA3</i> , Km ^r , Amp ^r	Triscari-Barberi, 2013
KFΔ <i>cheA2</i> /cheA3	Deletion of <i>cheA2</i> and <i>cheA3</i> , Amp ^r	Triscari-Barberi, 2013
<i>E. coli</i>		
DH5α	<i>supE44, hsdR17, recA1, endA1, gyrA96, thi1, relA1</i>	Hanahan, 1983
HB101	Sm ^r , <i>recA, thi, pro, leu, hsdR</i>	Boyer and Roland-Dussoix, 1969
Top10F'	F' [<i>lacIq, Tn10</i> (TetR)], <i>mcrA, Δ(mrr-hsdRMS-mrcBC), Φ80lacZΔM15ΔlacX74, recA1, araD139, Δ(ara leu), 7697 galU, galK, rpsL</i> (StrR), <i>endA1, nupG</i>	
Plasmids	Relevant Genotype	Reference
pG19II	Gm ^r , <i>sacB, lacZ</i> , cloning vector and conjugative plasmid	Maseda et al., 2004
pG19IIΔ <i>cheA2</i>	Gm ^r , <i>sacB, lacZ</i> , carrying Δ <i>cheA2</i> deleted fragment	Triscari-Barberi, 2013
pG19IIΔ <i>cheA3</i>	Gm ^r , <i>sacB, lacZ</i> , carrying Δ <i>cheA3</i> deleted fragment	Triscari-Barberi, 2013
pSEVA342	Cm ^r , pRO1600/Cole1, <i>lacZα</i> -pUC19	This study
pSEVA532	Tc ^r , pBBR1, <i>lacZα</i> -pUC19	This study
pSEVA342- <i>cheA1</i>	Cm ^r , pSEVA342 with <i>cheA1</i> gene in the MCS	This study
pSEVA532- <i>cheA1</i>	Tc ^r , pSEVA532 with <i>cheA1</i> gene in the MCS	This study
pSEVA342- <i>cheA2</i>	Cm ^r , pSEVA342 with <i>cheA2</i> gene in the MCS	This study
pSEVA532- <i>cheA3</i>	Tc ^r , pSEVA532 with <i>cheA3</i> gene in the MCS	This study

1.2.2 KF707 deletion mutant and complemented strains for *cheA* genes

KFcheA1::Km mutant was obtained in a previous work [Tremaroli et al., 2011] by using a KF707 mutant library generated by random mutagenesis with the miniTn5-*lacZ1* transposon (Km^r). Deletion mutant strains were obtained by using Gene SOEing PCR technique and conjugation protocol during Triscari-Barberi PhD work (2013).

All the primers used for the deletion Δ constructs and for the amplification of the *cheA* genes for the KF707 complementation mutant strains are listed in Table 1.3.

Table 1.3: Primers used for the construction of the deletion fragments (Δ) and for the *cheA* genes. The red nucleotides form the overlap region for the UP and DOWN deletion fragments union PCR, while the nucleotides that form the cutting site for the restriction enzymes are in bold.

Gene	Primer name	Sequence	Restriction enzyme
ΔcheA2	FOR up	GCCGA AAGCTT TGTTGTCCTG	<i>Hind</i> III
	REV up	CTATAAGTGTAGCAT GGTTGTCCGGG	
	FOR down	ATGCTACACTTATAG GACCGTGCGC	
	REV down	AAGCG GATCC GATGTCTTCTCTGTC	<i>Bam</i> HI
ΔcheA3	FOR up	GCCGA AAGCTT TACCACCTGGTGTT	<i>Hind</i> III
	REV up	CTATAAGTGTAGCAT TGGGTCACGGCG	
	FOR down	ATGCTACACTTATAG TGATCCGGGTCCG	
	REV down	AAGCG GATCC ACGATGGGAACGATG	<i>Bam</i> HI
<i>cheA1</i>	FOR	GCGAGA AAGCTT CGACGCCGATGAAGAA	<i>Hind</i> III
	REV	ATAGT GATCCT CAGCCACGGCGCGTA	<i>Bam</i> HI
<i>cheA2</i>	FOR	AACAAT CTAGAT CATGTCCGTTTGACCAG	<i>Xba</i> HI
	REV	ATTAT CCTGCAGG ACTGATCGGCATGACTA	<i>Sbf</i> I
<i>cheA3</i>	FOR	TACGTA AAGCTT GAAATGACGGGATGAACCAGTTC	<i>Hind</i> III
	REV	GATCA AGGATCCT AGGGGAGTTCATGCAG	<i>Bam</i> HI

To restore the wild type genotype in KF707 *cheA* deletion mutant strains, the three *cheA* genes were reintroduced using pSEVA342 and pSEVA532 vectors.

As a first step, the three genes *cheA1*, *cheA2* and *cheA3* were amplified, using a High Fidelity Taq Polymerase (Thermo Fisher), provided with a proofreading activity in order to avoid errors during polymerization; the reagents were added according with the datasheet.

The primers used for the three reactions are reported in Table 1.3, while the PCR programs are shown in Table 1.4.

Table 1.4: PCR programs for the amplification of *cheA* genes, for complementation protocol.

Gene	Step	Temperature	Time
<i>cheA1</i> - 35 cycles			
	Initial denaturation	98°C	2 minutes
	Denaturation	98°C	30 seconds
	Annealing	64°C	30 seconds
	Extension	72°C	30 seconds
	Final extension	72°C	10 minutes
<i>cheA2</i> - 32 cycles			
	Initial denaturation	94°C	3 minutes
	Denaturation	94°C	20 seconds
	Annealing	58°C	30 seconds
	Extension	68°C	6 minutes
	Final extension	68°C	10 minutes
<i>cheA3</i> - 35 cycles			
	Initial denaturation	98°C	2 minutes
	Denaturation	98°C	30 seconds
	Annealing	60°C	30 seconds
	Extension	72°C	30 seconds
	Final extension	72°C	10 minutes

After the reactions, PCR products were purified with a Gel Extraction kit (QIAquick – QIAGEN) and cloned into *E. coli* Top10F' competent cells using the TOPO TA cloning kit (Invitrogen); subsequently, the PCR products were double digested with specific restriction enzymes, and individually ligated into pSEVA342 and pSEVA532; the correct cloning was confirmed by plasmid DNA extraction, colony PCR and sequencing analysis.

Finally, the conjugation protocol (General Materials and Methods – until the day 4) was performed by using KF707 *cheA* deletion mutant strains, recombined pSEVA plasmids and *E. coli* HB101 helper strain. Through this method was possible reintroduced the wild type *cheA* genes in the deletion mutants strain. At the end through Colony PCR and DNA sequencing analysis, complementations were confirmed.

1.2.3 Motility assay

The swimming and swarming behavior of KF707 W.T., *cheA* deletion mutants and complementation strains were analyzed, in order to observe phenotypic differences, as described in the following protocols.

Swimming assay: swimming motility is mediated by flagellar rotation; to observe this type of motility first of all KF707 W.T., deletion mutants and complementation strains were streaked on LB plates, with the appropriate antibiotics and were grown overnight at 30°C. The next day, a single colony, for each strains, was inoculated in 10 mL of LB, in 50 mL flasks, and grown at 30°C and at 130 rpm for 16-18 hours. These cultures were later used to inoculate (2%) 10 mL of new LB, in 50 mL flasks; in these cases cells were grown until exponential phase, with $OD_{600\text{ nm}}$ around 0.5-0.6, and 1 mL of these preparation was collected, centrifuged for 5 minutes at 13.000 rpm at room temperature, and suspended at the same OD in 0.9% saline. Finally, 10 μ L of each suspension were spotted in the middle of the appropriate swimming plate, and incubated at 30°C for 24 hours. At the end the motility was qualitatively examined by measuring the swimming haloes formed, around the initial inoculum, by the bacterial cells.

- Preparation of swimming plates: pH 7.0, NaCl [5 g/L], Triptone [10 g/L] and Difco Bacto Agar [0.3% w/v], plate diameter of 8.8 cm.

Swarming assay: swarming is an organized translocation, is the capacity of bacterial cells to spread over the agar surface [Harshey, 2003]; to analyze these type of “movement”, also in this case KF707 W.T., deletion mutants and complementation strains were streaked on LB plates containing the specific antibiotics, and they were grown, overnight at 30°C. Later, like for the swimming assays, these cultures were used to inoculate (2%) 10 mL of swarming liquid media, in 50 mL flasks; in these case cells were grown overnight at 30°C at 130 rpm, and, the day after, a single drop of each culture, was spotted in the middle of a swarming plate. Finally, plates were incubated for one week at 30°C and swarming areas were measured.

- Preparation of swarming plate and liquid medium: pH 7.0, K_2HPO_4 [0.01% w/v], NaCl [0.01% w/v], $MgSO_4 (7 H_2O)$ [0.02% w/v], KH_2PO_4 [0.04% w/v], Yeast extract [0.4% w/v], carbon source (glucose or sucrose) [0.5% w/v] and, only for plates, Difco Bacto Agar [0.7% w/v].

1.3 Results

1.3.1 KF707 *cheA* genes complemented strains

KFcheA1::Km mutant was obtained in a previous work [Tremaroli et al., 2011] by using a KF707 mutant library generated by random mutagenesis with the miniTn5-*lacZ1* transposon (Km^r) while, the KF707 deletion mutant strains for *cheA2* and *cheA3* genes, were obtained by using Gene SOEing PCR technique and conjugation protocol during Triscari-Barberi PhD work (2013).

Here, in KF707 deleted mutants the wild type genotype was restored by using pSEVA342 or pSEVA532 vectors. The three genes were initially amplified, with High Fidelity Taq Polymerase (Figure 1.5), and then they were directly cloned by using TOPO TA cloning kit (Invitrogen). Subsequently *cheA1*, *cheA2* and *cheA3* genes were excised from the plasmid with specific restriction enzymes and cloned into pSEVA plasmids.

Finally, the recombinant pSEVA plasmids were used, with helper strain *E. coli* HB101 for conjugation protocol, in order to restore in each deletion mutant strain the initial genotype, adding one or two plasmids according to the number of deleted genes. All the KF707 complemented strains obtained are listed in Table 1.5, in which the conjugation mixes used are also described. To confirm the correct complementation, strains were examined with Colony PCR and DNA sequencing analysis.

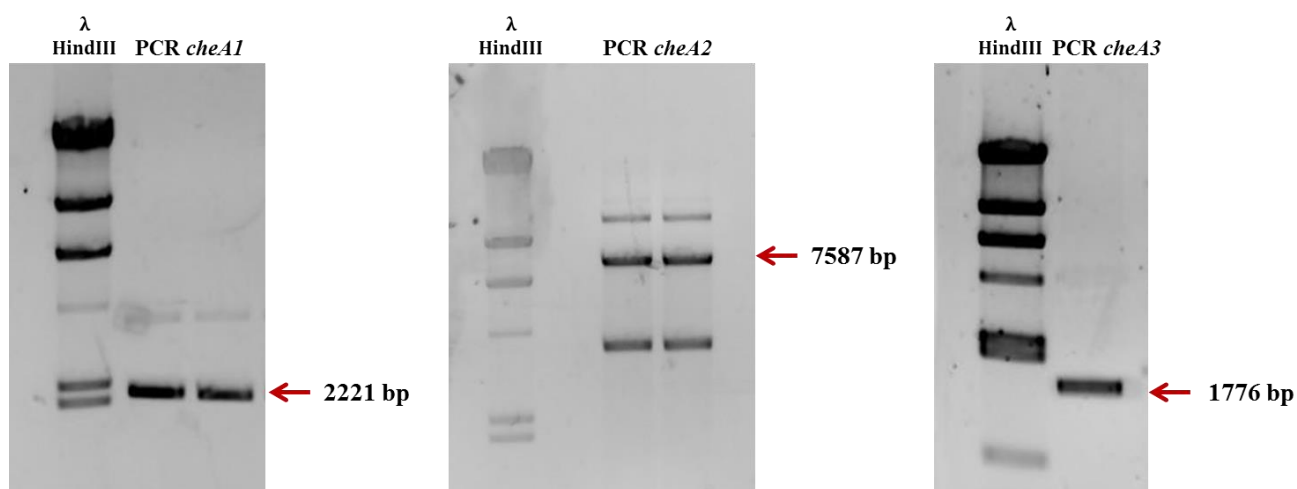
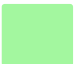
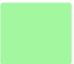
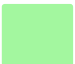
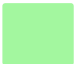
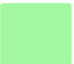
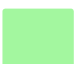


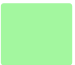



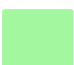

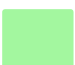

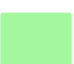
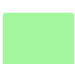
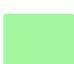
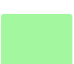
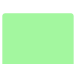
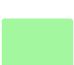
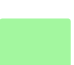




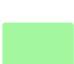

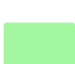
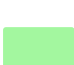
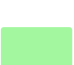

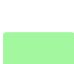

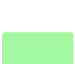
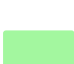
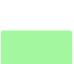
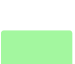


Figure 1.5: Amplifications of *cheA* wild type genes. These genes were amplified using High Fidelity Taq Polymerase in order to obtain the perfect amplification of the three genes: *cheA1* 2221 bp, *cheA2* 7587 bp and *cheA3* 1776 bp.

Table 1.5: List of KF707 complemented mutant strains obtained using conjugation protocol. The table shows the name of the mutant, the deleted proteins and the conjugation mix used.

Mutant strain	cheA genes			Conjugation mix
	cheA1	cheA2	cheA3	
KFcheA1::Km+cheA1				D: <i>E. coli</i> DH5α pSEVA342cheA1 R: KFcheA1::Km H: <i>E. coli</i> HB101 pRK2013
KFcheA1::Km+cheA1				D: <i>E. coli</i> DH5α pSEVA532cheA1 R: KFcheA1::Km H: <i>E. coli</i> HB101 pRK2013
KFΔcheA2+cheA2				D: <i>E. coli</i> DH5α pSEVA342cheA2 R: KFΔcheA2 H: <i>E. coli</i> HB101 pRK2013
KFΔcheA3+cheA3				D: <i>E. coli</i> DH5α pSEVA532cheA3 R: KFΔcheA3 H: <i>E. coli</i> HB101 pRK2013
KFcheA1::Km/ΔcheA2+cheA1				D: <i>E. coli</i> DH5α pSEVA532cheA1 R: KFcheA1::Km/ΔcheA2 H: <i>E. coli</i> HB101 pRK2013
KFcheA1::Km/ΔcheA2+cheA2				D: <i>E. coli</i> DH5α pSEVA342cheA2 R: KFcheA1::Km/ΔcheA2 H: <i>E. coli</i> HB101 pRK2013
KFcheA1::Km/ΔcheA2+cheA1+cheA2				D: <i>E. coli</i> DH5α pSEVA532cheA1 R: KFcheA1::Km/ΔcheA2+cheA2 H: <i>E. coli</i> HB101 pRK2013
KFcheA1::Km/ΔcheA3+cheA1				D: <i>E. coli</i> DH5α pSEVA342cheA1 R: KFcheA1::Km/ΔcheA3 H: <i>E. coli</i> HB101 pRK2013
KFcheA1::Km/ΔcheA3+cheA3				D: <i>E. coli</i> DH5α pSEVA532cheA3 R: KFcheA1::Km/ΔcheA3 H: <i>E. coli</i> HB101 pRK2013
KFcheA1::Km/ΔcheA3+cheA1+cheA3				D: <i>E. coli</i> DH5α pSEVA342cheA1 R: KFcheA1::Km/ΔcheA3+cheA3 H: <i>E. coli</i> HB101 pRK2013
KFΔcheA2/ΔcheA3+cheA2				D: <i>E. coli</i> DH5α pSEVA342cheA2 R: KFΔcheA2/ΔcheA3 H: <i>E. coli</i> HB101 pRK2013
KFΔcheA2/ΔcheA3+cheA3				D: <i>E. coli</i> DH5α pSEVA532cheA3 R: KFΔcheA2/ΔcheA3 H: <i>E. coli</i> HB101 pRK2013
KFΔcheA2/ΔcheA3+cheA2+cheA3				D: <i>E. coli</i> DH5α pSEVA342cheA2 R: KFΔcheA2/ΔcheA3+cheA3 H: <i>E. coli</i> HB101 pRK2013

Green squares indicate the cheA genes present, red one indicate the eliminated one.

In the mix: R = receiver, D = donor and H = helper.

1.3.2 Swimming motility assay

The ability of swimming type motility was analyzed, for KF707 *cheA* deletion mutants or *cheA* trans conjugant strains, on plates containing the appropriate growth medium with only 0.3% w/v of Difco Bacto Agar; bacteria were grown at 30°C for 24 hours.

As shown in Figure 1.6, observing the haloes that were formed in each plates, it was possible to prove that only *cheA1* seems to be necessary and involved in this type of motility, in fact, *cheA2* or *cheA3* mutant showed a phenotype similar to that of KF707 W.T. strain. In addition, analyzing the KF707 complemented strains plates, with the *cheA1* gene product the wild type phenotype was immediately restored (Figure 1.6).

Swimming plates

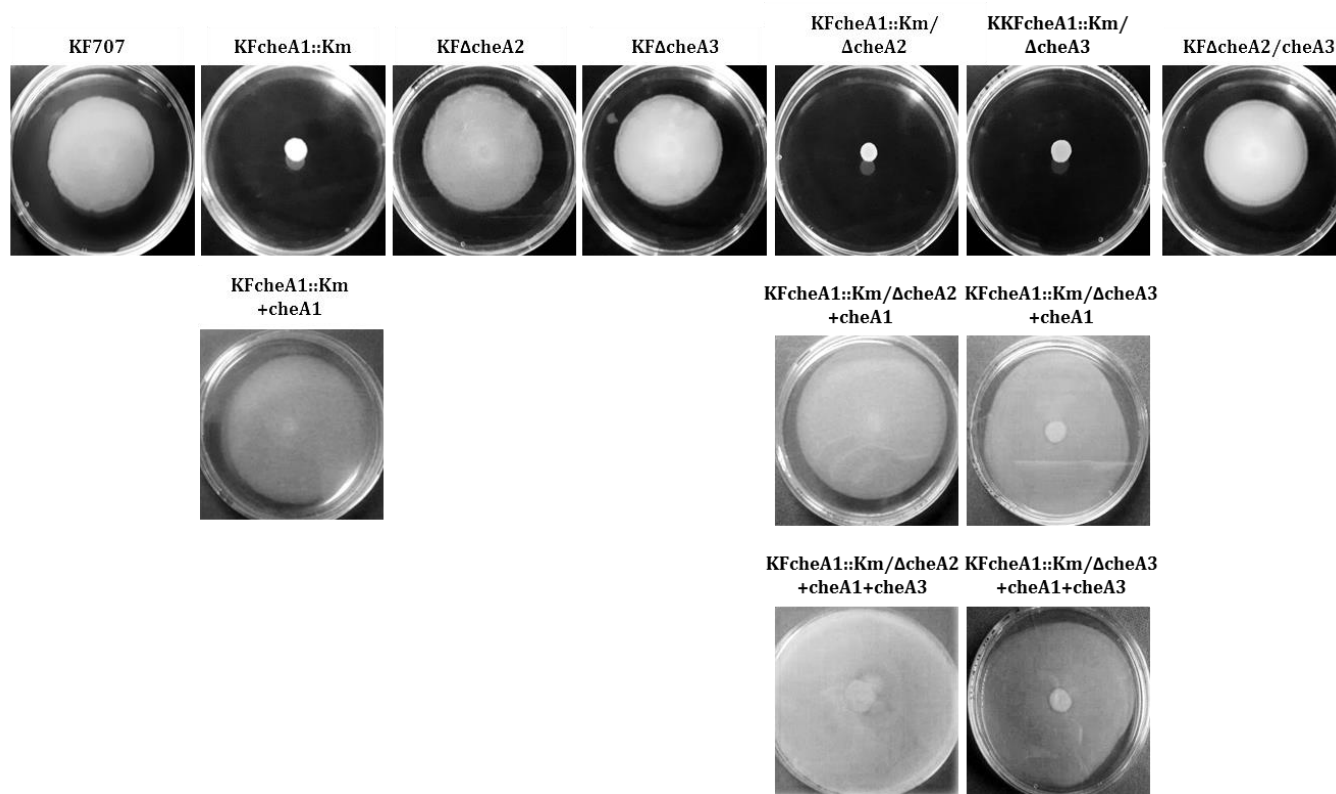


Figure 1.6: Swimming phenotype of KF707 W.T., single and double deletion *cheA* mutants, single and double complemented mutants. The swimming haloes were determined after 24 hours of incubation.

1.3.3 Swarming motility assay

Swarming assays were performed with the specific medium, containing 0.7% w/v of Difco Bacto Agar; 2 μ L of cells were spotted, after overnight growth in liquid swarming medium, in the middle of the plates and then they were incubated at 30°C for seven days. In these case the swarming motility does not appear as a turbid ring zone around the inoculum, but as ramifications that arise from the drop at the center of the plate; the extent of the ramification was measured in order to obtain a quantitative data and compare the different mutant strains.

Figure 1.7A and B show that in the cases of *cheA1* and/or *cheA2* KF707 deletion mutant strains, there is a significant reduction of the swarming area, compared to the W.T. strain. These results suggested that the deletion of only *cheA1* and/or *cheA2* genes influenced negatively swarming motility. On the contrary, the addition of *cheA3* deletion, in *cheA1::Km* and *cheA2* mutants, results in a significant increase in the swarming diameter compared to the single mutants. Conversely, the increase that had been observed in the single $KF\Delta cheA3$ mutant did not appear to be significant (Figures 1.7A and 1.7B). This phenomenon suggests that the deletion of the single *cheA3* gene may not be sufficient to induce a significant increase in the swarming area due to the interactions between the CheA proteins and the interference of other unknown factors such as cyclic GMP, c-AMP and quorum sensing signals [O'Toole and Kolter, 1998; Luo et al., 2015].

As shown in Figure 1.8, the transconjugant strains, in which the genotype was completely or partially restored by using pSEVA vectors, the *cheA1* gene product partially complemented the swarming motility in all *cheA1::Km* mutant strains. Also, with the introduction of *cheA2* gene, the phenotype resulted partially complemented in $KF\Delta cheA2$, $KFcheA1::Km/\Delta cheA2$ and $KF\Delta cheA2/cheA3$ mutants. Finally, with the addition of the restoration of *cheA3*, the wild type phenotype was completely recovered in double deletion mutant strains and the swarming diameter decreased; on the contrary, the production of only the CheA3 protein in double mutant strains did not restore the wild type phenotype. These analyses taken together demonstrated that CheA1 and CheA2 proteins play a direct and specific role in the motility behavior, while CheA3 may interacts with the other two proteins affecting negatively the swarming motility.

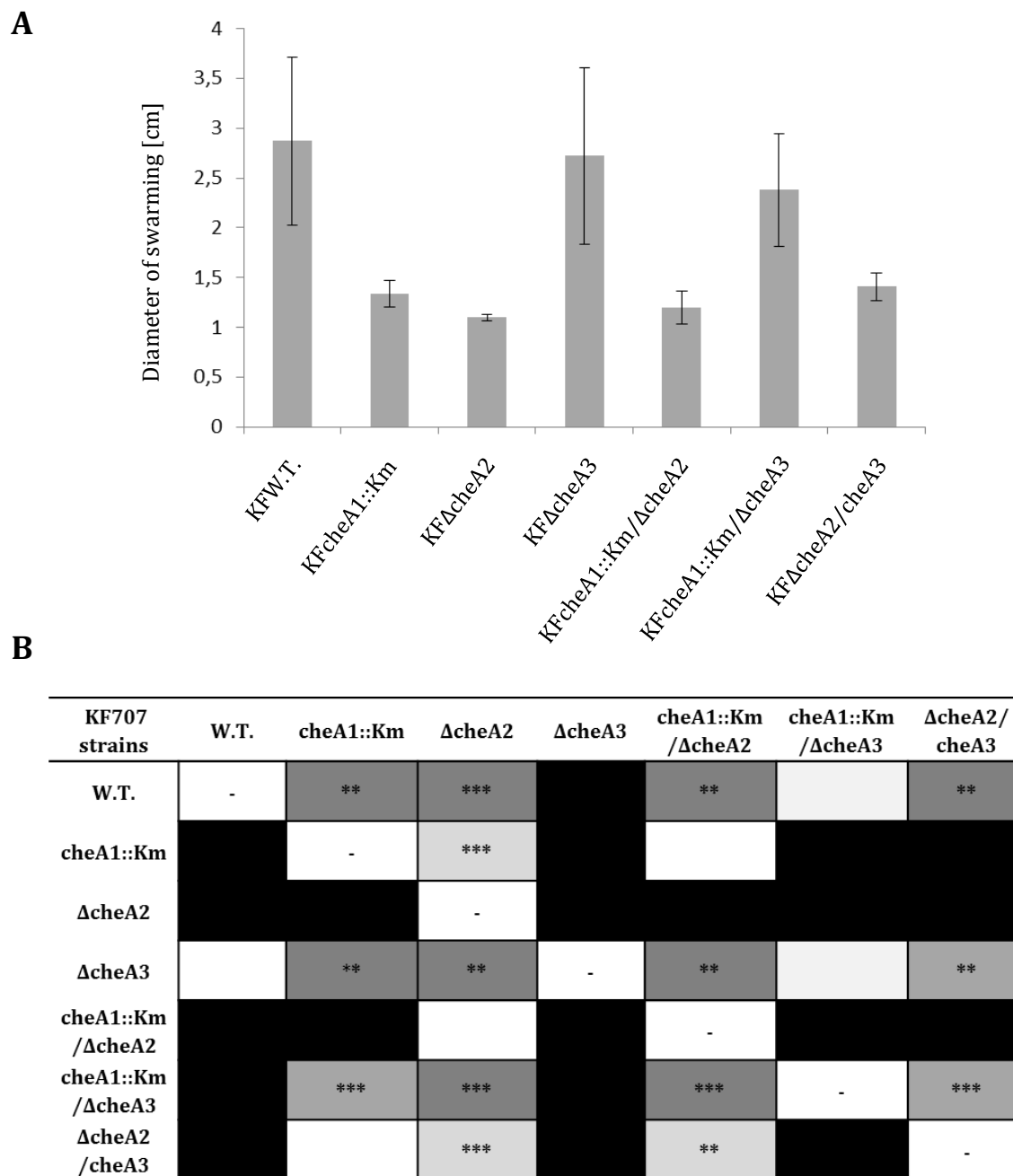


Figure 1.7: Swarming abilities of KF707 W.T. and *cheA* mutant strains. **A)** The diameters of swarming areas and the standard deviations measured after seven days are reported (growth on swarming medium plates with sucrose as carbon source, agar [0.7% w/v], plates diameter 8.8 cm). **B)** A reduction in the swarming diameter is expressed as percentage. The colors represent four ranges of diameter reduction percentages: white, 0-25%; light gray, 25-50%; medium gray 50-75% and dark gray 75-100%. The black color represents a percentage value indicating an increase in diameter instead of a reduction. A one-way ANOVA was performed to test the null hypothesis that there were no significant differences in the mean of swarming diameters of the seven strains, followed by Tukey's post-hoc test. The obtained results were verified by performing a two-sample *T*-test within pairs of strains. ** $p < 0.01$; *** $p < 0.001$. Results reflect five experimental replicates for each strain.

Swarming plates

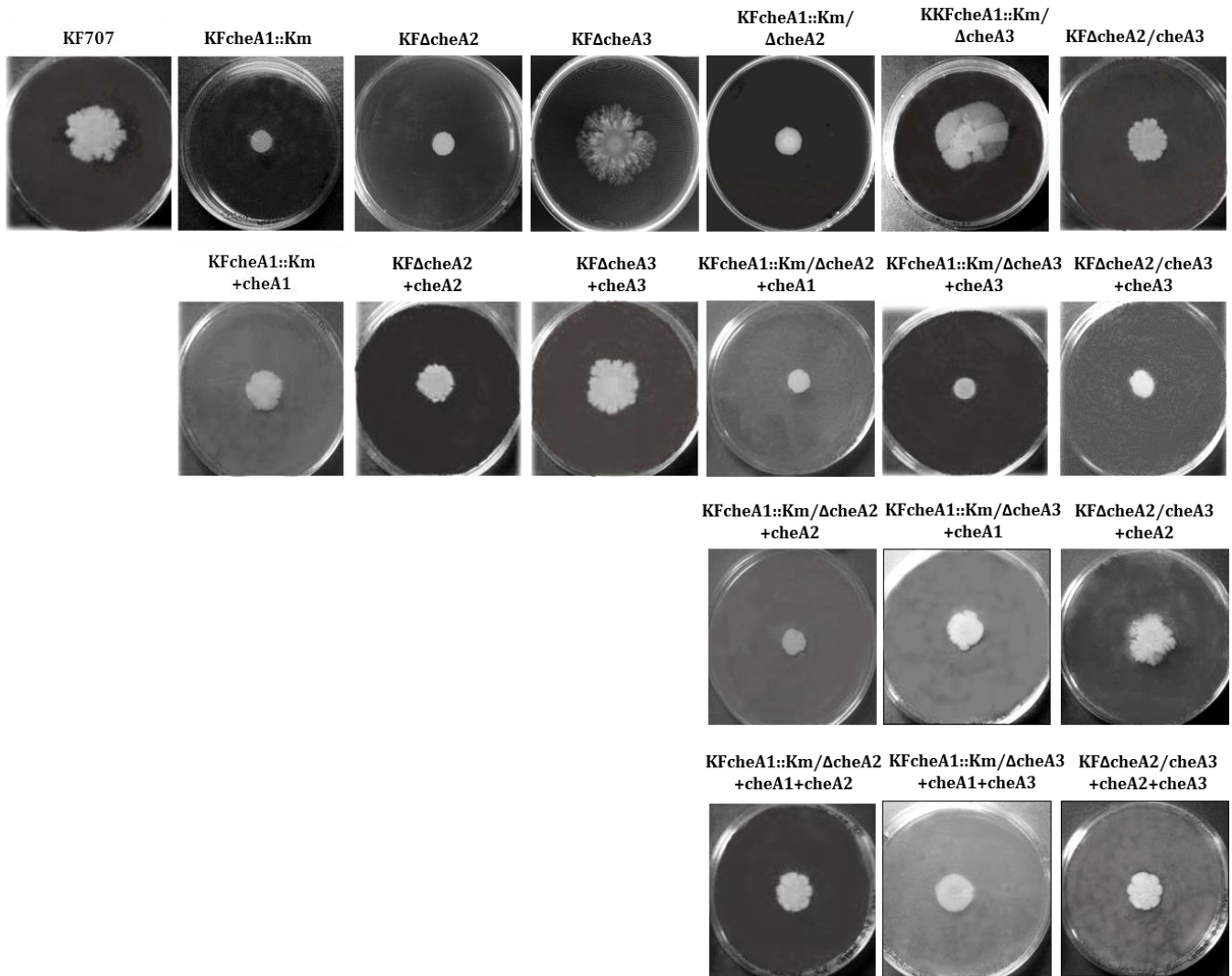


Figure 1.8: Swarming phenotypes of KF707 W.T., single and double deletion *cheA* mutants, single and double complemented mutants. The swarming areas were measured after a seven days incubation.

1.4 Discussion

The results obtained from swimming and swarming analyses suggest that in KF707 strain, multiple factors determine the motility phenotypes, which may play different roles depending on the environmental conditions.

In particular, the **swimming motility** analysis showed that only the *cheA1* gene is involved in this mechanism, while *cheA2* and *cheA3* genes do not influence the swimming motility.

This was also confirmed by the double mutant strains, KF7*cheA1*::Km/ Δ *cheA2* and KF*cheA1*::Km/ Δ *cheA3*, that do not show any swimming haloes, while the KF Δ *cheA2/cheA3* strain motility phenotype is the same of the KF707 W.T. Additional confirmations were obtained from the KF707 complementation mutants. In particular, in KF707 mutant strains, the restoration of the *cheA1* gene led to the recovery of the swimming-type motility.

Concerning the **swarming motility** of KF707, the gene *cheA2* plays an important role, since its deletion determines the absence of motility and of ramifications. In addition, in this latter case, the *cheA1* gene deletion also affects motility, while the lack of *cheA3*, in the presence of the other two genes, leads to an increase of swarming motility as compared to KF707 W.T. Apparently, it seems that *cheA3* gene has a negative effect on the other two gene clusters since, in the case of single *cheA1* and/or *cheA2* mutations, the presence of only one of these two proteins in association with the CheA3, generates alterations in the swarming phenotype. The potential negative effect of the *cheA3* gene has also been observed in previous studies, where it is reported that the overexpression in *E. coli* of the *P. aeruginosa* PAO1 genes *cheA2* and *cheW2*, homologous of the *cheA3* and *cheW3* genes in KF707, inhibits the chemotactic response [Kato et al., 2008]. Based on these results and according to the findings obtained in *P. aeruginosa* PAO1, CheA3 activity is likely to modulate KF707's swarming motility.

As reported in the past, swarming motility is a very complex system in which several proteins and regulators are involved. Previous studies have shown that swarming motility is also governed by a hierarchical secondary-messengers cascade including cyclic di-GMP, c-AMP, biosurfactants and quorum sensing signals [Kato et al., 2008; Lou et al., 2015]. Recently it has been observed in *P. aeruginosa*, that this type of motility is inhibited by

naphthalene degradation intermediates such as 1-naphtol [Oura et al., 2015]; in particular, this compound is also known as *mexAB* gene expression regulator and MexAB is an efflux pump involved in antibiotic resistance [Oura et al., 2015]. It is also known that, in *P. aeruginosa* PAO1, ChpA (KF707 CheA2 homologue) acts as a histidine kinase that regulates the two response regulators, PilG and PilH, using a phosphorylation mechanism. These two regulators are similar to CheY proteins (coded by *che1* and *che3* gene clusters) and lead to cAMP production mediated by cAMP cyclase activity. In turn, cAMP adjusts the motility of swarming through a signal cascade regulation [Lou et al., 2015].

Overall, the results obtained in this chapter have been useful in providing new knowledge about the motility of KF707 and to better understand the role of *cheA* genes in swimming and swarming motility.

Future studies will be required to understand how these three gene clusters interact with each other during the biofilm formation and how their expression is regulated under different growth conditions (different environmental conditions such as the presence of xenobiotic compounds or pH variation); this further results will help to improve the use of KF707 cells as a tool for bioremediation applications.

Chapter 2

Biphenyl modulates the expression and function of respiratory oxidases in the polychlorinated-biphenyls degrader

Pseudomonas pseudoalcaligenes KF707

This chapter is based on:

F. Sandri, S. Fedi, M. Cappelletti, F.M. Calabrese, R.J. Turner and D. Zannoni, Frontiers in Microbiology. Vol. 8 – 1223 (2017).

Background: The microbial aerobic respiration

Energy is a fundamental requirement for all living organisms [Lyons et al., 2016]. Bacteria transform the various forms of energy available from their environment in metabolic energy such as membrane electrochemical potential, ATP or reducing power [Dehò and Galli, 2015]. The metabolism includes a large variety of chemical reactions mediated by enzymes that belong to catabolism (degradative reactions) or to anabolism (biosynthetic reactions).

The variety of metabolic pathways in microorganisms is surprising; in fact, the ability to colonize extremely different environments depends on the bacterial ability to use a large number of compounds as carbon and energy sources. In all cases, energy metabolism is based on redox processes between electron donor pairs at low redox potential and electron acceptors at high potential [Dehò and Galli, 2015].

In order to obtain energy, all microorganisms must find in their environment, the source to produce adenosine-5'-triphosphate (ATP) (Figure 2.1), the molecule required for many but not all the cellular biosynthetic and mechanical processes since the membrane potential is an intermediate step in energy transduction. In animals, the energy used by cells derives from organic material, such as carbohydrates and while bacteria, do not strictly depend on organic sources for growth. Indeed, microorganisms possess a multitude of metabolic pathways that also include the use of inorganic molecules, since many bacteria are able to

drive CO₂ assimilation by light energy, while others need inorganic molecules such as elemental sulfur, nitrogen, or iron functioning as both electron donors and/or acceptors in respiratory processes. These latter features allow bacteria to survive in a variety of extreme habitats [Wessner et al., 2015].

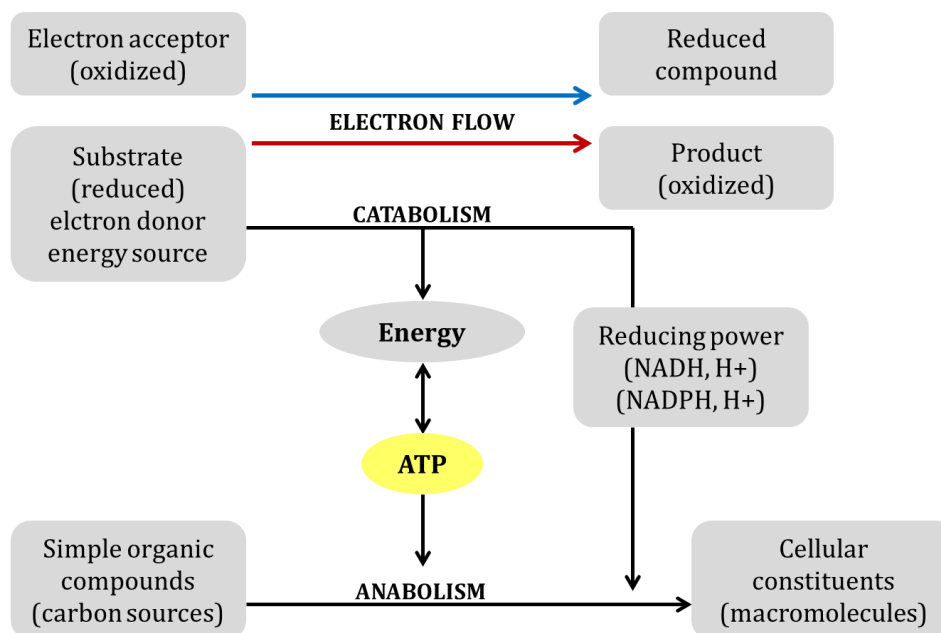


Figure 2.1: General scheme of cellular metabolism [Matheron and Caumette, 2011].

The aerobic respiration in bacteria

Some bacteria possess an exclusively aerobic or anaerobic metabolism, in this case the ATP required for survival is produced through a process called phosphorylation which is linked to the electron transfer chain (also called “**respiratory chain**”). This is the mechanism of ATP formation throughout aerobic or anaerobic respiration (oxidative phosphorylation) [Matheron and Caumette, 2011].

In prokaryotic microorganisms, the respiratory metabolism is different from that of eukaryotic organisms. In order to adapt to different environmental conditions, microbes developed an enormous variety of electron transport chains [Hernandez and Newman, 2001]. Bacteria are able to utilize multiple electron donors and acceptors to provide the

respiratory flexibility required for the changes of the environmental niches in which they reside.

The respiratory flexibility in the mammalian mitochondrion is relatively poor, having limited options at the level of electron acceptor in cytochrome *c* oxidase (cytochrome *aa*₃-type), in plants mitochondria are slightly more flexible, where a number of alternative NADH dehydrogenase and two terminal oxidases permit respiratory functions beyond the synthesis of ATP. Instead, bacteria comprise multiple dehydrogenases, quinone electron carriers, a cytochrome *bc*₁ complex, and a range of quinol oxidases and reductase complexes that can reduce molecular oxygen and various inorganic electron acceptors (such as nitrate, sulfate, iron or manganese) (Figure 2.2). Depending on the growth conditions, different combinations of these complexes predominate, in addition to the individual components often being expressed in response to specific environmental stimuli. This flexibility explains why bacterial respiratory chains are often described as being branched, modular and inducible.

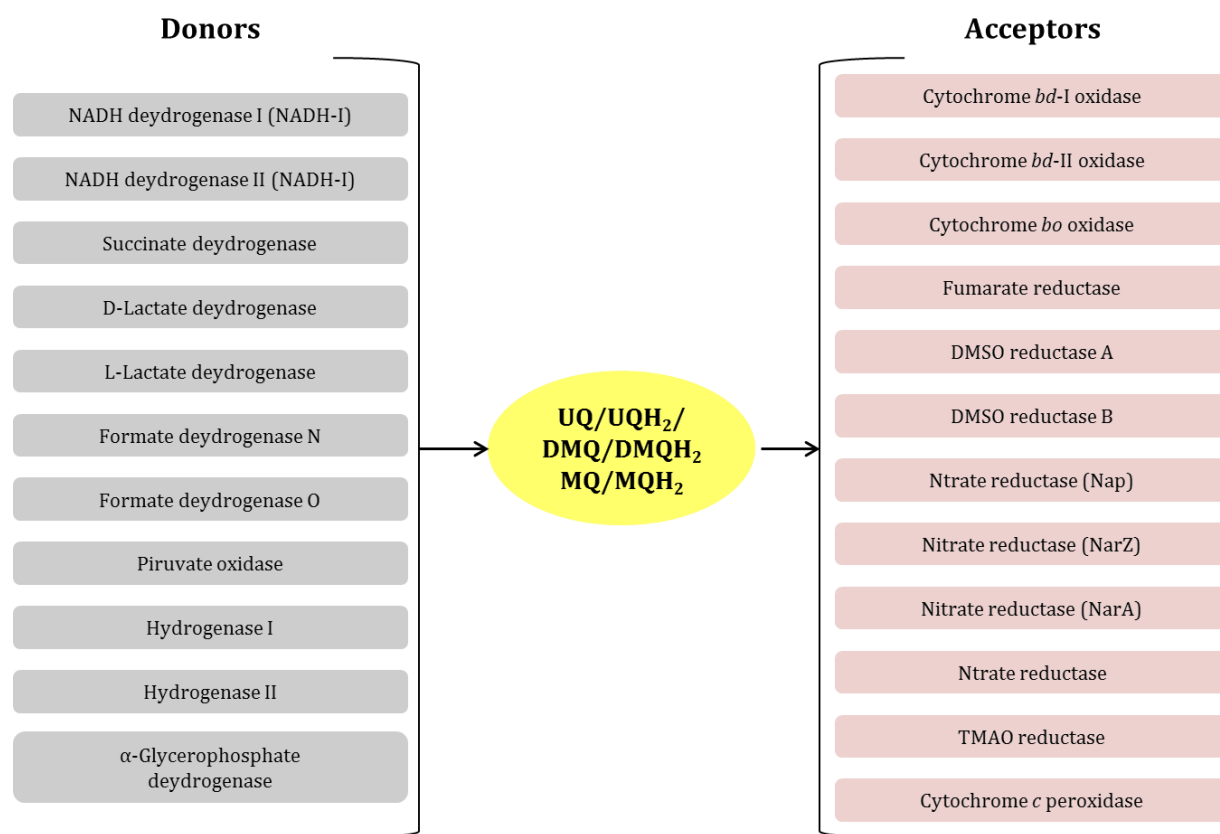


Figure 2.2: Respiratory flexibility in *Escherichia coli*. UQ ubiquinone, DMQ dimethylmenaquinone, MQ menaquinone [Gennis and Stewart, 1996; Richardson, 2000].

The electron transport chain

The electron transport chain (Figure 2.3) is the last step of cellular respiration and in bacteria it is (mainly) localized in the cytoplasmic membrane. It includes a series of redox carriers divided into two categories: electron and proton carriers (flavoproteins and quinones) and electron carriers only (protein Fe/S and cytochromes).

The oxidation reactions are different according to the transporter involved and the prosthetic group that it contains. The chain components are composed by a series of different carriers, namely; there are proteins containing one or two prosthetic groups, such as haem(s) in cytochromes or non-haem in iron-sulfur proteins, and relatively small molecules, like quinones. The type of molecules involved in these oxidoreduction reactions and their interaction in the electrons transport chain, result in a transfer of protons from the inside to the outside of the cell through the cytoplasmic membrane. Because plasma membrane is impermeable to protons this proton efflux determines the formation of a proton gradient called proton-motive force, **ATP synthesis** takes place when protons, which are concentrated outside the membrane (that is the periplasmic space of Gram-negative bacteria), return into the cell by means of the F_0F_1 -ATP synthase complex.

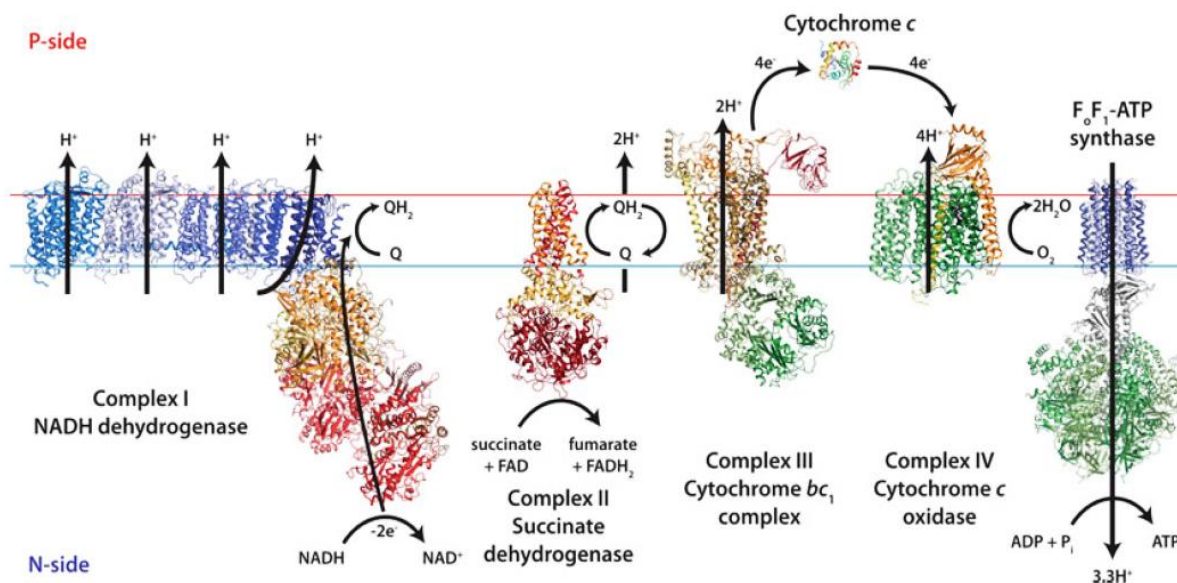


Figure 2.3: The electron transport chain. Complex I – NADH dehydrogenase *Thermus thermophilus*, Complex II – Succinate dehydrogenase *Escherichia coli*, Complex III – Cytochrome bc_1 complex *Saccharomyces cerevisiae*, Complex IV – Cytochrome c oxidase *Paracoccus denitrificans* and F_0F_1 ATP synthase [Lyons et al., 2016].

The four major complexes that form the redox chain are: NADH:quinone reductase (Complex I), succinate:quinone reductase (Complex II), Cytochrome *bc*₁ complex (Complex III) and Cytochrome *c* oxidase (Complex IV) (Figure 2.3).

NADH + Q_(ox) → Complex I → NAD⁺ + Q_(red)

The electrons transport pathway starts with the Complex I also called NADH dehydrogenase, which is the largest redox complex in the respiratory chain and consists of various flavoproteins and a non-haem iron-sulfur center. In this step, two protons and two electrons are transferred by oxidizing NADH to NAD⁺-H⁺ in parallel to reduction of the quinone pool to quinol (QH₂). Quinones are lipid-soluble molecules that reside in the inner membrane transferring electrons and protons between various respiratory complexes. Bacterial species use different types of quinones having mid-point redox potentials which respond to various ambient redox poise (aerobic or anaerobic). During this process, protons move across the plasma membrane to generate the proton-motive force which is necessary for ATP synthesis [Lyons et al., 2016].

FADH₂ + Q_(ox) → Complex II → FAD⁺ + Q_(red)

The second complex of the respiratory chain is the succinate:quinone reductase, or succinate dehydrogenase. This linear transmembrane enzyme reduces quinone molecules to quinols and catalyzes the transfer of two electrons from succinate, via FADH₂ [Roy and Lancaster, 2002]. This complex is known as the only membrane bound component that also participates in the Krebs cycle [Cecchini, 2003]. Unlike Complex I, this enzyme is unable to translocate protons across the membrane.

Q_(red) + cyt *c*_(ox) → Complex III → Q_(ox) + cyt *c*_(red)

The cytochrome *bc*₁ complex is the most common transfer complex, and it has been isolated from Gram-negative and Gram-positives, both aerobic and anaerobic bacteria [Trumpower, 1990]. Electrons arriving to Complex III move through two *b*-type haems, an iron-sulfur center and a cytochrome *c*, then they are transferred to a specific (soluble) cytochrome *c* located on the outer side of the membrane [Crofts, 2004]. The structure of this enzyme can be divided into three regions: the membrane spanning, the inter-membrane space (periplasm), and the matrix (cytoplasm) regions.



Complex IV is a member of the Haem Copper Oxidase (HCO) superfamily. It catalyzes the four-electron reduction of dioxygen to water and uses the released free energy to translocate protons across the periplasmic membrane, and for this reason it contributes to the increase of the proton-motive force production [Ferguson-Miller and Babcock, 1996].

It should also be underline that bacterial species use a variety of electron donors and acceptors for respiration along with more complex and flexible Electron Transport Systems (ETS) than eukaryotic organisms. Microorganisms can modify their ETS by activating or deactivating specific proteins and/or cofactors in response to environmental conditions a phenomenon which has specifically been faced in the present experimental work.

The terminal oxidase enzymes

The terminal oxidases are the terminal enzymes of the respiratory electron transport chain that catalyze the four-electron reduction of dioxygen to water by means of the following reaction:

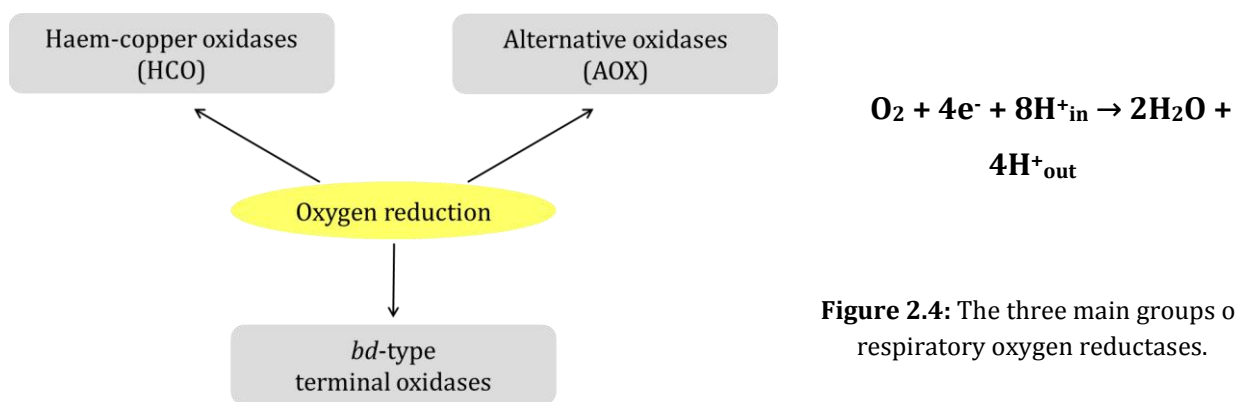


Figure 2.4: The three main groups of respiratory oxygen reductases.

In particular, these enzymes can be divided into three families (Figure 2.4):

Haem-copper superfamily (HCO): they are the most common oxidases in bacteria, the subunit I is highly conserved and it contains a high-spin haem copper binuclear center responsible for the oxygen reduction. These enzymes are phylogenetically closer to the mitochondrial oxidases found in eukaryotic cells [Pitcher and Watmough, 2004].

Alternative oxidase family (AOX): these enzymes have been found in mitochondria of plants, fungi and protists [Albury et al., 2009], and include cyanide-resistant proteins. They do not translocate protons across the membrane and therefore they do not generate proton motive force.

bd-type terminal oxidases: they are present in several microorganisms and they function as quinol oxidases; these enzymes do not show sequence homologies to any HCO or AOX and do not contain the haem-copper binuclear center. *bd* oxidases generate a membrane potential by means of the transmembrane charge separation [Borisov et al., 2011].

The haem-copper oxidases (HCO)

Most of the terminal oxidases are haem copper oxidases, and use cytochrome *c* as the electron donor (Figure 2.5). Enzymes belonging to this group have a rich diversity in substrates, prosthetic groups, haem-types, subunits composition and in amino acid sequences of D- and K- pathways [Pereira et al., 2001, 2008; Sousa et al., 2012]. Members of the HCO superfamily are characterized by the presence, in the conserved subunit I, of the high-spin copper-binuclear catalytic center, named Cu_B , and a low-spin haem. Some HCO enzymes contain, in their subunit II, an additional copper center (Cu_A) that transfers electrons between cytochrome *c* and the low-spin haem [Lyons et al., 2016].

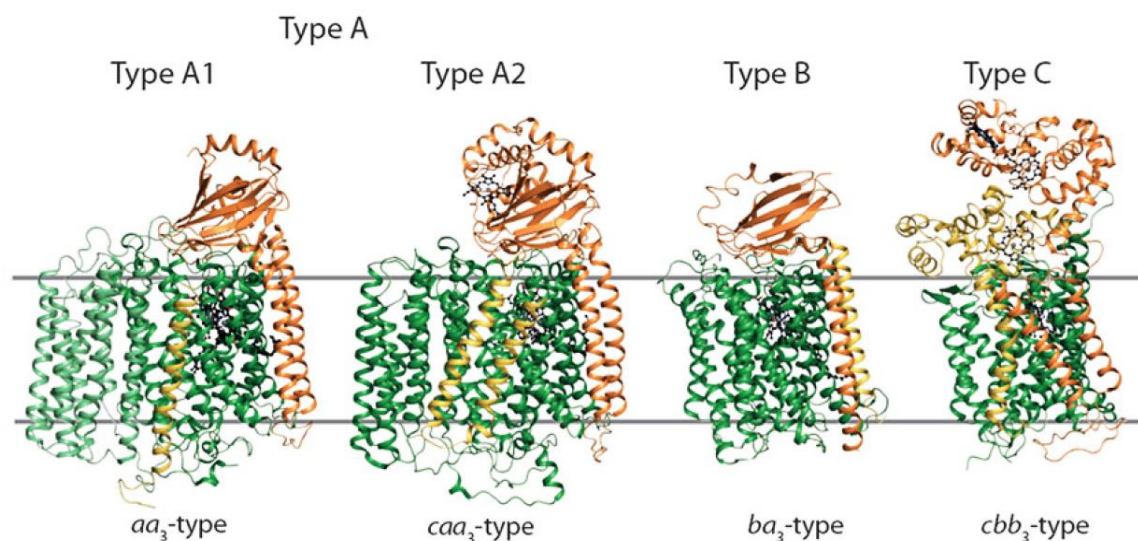


Figure 2.5: Models of different HCO types: Type A1 *aa*₃ protein; Type A2 *caa*₃; Type B *ba*₃ and Type C *cbb*₃. Proteins are displayed as ribbons with subunit I-IV colored in green, orange, light green and yellow, respectively [Lyons et al., 2016].

HCO superfamily is divided into three categories (Figure 2.5): Type A, B and C, based on amino acid sequence and the conservation degree of the D- and K- proton pathways. These pathways are essential for the oxygen reactions, and through these pathways protons and oxygen can reach the binuclear center and water can be released. The name of the D-pathway is related to the conserved aspartate present at the entrance of the pathway, while the K-pathway is named in this way for the centrally located lysine residue.

- ✓ **Type A:** it includes the mitochondrial and many bacterial cytochrome *c* oxidases. This type is divided into two subclasses, A1 and A2, on the basis of the amino acid composition at the end of the D-pathway. Type A1 contains, on the helix IV, a highly conserved glutamate in the sequence motif – XGHPEV –, while in Type A2 the glutamate is replaced by a consecutive tyrosine and serine (YS) in – YSHPXV – motif [Pereira et al., 1999].
- ✓ **Type B:** are a particular type of oxidases found in archaea and in some bacteria such as *Thermus thermophilus*. These enzymes don't have a canonical D- and K-pathways but they present an alternative K-pathway situated in the subunit I. These oxidases are peculiar, in fact they don't show sequence homology with Type A or Type C enzymes [Lyons et al., 2012 and 2016].
- ✓ **Type C:** *cbh₃*-type oxidases are found exclusively in Proteobacteria and they probably are the oldest member of the HCO superfamily and comprise ~20% of HCOs. Type C represents a distinctive class of proton-pumping respiratory HCO; the structure of these enzymes diverges from Type A and B because they contain an extra subunit that is involved in the electron transport [Pitcher and Watmough, 2004]. These oxidases are supposed to be originated from a NO reductase, in fact this subfamily of enzymes can also reduce NO to N₂O. They are characterized by reduced proton pumping and by a higher catalytic activity at low oxygen concentrations (Michaelis constant K_M for O₂ is around 7 nM and is 6-8 times lower than that determined for Type A); for this reasons, their expression is required for the successful colonization of virtually anoxic habitats and they also have a role in bacterial pathogenicity.

For all of these types of enzymes, the crystal structure is available and the three canonical subunits consist of (Figure 2.6 and 2.7):

Subunit I (SU I): it is conserved in all three families and is composed of 12 transmembrane helices. This is the most important subunit and contains the low-spin, the high-spin haem and the copper ion center Cu_B , these components together constitute the enzyme's active site; they are situated in the hydrophobic core of the protein, near the periplasmic side of the membrane [Iwata et al., 1995; Verkhovsky et al., 1999]. In Type A and Type C oxidases there is, situated at the interface between SU I and SU II, a functionally relevant non-redox active metal center, Mg^{2+} and Mn^{2+} in Type A, Ca^{2+} in Type C.

Subunit II (SU II): in Type A and Type B, it is composed by two N-terminal transmembrane helices associated to a cupredoxin domain located in the periplasm; this latter domain contains an additional copper center Cu_A , that acts as a primary electron acceptor. In addition, some Type A enzymes include a C-terminally fused cytochrome *c* domain. Type C oxidases do not have the binuclear copper center Cu_A in the SU II; in these proteins, the redox center is situated in two accessory subunits (CcoP and CcoO). CcoO is a single transmembrane helix containing a soluble cytochrome *c* domain, while CcoP is composed by a pair of N-terminal transmembrane helices, connected with a globular domain that harbors two cytochrome *c* domains.

Subunit III (SU III): this domain was identified only in Type A enzymes and comprises seven transmembrane helices. Its role is not very clear but it is known that the deletion of this subunit leads to a suicide inactivation of the enzyme [Bratton et al., 1999; Hosler, 2004]; in addition, its presence is important for the correct efficiency of the proton flow through the D-pathway [Mills and Hosler, 2005].

The simultaneous presence of enzymes belonging to different HCO types, in the same strain, indicates the high capacity that microorganisms have to respond, by modulating the activation of different respiratory chain's enzymes, to external environmental stimuli.

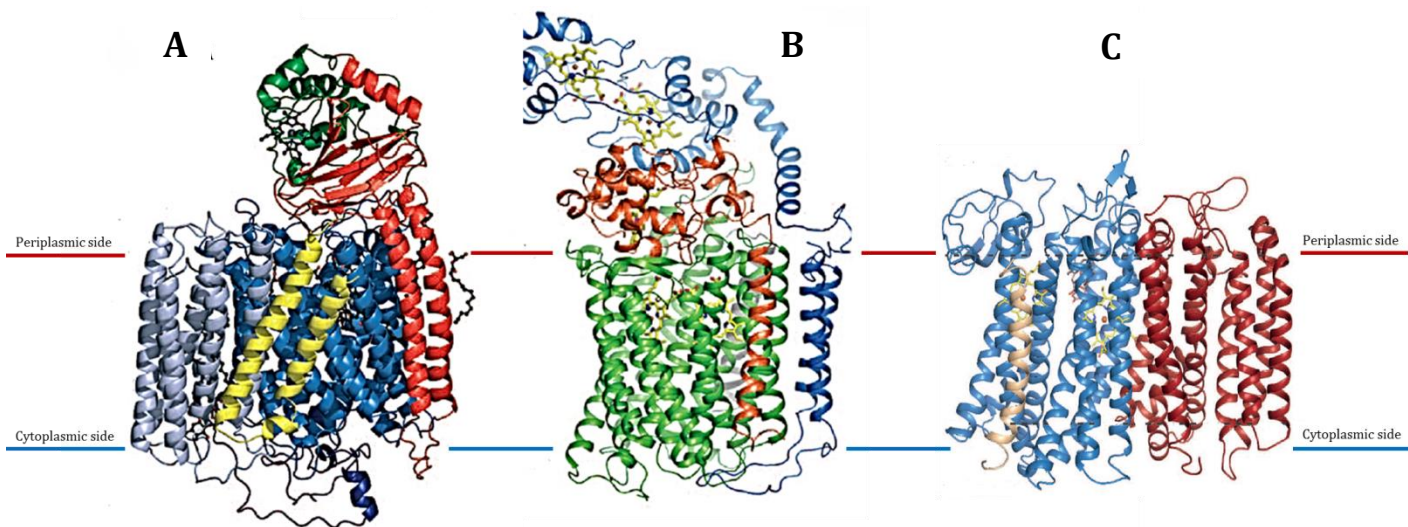


Figure 2.6: **A)** Structure of *Thermus thermophilus caa₃* oxidase. Subunit I/III are blue and grey respectively, and the fusion linker is dark blue, subunit II in red and the fused cytochrome *c* domain in green, subunit IV in yellow. The haems are in balls and sticks with the iron and copper metal centers as grey and copper spheres, respectively [Lyons et al., 2012]. **B)** Structure of *Pseudomonas stutzeri Cbb₃* oxidase. The multisubunit complex consists of subunits CcoN in green, CcoO in red and CcoP in blue. An additional transmembrane helix (gray) could be detected as subunit Q. The haems are shown as sticks; iron and copper as spheres [Buschmann et al., 2010]. **C)** Structure of *Geobacillus thermodenitrificans bd* oxidase subunits CydA in blue, CydB in red, and CydS in beige [Safarian et al., 2016].

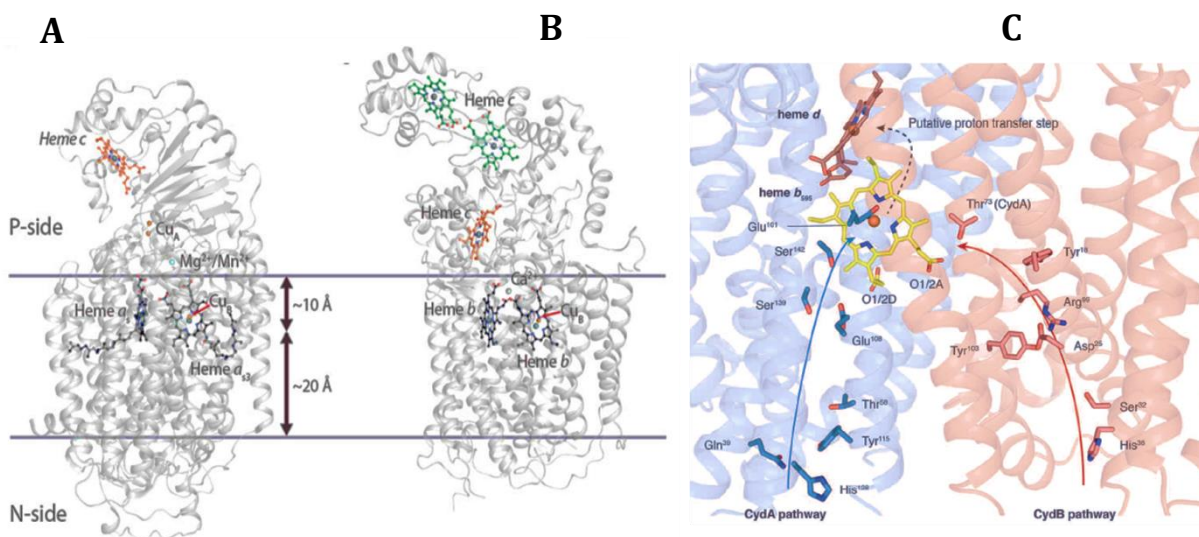


Figure 2.7: Architecture of Type A HCOs using *caa₃*-type oxidase **(A)** and architecture of Type C HCOs using *cbb₃*-type oxidase **(B)**; haems are displayed as balls and sticks with metal ions as spheres. The position of the metal centers relative to the sides of the membrane is indicated by *double headed arrows* [Lyons et al., 2016]. **C)** The potential proton transfer pathways in the *bd* oxidase [Safarian et al., 2016].

***bd*-type terminal oxidases**

The *bd*-type terminal oxidases constitute a large family of terminal oxidase enzymes present in bacteria. They are generally divided into two categories, the classic *bd*-type and the cyanide-insensitive oxidases (CIO); both of these enzymes use quinol as electron donor and they generally have a low sensitivity to cyanide [Borisov et al., 2011]. They are also characterized by a high affinity for oxygen that determines a protective role from oxidative stress [Edwards et al., 2000] and leads to the colonization of poor oxygen environments by pathogenic bacteria [Shi et al., 2005].

In *E. coli*, *bd*-type enzyme is composed by two subunits, CydA and CydB [Miller and Gennis, 1983] while, some Proteobacteria have an additional subunit consisting of a single helix. This type of enzyme contains, in the CydA subunit, a low-spin *b*₅₅₈ haem, a high-spin *b*₅₉₅ haem while an additional *d*-type haem is situated in CydB. In an orthodox *bd*-type enzyme, quinol interacts with a conserved hydrophilic region (Q-loop) connecting the 6th and 7th transmembrane helices situated in the extracellular portion of the protein. The *b*₅₅₈ haem acts as the primary electron acceptor then, electrons are transferred to the active site of the enzyme composed by *b*₅₉₅ and *d* haems. In this latter region, the oxygen reduction and the water formation take place [Borisov et al., 2011](Figure 2.6 and 2.7).

In the case of the *bd*-type cyanide insensitive oxidase (CIO) of *P. aeruginosa* PAO1, although the genes are homologous to those of *E. coli* enzyme (*cydAB*), the protein does not show the typical absorption spectra belonging to *b*₅₉₅ and *d* haems [Cunningham et al., 1997; Jackson et al., 2007]. In addition, comparing the two proteins, the conserved Q-loop sequence in the CioA subunit is shorter than that of CydA [Cunningham et al., 1997].

Usually, these enzymes are not essential for bacterial growth, in aerobic conditions [Winstedt and von Wachenfeldt, 2000], while *bd* oxidases are required for growth under copper starvation or in the presence of cyanide [Borisov et al., 2011].

2.1 Introduction

As described in the General Introduction paragraph, the bacterium *Pseudomonas pseudoalcaligenes* KF707, isolated in the 1980s near a biphenyl manufacturing plant in Japan [Furukawa and Miyazaki, 1986], is known as one of the most effective aerobic degraders of polychlorinated-biphenyls (PCBs) [Fedi et al., 2001]. Despite the fact that most of the biphenyl degradation enzymes required for PCBs degradation are expressed during the aerobic growth of KF707 [Furukawa et al., 1993], no report is available on the functional arrangement of KF707 respiratory chain with biphenyl as carbon source. Indeed, an early biochemical study was published, which aimed to define the effect of the toxic oxyanion tellurite on aerobic growth of KF707 in rich medium (LB) [Di Tomaso et al., 2002]. This work suggested the presence, in KF707, of a branched respiratory chain leading to two cytochrome *c* oxidases and one cyanide insensitive quinol oxidase (CIO) [Di Tomaso et al., 2002].

Since then, no other studies on function and composition of the respiratory redox chain of this aerobic PCBs degrader have been published. In the meantime, the expression and arrangement of the respiratory chains in species such as *P. putida* KT2440 and *P. aeruginosa* PAO1, were elucidated [Kawakami et al., 2010; Arai et al., 2011; Sevilla et al., 2013 1-2; Arai et al., 2014] (Figure 2.8).

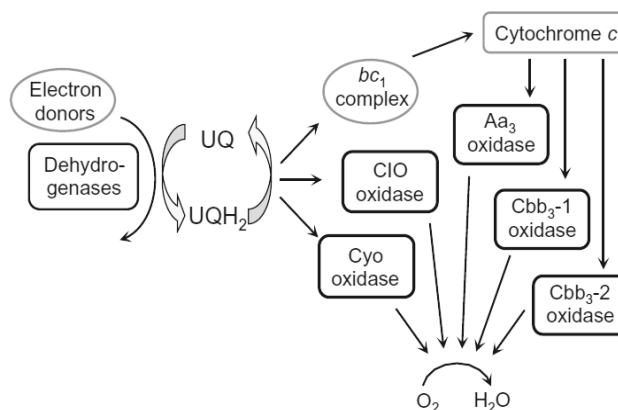


Figure 2.8: Model for the *P. putida* and *P. aeruginosa* PAO1 electron transport chain. Different reduced compounds move the electrons to the ubiquinone of the membrane cell (UQ), and then they flow to the *bc*₁ complex or to the Cyo or CIO terminal ubiquinol oxidases. Through *bc*₁ complex electrons arrive to the Aa₃, Cbb₃1 and Cbb₃2 terminal oxidases and are finally transferred to the oxygen [Ugidos et al., 2008; Arai, 2011; Sevilla et al., 2013 1-2].

In *P. aeruginosa* PAO1 strain, whose genome has a high homology with that of KF707, it was shown that there are five different terminal oxidases (Figure 2.8) that catalyze the four-electron reduction of molecular dioxygen to water [Cunningham and Williams, 1995; Cunningham et al., 1997; Stover et al., 2000; Comolli and Donohue, 2002, 2004]; the same situation was observed in *P. putida* KT2440, and also in this case **five terminal oxidases** were found in the genome [Ugidos et al., 2008]. Two of these enzymes, which receive electrons directly from ubiquinone, are considered quinol oxidases (CYO and CIO), while the remaining three protein complexes are cytochrome *c* oxidases (two *cbb*₃-type and one *aa*₃-type), receiving electrons from the cytochrome *bc*₁ complex and *c*-type cytochromes. The analysis of a differential expression of multiple terminal oxidases in *P. aeruginosa* PAO1 [Kawakami et al., 2010] demonstrated, through the construction of deletion mutant and *lacZ* transcriptional fusion strains, that each oxidase has a specific affinity for oxygen, efficiency in energy coupling, tolerance to various stresses and positively or negatively regulated by various transcriptional factors (Figure 2.9).

In particular, the *P. aeruginosa* PAO1 *aa*₃-type oxidase has low affinity for oxygen plays a major role during aerobic respiration [Poole and Cook, 2000]; this oxidase is expressed, primarily, under nutrient-limited conditions while it is otherwise a minor player under nutrient-rich growth conditions, e.g. LB [Kawakami et al., 2010]. The *aa*₃-type enzyme is inhibited by RoxSR and activated on a stationary phase by the sigma factor RpoS [Schuster et al., 2004; Kawakami et al., 2010]. In *P. aeruginosa* PAO1, the gene cluster coding for the *aa*₃-type oxidase contains three genes named *coxA*, *coxB* and *coxC*, respectively [Stover et al., 2000].

In contrast to *aa*₃-type, the two *cbb*₃-type oxidases (Cbb₃1 and Cbb₃2) are crucial when oxygen becomes limiting in bacterial strains such as *Par. denitrificans*, *R. sphaeroides* and *R. capsulatus* [Mouncey and Kaplan, 1998; Swem and Bauer, 2002]; in fact, this type of enzymes are characterized by high affinity for oxygen and low proton-translocation efficiency. Both of them are activated by RoxSR regulator whereas ANR factor, is involved in the expression of Cbb₃2 when the oxygen concentration is low [Comolli and Donohue, 2004; Kawakami et al., 2010]. These two enzymes are, in most cases, tandemly clustered, including *P. aeruginosa* PAO1 strain; each cluster is composed by four different genes: *ccoN*, *ccoO*, *ccoQ* and *ccoP*. In *P. aeruginosa* PAO1, Cbb₃1 oxidase is expressed constitutively, while

the Cbb₃2 is induced through oxygen limitation [Comolli and Donohue, 2004; Kawakami et al., 2010]. Notably, mutation of the *cco1* gene cluster coding for the Cbb₃1 oxidase causes up-regulation of the CIO promoter in *P. aeruginosa* PAO1 [Kawakami et al., 2010].

Regarding the quinol *bo*₃ oxidase, it is a haem-copper enzyme encoded by *cyoABCDE* gene cluster. The stationary phase of growth and the drop of oxygen concentration down-regulate its expression that, on the contrary, is stimulated by iron starvation; indeed the transcriptional regulator Fur (ferric uptake regulator that is known as DNA binding protein in the presence of Fe²⁺) represses this oxidase [Kawakami et al., 2010; Vasil, 2007]. Finally, the second quinol oxidase is a cyanide insensitive oxidase, a copper-free enzyme encoded by two genes *cioA* and *cioB* [Cunningham et al., 1997]. This oxidase is up-regulated by the presence of cyanide and by copper starvation [Frangipani et al., 2008]. In addition, in *P. aeruginosa* PAO1 it is known that this enzyme is usually expressed during stationary phase of growth or when the oxygen concentration decreases [Alvarez-Ortega and Harwood, 2007; Kawakami et al., 2010]; furthermore, it seems to be positively regulated by RoxSR and, in particular, by the deletion of Cbb₃1 oxidase [Comolli and Danohue, 2004].

In *P. putida*, which is also able to grow under semiaerobic or microaerobic conditions, there are five different terminal oxidase enzymes, like in *P. aeruginosa* PAO1; in this latter case, the only difference is that the Cbb₃1 oxidase is the equivalent of Cbb₃2 oxidase of *P. aeruginosa* PAO1 and vice versa for the Cbb₃2, which corresponds to Cbb₃1 of *P. aeruginosa* PAO1 [Ugidos et al., 2008]. All these enzymes are regulated and expressed in the most appropriate way according to environmental conditions, as described above for *P. aeruginosa* PAO1. In addition a novel regulator or a hybrid sensor kinase protein, HskA, has been recently studied for its influence in the electron transport chain composition [Sevilla et al., 2013-1]; in particular, this protein activates the expression of both CIO and Cbb₃1 oxidases inhibits the expression of Cyo and induces that of Aa₃ oxidase, during the stationary growth phase [Sevilla et al., 2013-2].

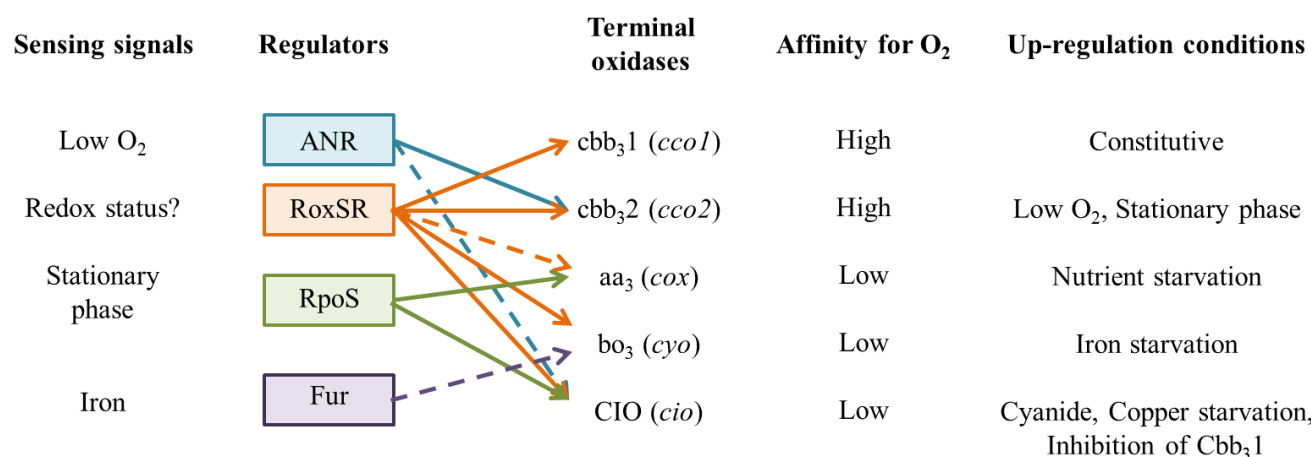


Figure 2.9: Schematic model of the regulatory network controlling the multiple terminal oxidases in *P. aeruginosa* PAO1. The left column represents the sensing signals for regulators; instead, in the right columns, the affinity for oxygen and the up-regulation conditions are shown. Normal arrows indicate the activation while, dotted arrows represent the inhibition [Arai, 2011].

To fill up the molecular and functional gap between our present knowledge of the respiratory chain in KF707 and the most investigated *Pseudomonas* spp. redox chains, here we provide the first functional analysis of the KF707 respiratory genes (GenBank Acc. no. AP014862; Triscari-Barberi et al., 2012) in relation with different primary carbon sources for growth while, the remaining growth conditions, were kept constant. This is an important aspect, as the response of the central carbon catabolism to nutritional compounds is an absolute requirement for an effective microbial colonization of a given environment [Rojo, 2010]. Oddly, the effect of the carbon source on the modulation of the oxidative Electron Transport Chain (ETC), that is the machinery which transduces the reducing metabolic power into energy, still remains a puzzling issue [Dominguez-Cuevas et al., 2006; Nikel et al., 2015].

KF707 contains five different aerobic terminal oxidases: two of *caa*₃-type (**Caa₃** and **Ccaa₃**), two isoforms of *cbb*₃-type (**Cbb₃1** and **Cbb₃2**) and one *bd*-type cyanide-insensitive quinol oxidase (**CIO**). However, while the function and expression of both Cbb₃1 and Cbb₃2 oxidases prevail in cells grown in LB or in minimal salt medium with all the carbon sources tested the expressions of Caa₃ and Cbb₃2 oxidases were 4-fold increased and 7-fold decreased, respectively, when biphenyl was used as the sole carbon source along with a very low contribution to respiration of CIO. This present Chapter 2 not only reveals unexpected features of the KF707 respiratory chain, such as, for example, the presence of a Caa₃ oxidase induced by growth in biphenyl, but it also integrates the functional and genetic data obtained in the past with this PCBs-degrader [Taira et al., 1992; Furukawa et al., 1993; Fujihara et al., 2006; Tremaroli et al., 2008, 2010, 2011], allowing the establishment of solid molecular basis to better understand the use of toxic aromatics as energy and carbon sources.

2.2 Materials and Methods

2.2.1 Bacterial strains and plasmids

All strains and plasmids, used in this chapter, are listed in Table 2.1:

Table 2.1: Bacterial strains and plasmids.

Bacterial Strains	Relevant Genotype	Reference
<i>P. pseudoalcaligenes</i> KF707		
Wild type (W.T.)	Amp ^r	Furukawa and Miyazaki, 1986
KFΔcox1	Deletion of <i>coxI-II-III</i> , Amp ^r	This study
KFΔcox2	Deletion of <i>coxMNOP</i> , Amp ^r	This study
KFΔcox1-2	Deletion of <i>coxI-II-III</i> and <i>coxMNOP</i> , Amp ^r	This study
KFΔcco1	Deletion of <i>ccoN101Q1P1</i> , Amp ^r	This study
KFΔcco2	Deletion of <i>ccoN202Q2P2</i> , Amp ^r	This study
KFΔcco1-2	Deletion of <i>ccoN101Q1P1</i> and <i>ccoN202Q2P2</i> , Amp ^r	This study
KFΔcox1-2/ <i>cco1-2</i>	Deletion of <i>coxI-II-III</i> , <i>coxMNOP</i> , <i>ccoN101Q1P1</i> and <i>ccoN202Q2P2</i> , Amp ^r	This study
KFΔCIO	Deletion of <i>cioABC</i> , Amp ^r	This study
KFΔcox1-2/ <i>CIO</i>	Deletion of <i>coxI-II-III</i> , <i>coxMNOP</i> and <i>cioABC</i> , Amp ^r	This study
KFLac	KF707 <i>lacZ</i> with no insertion, Amp ^r	This study
KFcox1Lac	KF707 <i>coxII::lacZ</i> translational fusion, Amp ^r	This study
KFcox2Lac	KF707 <i>coxM::lacZ</i> translational fusion, Amp ^r	This study
KFcco1Lac	KF707 <i>ccoN1::lacZ</i> translational fusion, Amp ^r	This study
KFcco2Lac	KF707 <i>ccoN2::lacZ</i> translational fusion, Amp ^r	This study
KFCIOlac	KF707 <i>cioA::lacZ</i> translational fusion, Amp ^r	This study
KFΔcco1-2 <i>CIOlac</i>	Deletion of <i>ccoN101Q1P1</i> and <i>ccoN202Q2P2</i> , <i>cioA::lacZ</i> translational fusion, Amp ^r	This study
KFΔcox1-2/ <i>cco1-2</i> <i>CIOlac</i>	Deletion of <i>coxI-II-III</i> , <i>coxMNOP</i> , <i>ccoN101Q1P1</i> and <i>ccoN202Q2P2</i> , <i>cioA::lacZ</i> translational fusion Amp ^r	This study
KFΔcco1 <i>CIOlac</i>	Deletion of <i>ccoN101Q1P1</i> , <i>cioA::lacZ</i> translational fusion, Amp ^r	This study
KFΔcco2 <i>CIOlac</i>	Deletion of <i>ccoN202Q2P2</i> , <i>cioA::lacZ</i> translational fusion, Amp ^r	This study

Escherichia coli

DH5 α	<i>supE44, hsdR17, recA1, endA1, gyrA96, thi1, relA1</i>	Hanahan, 1983
HB101	<i>Sm^r, recA, thi, pro, leu, hsdR</i>	Boyer and Rolland-Dussoix, 1969

Plasmids	Relevant Genotype	Reference
pRK2013	Km ^r , <i>ori</i> ColE1, RK2-Mob+, Rka-Tra+	Figursky and Helinski, 1979
pG19II	Gm ^r , <i>sacB, lacZ</i> , cloning vector and conjugative plasmid	Maseda <i>et al.</i> , 2004
pG19II Δ cox1	Gm ^r , <i>sacB, lacZ</i> , carrying Δ cox1 (<i>coxI-II-III</i>) deleted fragment	This study
pG19II Δ cox2	Gm ^r , <i>sacB, lacZ</i> , carrying Δ cox2 (<i>coxMNOP</i>) deleted fragment	This study
pG19II Δ cco1	Gm ^r , <i>sacB, lacZ</i> , carrying Δ cco1 (<i>ccoN1O1Q1P1</i>) deleted fragment	This study
pG19II Δ cco2	Gm ^r , <i>sacB, lacZ</i> , carrying Δ cco2 (<i>ccoN2O2Q2P2</i>) deleted fragment	This study
pG19II Δ CIO	Gm ^r , <i>sacB, lacZ</i> , carrying Δ CIO (<i>cioABC</i>) deleted fragment	This study
pTNS3	RK6 replicon, encodes the TnsABC+D specific transposition pathway, helper plasmid DNA, Amp ^r	Choi <i>et al.</i> , 2005
pFLP2	Flp recombinase-expressing plasmid, Ap ^r	Hoang <i>et al.</i> , 1998
pFLP2-Km	Flp recombinase-expressing plasmid, Ap ^r , Km ^r	This study
pUC18-mini-Tn7T-Gm- <i>lacZ</i>	mini-Tn7, for construction of β -galactosidase protein fusions, <i>lacZ</i> , Gm ^r	Choi and Schweizer, 2006
pUC-cox1- <i>lacZ</i>	mini-Tn7T, <i>coxII::lacZ</i> translational fusion, Gm ^r	This study
pUC-cox2- <i>lacZ</i>	mini-Tn7T, <i>coxM::lacZ</i> translational fusion, Gm ^r	This study
pUC-cco1- <i>lacZ</i>	mini-Tn7T, <i>ccoN1::lacZ</i> translational fusion, Gm ^r	This study
pUC-cco2- <i>lacZ</i>	mini-Tn7T, <i>ccoN2::lacZ</i> translational fusion, Gm ^r	This study
pUC-CIO- <i>lacZ</i>	mini-Tn7T, <i>cioA::lacZ</i> translational fusion, Gm ^r	This study

2.2.2 KF707 deletion mutant strains

The KF707 knockout mutant strains, for single or multiple oxidases, were obtained by using the Gene SOEing PCR technique and the conjugation protocol (General Materials and Methods). All the primers used for the deletion Δ constructs are listed in Table 2.2.

Table 2.2: Primers used for the construction of the deletion fragments (Δ). The red nucleotides form the overlap region for the UP and DOWN deletion fragments union PCR, while the nucleotides that form the cutting site for the restriction enzymes are in bold.

Gene	Primer name	Sequence	Restriction enzyme
Δ cox1	FOR up	ACGTGTA AGCTT CCTTCACAGTTATTCGGCGCA	<i>HindIII</i>
	REV up	AGGAGTAAGTATGGAACAGT AGCGGGCGGTGGATGATCATC	
	FOR down	ACTGTTCCATACTTACTCCT ACCCAAGGCGGTGATCGAT	
	REV down	ATTT CGAATT TCTCTCGTCCAGCCGCGCTAAAG	<i>EcoRI</i>
	FOR control	TTCGCCATGTTCTCGCTGGG	
	REV control	CCGCGTTGAAGAAGCTGGTG	
Δ cox2	FOR up	CGGGCT GGATCC GCGAGACCC	<i>BamHI</i>
	REV up	ACATTGATCTTAATTGTACCT TCAGCCGGGAGCCGTCCG	
	FOR down	AGGTACAATTAAGATCAATGT CCTGCTTCCTCACCGGTA	
	REV down	ATCCC GAATT TCTCACTCCCCTGCGTACCAC	<i>EcoRI</i>
	FOR control	TAGGCCAGCGATGCACCAC	
	REV control	CGATCCTCTCCAGCACCTG	
Δ cco1	FOR up	ATTAGT GGATCCA AGAGGACGGGGCGACGCAG	<i>BamHI</i>
	REV up	TAGGAGTCAGAATGGTTCAGT TAGGGGTTCCACGGTTAAT	
	FOR down	ACTGAACCATTCTGACTCCTA AAGTAACACCCTGCCTGC	
	REV down	GGGCT GAATT CGATGTAGAACTTGCGCTCGGG	<i>EcoRI</i>
	FOR control	GGTGCCGCTTTCGTTGACTG	
	REV control	CACCGCTTCTGGGGATGAT	
Δ cco2	FOR up	AATC AGGATCC GACCCGAGGCTTGTCCGCTT	<i>BamHI</i>
	REV up	AGGAGTCAGTATGGAACAGT GTAGTTATAGGCGGTGCTGC	
	FOR down	ACTGTTCCATACTGACTCCTA AAGAGGACGGGGCGACGCAG	
	REV down	CTCCC GAATT CTAGGGGTTCCACGGTTAAT	<i>EcoRI</i>
	FOR control	GGTGATGCCATTGACCCACA	
	REV control	CATCTACGTGGCAACTGGT	
Δ CIO	FOR up	AATC AGGATCC GACTTACCTCAGCCCAAGG	<i>BamHI</i>
	REV up	TATCAGTCAGTATAGAACAGT ATCTTCTCGGTTACAGCG	
	FOR down	ACTGTTCTATACTGACTGATA CCGGACACCAGCCCATGC	
	REV down	CTCA AGAATT CCCAGGACTGCGGCGAGCC	<i>EcoRI</i>
	FOR control	TCAGGATCAGCGGCAGGTA	
	REV control	CACAGCGTGACCCAGATGA	

2.2.3 NADI assay

The NADI assay is an oxidase test used in microbiology to determine if a bacterium produces certain cytochrome *c* oxidases [Marrs and Gest, 1973]. The reaction consists in the formation of indophenol blue from *N,N*-dimethyl-*p*-phenylenediamine (DMPD), which is also a redox indicator, and α -naphthol. The DMPD reagent shows a dark-blue color when oxidized (because the oxidized reagent forms the colored compound indophenol blue), and colorless when reduced; this reagent acts as an artificial electron donor for the oxidase enzymes.

The assay was performed in liquid or on plates, with cells grown until stationary phase.

- ✓ In the case of the liquid assay, cells were grown overnight until the stationary phase ($OD_{600\text{ nm}}$ 0.8-1.0), in 50 mL of LB or MSM plus a single specific carbon source (glucose, fumarate, benzoate, *p*-hydroxybenzoate and biphenyl [6 mM]), at 30°C and 130 rpm. After growth, 2 mL of culture were centrifuged for 2 minutes at 13.000 rpm, the supernatant was discarded and the pellet was suspended in 1 mL of Tris HCl [10 mM pH 7.5], this step was repeated twice. At the end, the suspended solution was placed in small glass tube and 100 μ L of a mixture containing DMPD [30 mM in water] and α -naphthol [35 mM in 90% ethanol] was added; after 30 seconds, the samples containing active cytochrome *c* oxidase enzymes became blue and all the samples were photographed.
- ✓ For plates assay, cells were grown on LB plates for 24 hours at 30°C. The day after, 4 mL of NADI solution [30 mM DMPD in water and 35 mM of α -naphthol in ethanol], were added over the plates and left to act for 30 seconds. Also in this case, strains containing active cytochrome *c* oxidase enzymes became blue and a photograph was taken for each plate.

2.2.4 Growth curves

Growth curves were performed to compare the growth rate of the KF707 W.T. strain with that of deletion mutant strains. The experiment was repeated at least six times for each strain in LB medium or minimal salt medium (MSM) with different single carbon sources [6 mM], glucose, fumarate, benzoate, *p*-hydroxybenzoate or biphenyl.

- For MSM with biphenyl, 1 g of biphenyl was dissolved in 10 mL of 98% pure hexane and added in 1 L of MSM media; flasks were left stirring overnight to permit the evaporation of the hexane.

Day I: KF707 W.T. and mutant strain were streaked out on LB plates and incubated overnight at 30°C.

Day II: a single colony for each strain was inoculated in falcon with 10 mL of LB, and incubated overnight at 30°C at 130 rpm.

Day III: each culture was centrifuged for 5 minutes at 5.000 rpm at room temperature, and the cells pellet was washed twice with 10 mL of buffer phosphate. Around 1 mL of overnight culture was inoculated in 250 mL flask, containing 50 mL of the medium; the start OD_{600 nm} was comprised between 0.03-0.05. Flasks were incubated at 30°C at 130 rpm and the OD_{600 nm} was monitored, every two hours, for 16 or 30 hours, depending on the carbon source, until the stationary phase.

2.2.5 KF707 *lacZ* translational fusion strains

To evaluate the expression of the different cytochrome oxidases in KF707 W.T. and mutant strains, strains that carry translational fusions of the promoter region with the first 10-11 amino acids of the terminal oxidase genes with *lacZ* on the genomic DNA were obtained. The *lacZ* fusions were designed to evaluate the promoter expression at the translational level; *lacZ* gene is commonly used in molecular biology as a marker for the gene expression. The *lacZ*-containing strains were constructed by utilizing a Tn7-based method [Choi and Schweizer, 2006].

This system is extremely useful for different reasons: Tn7 has extremely broad host-range capabilities, it has been shown to transpose in over 20 bacterial species so far, it is easy and efficient to use, mini-Tn7 elements can be readily transferred into different mutant backgrounds and the molecular biology of Tn7 is well understood. The TnsABCD

transposase components of Tn7 catalyze site- and orientation-specific insertion with high frequency into bacterial chromosomes at Tn7 attachment (*att*Tn7) sites. Usually, these sites are located downstream of highly conserved *glmS* genes encoding essential glucosamine-6-phosphate synthetase [Choi and Schweizer, 2006].

The method comprises three different steps: the amplification and cloning of the fragment of interest in the plasmid pUC18-mini-Tn7-Gm-*lacZ*, then the transfer of the plasmids into KF707 (by electroporation) and at the end, the excision of the plasmid by Flp system (Figure 2.10).

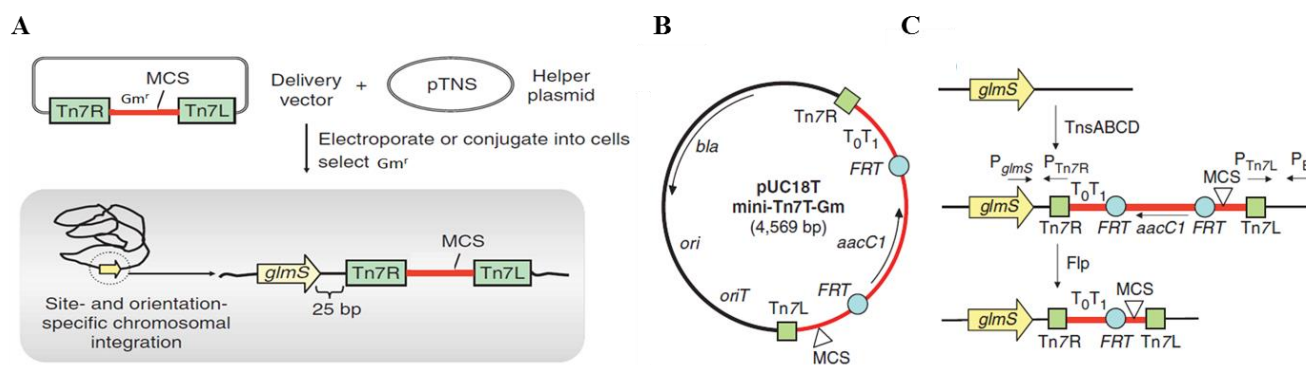


Figure 2.10: **A**) Components of the Tn7 cloning and integration system. The system consists of two components: the mini-Tn7 suicide delivery vector and a helper plasmid. The mini-Tn7 element (red bar flanked by green boxes labeled Tn7L and Tn7R) contains an antibiotic resistance (*Gm^r*) selection marker and a multiple cloning site (MCS). The pTNS helper plasmid carries the genes encoding components of the TnsABCD site-specific transposition pathway. After the transfer of both plasmids into the recipient cell, *Gm^r* transformants contain the transposon inserted into the chromosome (black lines) site and orientation specifically. Insertion generally occurs 25 nucleotides downstream of the respective *glmS* genes. Boxed arrow marks the *glmS* gene and its transcriptional orientation. **B**) Map of a mobilizable pUC18-based suicide delivery vector. The extent of the suicide vector and mini-Tn7 DNA is indicated by the black and red line, respectively. Abbreviations: *aacC1*, gentamycin acetyl transferase-encoding gene; *bla*, β -lactamase-encoding gene; *FRT*, Flp recombinase target; MCS, multiple cloning site; *ori*, ColE1-derived origin of replication; *oriT*, origin of conjugative transfer; *T₀T₁*, transcriptional terminators *T₀* and *T₁* from bacteriophage λ and *E. coli rrnB* operon, respectively; Tn7L and Tn7R, left and right end of Tn7, respectively. Arrows indicate the extent and transcriptional orientation of the *aacC1* and *bla* genes. **C**) Chromosomal integration of mini-Tn7. In this example, mini-Tn7T-Gm is transposed into a bacterial chromosome (black line) after co-electroporation of pUC18T-mini-Tn7T-Gm and the pTNS helper plasmid encoding the TnsABCD transposase subunits, and *Gm^r* transformants resulting from transposition of mini-Tn7T-Gm (red line delimited by green squares) into the chromosome are selected. Optionally, the *Gm^r* marker can be removed by Flp-mediated excision, resulting in strains with unmarked mini-Tn7 insertions [Choi and Schweizer, 2006].

Amplification and cloning of promoter fragments for translational fusion strains

For each oxidase, a pair of primers was designed to amplify a DNA fragment (approximately 500 bp), comprising the promoter region and the first 10-11 amino acids, in order to obtain translational type fusions. Both primers, forward and reverse, contain a restriction enzyme site useful for cloning the amplified fragment into pUC18-mini-Tn7-Gm-*lacZ* vector. The primers used in this step are listed in the Table 2.3. PCR reaction mixtures, 50 μ L, were prepared according to the data sheet of Taq DNA Polymerase, recombinant [5 U/ μ L] (Thermo Fisher Scientific). Amplifications were performed in a Life-Pro™ Gradient Thermo Cycler (Bioer Technology). Optimal conditions of denaturation, annealing and extension were used for each pair of primers. In general, the following parameters were applied: initial denaturation at 95°C for 3 minutes followed by 30 cycles consisting of denaturation at 95°C for 1 minute, annealing at the optimal temperature for each primers pair for 45 seconds, elongation at 72°C for 1 min/Kb and a final extension step at 72°C for 10 minutes. PCR products were separated by electrophoresis on agarose gel [0.7% (w/v)], and after staining in Gel-Red solution, they were visualized under UV-light: when clear and clean bands were observed, the PCR reactions were cleaned-up using QIAGEN PCR purification kit; otherwise, if no specific products were observed, the correct bands were cut from gel and cleaned-up using the QIAGEN gel extraction kit.

Subsequently, each fragment was cloned into the pUC18-mini-Tn7-Gm-*lacZ* plasmid [Choi and Schweizer, 2006], double digested with the specific restriction enzymes. pUC18-mini-Tn7-Gm-*lacZ* is an integrating vector with two Tn7 portions (L and R) capable of site-specific integration by transposition, in the presence of transposase. This mini-Tn7 plasmid contains the *lacZ* gene for the β -galactosidase enzyme expression, without its promoter, and it is located downstream of the MCS. In addition, this vector contains a gentamicin resistance cassette (*aacC1*) as a selection marker, used to verify the insertion of the plasmid in the genome. Up and down this region there are two FRT sequences; these sites are targets of a Flp recombinase enzyme, carried by pFLP2 vector, necessary for the deletion of the gentamicin resistance cassette from the pUC18-mini-Tn7 plasmid after its integration into the bacterial genome.

Table 2.3: Primers used to obtain KF707 translational fusion strains.

Construct	Primer name	Sequence	Restriction enzyme
cox1-lacZ	FOR	TTTAA ACTGCAG GTGGAGGCTGGCGACCTG	<i>Pst</i> I
	REV	ATATCCA AAGCTT AACAGACCACAGCAGCAG	<i>Hind</i> III
cox2-lacZ	FOR	TTGTT AAGCTT GAGAGCCAGGATGATTGC	<i>Hind</i> III
	REV	TTATT GGATCC CTTCGGCTTCGCCGC	<i>Bam</i> HI
cco1-lacZ	FOR	ATTACT AAGCTT AGCAGTCTGACTGATTGC	<i>Hind</i> III
	REV	ATTAC GGATCC ATTGCACCGCTTGCCACGG	<i>Bam</i> HI
cco2-lacZ	FOR	TTT CTGCAG CTGTAGTTATAGGCGGTGCT	<i>Pst</i> I
	REV	TTATT GGATCC CTGCTCGTGGGTGAAACCG	<i>Bam</i> HI
CIO-lacZ	FOR	TAA AGGATC CTGCCGAACAGGGCATG	<i>Bam</i> HI
	REV	ATACA AAGCTT GTGGAAGGAGACCGTG	<i>Hind</i> III

The nucleotides that form the cutting site for the restriction enzymes are in bold.

Construction of KF707 translational fusion strains

Day I. KF707 W.T. or mutant strain was streaked out on LB agar plates and incubated overnight at 37°C.

Day II. KF707 strain was inoculated in 10 mL of LB medium from a single colony grown on the agar plates. LB liquid culture was grown overnight at 30°C under agitation at 130 rpm. pUC18-mini-Tn7-Gm-*lacZ* carrying the promoter fragment insertion and pTNS3 vector were purified using QIAGEN Miniprep kit and quantified by NanoDrop ND-1000 UV-Vis Spectrophotometer. pTNS3 is a mobilizable helper plasmid encoding for a transposase enzyme (*tnsABCD* gene cluster) required to integrate the internal portion of the mini-Tn7 vector into the bacterial genome.

Day III. After overnight growth, 1 mL aliquot of KF707 strain was collected in a sterile tube and washed twice with a sucrose solution [300 mM]. At the end, cells were suspended in 400 µL of sucrose [300 mM] and kept in ice. Electroporation was performed shortly after electro-competent cells preparation with 500 ng of plasmids DNA (250 ng of pUC18-mini-Tn7 plasmid type and 250 ng of pTNS3), using 400 µL of cells and no more than 10 µL of plasmid with the following settings: 25 µF, 200 Ω, 2.5 kV (the time constant should be less

than 5 ms). Immediately after the electroporation, 1 mL of LB medium was added to electroporated cells and then they were incubated for two hours at 30°C with shaking (130 rpm). After the incubation, 100 µL of the mixture were plated on LB+Gm+X-gal plate; the remaining culture was centrifuged for 2 minutes at room temperature at 13.000 rpm, after that the supernatant was discarded and cells were suspended in 200 µL of LB and plated on another LB+Gm+X-gal plate. Plates were incubated at 30°C for 48 hours.

Day IV. One single and large colony was *tooth-picked* in fresh LB+Gm+X-gal agar medium and incubated at 30°C until growth was clearly visible (24 hours).

Day V. One single colony was inoculated in 10 mL of LB+Gm medium in the afternoon; the liquid culture was grown overnight at 30°C under agitation at 130 rpm. pFLP2-Km was purified using QIAGEN Miniprep kit and quantified by NanoDrop ND-1000 UV-Vis Spectrophotometer. pFLP2-Km (Hoang et al., 1998) encodes for a Flp recombinase enzyme that catalyzes the recombination of FRT sites situated in pUC18-mini-Tn7 vector, it is necessary for the excision of the Gm^r marker. In addition, this plasmid contains also a *sacB* gene that confers sensitivity to sucrose and was engineered by adding kanamycin resistance cassette as a second selective marker.

Day VI. After overnight growth, 1 mL aliquot of KF707+pUC18-mini-Tn7-Gm-*lacZ* strain was collected in a sterile tube and washed twice with a 300 mM sucrose solution. At the end, cells were suspended in 400 µL of 300 mM sucrose and kept in ice. For the excision of Gm^r marker, a new step of electroporation was performed shortly after electro-competent cells preparation with 500 ng of pFLP2-Km DNA and the following settings: 25 µF, 200 Ω, 2.5 kV (the time constant should be less than 5 ms). Immediately after electroporation, 1 mL of LB medium was added and cells were incubated for two hours at 30°C with shaking (130 rpm). After the incubation, 100 µL of the mixture were plated on LB+Km+X-gal plate; the remaining culture was centrifuged for 2 minutes at room temperature at 13.000 rpm, after that the supernatant was discarded and cells were suspended in 200 µL of LB and plated on another LB+Km+X-gal plate. Plates were incubated at 30°C for 48 hours.

Day VII. To confirm the deletion of the gentamicin resistance cassette, a Plating Replica was performed by picking 50 single colonies grown on LB+Km+X-gal on the same medium and on LB+Gm+X-gal; plates were incubated overnight at 30°C.

Day VIII. After overnight incubation the growth in the two kinds of media was compared, a single colony able to grow only in LB+Km+X-gal but not in LB+Gm+X-gal was selected, inoculated and incubated at 30°C for 48 hours, in 10 mL of modified LB broth without NaCl, in order to force the emission of the pFLP-Km plasmid.

Day IX. After 48 hours growth, serial dilutions were performed and 100 μ L of dilutions, between 10^{-2} to 10^{-5} , were plated on LB+10% of sucrose+X-gal. Since pFLP2-Km harbors the *sacB* gene, which codifies for the levansucrase, an enzyme that does not allow growth on sucrose, this carbon source was added at high concentration to stimulate the expulsion of the plasmid. Plates were incubated at 30°C for 48 hours.

Day X. After incubation, grown clones were *tooth-picked* onto both LB+10% sucrose+X-gal and LB+Km+X-gal; plates were incubated at 30°C overnight.

Day XI. After overnight incubation, the growth of the selected clones in the two kinds of media was compared: the colonies that still contained the replicative pFLP2-Km plasmid were discarded and one colony able to grow only in LB+10% of sucrose+X-gal was selected.

2.2.6 β -galactosidase assay

β -galactosidase assay provides an easy, rapid, and highly sensitive method for determining the activity in the lysates of cells that contain a β -galactosidase expression construct. The enzyme converts o-nitrophenyl- β -D-galactopyranoside (ONPG, substrate used in the assay) into o-nitrophenol (ONP); this compound determines a color change of the solution, which becomes yellow; in this way it is possible to measure the color intensity with a spectrophotometer (λ 420 nm) and relate it to the quantity of cells tested. In our case, the assay was performed at least six different times for each KF707 translational fusion strain grown in LB or MSM medium with different carbon source [6 mM], and at two different stages of the growth: exponential phase ($OD_{600\text{ nm}}$ 0.35-0.50) and stationary phase ($OD_{600\text{ nm}}$ 0.80-1.00).

The protocol used for the assay is described below.

Day I: KF707 translational fusion strains were inoculated into LB liquid medium (10 mL) by expressing the *lacZ* gene under the control of the promoter of the different oxidases. Cultures were incubated overnight at 30°C and 130 rpm of shaking.

Day II: cultures grown overnight were centrifuged and pellet was washed twice with phosphate buffer. Cells were inoculated in 50 mL of LB or MSM with a single carbon source (glucose, fumarate, benzoate, *p*-hydroxybenzoate and biphenyl (dissolved in 10 mL of *n*-hexane) [6 mM]) in 250 mL flasks. The initial OD_{600 nm} was comprised between 0.03-0.05; then the flasks with the cultures were incubated at 30°C and at 130 rpm.

For the assay, the Miller protocol was followed. The cultures were stopped during the exponential phase (OD_{600 nm} 0.35-0.50) and at the end of the growth (OD_{600 nm} 0.80-1.0), and 1 mL was taken, both times, to perform the assay. The cultures were centrifuged at 13.000 rpm for 5 minutes and the supernatant was discarded. The pellet were suspended in 500 µL of BufferZ [Na₂HPO₄ 2H₂O 60 mM - NaH₂PO₄ 40 mM - KCl 10 mM - MgSO₄ 7H₂O 1 mM - β-mercaptoethanol 50 mM, pH 7.0] with the addition of 50 µL of chloroform and 20 µL of SDS [0.1 % w/v]. Then cells were vortexed and incubated for 7 minutes at 30°C; at the end of the incubation, 200 µL of ONPG solution [4 mg/mL in BufferZ solution] were added and the eppendorfs were incubated at 30°C for 15 minutes; 500 µL of Na₂CO₃ [1 M] were added to block the ONPG reaction. Finally, the cells were vortexed and centrifuged for 5 minutes at 4°C and 13.000 rpm, the supernatant was transferred to the quartz cuvette to measure absorbance at 420 nm and at 550 nm with the Jasco 7800 Spectrophotometer.

For each measurement, Miller Unit number was calculated using the following formula:

$$\text{Miller Units} = 1000 \times [(\text{OD}_{420 \text{ nm}} - 1.75 \times \text{OD}_{550 \text{ nm}})] / (\text{T} \times \text{V} \times \text{OD}_{600 \text{ nm}})$$

- OD_{420 nm} and OD_{550 nm} are read from the reaction mixture.
- OD_{600 nm} reflects cell density in the washed cell suspension.
- T = time of the reaction in minutes (15 minutes).
- V = culture volume used in the assay in mLs (1 mL).

2.2.7 Preparation of membrane fragments

For the preparation of membrane fragments, KF707 cells were inoculated (after overnight growth in 10 mL LB medium at 30°C and 130 rpm) at a cell density close to 0.03-0.05 OD_{600 nm}. Then, cells were grown aerobically until the stationary phase (OD_{600 nm} 0.8-1.0) in 3 L Erlenmeyer flasks containing 1 L of MSM medium, pH 7.2, at 30°C and 130 rpm, with glucose or biphenyl [6 mM] as single carbon source. Cells were harvested and centrifuged after 16 and/or 30 hours for glucose or biphenyl medium, respectively. Cell pellets were collected and washed twice with 10 mL of phosphate buffer [0.1 mM] to reach about 1.6 g of wet weight cells for KF707 W.T. and mutant strains.

To prepare membrane fragments to be used for respiratory activity measurements and spectroscopic analysis, pellets were suspended in 25 mL of MOPSO buffer [50 mM, pH 7.2] containing MgCl₂ [5 mM] and cells were sonicated for three times, 45 seconds each, and subjected to French pressure mechanical treatment. Broken cells were centrifuged at 5.000 rpm for 20 minutes at 4°C, and the supernatant was centrifuged for 2.30 hours at 35.000 rpm (4°C). The supernatant was removed and the pellet formed by membrane fragments was suspended in 1-2 mL of MOPSO buffer to reach a protein concentration between 5 and 15 mg/mL. Proteins concentration was determined using the method of Lowry [Lowry et al., 1951], or the bicinchoninic (BCA) acid assay according to the supplier's recommendations (Sigma Inc.; procedure TPRO-562), with bovine serum albumin (BSA) as a standard. For both respiratory activities and spectroscopic analysis, cells were used immediately after ultra-centrifugation.

All experiments conducted with membranes from KF707 W.T. and/or mutant cells were repeated at least in two/three independent cell preparations.

2.2.8 Spectroscopic analysis and Respiratory activities

- The amount of cytochromes in W.T. and deletion mutants membrane fragments (prepared according to the method previously described) were estimated by recording reduced (with [0.5 mM] NADH plus [5 mM KCN] and/or a few crystals of sodium dithionite)-*minus*-oxidized (with a few crystals of potassium ferricyanide) optical difference spectra at room temperature with a Jasco 7800 spectrophotometer. For each sample ~ 1.5 mg of membrane fragments, suspended in 2 mL of MOPSO buffer, were used; spectra were repeated at least three times for each sample. Haem amounts were estimated using the following molar extinction coefficients: $\epsilon_{603-630}$ of $11.6 \text{ mM}^{-1}\text{cm}^{-1}$, $\epsilon_{561-575}$ of $22 \text{ mM}^{-1}\text{cm}^{-1}$ and $\epsilon_{551-542}$ of $19.1 \text{ mM}^{-1}\text{cm}^{-1}$ for *a*-, *b*- and *c*-type cytochromes, respectively.
- Respiratory activities in membrane fragments isolated from W.T. and mutant strains were determined by monitoring the oxygen consumption, at 28°C, with a Clark-type oxygen electrode YSI 53 (Yellow Spring Instrument). 0.25 to 0.30 mg of membrane fragments per mL (2 mL total volume) were used suspended in MOPSO buffer; the activities in the presence or in the absence of specific inhibitors were measured within a few hours the completion of the membrane isolation procedure.
The total oxygen consumption was observed by adding NADH [200 μM] (electron donor to both quinol and cytochrome oxidases); to observe cytochrome *c* oxidases activity, 2 mM of sodium ascorbate plus horse heart cytochrome *c* [50 μM] or N,N,N',N'-tetramethyl-*p*-phenylenediamine (TMPD) [50 μM] were used. Conversely potassium cyanide [50 μM] or sodium azide [50 μM] were added to inhibit the different cytochrome oxidase enzymes. The enzymatic activity for each experiment was expressed in moles of substrate consumed per minute per milligram of protein.
With this technique, the inhibitory concentration IC_{50} was also measured, which corresponds to the concentration of a defined inhibitor which is required to inhibit 50% of the target enzymatic activity.

2.3 Results

2.3.1 Putative genes for terminal oxidases

The genome analysis of KF707 revealed the presence of five different clusters for aerobic terminal oxidases. The gene clusters are listed in Table 2.4 and represented in Figure 2.11; there are two *caa3*-type (Caa₃ and Ccaa₃), two isoforms of *ccb3*-type (Cbb₃₁ and Cbb₃₂) and one *bd*-type cyanide-insensitive quinol oxidase (CIO).

Table 2.4: KF707 oxidases gene clusters compared to *P. aeruginosa* PAO1 homologues. Names of the genes from which are encoded, lengths of the products in amino acids and the Gene Bank accession number (*P. pseudoalcaligenes* KF707 = NBRC 110670 – Nov. 2016), are reported. For each gene, the Gene Bank accession number resulting as best hit from BLASTP against the *P. aeruginosa* PAO1 genome is reported, together with the related amino acids % of identity (aa % ID PAO1).

Oxidase gene cluster	Gene	Gene product (aa)	Gene Bank KF707	aa % ID PAO1	Gene Bank PAO1
Caa₃ (cox1)	<i>coxI</i>	529	BAU71738	93%	AAG03496
	<i>coxII</i>	374	BAU71737	81%	AAG03495
	<i>coxIII</i>	295	BAU71740	85%	AAG03498
	<i>cox11-ctaG</i>	181	BAU71739	73%	AAG03497
	<i>MFS</i>	67	BAU71741	81%	AAG03499
	<i>surf1</i>	241	BAU71742	60%	AAG03500
	<i>cox15-ctaA</i>	361	BAU71744	77%	AAG03502
	<i>cox10-ctaB</i>	301	BAU71745	82%	AAG03503
	<i>scoI</i>	208	BAU71746	69%	AAG03504
Ccaa₃ (cox2)	<i>coxM</i>	481	BAU74428	26%	AAG03495
	<i>coxN</i>	588	BAU74429	42%	AAG03496
	<i>coxO</i>	229	BAU74430	29%	AAG03498
	<i>coxP</i>	227	BAU74431	37%	AAG03498
	<i>coxX</i>	105	BAU74432	/	/
Cbb₃₁ Cbb₃₂ (cco1-cco2)	<i>ccoN1</i>	480	BAU73555	90%	AAG04943
	<i>ccoO1</i>	203	BAU73554	94%	AAG04942
	<i>ccoQ1</i>	61	BAU73553	98%	ADN93060
	<i>ccoP1</i>	324	BAU73552	79%	AAG04941
	<i>ccoN2</i>	478	BAU73559	89%	AAG04946
	<i>ccoO2</i>	203	BAU73558	99%	AAG04945
	<i>ccoQ2</i>	55	BAU73557	70%	ADN93059
	<i>ccoP2</i>	311	BAU73556	72%	AAG04944
	<i>ccoG</i>	471	BAU73551	80%	AAG04940
	<i>ccoH</i>	165	BAU73550	57%	AAG03939
	<i>ccoI</i>	799	BAU73549	83%	AAG04938
	<i>ccoS</i>	73	BAU73548	74%	AAG04937
CIO (cio)	<i>cioA</i>	479	BAU72498	87%	AAG07317
	<i>cioB</i>	335	BAU72499	85%	AAG07316
	<i>cioC</i>	141	BAU72500	71%	AAG07315

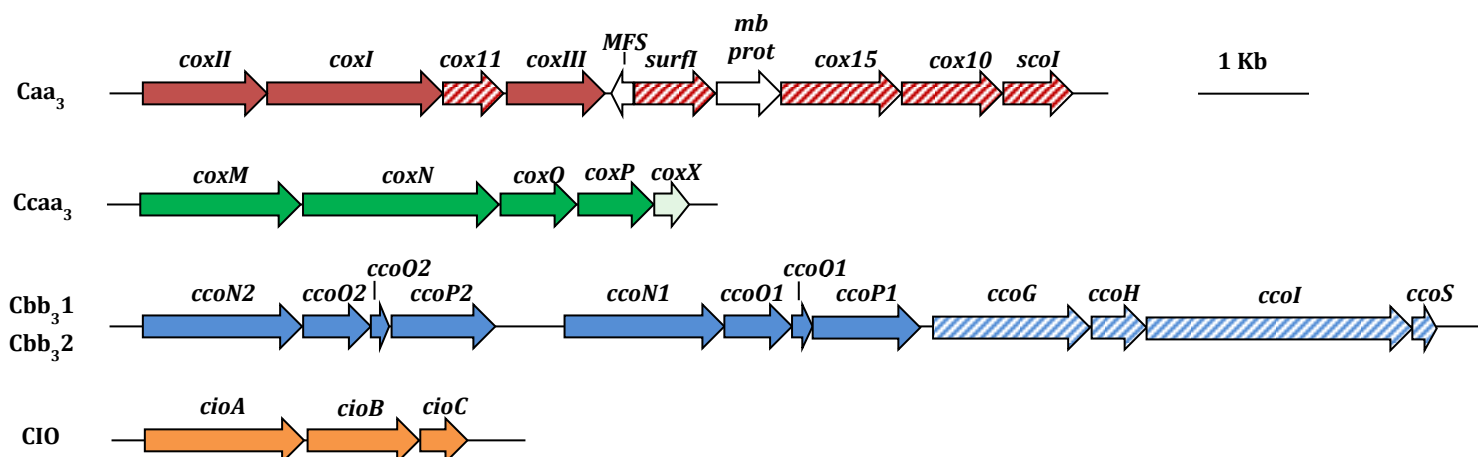


Figure 2.11: Organization of the terminal oxidase gene clusters in KF707: *cox*, encoding for cytochrome *c* oxidases of *caa*₃-type (*coxII-I-III* and *coxMNO**P*); *cco*, encoding for gene products involved in the synthesis of two cytochrome *c* oxidases *ccb*₃-type (*ccoN1O1Q1P1* and *ccoN2O2Q2P2*); *cio*, gene cluster for the quinol oxidase CIO (*cioABC*). Genes (listed in Table 2.4) are represented by arrows and by different colors or stripes: full color, functional genes; dashed stripes, genes for cytochrome biogenesis; light color, cytochrome *c* oxidase accessory membrane protein (CoxX); white genes are supposedly not directly related with the gene clusters under analysis. Full names and abbreviation used: MFS, Major Facilitator Superfamily permease; mb prot, membrane protein.

The *caa*₃-type cytochrome oxidases

The analysis of KF707 genome shows the presence of two gene clusters for two different *cox* oxidases of *caa*₃-type whose subunits are predicted to contain *c*-type haems: Caa₃ and Ccaa₃ oxidases. The Caa₃ oxidase is encoded by *coxI-II-III* (BAU71738-71737-71740) gene cluster (Figure 2.11; Table 2.4). The three subunits, which are annotated as part of the *caa*₃-type cytochrome *c* oxidase in the KF707 genome, have sequences with high similarity (~90%) to CoxB, CoxA, and CoxC of *P. aeruginosa* [Stover et al., 2000]. Similarly to *P. aeruginosa*, subunit I (58.8 kDa) of KF707 is predicted to carry a low spin *a*-type haem and one hem *a*₃-Cu_B binuclear catalytic center. The predicted subunit II (42 kDa) consists of a membrane anchored cupredoxin domain, containing the electron-accepting homo-binuclear copper-center, Cu_A, with a carboxy-terminal fusion to a cytochrome *c* domain [Lyons et al., 2012]. The presence of a *c*-type haem in the *caa*₃-type oxidase of KF707 was suggested by an alignment analysis (see Alignment 1) which showed, in the C-terminal region, the typical amino-acids residues (CXXCH), that coordinate the haem *c* in *T. thermophilus* and *Rhodothermus marinus* Caa₃ oxidases [Lyons et al., 2012]; these characteristic residues are

absent from *R. sphaeroides* and *Par. denitrificans* Aa₃ oxidases while the CoxII amino acid sequence of KF707 has 81% similarity with the CoxB of *P. aeruginosa* PAO1. In KF707, an additional **Ccaa₃** oxidase is predicted to be encoded by the gene cluster **coxMNOP** (BAU74428- 74432) (Figure 2.11; Table 2.4). Sequence analyses showed that this alternative complex is characterized by an organization which is typical of aa₃-type cytochrome oxidases present in *Sinorhizobium meliloti* 1021, *Cupriavidus metallidurans* CH34, *Mesorhizobium sp.* and *Polaromonas* [Preisig et al., 1996]. Previous studies have shown that the *coxMNOP* gene cluster encodes a complex with homology to Cu-containing cytochrome *c* oxidase; indeed it was observed that the subunit I (66 kDa), encoded by *coxN*, was very similar to CoxA of *P. aeruginosa* [Bott et al., 1992] and to CoxI of KF707's Caa₃. The alignment suggested that CoxM (52 kDa) of KF707 showed, in the C-terminal portion, two *c*-type haems (see Alignment 2) and therefore this oxidase is a Ccaa₃ cytochrome oxidase; in this case, in the C-terminal portion, there is a repetition of the residues (CXXCH) that coordinate the *c*-type haems. These enzymes are not common, but they have also been found in bacteria such as *Desulfovibrio vulgaris* [Lobo et al., 2008] and *Shewanella oneidensis* MR-1 [Le Laz et al., 2014]. In KF707, CoxP and CoxO amino acid sequences are homologs to subunit III of the Aa₃ complex.

The *cbb₃*-type cytochrome oxidases

Two complete sets of genes encoding for cytochrome *c* oxidases of *cbb₃*-type (**Cbb₃1** and **Cbb₃2**) are present in KF707 (Figure 2.11; Table 2.4). These genes, tandemly clustered in the genome of KF707, are situated in the **ccoN101Q1P1** (BAU73552-73555) and **ccoN202Q2P2** (BAU73556-73559) clusters, as previously shown in *P. aeruginosa* strains PAO1 and PA7, *P. putida* KT2440 and *P. fluorescens* [Stover et al., 2000]. Similarly to orthodox *cbb₃*-type oxidases, the catalytic subunit I (~50 kDa) of KF707, encoded by *ccoN* gene, is expected to comprise 12 transmembrane helices and to contain, in addition to the low spin *b*-type haem, a binuclear center formed by high spin *b₃* haem and Cu_B. In general, the two transmembrane cytochrome *c* subunits with *c*-type monohaem and dihaem groups are encoded by the genes *ccoO* (~22 kDa) and *ccoP* (~40 kDa) respectively, while CcoQ (~7 kDa) are necessary for the stability of the complex. These oxidases utilize cytochrome *c* as an electron donor and they lack a Cu_A site. In general, the *ccoNOQP* operons, encoding *cbb₃*-

type oxidase subunits, are found in association with the *ccoGHIS* (BAU73548- 73551) gene cluster, which is located in the downstream region and whose expression is required for the maturation and assembly of a functional Cbb₃ oxidase and this type of gene organization is also present in KF707 (Figure 2.11; Table 2.4) [Preisig et al., 1996; Koch et al., 2000; Pitcher and Watmough, 2004]. Homology searching of both *ccoNOQP* and *ccoGHIS*, showed the same gene arrangement among *P. aeruginosa* strains PAO1 and PA7, *P. putida* KT2440 and *P. entomophila* L48 while *P. aeruginosa* strains UCBPP-PA14 and LESB58, *P. stutzeri* A1501 and *P. mendocina* YMP showed similar features except that some of them lack one copy of the *ccoQ* gene.

The *bd*-type oxidase

In the past, an oxidase activity insensitive to cyanide (**CIO**), which accounts for ~20% of the total NADH-dependent respiration of LB-grown KF707 cells, has been reported [Di Tomaso et al., 2002]. KF707 genome contains two genes coding for two subunits, which are highly similar to those of cytochrome *bd*-type quinol oxidases of *P. fulva* 12-X and *P. mendocina* (Figure 2.11; Table 2.4). In *E. coli* and other Gram negative bacteria, the cytochrome *bd*-I complex consists of two subunits named CydA (subunit I) and CydB (subunit II), while in *Pseudomonas spp.* it is encoded by the *cioA* and *cioB* genes, respectively [Cunningham et al., 1997]. In KF707, genes *cioA* (BAU72498) and *cioB* (BAU72499) code for two orthodox subunits in addition to a third accessory subunit encoded by *cioC* (BAU72500). The CIO oxidase functions as a quinol oxidase with a relatively low sensitivity to cyanide and it often shows high affinity for oxygen [D'mello et al., 1996]. CIO contains low-spin haem *b*₅₅₈, high spin haem *b*₅₉₅ and haem *d* [Jünemann, 1997; Siletsky et al., 2016]. It should be noted that, although both the *cioA* and *cioB* genes are highly similar to the *cydAB* genes encoding a *bd*-type oxidase, the CIO from KF707 lacks the spectral features of haem *b*₅₉₅ and haem *d* [Matsushita et al., 1983; Di Tomaso et al., 2002].

Alignment 1: Alignment of Caa₃ oxidases from various bacterial species: KF707, *Pseudomonas pseudoalcaligenes* KF707; PAO1, *Pseudomonas aeruginosa* PAO1; THER, *Thermus thermophilus* and RHOD, *Rhodothermus marinus*. Residues that coordinate the c-type haem are indicated in black (CXXCH and M).

KF707	-MRHPRVWMGLLLLS--VLSQAQAAWTVNMTPGATEVSRVFDLHMTIFWICVVIGVIVF	57
PAO1	MLRHPRVWMGFLLLS--AISQANAAWTVNMAPGATEVSRVFDLHMTIFWICVVIGVLVF	58
THER	---MQRSF AALGLWGLSLAQEAHRVAITHP---GGSFNQEVAF LFPWVYFFSFLIFLVVA	54
RHOD	-----MSGMILLQN--TAWLPEA---ASSIAPEVDSL FHFWTLVSAIIFIGVV	43
	: . .: * * . .. : * : *	
KF707	GAMFWSMII--HRRSTGQQPAHFHESTTVEILWTVVPFVILVLM AIPATKTLIDIYDTSE	115
PAO1	GAMFWSMIV--HRRSTGQQPAHFHESTTVEILWTVVPFVILVVM AVPATRTLIIHYDTSE	116
THER	GSLAYVTWKFRARPEDQEPPQIHGNDRLLEVWTLIPLAIVFVFLG LTAKALIQVNRPIP	114
RHOD	GAMTFFVVRYYYYRRRDE-VPEPVQEKVVELAWIVVPTILV L VFAWGRVYIKMYTAPP	102
	* : : * * . . : * : * : : : : : . * : *	
KF707	SGLDVQITGYQWKWHYKYLGDVEFFSNLATPSEQIHNKAPKDEHYL LEVDQPLVVPVGT	175
PAO1	PELQVQVTGYQWKWKYKYLGDVEYFSNLATPQDQIHNQAKDEHYL LEVDEPLVLPVGT	176
THER	GAMKVEVTGYQFWWDFHYPELGL-----RNSNELVLPAGV	149
RHOD	DAYEILVHGYSWYWEFEYFN-GV-----KTTNELHVPAGQ	136
	. : : * * * : * . . * . : . : * : * . *	
KF707	KVRFLITAAADV IHSWVVPALAVKKDAIPGFVNESWTRIEKPGLYRGQCTELCGKDHGFMP	235
PAO1	KVRFLITSSDVIHSWVVPFAFAVKRDAIPGFVNEAWTKVDEPGIYRGQCAELCGKDHGFMP	236
THER	PVELEITSKDVIHSFWVPLAGKRDAIPGQTTTRISFEPKPEGLYGFCAELCGSHARML	209
RHOD	PVKLRMTSADVIHSFYVPAFRVKQDVLDPDRYSALWFEATKPGEYTVFCTEYCGTQHAGML	196
	* . : : * : * * * * : * * . : * : * . * . . : * * * . * . *	
KF707	IVVEAKSQEDFAKWL AARKEETAKLKELTDKEWTLDELVARGDKVY-HTSCAACHQPEGQ	294
PAO1	IVVDVKPKAEFDQWLAKRKEEAAKVELTSKEWTKEELVARGDKVY-HTICAAACHQAEQG	295
THER	FRVVVLPKEEFDRFVEAAKASPAPV-----ADERGQVF-QQNCAACHGVARS	256
RHOD	AKVIVHPREEFEQWLESAGIPEDMP-----LAELGARLYREKACFSCHSIDGS	244
	* . : * : : * : : . * : * * . : * * .	
KF707	GMP----PMFPALKGSKIATGPKA-----DHLNIVFHGKPGTSM AAFGKQL	336
PAO1	GMP----PMFPALKGSKIIVTGPKE-----HHLEVVFNGVPGTAM AAFGKQL	337
THER	MPPAVIGPE-LGLWGNRTSLGAGIVENTPENLK-AWIRDPA----GMKPGVKMPGFP-QL	309
RHOD	R---LVGPSFKGLYGSTRTFEDGTTAVADENYLRESILQPGAKIVQGYPNVMPASYA-SL	300
	* . * * . . * . . . : . *	
KF707	SEVDIAAVITYERNAWGNNTGDMVTPKEVLALKQAESQ 374	
PAO1	NEVDLAAVITYERNAWGNDDGDMVTPKDVVAYKQKQQ- 374	
THER	SEEDLDALVRYLEGLKVEGFDFGALPKF----- 337	
RHOD	SEREVAALIEFIKQQQ----- 316	
	. * : : * : : . .	

Alignment 2: Alignment of Ccaa3 oxidases from various bacterial species: KF707, *Pseudomonas pseudoalcaligenes* KF707; MR-1, *Shewanella oneidensis* MR-1 and DES, *Desulfovibrio vulgaris*. Residues that coordinate the two c-type haems are indicated in black (CXXCH and M).

KF707	MAIAI-ILALILVASVLFHFLAPWHLTPPASNW-GSIDTLLITLVITGVFFIAVVGFMV	58
MR-1	MKQWLYCLLVVLFAPPLAASDMRYNMTPGVTEISGKVYHLHMTILYICCAIGLVVFGVMI	60
DES	-----MYPQSLSPV-----QQVDLAFYVIFGVSAMLLGITATML	35
	:* .: : : .: : : . *:	
KF707	VAIIRFRHREGRRARYEPESRRLEWWMVVTSLGIVGMLAPGLVVYSDFVRVPKDAYPLE	118
MR-1	YAMINHRKSKGAVASHFHSTKVEIAWTVIPFVILILMAIPATKTLIAMEDPSNADLTVK	120
DES	WFWVRYDHRRNPVATEIPGSVLAETAWTLIPTLIVMALFYYGWAGYKALRTVPADALEVG	95
	: . . : . . * * * .: : : : . : :	
KF707	VVAQQWQWAFRFPQGQDLGRADVSVDARNPLGLDPRDPHGQDDVLVRGNEVRLPLDRP	178
MR-1	VTGSQWKWHYSYFDQDIEFYSI-----LATPRPQIEGNEVKGEHYLLEVDKPLVLPVNRK	175
DES	VKARMSWIFWEYPNGKR-----SSVLYVPAGKP	123
	* . * . * : : : : * . :	
KF707	VKVLRSKDVLNHFYIPQIRGKMDMVPGMVSHFWFTPTLAGEYEILCAEFCGVGHFNMRG	238
MR-1	IRFLMTSEDVIHSWVPDFAVKKDANPGFINEAWTRIDKPGIYRGGCAELCGKDHGFMP	235
DES	VKLDMTSVDVIHSLYIPAFRIKMDTVPGMQTYAWFKTDGPGEFDILCAEYCGLKHANMLS	183
	: : . : * ** : . : * : * * * : * * * * * * * *	
KF707	KLQVEPAPAFEQWLATQPTFAQVVASAGAP-----SQGLIERGRQLADTHGCPACHSQ	292
MR-1	VVKALPEAEFEAWVKEQKQAADAAAQAAQAALSQNLKSKEELMTQGEQV-YLGHCAACHQP	294
DES	VVKAVEPDEFKWLSESE-----APGGKGRALLDAYGCTISCHSL	222
	: : . * . * : . : * . : * : * .	
KF707	DGSQSLGPGWKDLYGREVQLAD---GSRLKADAAYLRESILDPRARLVQGYPPVMPVPT	348
MR-1	NGEGLKG-VFPHLKGSPIAMGPLGAH-----IEIVLNGKAGTAMQAFS	336
DES	DGSPGPGTTFKGLYGAERVVVLGDGSKRKVIVDEAYLRRALKDPNAELVEGFEPIMPSTE	282
	: * . * : * * : . * *	
KF707	FS--QDELAALVAFIRSLSAVGQ-----QE-----	371
MR-1	KQLTTQEIAAAVITYERNAWGNNTGDAAQAKDVDAHKSGGTNSEPVATTQPPSTTDAPKAV	396
DES	GVVPEQDFEDMIAWF-----	297
	: : : : : : :	
KF707	-----SGGAGNLVEQGEKLAQSLGCLACHSLDGSKGVGPSWKGLYGHVPTLA	418
MR-1	TEPIASVDPASLPTLTHEALMAEGEKVY-VTFCAACHQVTGA-GMPPAFPALAGSAIATG	454
DES	-----MHGNGLTREEGRRLMEQEGCLSCHSTDGSSVAGPTFKNLWGSEVDVL	344
	* : * . * : * : : * * :	
KF707	---DGSQVEADAAYLRESVLAPAARLVQGSPLMPAFT-PSDT-ELDALIAFIRSRADPD	473
MR-1	PSTN---HIDI-----VVQGKTGTAMQAFGKQLTPQQLAAVITYERNAWGN	498
DES	VDGVPKRVKVDADYVRESIVAPQKLSKGDPLMPGYD-SFTPEQMEAMMDYMRSLSGTP	403
	. * : . * . : : : * : : * . .	
KF707	SDDQEAP-----	481
MR-1	TGDTVQPADIARHGK-----	513
DES	DKAPADASSPGLHGGTSPAGKTQ	426
	:	

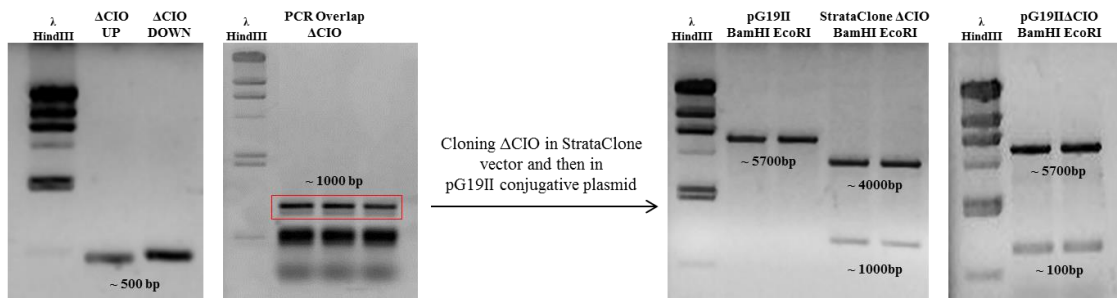
2.3.2 KF707 terminal oxidases mutant strains

KF707 deleted mutants for single or multiple oxidases (Table 2.5) were obtained by Gene SOEing PCR technique [Izumi et al., 2007]. The approach used to obtain these mutants is described in General Materials and Methods.

Figure 2.12 schematically shows the procedure for obtaining the KF707 Δ CIO mutant; analogous approaches were adopted for all other mutant strains listed in Table 2.5, whereas all conjugation mixtures are reported in Table 2.5. Only in the case of the KF707 Δ cco1-2 mutant the Gene SOEing PCR approach was changed; in fact, because *ccoN101Q1P1* and *ccoN202Q2P2* are tandemly clustered in the genome, for the simultaneous deletion of these two oxidases the primers for UP Δ cco1, as upstream flanking region, and the primers for DOWN Δ cco2, as downstream flanking region, were used.

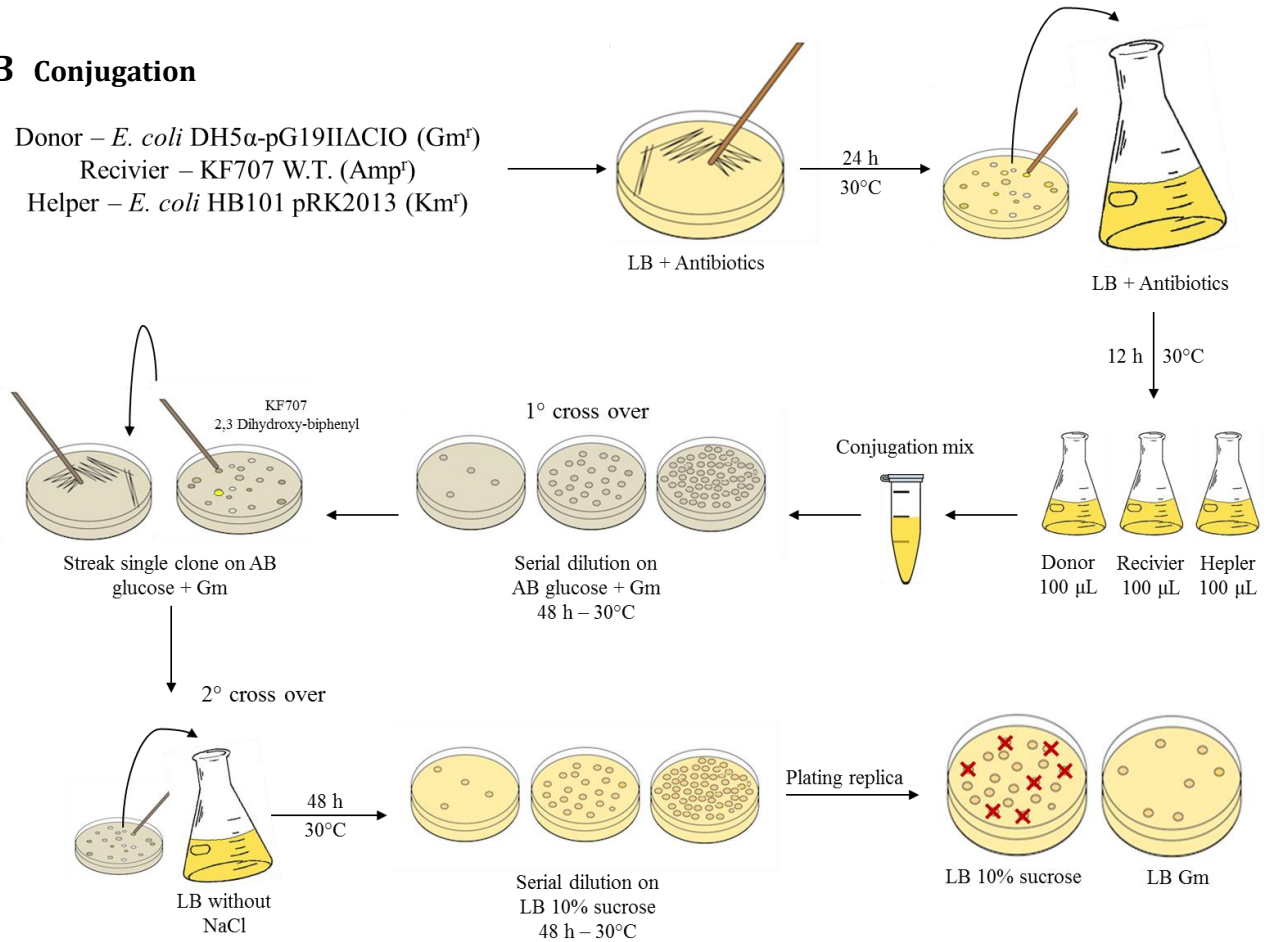
With this method, it was not possible to obtain a triple oxidase mutant lacking simultaneously the CIO, Cbb₃1 and Cbb₃2 oxidases; this result is in line with a previous data, reported in *P. aeruginosa* PAO1, in which, a mutant lacking four terminal oxidase gene clusters except for the *cox* gene (strain QXAa), did not grow aerobically because of the low expression level of the *aa*₃-type oxidase [Arai et al., 2014]. More recently, a suppressor mutant of QXAa (named QXAa2) that grew aerobically using the Aa₃ as the only terminal oxidase, emerged after a series of aerobic sub-culturing procedures [Osamura et al., 2017].

A Gene SOEing PCR



B Conjugation

Donor – *E. coli* DH5 α -pG19II $\Delta C10$ (Gm^r)
 Recivier – KF707 W.T. (Amp^r)
 Helper – *E. coli* HB101 pRK2013 (Km^r)



C Colony PCR

Colony PCR and sequencing analysis to confirm the deletion

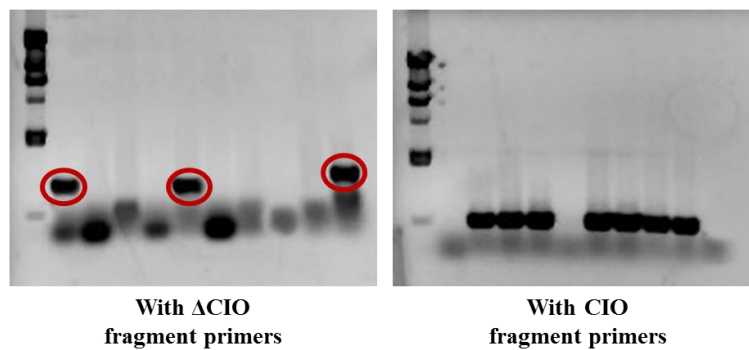















































Figure 2.12: Example for obtaining KF Δ CIO mutant strain. **A)** Gene SOEing technique; PCR for amplification of upstream and downstream 500 bp fragment, PCR overlap for Δ CIO deletion construct, cloning Δ CIO fragment in pG19II conjugation vector using *Bam*HI and *Eco*RI enzymes. **B)** Conjugation protocol with two steps of homologous recombination. **C)** Screening by two different Colony PCR to obtain KF Δ CIO.

Table 2.5: List of KF707 mutant strains obtained using Gene SOEing PCR technique and conjugation. The table shows the name of the mutant, the deleted proteins and the conjugation mix used.

Mutant strain	Terminal oxidases					Conjugation mix
	Caa ₃	Caa ₃	Cbb ₃ 1	Cbb ₃ 2	CIO	
KF Δ cox1						D: <i>E. coli</i> DH5 α pG19II Δ cox1 R: KF707 W.T. H: <i>E. coli</i> HB101 pRK2013
KF Δ cox2						D: <i>E. coli</i> DH5 α pG19II Δ cox2 R: KF707 W.T. H: <i>E. coli</i> HB101 pRK2013
KF Δ cox1-2						D: <i>E. coli</i> DH5 α pG19II Δ cox1 R: KF Δ cox2 H: <i>E. coli</i> HB101 pRK2013
KF Δ cco1						D: <i>E. coli</i> DH5 α pG19II Δ cco1 R: KF707 W.T. H: <i>E. coli</i> HB101 pRK2013
KF Δ cco2						D: <i>E. coli</i> DH5 α pG19II Δ cco2 R: KF707 W.T. H: <i>E. coli</i> HB101 pRK2013
KF Δ cco1-2						D: <i>E. coli</i> DH5 α pG19II Δ cco1-2 R: KF707 W.T. H: <i>E. coli</i> HB101 pRK2013
KF Δ CIO						D: <i>E. coli</i> DH5 α pG19II Δ CIO R: KF707 W.T. H: <i>E. coli</i> HB101 pRK2013
KF Δ cox1-2/CIO						D: <i>E. coli</i> DH5 α pG19II Δ CIO R: KF Δ cox1-2 H: <i>E. coli</i> HB101 pRK2013
KF Δ cox1-2/cco1-2						D: <i>E. coli</i> DH5 α pG19II Δ cco1-2 R: KF Δ cox1-2 H: <i>E. coli</i> HB101 pRK2013

The green squares indicate the oxidases present, the red ones the oxidases eliminated.

In the mix: R = receiver, D = donor and H = helper.

2.3.3 Phenotype analysis of KF707 mutant strains

Phenotypical analyses were conducted using KF707 W.T. and mutants lacking one or multiple oxidases; in these first set of experiments, single mutants were not used in order to understand the contribution of each type of oxidase to the cell phenotype.

We initially used the NADI assay (Figure 2.13). This test was performed, in KF707 W.T. and mutant strains, on solid medium (LB plates) and in liquid minimal medium (MSM), adding different single carbon sources [6 mM each]. The NADI assay aims to visualize the cytochrome *c* oxidase respiratory activity following the time-course oxidation of the artificial electron donor *N,N*-dimethyl-*p*-phenylenediamine (DMPD), which appears colorless in its reduced state and blue/purple when oxidized to indophenol. In cells grown on LB and MSM medium with glucose, fumarate, benzoate and *p*-hydroxybenzoate, the assay was negative in the case of KF Δ cco1-2 and KF Δ cox1-2/cco1-2 mutants, suggesting a negligible activity of *caa*₃-type oxidase. On the contrary, in cells grown on biphenyl, the assay was negative only in the case of Δ cox1-2/cco1-2, suggesting a role of the *caa*₃-type oxidase with this carbon source (Figure 2.13 red square).

In the second set of experiments, the growth rate of KF707 W.T. and mutant strains were analyzed for their capacity to grow aerobically in LB or minimal medium with the same single carbon source used for the previous experiment. In all experiments (repeated three times for each strain), the growth curves were determined by monitoring the cell density (OD_{600 nm}), every two hours until the stationary phase was reached. As shown in Figure 2.14, the two mutants KF Δ cco1-2 and KF Δ cox1-2/cco1-2 were clearly impaired in their aerobic growth rate as compared to KF W.T. except in the case of biphenyl. Notably, these two mutants do not reach the final OD_{600 nm} value of the W.T. strain. Similarly, KF Δ cco1-2 and KF Δ cox1-2/cco1-2 strains were shown to grow slowly in biphenyl during the exponential phase, as compared to W.T. although, at the end of the growth they were able to reach the same OD_{600 nm} value of the W.T. strain. The results indicated also that the KF Δ CIO, KF Δ cox1-2 and KF Δ cox1-2/CIO mutant growth curves were similar to KF707 W.T strain regardless of the carbon source used for growth (Figure 2.14).

These results, taken together, indicate that the KF707 optimal growth rates, with these carbon sources, depends on the presence of *cbb3*-type oxidases. In addition, the ability of the KF Δ cco1-2 and KF Δ cox1-2/*cco1-2* mutant cells to reach the same OD_{600 nm} of the KF W.T. strain could suggest that, during the stationary phase, with biphenyl, there is a different modulation of the terminal oxidases.

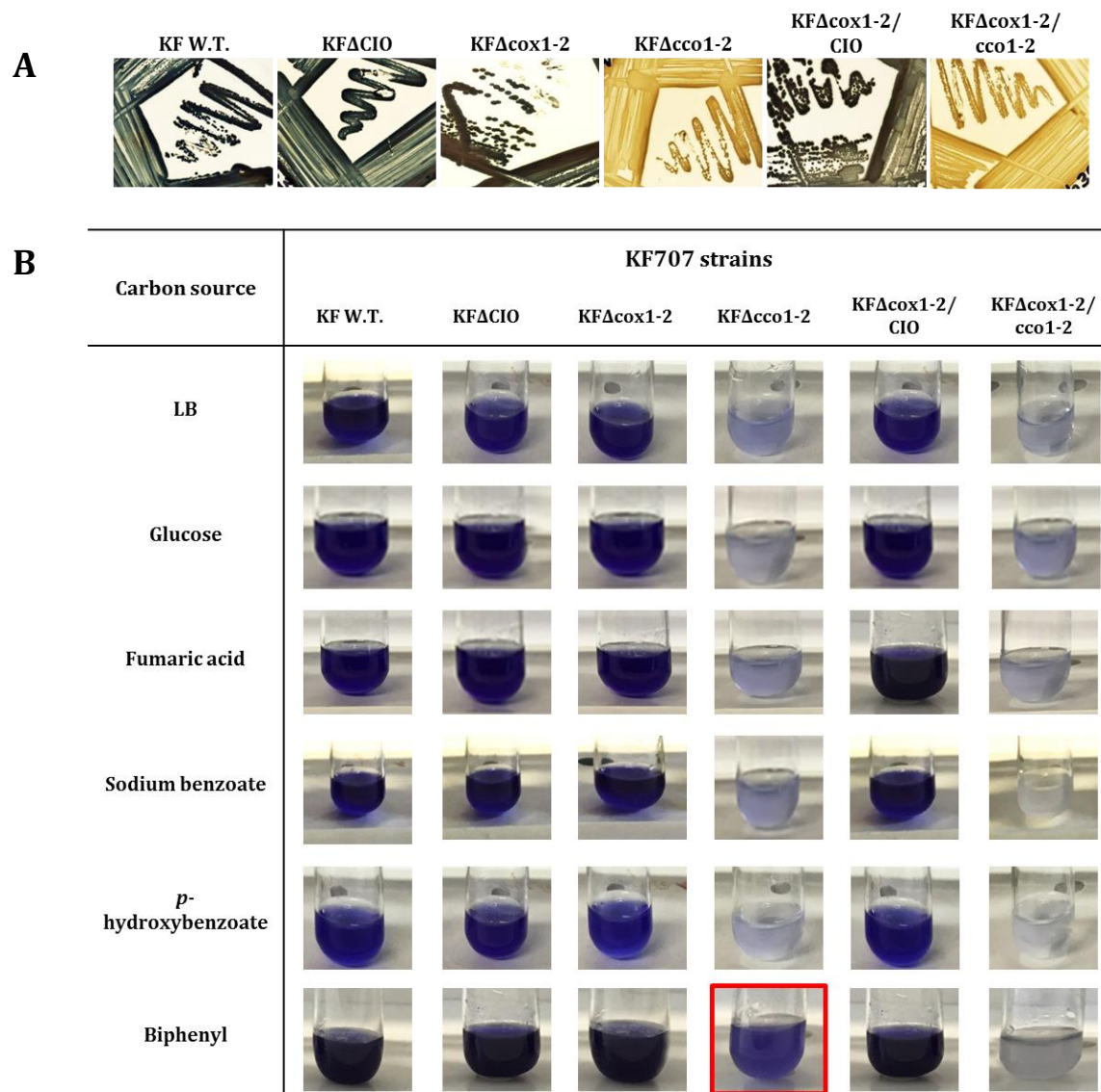


Figure 2.13: NADH assay in KF707 W.T. and mutant strains (KF Δ C10, KF Δ cox1-2, KF Δ cco1-2, KF Δ cox1-2/C10 and KF Δ cox1-2/*cco1-2*). **A)** NADH assay on LB plates, after an overnight growth at stationary phase. **B)** NADH assay in liquid, LB, or MSM medium with glucose, fumarate, benzoate, *p*-hydroxybenzoate and biphenyl [6 mM]; the assay was performed after an overnight growth with 1 mL of culture. In both cases were used 3 mL or 100 μ L, respectively, of a 1:1 mixture of 35 mM α -naphthol, in ethanol, and 30 mM N,N-dimethyl-*p*-phenylenediamine (DMPD) in water.

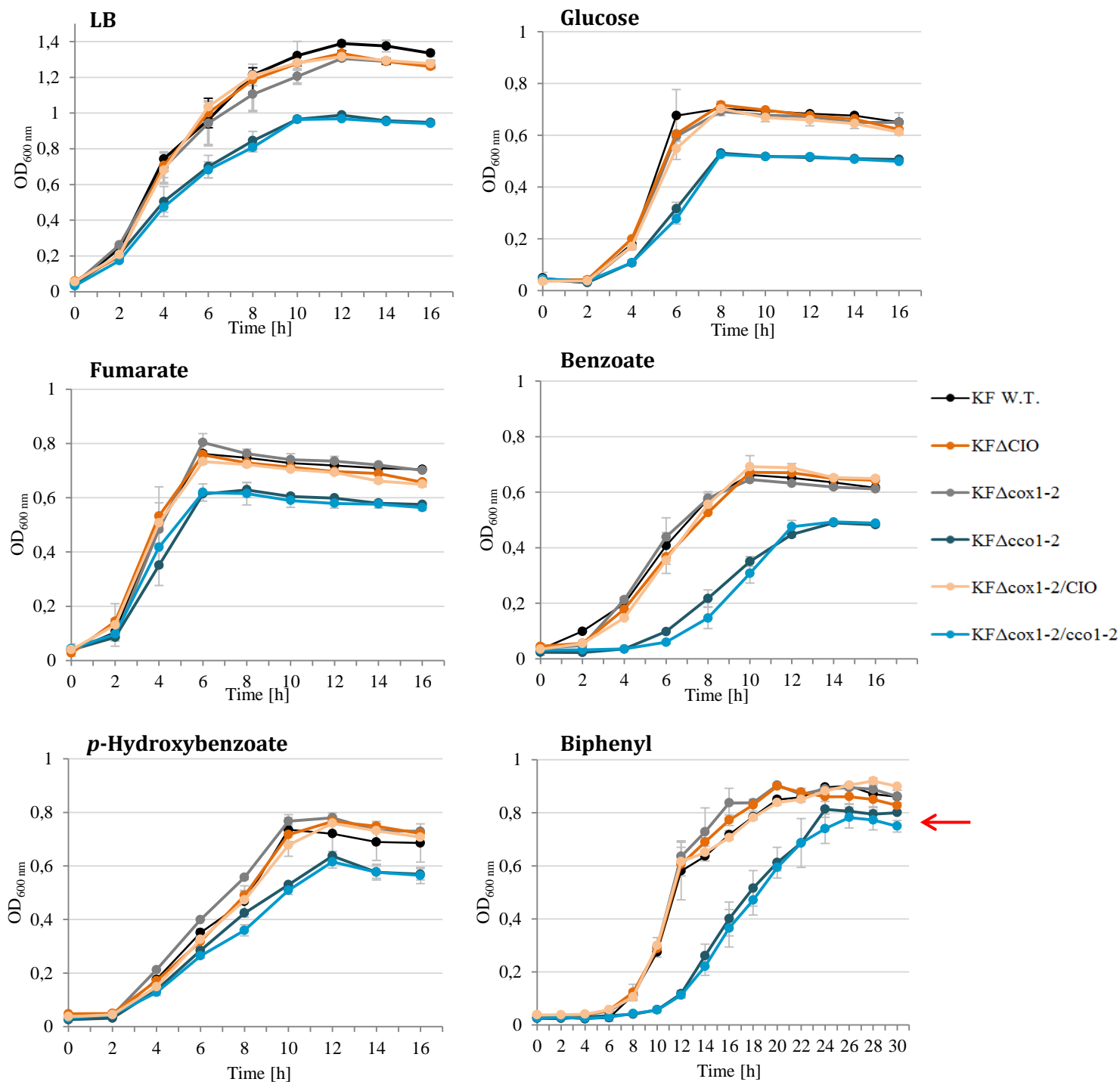


Figure 2.14: Growth curves of KF707 W.T. and deletion mutant strains. Strains were grown in 50 mL of LB or MSM medium in 250 mL flasks shaken at 130 rpm, with 6 mM of glucose, fumarate, benzoate, *p*-hydroxybenzoate and biphenyl. The optical densities were evaluated at 600 nm every two hours and growth was stopped at late-stationary phase. The red arrow indicates that in MSM with biphenyl, the two mutant strains KF Δ cco1-2 and KF Δ cox1-2/cco1-2, at the stationary phase, reach the same OD value of the KF W.T. strain.

2.3.4 KF707 *lacZ* translational fusion strains and oxidases expression

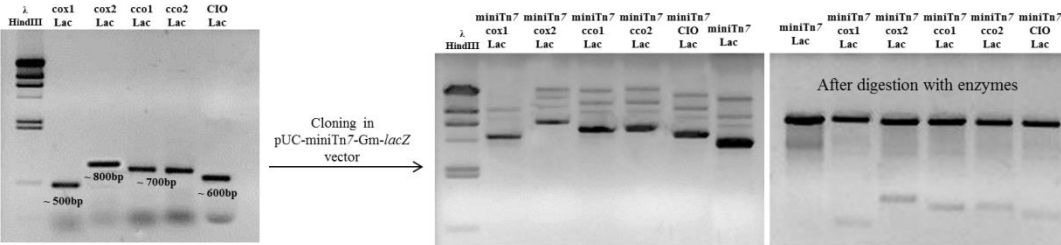
Since the phenotype analysis conducted on KF707 W.T. and oxidase mutant strains showed the possible involvement of the *caa*₃-type oxidases during the growth in MSM with biphenyl (KF707 is capable to aerobically degrade PCBs in the presence of biphenyl as co-metabolite [Abramowicz, 1990]), we thought to determine the expression of the entire set of putative genes for KF707 terminal oxidases in cells grown in LB medium, and in MSM with defined carbon sources [6 mM] such as glucose, fumarate, benzoate, *p*-hydroxybenzoate and biphenyl, to better understand if the modulation of these enzymes really depends on the carbon source used. To evaluate the activity of the terminal oxidases, β -galactosidase assays were performed in mutant strains containing translational fusions of the terminal oxidases with the *lacZ* gene. The *lacZ*-containing strains were constructed utilizing a Tn7-based method and the translational fusion fragments were inserted into the genome of KF707 at the *attTn7* site located downstream of *glmS* [Choi and Schweizer, 2006; 2.2.5 Materials and Methods].

For each terminal oxidase, the respective translational fusion strains were obtained: KFcox1Lac, KFcox2Lac, KFcco1Lac, KFcco2Lac and KFCIOLac. The promoter region, the ATG start codon and the coding region for the first 10 amino acids of *coxII* (for Caa₃ – KFcox1Lac), *coxM* (for Ccaa₃ – KFcox2Lac), *ccoN1* (for Cbb₃1 – KFcco1Lac), *ccoN2* (for Cbb₃2 – KFcco2Lac) and *cioA* (for CIO – KFCIOLac), were amplified obtaining ~500-800 bp fragments (Figure 2.15A). Then, these fragments were cloned into the pUC-miniTn7-Gm-*lacZ* vector and the resultant plasmids were electroporated, with the helper plasmid pTNS3 [Choi et al., 2005], into KF707 electrocompetent cells; then, cells containing the Tn7 insertion, were selected by gentamicin and X-gal. After that, the gentamicin-resistant gene was removed by the Flp-*FRT* recombinase system [Hoang et al., 1998]. pFLP2, encoding Flp recombinase, was transferred by electroporation to the Tn7-containing cells, and colonies that carried pFLP2 were selected by kanamycin and X-gal. At the end, pFLP2 was removed from the obtained transformants by *sacB*-based counter selection on LB plates containing 10% of sucrose and X-gal (Figure 2.15B). With this method, all five KF707 translational fusion strains were obtained. As Figure 2.8C shows, once the mutants were streaked on LB plates with X-gal, they showed different blue color intensity. KFcox2Lac and KFCIOLac were less colorful compared to the other strains, while the KFcco2 was the one with the most

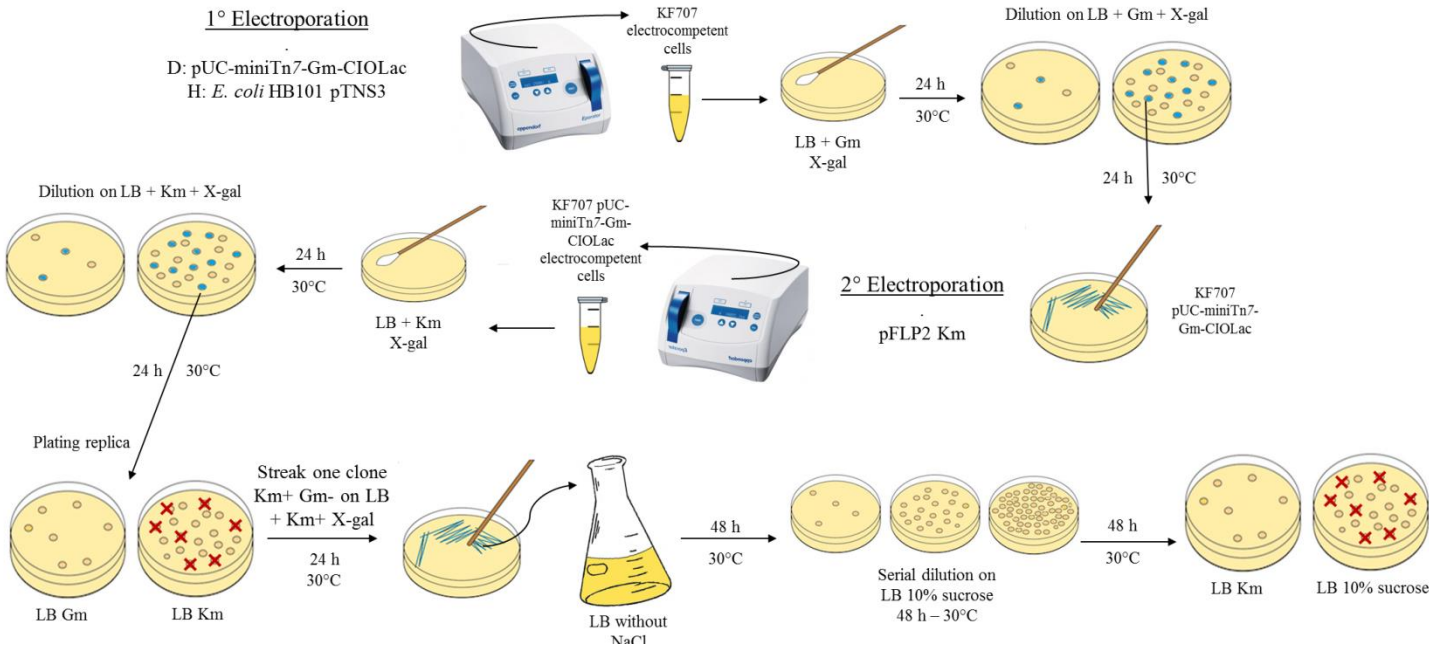
intense coloration (Figure 2.15C); this latter phenotypic evidence supports the previous results, obtained through the deletion mutants, where *cbb3*-type cytochrome *c* oxidases were crucial for the proper functioning of the respiratory chain and the growth.

Using the translational fusion strains, the β -galactosidase assay were performed at 30°C in cells grown in LB medium or MSM minimal medium with different carbon sources [6 mM each], at two different growth phases: exponential phase ($OD_{600\text{ nm}}$ 0.3-0.5) or stationary phase ($OD_{600\text{ nm}}$ 0.7-0.9), using standard protocols reported in Chapter 2.2.6; each experiment was repeated at least six times. As shown in Figure 2.9 the single contribution of each oxidase was calculated as the percentage of the total expression. With LB and all the single carbon sources used for these experiments, the *cco1* promoter for the Cbb₃₁ exhibited similar basic level of expression (between 20-30 %) in both exponential and stationary phase. The contribution to the respiratory chain for the *cox2* promoter, of the Ccaa₃ oxidase, and for the *cioA* promoter, of the CIO oxidase, showed very low levels (always less than 5%) in LB and with all carbon sources, in both exponential and/or stationary grown cells. With the *cco2* promoter for the Cbb₃₂, an higher contribute (more than 50-60%) was observed in cells grown on LB, glucose, fumarate, benzoate and *p*-hydroxybenzoate, under exponential and stationary phases. In contrast to *cco2*, in LB and the carbon sources mentioned above, the *cox1* promoter for the Caa₃ oxidase had a low expression in cells harvested at their exponential growth phase (less than 10%), while an increase in its expression (~20%) was seen during the stationary growth phase (Figure 2.16). The most relevant case was seen in cells grown with biphenyl; here the *cco2* promoter showed a high expression level (57%) in the exponential phase that became very low (10%) in the stationary phase of growth. Interestingly, the drop of the *cco2* contribution, in stationary phase, was paralleled with a drastic increase of *cox1* expression, being 13% during exponential phase and 60% during stationary phase (Figure 2.16).

A Translational fusion constructs



B Translational fusion strains



C

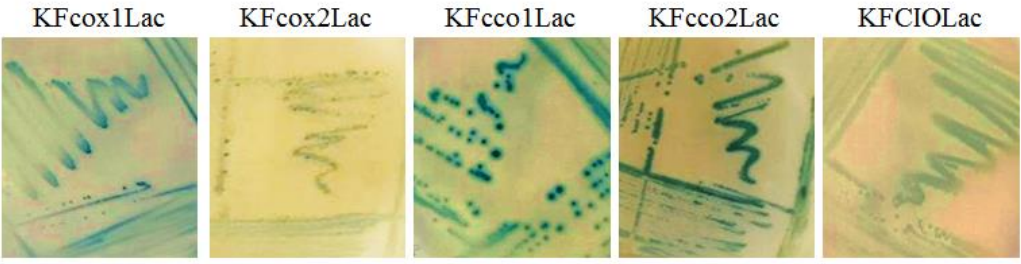


Figure 2.15: KF707 translational fusion strains obtained. **A)** Amplification of oxidases “promoter fragments” containing promoter region, ATG start codon and the first 10 amino acids; cloning of these fragments into pUC-miniTn7-Gm-lacZ vector. **B)** Protocol for translational fusion strains; see Chapter 2.2.6 for the details. **C)** KF707 mutant strains obtained, streaked on LB plates + X-gal to confirm the presence of the lacZ gene fusion.

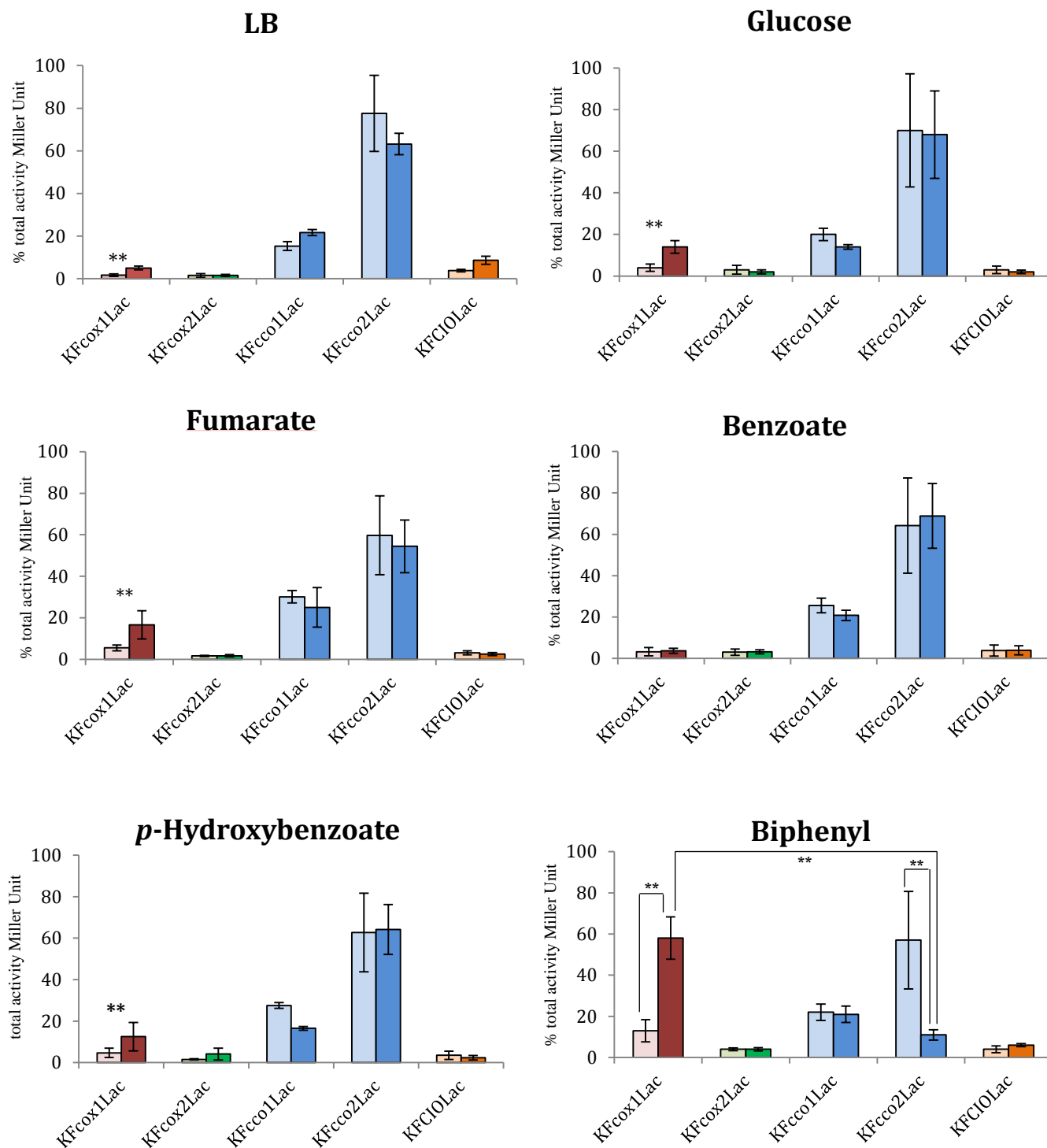


Figure 2.16: β -galactosidase activities measured in cell extracts derived from the KF707 translational fusion strains, grown aerobically in LB or MSM medium with glucose, fumarate, benzoate, *p*-hydroxybenzoate and biphenyl [6 mM each] as sole carbon source. The assays were performed at two different stages of growth (**exponential** - light bars / **stationary** - dark bars) and the activities are presented as percentage of total activity. Asterisks indicate that mean values are significantly different according to one-way ANOVA and verified by a two samples *T*-test within pairs of strains (** $p < 0.01$).

2.3.5 Spectroscopic analysis and Respiratory activities

To further analyze the role and contribution of the *caa₃*-type oxidases in cells grown in biphenyl during the stationary phase, spectroscopic analysis and respiratory activities assays were conducted on KF707 W.T. and deletion mutant strains in order to compare the situation of the strains grown in biphenyl with strains grown on a defined carbon source such as glucose. For the haem-spectroscopic analysis and respiratory activities, cells were grown on glucose and/or biphenyl until stationary phase, then cells were harvested and washed twice with phosphate buffer [0.1 M] before membrane fragments were obtained using French pressure cell and ultracentrifugation in MOPSO buffer [50 mM, pH 7.2] containing MgCl₂ [5 mM]. Finally, membranes were suspended at a known protein concentration [5-10 mg/mL] in the same buffer.

The haem-spectroscopic features of membranes isolated from cells grown in glucose or/and in biphenyl and harvested at their stationary phase of growth, was evaluated with a Jasco 7800 spectrophotometer and all the collected data are reported in Table 2.6 and Figure 2.17.

The spectroscopic evaluation of membranes from glucose grown cells showed that the α band, attributable to *a*-type haem, is barely detectable at 600-605 nm. Conversely, an evident peak at 600-605 nm, which is given by *a*-type haem, was seen in KF707 W.T. membranes from cells grown on biphenyl (Figure 2.17; Table 2.6). This observation is in line with the results obtained with the β -galactosidase experiments (reported in the previous paragraph), showing that the *cox1* promoter activity for the Caa₃ oxidase is 4-times (15% versus 60%) enhanced in KF707 biphenyl grown cells during the stationary phase.

Regarding the presence of other haem types, the spectroscopic results also indicate a significant drop of the peak at 550-555 nm, attributable to *c*-type haem, in KF Δ *cox1-2* and/or KF Δ *cco1-2* mutants, this decrease being even more significant in KF Δ *cox1-2/cco1-2* mutant cells grown in both of glucose and biphenyl (Figure 2.17; Table 2.6). These data suggest that the protein subunits encoded by the gene clusters *coxI-II-III*, *coxMNOP*, *ccoN101Q1P1* and *ccoN202Q2P2* all contain considerable amounts of *c*-type haems as predicted by BLASTP search and alignment analysis.

Table 2.6: Haem amounts of *a*-, *b*- and *c*-type in membranes isolated from KF707 W.T. and mutant strains grown in MSM medium with glucose or biphenyl [6 mM] as sole carbon source.

Carbon source	Strain	<i>c</i> -type haem	<i>b</i> -type haem	<i>a</i> -type haem
		$\epsilon_{551-540} = 19.1$ [nmoles/mg protein]	$\epsilon_{561-575} = 22$ [nmoles/mg protein]	$\epsilon_{603-630} = 11.6$ [nmoles/mg protein]
GLUCOSE	KF707 W.T.	1,65±0,20	0,77±0,08	0,10±0,05
	KF Δ cox1-2	1,50±0,20	0,80±0,09	n.d.
	KF Δ cco1-2	0,95±0,15	0,62±0,07	0,12±0,05
	KF Δ cox1-2/ <i>cco</i> 1-2	0,74±0,10	0,64±0,07	n.d.
	KF Δ CIO	1,42±0,15	0,84±0,10	0,12±0,05
	KF Δ cox1-2/CIO	1,09±0,12	0,61±0,07	n.d.
BIPHENYL	KF707 W.T.	1,80±0,20	0,87±0,10	0,45±0,03
	KF Δ cox1-2	1,10±0,09	0,82±0,10	n.d.
	KF Δ cco1-2	0,86±0,07	0,59±0,06	0,27±0,02
	KF Δ cox1-2/ <i>cco</i> 1-2	0,65±0,08	0,32±0,01	n.d.
	KF Δ CIO	0,78±0,09	0,50±0,03	0,30±0,02
	KF Δ cox1-2/CIO	0,81±0,07	0,55±0,03	n.d.

Symbols and abbreviations used: n.d., not-detectable by optical spectroscopy at room temperature. Values are the mean of at least two membrane preparations from different growth cultures for each strain.

Respiratory activities assays, in membrane fragments isolated from KF707 W.T. and deletion mutant strains, grown until stationary phase with glucose or biphenyl [6 mM] as sole carbon source, were determined by monitoring the oxygen consumption with a Clark-type oxygen electrode YSI 53, as described in 2.2 Materials and Methods. Early results in *R. sphaeroides* indicated that both *aa*₃ and *cbb*₃-type oxidases [Cramer and Knaff, 1990], were inhibited by cyanide (CN⁻) and azide (N₃⁻) anions. However, while 50 μ M CN⁻ fully inhibited both the *aa*₃ and *cbb*₃-type cytochrome *c* oxidase activities, 50 μ M N₃⁻ only inhibited the *cbb*₃ dependent activities. In this way, in the presence of 50 μ M cyanide or azide, it was possible to determine the contribution of *aa*₃-type and/or *cbb*₃-type oxidases to the total respiratory activity catalyzed by cytochrome *c* oxidases [Daldal et al., 2001].

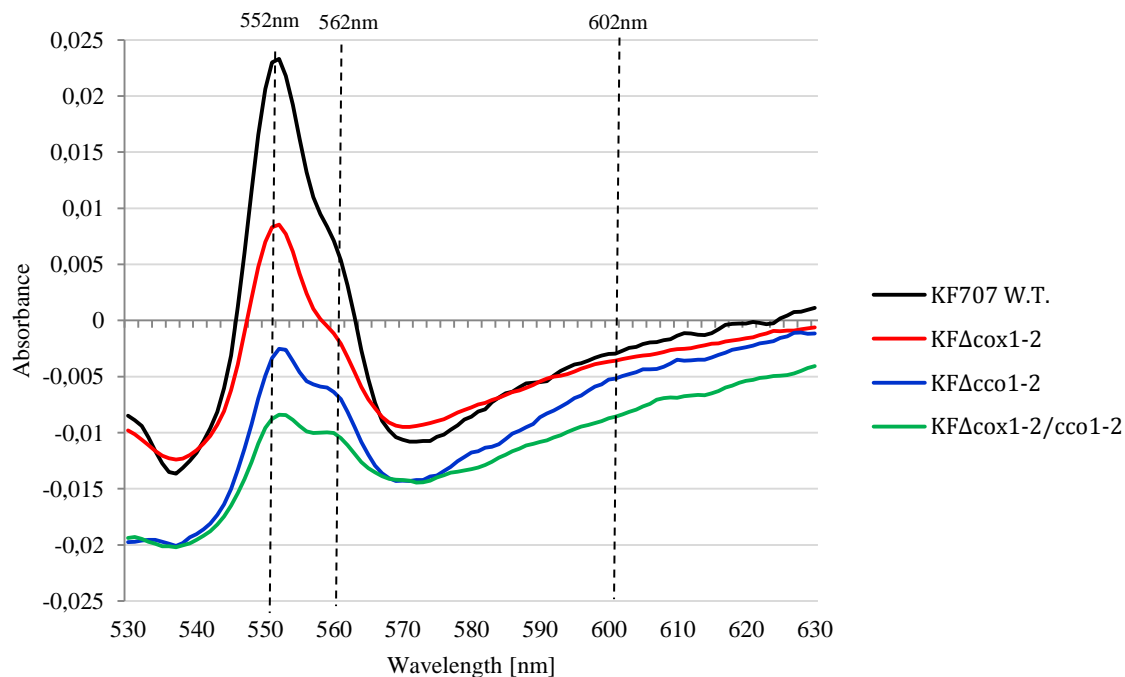
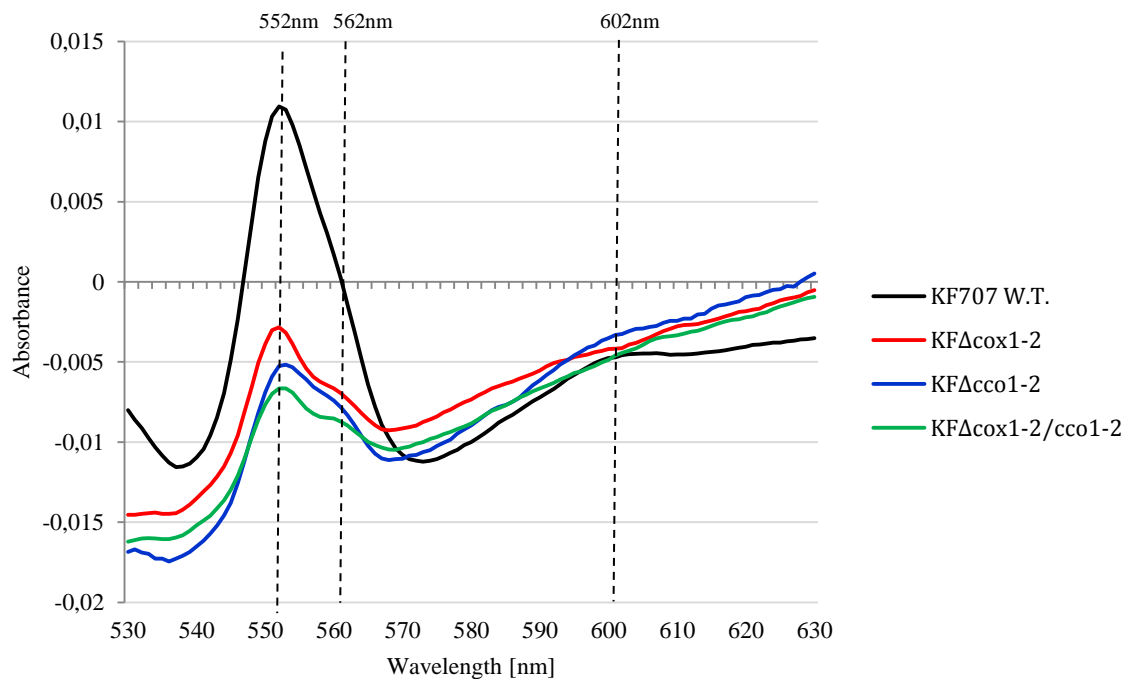
A Glucose**B Biphenyl**

Figure 2.17: Reduced-minus-oxidized different spectra of membrane fragments from cells of KF707 W.T. and mutants grown with glucose and/or biphenyl as carbon source. Samples were oxidized with a few crystals of $K_4[Fe(CN)_6]$ and reduced with NADH [0.5 mM]. Spectra were recorded from samples having the following membrane protein concentrations: **A)** glucose: W.T., 10.7 mg/mL, $KF\Delta\text{cox1-2}$, 11.9 mg/mL, $KF\Delta\text{cco1-2}$ and $KF\Delta\text{cox1-2}/\text{cco1-2}$, 11 mg/mL. **B)** biphenyl: W.T., 8 mg/mL, $KF\Delta\text{cox1-2}$, 6 mg/mL, $KF\Delta\text{cco1-2}$ and $KF\Delta\text{cox1-2}/\text{cco1-2}$, 7 mg/mL.

The data reported in Table 2.7 were obtained from experiments performed in membrane from KF707 W.T. and mutant strains. In these cases, the same inhibitor concentration was used to estimate the activities of KF707 *caa3* and *ccb3* oxidase types in the or absence of cyanide and azide; all values were expressed as nanomoles of O₂ consumed min⁻¹ mg of proteins⁻¹. As shown in Table 2.7 (left part), with NADH as electron donor, the total oxygen consumption by KF707 W.T. membrane from cells grown in glucose was 57% inhibited by azide [50 μM] (from 165±10 to 72±3.3), this inhibition value represents the contribution of *ccb3*-type oxidases to respiration, while only a further 26% was inhibited by cyanide [50 μM] (from 72±3.3 to 29±5) indicating the contribution by *caa3*-type oxidases. The NADH oxidation, when measured in membranes from biphenyl grown cells, was 42% inhibited by azide [50 μM] (from 111±2.5 to 64±9.5), while a further 52% (from 64±9.5 to 7±0.3) of the total respiration was sensitive to cyanide [50 μM]. From these results, it appears that the % contribution to the NADH respiration of *caa3*-type oxidases, that are resistant to azide [50 μM] but sensitive to cyanide [50 μM], was 2-fold higher in biphenyl (52%) than in glucose (26%).

Similar experiments were also conducted with ascorbate/TMPD as electron donor, Table 2.7 (right part); in these cases, the activity observed indicate the overall oxygen consumption catalyzed by cytochrome *c* oxidases. In glucose, the activity was 80% (from 157±20 to 32±3) inhibited by azide, versus the 47% (from 165±13 to 88±13) showed in biphenyl membranes, confirming the main role of *ccb3*-type oxidases in glucose but not in biphenyl.

All the results obtained in W.T. membranes were confirmed by activities determined in membranes from oxidase mutant cells. The mutant lacking both Cbb31 and Cbb32 oxidases (KFΔcco1-2) showed strong activation of the CIO dependent activity in glucose (72% resistant to cyanide, from 175±15 to 125±1); interestingly, the CIO activation in these mutant cells grown in biphenyl, was less evident (30% resistant to cyanide, from 96±9.3 to 29±0.4). In this latter case, the 83% (from 96±9.3 to 80±12) of the NADH activity was insensitive to azide, confirming the main role of *caa3*-type oxidases using biphenyl as carbon source (Table 2.7 left part). Accordingly, in the same mutant KFΔcco1-2, the ascorbate/TMPD oxidation was only 8% (from 117±12 to 108±5) inhibited by azide, while 95% was sensitive to cyanide (Table 2.7 right part).

The activation and the functional role of CIO in supporting NADH dependent respiration in glucose was also seen in the quadruple mutant KF Δ cox1-2/*cco1-2*, whose respiratory activity was 96% insensitive to cyanide [50 μ M] (from 174 \pm 15 to 167 \pm 15) (Table 2.7 right part). These data were also used to determine in KF Δ cox1-2 in glucose, in KF Δ cco1-2 in biphenyl and in KF Δ cox1-2/*cco1-2* grown in biphenyl, the inhibitory concentrations (IC₅₀) for cyanide of *cbb*₃-type, *caa*₃-type and CIO oxidase activities, which were in order of 4 10⁻⁷ M CN⁻, 5 10⁻⁶ M CN⁻ and 1 mM CN⁻, respectively (Figure 2.18) (IC₅₀ is the concentration of an inhibitor required to inhibit 50% of the target enzymatic activity).

Table 2.7: Respiratory activities in membranes from KF707 W.T. and oxidase mutant cells grown in glucose and/or in biphenyl, as sole carbon source, until the stationary phase.

	Electron donors	NADH			ASCORBATE			
		Additions	/	N ₃ ⁻	CN ⁻	Cyt <i>c</i>	TMPD	TMPD/N ₃ ⁻
Strains								
GLUCOSE	KF W.T.	165 ± 10	72 ± 3.3	29 ± 5.0	33 ± 1.0	157 ± 20	32 ± 3.0	7 ± 2.0
	KF Δ cox1-2	178 ± 20	38 ± 8.0	34 ± 10	59 ± 6.0	221 ± 14	21 ± 2.5	16 ± 1.0
	KF Δ cco1-2	175 ± 7.0	160 ± 2.0	125 ± 1.0	9 ± 0.5	38 ± 5.0	32 ± 3.3	8 ± 1.0
	KF Δ cox1-2/ <i>cco1-2</i>	174 ± 15	172 ± 15	167 ± 15	1 ± 0.2	11 ± 2.0	11 ± 2.0	11 ± 2.0
	KF Δ CIO	145 ± 30	29 ± 5.0	1 ± 0.2	37 ± 3.5	208 ± 31	35 ± 3.5	10 ± 0.5
	KF Δ cox1-2/CIO	145 ± 5.0	25 ± 5.0	2 ± 1	45 ± 7.0	163 ± 12	10 ± 2.5	10 ± 2.5
BIPHENYL	KK W.T.	111 ± 2.5	64 ± 9.5	7 ± 0.3	37 ± 2.0	165 ± 13	88 ± 15	7 ± 2.0
	KF Δ cox1-2	38 ± 5.0	9 ± 3.3	3 ± 0.2	17 ± 3.0	75 ± 10	5 ± 2.0	3 ± 2.0
	KF Δ cco1-2	96 ± 9.3	80 ± 12	29 ± 0.4	18 ± 3.0	117 ± 12	108 ± 5.0	6 ± 1.7
	KF Δ cox1-2/ <i>cco1-2</i>	36 ± 5.0	35 ± 5.0	35 ± 0.5	2 ± 1.0	6 ± 2.5	6 ± 2.5	6 ± 2.5
	KF Δ CIO	83 ± 4.0	60 ± 5.0	4 ± 2.0	37 ± 0.4	174 ± 1.0	110 ± 5.0	12 ± 1.0
	KF Δ cox1-2/CIO	104 ± 4.0	15 ± 2.5	3.5 ± 1.5	8.3 ± 3.5	67 ± 1.0	9.3 ± 2.0	8.3 ± 2.0

*Symbols and abbreviations used: N₃⁻, sodium azide [50 μ M]; CN⁻, potassium cyanide [50 μ M]; Cyt *c*, horse heart cytochrome *c* [50 μ M]; TMPD, N,N,N',N'-tetramethyl-*p*-phenylene diamine [50 μ M]. Rates, expressed as nmoles of O₂ consumed min⁻¹ mg of protein⁻¹, are the mean of at least two/three membrane preparations from independent cell cultures.*

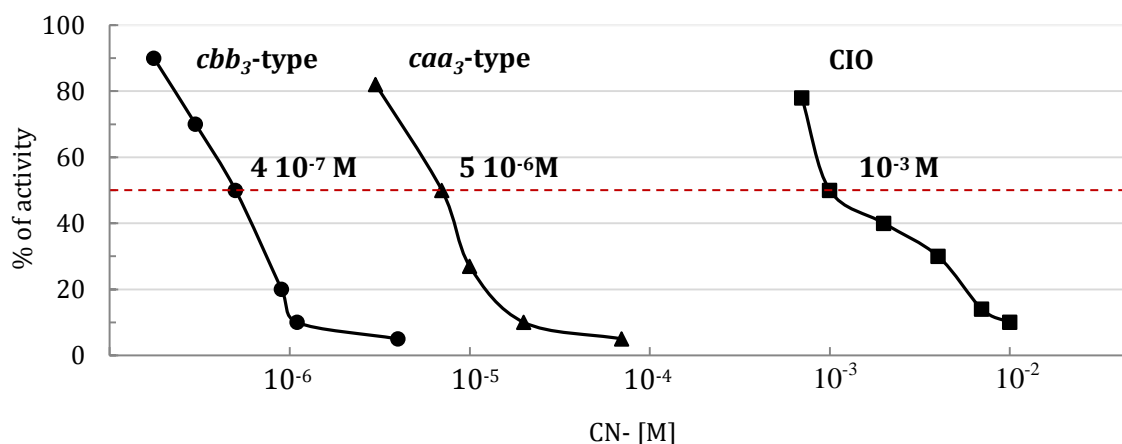


Figure 2.18: Inhibition of the terminal oxidase activities in KF707 membranes. Cytochrome *c* oxidase catalyzed by *cbb₃* and *caa₃*-type oxidases were determined as ascorbate/TMPD oxygen reduction in membranes of $KF\Delta\text{cox1-2}$ cells grown in glucose and $KF\Delta\text{cco1-2}$ cells grown in biphenyl, respectively. CIO oxidase was determined as NADH oxygen reduction in membranes of $KF\Delta\text{cox1-2}/\text{cco1-2}$ cells grown in biphenyl. The inhibition values are the mean of two independent membrane preparations. Continuous line connecting the experimental points do not represent a mathematical function. The three values for CI_{50} CN- are reported in the graph and the red line indicates the 50% of activities.

2.3.6 The cyanide-insensitive oxidase (CIO) overexpression

In order to better understand the overexpression of the CIO oxidase, a series of experiments were conducted on single mutants $KF\Delta\text{cco1}$ and $KF\Delta\text{cco2}$.

In *P. aeruginosa* PAO1, it has been observed that the deletion of the gene cluster for *Cbb₃1* oxidase causes an up-regulation of the CIO promoter, a phenomenon not seen when the *Cbb₃2* oxidase was deleted [Kawakami et al., 2010; Arai, 2011].

From results of Table 2.7 it is apparent that the deletion of *cbb₃*-type oxidases induces an increase of the cyanide resistant activity, which may be related to a higher expression of the CIO oxidase; this increase is not observed in the case of *caa₃*-type oxidase mutants.

To clarify the role of each of the two *Cbb₃* oxidases in determining the activation of the CIO oxidase activity and the contribution of each oxidase to the total respiration, the oxygen consumptions in membranes from $KF\Delta\text{cco1}$ and $KF\Delta\text{cco2}$ were observed. Membranes were derived from cells grown with glucose or biphenyl as sole carbon source until stationary phase; the experiments were conducted as previously described.

As Table 2.8 shows, in glucose grown cells, the CIO catalyzes 56% (from 196 ± 7 to 110 ± 3.0) of the total respiration of $KF\Delta\text{cco1}$, being 3 times higher than the corresponding activity

measured in KF Δ cco2 and W.T. membranes, with a parallel minor role (16%) of the Cbb₃2 oxidase. Differently, in KF Δ cco2 membranes the Cbb₃1 oxidase catalyzes 65% of the total respiration compensating the low CIO activity (only 23%). Interestingly, in biphenyl grown cells the CIO catalyzes 33% (from 111 \pm 8.0 to 37 \pm 2.0) of the total CN⁻ resistant NADH respiration of KF Δ cco1 with a parallel minor role of the Cbb₃2 oxidase (13%) and a prevalent contribution of the Caa₃ oxidase (54% observed with the addition of azide) to respiration. In KF Δ cco2, the CIO activity decreased to 12% of the total NADH oxidation with a parallel increase of the contribution to respiration of Cbb₃1 (52%) and a slight decrease of Caa₃ oxidase activity (36%).

Accordingly, the β -galactosidase assays performed in KF Δ cco1CIOlac and KF Δ cco2CIOlac translational fusion strains cells grown with glucose (Figure 2.19), indicated that the expression of CIO in KF Δ cco1-2 and KF Δ cco1 increases \sim 3.5 times as compared to that of KF Δ cco2; in addition, this expression was 10 times more than that of the CIO activity in W.T. strain. The same analysis, conducted in cells grown with biphenyl, showed different results (Figure 2.19); in this case, the CIO expression was almost the same for both mutant strains (KF Δ cco1 and KF Δ cco2), the level of the CIO promoter expression being only 4-5 times more as compared to the W.T. These data are in line with what we have previously observed as in cells grown with biphenyl and harvested in their stationary phase, the respiratory activity mainly depends on *caa*₃-type oxidases.

Table 2.8: Respiratory activities in membranes from KF707 W.T. and Cbb₃ oxidase mutant cells grown in glucose and/or in biphenyl, as sole carbon source, until the stationary phase.

Strain	NADH			
	/	N ₃ ⁻	CN ⁻	
GLUCOSE	KF W.T.	165 ± 10	72 ± 3.3	29 ± 5.0
	KFΔcco1-2	175 ± 7.0	160 ± 2.0	125 ± 1.0
	KFΔcco1	196 ± 7.0	165 ± 2.0	110 ± 3.0
	KFΔcco2	220 ± 15	78 ± 5.0	51 ± 5.0
BIPHENYL	KK W.T.	111 ± 2.5	64 ± 9.5	7 ± 0.3
	KFΔcco1-2	96 ± 9.3	80 ± 12	29 ± 0.4
	KFΔcco1	111 ± 8.0	97 ± 7.0	37 ± 2.0
	KFΔcco2	95 ± 5.0	46 ± 5.0	11 ± 3.0

Symbols and abbreviations used: N₃⁻, sodium azide [50 μM]; CN⁻, potassium cyanide [50 μM]. Rates, expressed as nmoles of O₂ consumed min⁻¹ mg of protein⁻¹, are the mean of at least two/three membrane preparations from independent cell cultures.

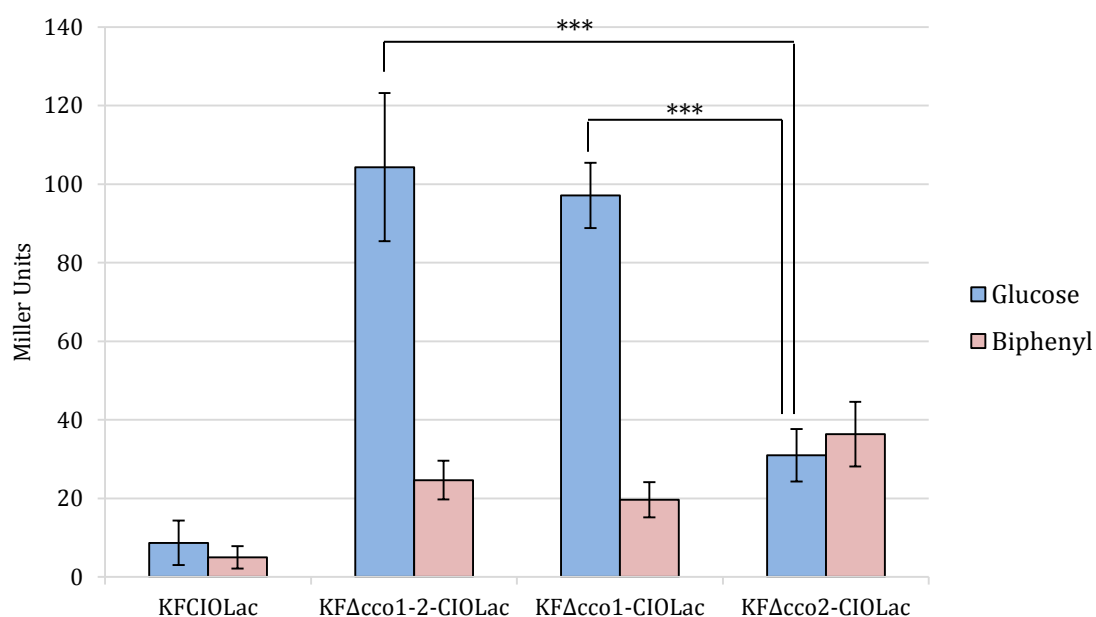


Figure 2.19: β-galactosidase activities measured in cell extracts derived from the KFCIOlac, KFΔcco1-2CIOlac, KFΔcco1CIOlac and KFΔcco2CIOlac translational fusion strains, grown aerobically in MSM medium with glucose or biphenyl [6 mM] as sole carbon source. The assays were performed at stationary phase of growth and the activities are presented as Miller Units. Asterisks indicate that mean values are significantly different according to two samples *T*-test within pairs of strains (***) ($p < 0.001$).

2.4 Discussion

2.4.1 The branched respiratory chain of KF707 terminal oxidases

In the past, the Haem-Copper Oxygen (HCO) reductases were classified into three families: (1) Type A or mitochondrial like oxidases of *aa₃*-type; (2) Type B or *ba₃*-type oxidases; and (3) Type C or *cbb₃*-type oxidases which are only detected in bacteria [Sousa et al., 2012]. Additionally, cytochrome *bd*-type oxidases, which are phylogenetically unrelated to HCO, represent a second major superfamily [Jünemann, 1997; Borisov et al., 2011] functioning as quinol oxidases.

Type A oxidases encoded by the *cox* gene cluster are present in a wide range of bacteria and they have a high proton-pumping activity [Brzezinski et al., 2004; Arai et al., 2014]. In general, *aa₃*-type oxidases show a low affinity for oxygen and usually play a dominant role under high-oxygen conditions in bacteria such as *R. sphaeroides* and *B. subtilis* [Gabel and Maier, 1993; Winstedt and von Wachenfeldt, 2000; Arai et al., 2008]. If we extend these widely accepted biochemical concepts to KF707 redox chain, the peculiarity of the membrane terminal oxidase content of this PCBs degrader becomes apparent. In fact, while the sequence analysis allowed classifying *coxMNOP* gene cluster in the Type A subfamily, the presence in the predicted subunit II (CoxM) of an uncommon extra C-terminal domain carrying two *c*-type haems binding consensus sequences, suggests that this protein is a *caa₃*-type HCO. In agreement to this, the C-terminal extension of subunit II (CoxB) from the facultative anaerobic proteobacterium *S. oneidensis* MR-1 was shown to bind two *c*-type haems [Le Laz et al., 2014]. Similarly, this unusual feature was reported in *Desulfovibrio* spp. [Lobo et al., 2008] and in some species of the genus *Psychromonas*, *Colwellia*, and *Methylosarcina* [Le Laz et al., 2014]. In *S. oneidensis* MR-1, the *Caa₃* oxidase was expressed at a low level but only under O₂-rich growth conditions in LB-medium [Le Laz et al., 2014], while in KF707 the *Caa₃* oxidase is always expressed at a low level regardless of the cell growth phase and the carbon source (Figure 2.16). As opposed to the CoxM subunit, the CoxB subunit II of *T. thermophilus*, *B. subtilis*, and *R. marinus* has an extra domain carrying only one *c*-type haem [Lauraeus et al., 1991; Mather et al., 1991]. This is the case of *caa₃*-type oxidase of KF707, which is always expressed during the stationary phase, in cells grown with biphenyl, its expression was higher than those of *cbb₃*-type oxidases (Figure 2.16). In KF707, the presence of *c*-type haems in the oxidase catalytic subunits is not only

predicted by the amino acid sequences (Alignment 1) but it was supported by spectroscopic analysis in which a decrease of the *c*-type haem content in membranes from KF1cox1-2 mutant (Caa₃/Ccaa₃ minus) is seen (Figure 2.17; Table 2.6).

Oxidases of *cbb*₃-type normally show a very high affinity for oxygen and low proton-translocation efficiency. In bacteria such as *P. denitrificans*, *R. sphaeroides*, and *R. capsulatus*, *cbb*₃ oxidases are known to be induced under low oxygen conditions [Preisig et al., 1996; Mouncey and Kaplan, 1998; Swem and Bauer, 2002]. In *P. aeruginosa* PAO1 one of these *cbb*₃-type oxidases, Cbb₃1, is constitutively expressed and plays a primary role in aerobic growth irrespective of oxygen concentration; on the contrary, the expression of Cbb₃2 varies under low oxygen conditions or at the stationary growth phase [Kawakami et al., 2010]. The latter regulatory mechanism is also present in KF707 grown on glucose or biphenyl, as clearly demonstrated by the constitutive expression of Cbb₃1, while the Cbb₃2 expression varies as a function of the carbon source and growth phase being repressed in the stationary phase of growth in biphenyl (Figure 2.16).

CIO oxidases are copper-free enzymes that are insensitive to millimolar concentration of cyanide and they function as quinol:oxygen oxidoreductases. In the past, a direct determination through the use of Q-electrodes of the Q-pool redox state in membranes from aerobically grown *R. capsulatus* endowed with Cbb₃ and CIO oxidases, indicated that the quinol oxidase of CIO type starts being involved in respiration when the Q-pool reduction level reaches ~25% [Zannoni and Moore, 1990]. If this observation is applied to analogous bacterial respiratory chains, as those of *R. sphaeroides*, *P. aeruginosa* and KF707, it is apparent that CIO pathways operate as redox valves to prevent the Q-pool from exceeding the 25–50% oxidation-reduction level that is the optimum Q-pool redox state to warrant an efficient energy transduction by the respiratory chain [Klamt et al., 2008]. This would explain why cytochrome *cbb*₃-type oxidases are prone to sense environmental redox changes and this is why *cioABC* genes coding for CIO, are up-regulated by deletion of the constitutive Cbb₃1 oxidase in *P. aeruginosa* [Comolli and Donohue, 2004]. Interestingly, also in KF707, the CIO promoter is up-regulated by deletion of the Cbb₃1 isoform (Figure 2.19), as also confirmed by respiratory activities measured in membranes from Cbb₃1 minus cells (KFΔcco1 mutant), in which the CIO pathway catalyzes 56% of respiration as compared to only 17% of W.T. cells (Table 2.8). In addition, the promoter expression analysis, performed

with CIO-*lacZ* fusion strains grown on glucose or biphenyl, supported the results obtained with the respiratory activities assays (CIO oxidase is 10 times more expressed in KF Δ cco1 mutant than in W.T. strain, Figure 2.19).

These data confirms that CIO has a minor role in KF707 respiration when the main electron transfer pathway, ending into cytochrome *c* terminal oxidases, works properly and, in particular when the Cbb₃1 oxidase is not deleted.

2.4.2 Effect of the carbon source on the arrangement of KF707 respiratory chain

KF707 cells grown in LB-medium do not contain detectable amounts of *a*-type haems, regardless the growth phase [Di Tomaso et al., 2002]. Conversely, here we show that spectroscopic significant amounts of *a*-type haems are present in KF707 cells grown in minimal salt media supplemented with biphenyl as sole carbon source (Table 2.6). Furthermore, results of Figure 2.16 and Table 2.7 indicate that both *coxI-II-III* gene expression and catalytic activity (Caa₃ oxidase) are greatly enhanced in biphenyl grown cells. This effect was paralleled by a drastic decrease (7- fold) in the expression of the Cbb₃2 oxidase, which was not compensated by a parallel increase of the CIO quinol oxidase activity while the Cbb₃1 oxidase was constitutively expressed (Figure 2.16; Table 2.7). These results are of particular interest because they outline a new bioenergetic scenario in which two respiratory oxidases of KF707 are modulated by biphenyl, which is the metabolite that allows the co-metabolic degradation of PCBs by KF707. In this respect, while the response of the central carbon catabolism to environmental signals such as oxygen and/or nutritional compounds has been analyzed in some detail [Arras et al., 1998; Krooneman et al., 1998], the modulation of the oxidative electron transport chain by the carbon source used for growth is far less documented [Dominguez-Cuevas et al., 2006; Arai, 2011; Arai et al., 2014]. It is known that oxidases of *aa*₃-type are affected by carbon starvation, which was shown to induce a *cox* gene up-regulation in *P. aeruginosa*. This regulatory mechanism is linked to a cell response towards a more efficient energy-transducing *aa*₃-type oxidase under low nutrient conditions [Kawakami et al., 2010; Arai, 2011].

As far as it concerns the role of *caa₃*-type oxidases in KF707 grown in biphenyl, the growth results can be summarized as the following (Figure 2.14 Biphenyl):

- ✓ (1) the growth rate of the *caa₃*-type oxidases double mutant ($g = 94 \pm 6.1$ min) is similar to that of W.T. ($g = 97 \pm 8.5$ min); (2) the lack of both Cbb₃1 and Cbb₃2 oxidases slows down KF707 cell growth ($g = 140 \pm 21$ min); (3) the Caa₃/Ccaa₃/CIO minus phenotype is only slightly affected in its growth rate ($g = 117 \pm 1.5$ min) as compared to W.T.; (4) the Cbb₃1 minus phenotype is impaired in its growth rate ($g = 151 \pm 1.7$ min) in spite of Caa₃ overexpression; (5) growth of the quadruple cytochrome oxidase mutant Cbb₃1-2/Caa₃/Ccaa₃, although impaired, is still supported by the oxidase activity of CIO which is up-regulated ($g = 146 \pm 16$ min), and finally (6), all attempts to obtain a KF707 mutant carrying a Cbb₃1-2/CIO minus phenotype were unsuccessful.

Overall, these data suggest that the *caa₃*-type oxidases of KF707 are unable to sustain aerobic growth when they are present as the only terminal oxidases as it was noticed in *S. oneidensis* MR-1, whose genome is predicted to encode for a terminal Cox oxidase annotated as Ccaa₃ oxidase [Le Laz et al., 2014]. In the past, it was shown that a mutant of *P. aeruginosa* PAO1 that lacked four terminal oxidase gene clusters, except for the *cox* genes (strain QXAa), was unable to grow aerobically in LB [Arai et al., 2014]. More recently, a suppressor mutant of QXAa (QXAaS2) that grew aerobically using only the *cox* genes for Caa₃ (formerly reported as Aa₃) was described, in which a mutation in the two-component regulator RoxSR was necessary for the aerobic growth of *P. aeruginosa* PAO1 in LB [Osamura et al., 2017]. Apparently, the expression and function of bacterial cytochrome *c* oxidases of *caa₃*-type under variable growth conditions is far from being fully examined [Brzezinski et al., 2004; Arai, 2011; Osamura et al., 2017]. The scheme in Figure 2.20 represents the state of knowledge on the functional arrangement of the electron transport chain in the PCBs degrader KF707. A study is currently underway to understand the electron transport chain's regulation mechanism as a function of the two major carbon sources here used for cell growth, glucose, and biphenyl, along with the search for growth conditions under which the Ccaa₃ oxidases of KF707 is significantly expressed.

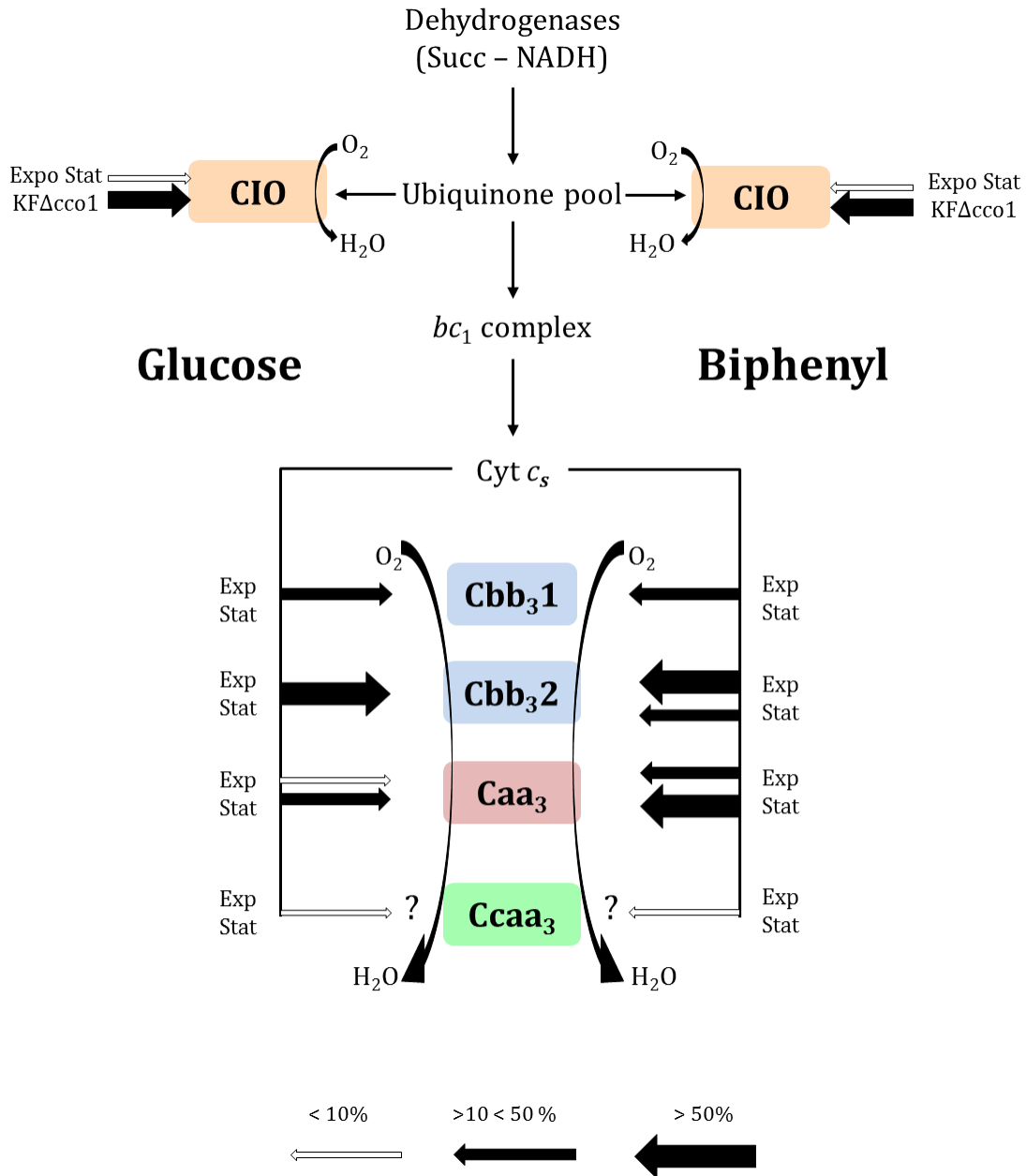


Figure 2.20: Block scheme illustrating the putative chain of KF707 based on spectroscopic, functional, and genetic analysis in cells grown in MSM medium with glucose or biphenyl as single carbon source. Symbols used: Succ, succinate dehydrogenase; NADH, NADH dehydrogenase; Cyt c_s , soluble cytochrome(s) c ; bc_1 complex, cytochrome bc_1 complex III; CIO, cyanide insensitive oxidase (*bd*-type) (encoded by *cioABC*); Caa₃, cytochrome c oxidase (encoded by *coxI-II-III* cluster); Ccaa₃, cytochrome c oxidase (encoded by *coxMNOP*); Cbb₃1, cytochrome c oxidase (encoded by *ccoN101Q1P1*); Cbb₃2, cytochrome c oxidase (encoded by *ccoN202Q2P2*); KFΔ*cco1*, Cbb₃1 minus mutant. The size and color of the arrows symbolize the % level of expression of terminal oxidases under the tested growth conditions, namely: cells grown in glucose or biphenyl and harvested during their exponential (Expo) or stationary (Stat) phase of growth. The actual expression values are those of Figure 2.16.

Chapter 3

Biochemical and structural evidence that *Pseudomonas pseudoalcaligenes* KF707 expresses a *caa*₃-type cytochrome *c* oxidase

This chapter is based on:

F. Sandri, F. Musiani, N. Selamoglu, F. Daldal and D. Zannoni.

FEBS Letters – February 2018.

3.1 Introduction

Cytochrome *c* oxidases belong to the Haem Copper Oxidase superfamily (HCO) [Lyons et al., 2016] and are classified into three main groups, Type A, B, and C, on the basis of the amino acids sequence of the D and K proton channels. As previously described in Chapter 2 Background, the Type A oxidases are usually divided into two subclasses: Type A1 and Type A2 the [Pereira et al., 1999]. The fundamental structure of the subunit I of these enzymes is conserved, but some of them contain an additional Cu_A copper binuclear center and/or a *c*-type haem domain in the subunit II (in this latter case enzymes are named *caa*₃-type oxidases). The first crystal structure of a Type A2 HCO was described from the thermophilic Gram negative bacterium *Thermus thermophilus* [Lyons et al., 2012]. This oxidase consists of two SUs, referred to as SU I/III and SU IIc, containing all metal centers characteristic of orthodox *caa*₃-type oxidases [Ferguson-Miller and Babcock, 1996]. In this enzyme, the SU I/III is a fusion of the classical SU I and SU III subunits, whereas SU IIc is a fusion between a canonical SU II and a cytochrome *c* domain. Due to this feature, the HCO of *T. thermophilus* is called Caa₃ cytochrome oxidase. In particular, oxidases with haems of *caa*₃-type were reported to be present also in the thermophilic Gram negative *R. marinus* and the spore-forming Gram positive *B. subtilis* species [Pereira et al., 1999; Bengtsson et al., 1999]. The occurrence of a cytochrome *c* domain fused with a canonical SU II seems to reflect the need for a better control of the respiratory electron transfer under harsh environmental conditions deriving from high temperatures or the absence of a periplasmic space in Gram positives [Lyons et al., 2016; Sone et al., 2004] (Figure 3.1). Similarly to *aa*₃ oxidases, the

proton pumping stoichiometry *caa*₃-type oxidases (0.8-1 H⁺/e⁻) is higher than *ba*₃- (0.5-0.75 H⁺/e⁻) and *cbb*₃- (0.2-0.5 H⁺/e⁻) type oxidases, which are also present in both thermophilic and mesophilic bacterial species [Kannt et al., 1998; Toledo-Cuevas et al., 1998; Pereira et al., 1999; Han et al., 2011].

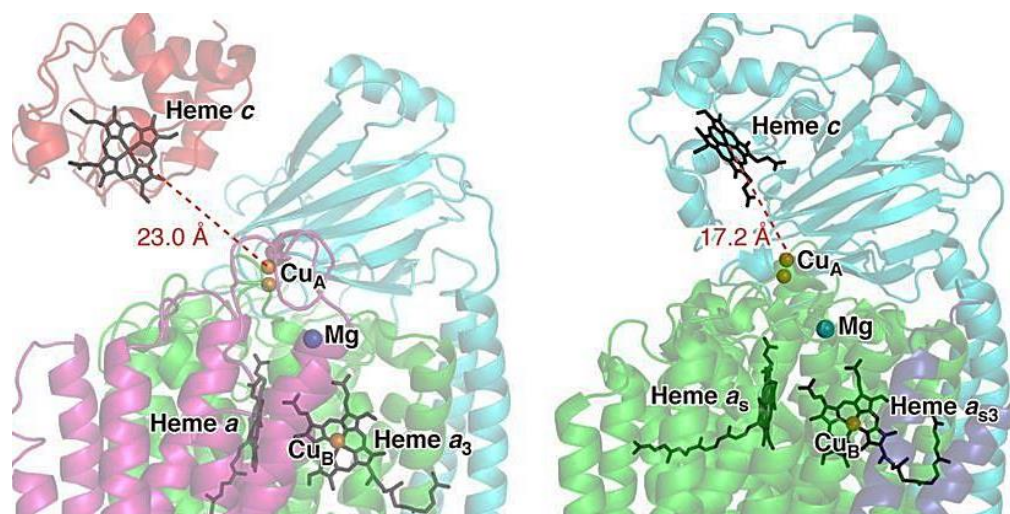


Figure 3.1: Arrangement of redox cofactor in the cytochrome *c* oxidases *aa*₃-type and *caa*₃-type [Shimada et al., 2017].

As described in Chapter 2, the genome analyses of the polychlorinated-biphenyl (PCBs) degrader *Pseudomonas pseudoalcaligenes* KF707, reported the presence of a gene cluster (BAU71738-71737-71740) encoding for a cytochrome *c* oxidase of *caa*₃-type composed of three subunits (SU I, SU IIc and SU III) [Sandri et al., 2017]. The predicted **SU IIc (42 kDa)** of KF707 was annotated as a membrane anchored cupredoxin domain containing one electron-accepting homo-binuclear copper center, Cu_A, with a carboxyl terminal fusion to a cytochrome *c* domain [Lyons et al., 2012; Sandri et al., 2017]. The occurrence of a *c*-type haem in the *aa*₃-type oxidase of KF707 was also suggested by alignment analyses which showed, at the C-terminal region, the typical amino acid residues (**CXXCH**) that coordinate the *c*-type haem in *B. subtilis* and *T. thermophilus* Caa₃ oxidases [Lyons et al., 2012; Sone et al., 2004] (Figure 3.2). These characteristic haem binding residues are absent from the *aa*₃-type oxidases of *R. sphaeroides* and *Par. denitrificans*. Notably, the SU IIc amino acid sequence of KF707 shows 81% of identity with CoxB (SU II) of the opportunistic pathogen *P. aeruginosa* PAO1 [Sandri et al., 2017; Stover et al., 2000]. In this latter species, the

presence of an orthodox *aa*₃-type oxidase was documented by Arai and co-workers [Kawakami et al., 2010; Arai, 2011; Arai et al., 2014], even though, in a recent publication by this group [Osamura et al., 2017], the product of the *cox* genes in *P. aeruginosa* PAO1 was referred as *caa*₃-type oxidase, despite the lack of any pertinent data supporting this affirmation.

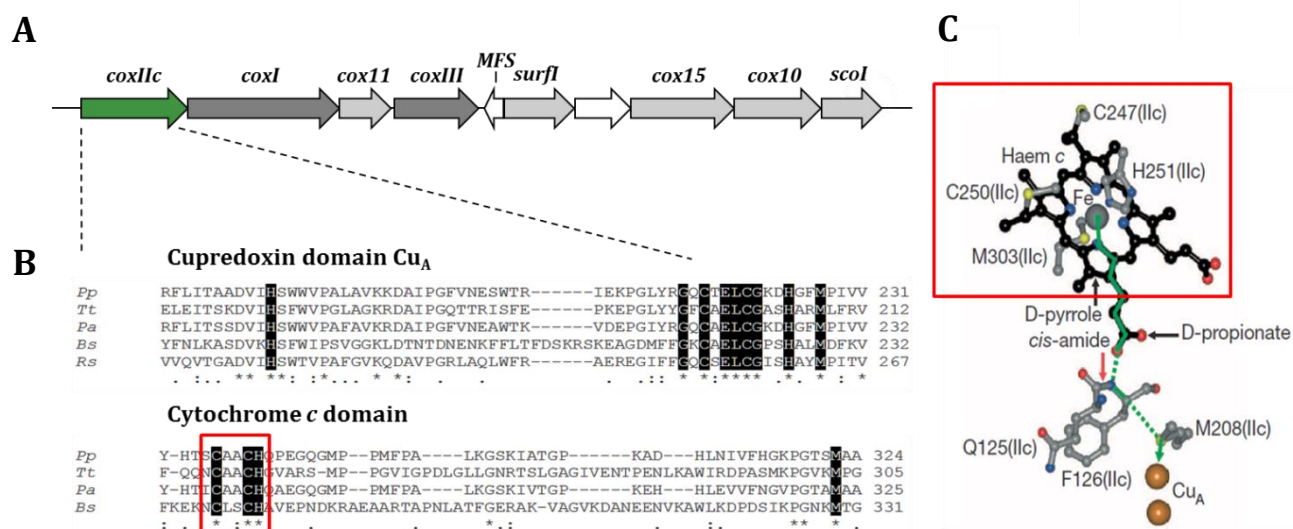


Figure 3.2: **A**) Organization of the *Caa*₃ oxidase gene cluster in KF707: green, *coxIIc* gene for subunit II; dark gray, functional genes; light gray, genes for *Caa*₃ biogenesis; white, genes probably not directly related to *Caa*₃. **B**) Alignment analysis for subunit II of *Caa*₃ from KF707 (*Pp*), *T. thermophilus* (*Tt*), *P. aeruginosa* PAO1 (*Pa*), *B. subtilis* (*Bs*) and *R. sphaeroides* (*Rs*). The first alignment focuses on the cupredoxin domain and the copper center Cu_A (N-terminal portion) and the second one shows the cytochrome *c* domain (C-terminal portion), absent in the *a*₃-type oxidase from *R. sphaeroides*. The dark boxes are the amino acids that are directly involved in the Cu_A and haem *c* binding, asterisks and dots represent the fully and partially conserved amino acid residues, respectively. Analyses were performed using the ClustalW software [Thompson et al., 1994]. **C**) The optimum electron transfer pathway, in *T. thermophilus*, between the haem *c* iron and the Cu_A center, the conserved residues are indicated [Lyons et al., 2012].

During the research studies reported in Chapter 2, aimed at understanding the remarkable metabolic abilities of KF707 in using biphenyl as a sole carbon source [Fedi et al., 2001; Tremaroli et al., 2010], it was observed that membranes from KF707 cells grown with different carbon sources, such as glucose or biphenyl, contained a number of membrane-bound *c*-type haem proteins possibly corresponding to subunits of *caa*₃- and *ccb*₃-type oxidases. In particular, by using SDS-PAGE and tetramethyl-benzidine (TMBZ) staining and appropriate tandem mass spectrometry analyses, in the present study we identified that a protein band of 37 kDa corresponded to the *c*-type cytochrome domain containing SU IIc of

the Caa₃ cytochrome *c* oxidase of KF707. As expected, the 37 kDa TMBZ-stained band was absent in a mutant derivative of KF707 lacking *cox* gene clusters (KFΔ*cox*₁₋₂). Moreover, we showed that this SU IIc is highly expressed in membranes from cells grown in the presence of biphenyl, while it is poorly expressed in those grown in the presence of glucose, in line with our recent findings related to the promoter activity of the *coxI-II-III* gene cluster [Sandri et al., 2017]. To further complete our analyses, a homology based structural model of the Caa₃ cytochrome *c* oxidase from KF707 was generated using the X-ray structure of that from *T. thermophilus* (PDB code 2YEV) [Lyons et al., 2012]. To the best of our knowledge, this work represents the first report that unequivocally demonstrates the presence of a *caa*₃-type oxidase in a *Pseudomonas* species.

Another important aspect to evaluate in order to better understand the physiological role of the *cbb*₃- and the *caa*₃-type cytochrome oxidases is the investigation of their electron donors, example cytochrome of *c*-type.

As shown in the past [Di Tomaso et al., 2002], both NADH- and succinic-dehydrogenases deliver their reducing equivalent into a quinol/cytochrome *c* oxido-reductase complex (also referred to as complex III or cytochrome *bc*₁ complex), which contains *b*- and *c*-type haem subunits coded by 1212 bp and 780 bp genes, respectively (BAU72674; BAU72675), while the ORF coding for the Rieske domain iron sulphur, [2Fe-S] reductase subunit of the *bc*₁ complex, is coded by a 591 bp gene (BAU72673). The latter genome annotation confirms early data indicating that the NADH-dependent respiration in KF707 is inhibited by the antibiotic antimycin A, which is a specific inhibitor of the cytochrome *bc*₁ complex at the haem *b*_H-Qi interaction site level [Cramer and Knaff, 1990; Di Tomaso et al., 2002].

In most Gram negatives, the cyt *c* maturation system (Ccm system) is encoded by the *ccm* gene cluster (***ccmABCDEFGHI***) and by *ccdA* (homolog of *E. coli dsbD*). In addition to these components, the thiol:oxidoreduction system, composed of the membrane-bound disulfide-bond forming proteins DsbB and DsbA, ensures oxidation of reduced apocyt *c* after its translocation across the membrane [Verissimo and Daldal, 2014]. In KF707, the *ccm* genes are clustered, while the genes coding for the disulphide binding proteins DsbA (BAU71766) and DsbB (BAU77178) were found in a different region of the genome.

The *cbb₃*-type oxidases of different α -Proteobacteria (*R. sphaeroides* [Toledo-Cuevas et al., 1998], *Par. denitrificans* [de Gier et al., 1996], *R. capsulatus* [Daldal et al., 2001], *Bradyrhizobium japonicum* [Arslan et al., 2000]) have been biochemically characterized and widely studied; in particular, it is known that cytochrome oxidases of *R. sphaeroides* can utilize the **mono-haem cytochrome *c₂*** or the membrane anchored cytochrome ***c_y***.

Analysis of sequenced genomes belonging to β - and γ -Proteobacteria containing *cbb₃*-type oxidases, noticed the presence of a di-haem cytochrome *c₄* [Chang et al., 2010]. One previous work on the electron donor to the unique Cbb₃ oxidase of in *Vibrio cholerae*, confirmed that the di-haem cytochrome *c₄*, unlike the mono-haem cytochrome *c₅*, is the substrate used by the in vitro Cbb₃ enzyme and it can support oxygen reductase activity at a rate of 300 e⁻¹/s; this latter value resulted 10-20 fold higher than that measured using cytochrome *c₅* or soluble horse heart cytochrome *c* [Chang et al., 2010]. Furthermore, in KF707 and other *Pseudomonas* spp. (*P. aeruginosa*, *P. fluorescens*, *P. putida* and *P. entomophila*), a gene cluster with genes encoding for soluble *c*-type cytochromes *c₄* and *c₅*, is present. A recent study revealed that in cells of *P. aeruginosa* PAO1, cytochrome *c₄* (PA5490) is constitutively expressed and its deletion causes a severe slowdown in growth which mainly depends on *cbb₃*-type oxidases [Arai et al., 2014].

3.2 Materials and Methods

3.2.1 Bacterial strains and plasmids

All bacterial strains and plasmids, used in this chapter, are listed in Table 3.1; in addition, we used the KF707 deletion mutant strains obtained in the previous chapter (KF Δ cox1-2, KF Δ cco1, KF Δ cco2, KF Δ cco1-2, KF Δ CIO, KF Δ CIO/cox1-2 and KF Δ cox1-2/cco1-2).

Table 3.1: Bacterial strains and plasmids.

Bacterial Strains	Relevant Genotype	Reference
<i>P. pseudoalcaligenes</i> KF707		
Wild type (W.T.)	Amp ^r	Furukawa and Miyazaki, 1986
KF Δ c ₄	Deletion of <i>cyt c₄</i> , Amp ^r	This study
KF Δ c ₅	Deletion of <i>cyt c₅</i> , Amp ^r	This study
KF Δ c ₄ /c ₅	Deletion of <i>cyt c₄</i> and <i>cyt c₅</i> , Amp ^r	This study
KF Δ c ₄ /cco1-2	Deletion of <i>cyt c₄</i> , <i>ccoN10I1Q1P1</i> and <i>ccoN202Q2P2</i> , Amp ^r	This study
KF Δ c ₄ cox1Lac	Deletion of <i>cyt c₄ coxII::lacZ</i> translational fusion, Amp ^r	This study
KF Δ c ₄ cox2Lac	Deletion of <i>cyt c₄ coxM::lacZ</i> translational fusion, Amp ^r	This study
KF Δ c ₄ cco1Lac	Deletion of <i>cyt c₄ ccoN1::lacZ</i> translational fusion, Amp ^r	This study
KF Δ c ₄ cco22Lac	Deletion of <i>cyt c₄ ccoN2::lacZ</i> translational fusion, Amp ^r	This study
KF Δ c ₄ CIOLac	Deletion of <i>cyt c₄ cioA::lacZ</i> translational fusion, Amp ^r	This study
Plasmids	Relevant Genotype	Reference
pG19II	Gm ^r , <i>sacB</i> , <i>lacZ</i> , cloning vector and conjugative plasmid	Maseda et al., 2004
pG19II Δ c ₄	Gm ^r , <i>sacB</i> , <i>lacZ</i> , carrying Δ c ₄ deleted fragment	This study
pG19II Δ c ₅	Gm ^r , <i>sacB</i> , <i>lacZ</i> , carrying Δ c ₅ deleted fragment	This study
pG19II Δ c ₄ /c ₅	Gm ^r , <i>sacB</i> , <i>lacZ</i> , carrying Δ c ₄ and c ₅ deleted fragments	This study

3.2.2 KF707 deletion mutant and *lacZ* translational fusion strains

The KF707 knockout mutant strains cytochrome *c*₄ or *c*₅ were obtained by using the Gene SOEing PCR technique; instead, the *LacZ* translational fusion strains for KF Δ *c*₄ were constructed with mini-Tn7 based method (as previously described Chapter 2). All the primers used for the deletion Δ constructs are listed in Table 3.2.

Table 3.2: Primers used for the construction of the deletion fragments (Δ). The red nucleotides from the overlap region for the UP and DOWN deletion fragments union PCR, while the nucleotides that form the cutting site for the restriction enzymes are in bold.

Gene	Primer name	Sequence	Restriction enzyme
Δc_4	FOR up	ACGTGTA AGCTT CCTTCACAGTTATTTCGGCGCA	<i>HindIII</i>
	REV up	AGGAGTAAGTATGGAACAGT AGCGGCGGTGGATGATCATC	
	FOR down	ACTGTTCCATACTTACTCCT ACCCAAGGCGGTGATCGAT	
	REV down	ATTTCGA ATTCT CTCTCGTCCAGCCGCGCTAAAG	<i>EcoRI</i>
	FOR control	TTCGCCATGTTCTGCTGGG	
	REV control	CCGCGTTGAAGAAGCTGGTG	
Δc_5	FOR up	CGGGCT GGATCC GCGAGACCC	<i>BamHI</i>
	REV up	ACATTGATCTTAATTGTACCT TCAGCCGGGAGCCGTCGG	
	FOR down	AGGTACAATTAAGATCAATGT CCTGCTTCCTACCCGGCTA	
	REV down	ATCCC GAATTCT CACTCCCCTGCGCTACCAC	<i>EcoRI</i>
	FOR control	TAGGCCCAGCGATGCACCAC	
	REV control	CGATCCTCTCCAGCACCTG	
$\Delta c_4/c_5$	FOR up	ATTAGT GGATCCA AGAGGACGGGGCGACGCAG	<i>BamHI</i>
	REV up	TAGGAGTCAGAATGGTTCAGT TAGGGGTTCACGGTAAAT	
	FOR down	ACTGAACCATTCTGACTCCTA AAGTAACACCCCTGCCTGC	
	REV down	GGGCT GAATTCT GATGTAGAACTTGCGCTCGGG	<i>EcoRI</i>
	FOR control	GGTGCCGTCTTCGTTGACTG	
	REV control	CACCGGCTTCCTGGGGATGAT	

3.2.3 Preparation of membrane fragments

For cell membrane fragments isolation, KF707 W.T. and mutant strains were grown aerobically at 30°C and 130 rpm in 3 L Erlenmeyer flasks containing 1 L MSM medium, pH 7.2 [Tremaroli et al., 2010] supplemented with glucose or biphenyl as the sole carbon source [6 mM]. Cells were harvested at their stationary phase ($OD_{600\text{ nm}}$ 0.7-0.9),

corresponding to 16 or 30 hours growth for glucose or biphenyl, respectively. Membrane fragments were prepared in MOPSO buffer [50 mM, pH 7.2] containing MgCl₂ [5 mM] using a French pressure cell mechanical treatment and ultracentrifugation, as previously described [Di Tomaso et al., 2002; Chapter 2].

Protein concentrations were determined using the bicinchoninic (BCA) acid assay, according to the supplier's recommendations (Sigma Inc.; procedure TPRO-562).

3.2.4 SDS-PAGE and *c*-type haem staining

The *c*-type cytochromes detection was performed using membrane fragments from KF707 W.T. and mutant strains grown in MSM medium with glucose or biphenyl [6 mM]. 150-200 µg of protein samples were denatured for 5 minutes at 37°C and separated by 15% SDS-PAGE [Laemmli, 1970]. The *c*-type cytochromes were revealed via their intrinsic peroxidase activity by using 3,3',5,5'-tetramethylbenzidine (TMBZ) and H₂O₂ [Thomas et al., 1976]. ImageJ was used to quantify the intensity of the gels bands.

3.2.5 Nano LC-MS/MS analysis and database searches

SDS-PAGE bands were excised, and after reduction (dithiothreitol, Sigma) and alkylation (iodoacetamide, Bio-Rad), were subjected to in-gel trypsin digestion (Promega, Sequencing Grade Modified Trypsin) overnight at 37°C. Peptides eluted from the gel samples were dried and desalted using ZipTips (Millipore U-C18 P10), lyophilized and stored at -80°C. They were resuspended in 10 µL 5% acetonitrile/0.1% formic acid prior to mass spectrometry.

A Q-Exactive Quadrupole-Orbitrap mass spectrometer (Thermo Fisher Scientific, San Jose, CA), coupled to an Easy-nLC™ 1000 nano liquid chromatography system (Thermo Fisher Scientific, San Jose, CA), was used for Nano LC-MS/MS analyses. Samples were loaded in buffer A (0.1% formic acid) onto a 20 cm long fused silica capillary column (75 µm ID), packed with reversed-phase Repro-Sil Pur C18-AQ 3 µm resin (Dr. Maisch GmbH, Germany). Peptides were eluted using a 45 min linear gradient from 4%–40% buffer B (100% acetonitrile, 0.1% formic acid), followed by a 7 minutes gradient from 40%–80% buffer B and 8 minutes wash with 80% B (constant flow rate 300 nl/min). The Q-Exactive was operated in data-dependent acquisition (DDA) mode with dynamic exclusion enabled

(repeat count: 1, exclusion duration: 20 sec). Full MS survey scans (mass range 300-1600 m/z) at high resolution (70,000 at 200 m/z) were followed by MS/MS fragmentation of the top 15 most intense ions with higher energy collisional dissociation (HCD) at a normalized collision energy of 22 (resolution 17,500 at 200 m/z). Dual lock mass calibration was enabled with 371.101233 m/z and 445.120024 m/z background ions.

MS spectra were searched against the KF707 protein FASTA database (UniProtKB) using Proteome Discoverer 1.4 Software (Thermo), with Sequest-HT search engine. Search parameters were set to full trypsin digestion, with a maximum of 3 missed cleavages and 3 equal modifications per peptide. Oxidation of methionine (+16 Da) and carboxyamidomethylation of cysteine (+57 Da) were selected as dynamic modifications. Precursor and fragment ion tolerances were set to 10 ppm and 0.6 Da, respectively. False discovery rates by target-decoy search (FDR) were set to 0.01 (high confidence) with X_{corr} of >2 for m/z=2, >2.5 for m/z=3, and > 2.6 for m/z=4 values.

3.2.6 Membrane protein modeling

Template search for each of the three subunits (SU) of Caa₃ cytochrome *c* oxidase (namely SU I, IIC and III) from KF707 (*Pp-caa₃*) was performed using the HHsearch method implemented in the HHpred server [Söding et al., 2005]. The server performs up to eight iterative PSI-BLAST [Altschult et al., 1997] searches through filtered versions of the non-redundant (nr) database from the NCBI. Using the final target alignment, a Hidden Markov Model (HMM) [Krogh et al., 1994; Jo and Cheng, 2014] profile is calculated. Homologous templates are identified by searching through a weekly updated database containing HMMs for a representative subset of PDB sequences. Finally, HHsearch ranks the database matches based on the probability of the match to be homologous to the target sequence. This approach is useful to distinguish homologous from non-homologous matches. Excluding PDB structures that were not solved by X-ray crystallography, HHpred identified the *caa₃*-type cytochrome *c* oxidase from *T. thermophilus* (*Tt-caa₃* hereafter). *Tt-caa₃* is composed by two protein chains homologous to the *Pp-caa₃* (SU) I/III and SU IIC sequences. SU I/III is a fusion of the canonical SU I with SU III, connected with a linker of ca. 70 residues. The pronounced sequence identity/sequence similarity of *Pp-caa₃* SU I, IIC and III with respect to the corresponding sequences of *Tt-caa₃* (45%-62%, 30%-45% and 31%-

42%, respectively) allows the generation of a reliable structural model. The target and template sequences were realigned using the Promals3D server [Pei et al., 2008]. Sequences of *aa*₃-type cytochrome *c* oxidase subunit II and III from *Par. denitrificans* (*Pd-aa*₃) were included to align two large insertions not present in the *Tt-caa*₃ sequences. The obtained alignment was then used to calculate 100 models of *Pp-caa*₃ structure using the available crystal structures of *Tt-caa*₃ (PDB code: 2YEV) [Lyons et al., 2012] and *Pd-aa*₃ (PDB code: 3HB3 [Koepke et al., 2009] and 1QLE [Harrenga and Michel 1999]) to model *Pp-caa*₃ subunit IIc and III, respectively, using the Modeller 9.18 software [Sali and Blundell, 1993]. The two haems *a*, the haem *c*, the binuclear and mononuclear copper centers (Cu_A and Cu_B, respectively) and the Mg(II) ion, together with the water molecules in direct contact with the metal ions and the lipid molecules found in the *Tt-caa*₃ structure, were included in the modelling procedure. The best model was selected using the DOPE potential function built into Modeller [Shen and Sali, 2006]. A loop optimization routine was used to refine the regions that showed higher than average energy as calculated using the DOPE potential function. The stereochemical quality of the model structure was established using ProCheck [Laskowski et al., 1993], and the results of this analysis confirmed the reliability of the model structure. The obtained molecular model and the molecular surface were displayed and analyzed using UCSF Chimera [Pettersen et al., 2004] and APBS [Baker et al., 2001] software. The position of the protein model in the membrane was predicted using the PPM web server [Lomize et al., 2012], and the residue conservation on the protein surface was evaluated using the ConSurf 2016 server [Ashkenazy et al., 2016].

3.2.7 Other analyses

All the experiments performed with the KF707 cytochrome *c* deletion mutant strains, including NADI tests, growth curves and β -galactosidase assay, were conducted as previously described in Chapter 2 – Materials and Methods. The membrane fragments were also used for respiratory activity analysis, performed as described in Chapter 2 – Materials and Methods.

3.3 Results

3.3.1 Cytochrome *c* profile and Nano LC-MS/MS analysis of KF707 W.T. and oxidase mutant strains

In the previous Chapter 2, KF707 deleted mutant strains, for single or multiple oxidases, were obtained. These mutants were crucial in understanding the peculiar metabolic abilities of KF707 [Fedi et al., 2001]. It was observed that membranes from KF707 cells, grown with different carbon sources, such as glucose or biphenyl, express several gene clusters coding for membrane-bound *c*-type haem proteins, corresponding to *caa₃* and *cbb₃*-type oxidases. In particular, five terminal oxidases were identified by genetic and functional analysis, namely: two *caa₃*-type oxidases (Caa₃ and Ccaa₃), two *cbb₃*-type oxidases (Cbb₃1 and Cbb₃2) and one cyanide-insensitive quinol oxidase (CIO).

The expression of the promoter for the Caa₃ oxidase increased considerably when biphenyl was used as sole carbon source, at stationary phase of growth, in contrast to the Cbb₃2 gene promoter, which was repressed; with the other carbon sources, like glucose, the *cbb₃*-type oxidases were prevalent in all stages of growth.

Up to now, there are no biochemical and structural data available in the literature supporting the genetic evidence for the presence of Caa₃ oxidases in *Pseudomonas* species [Le Laz et al., 2014; Lyons et al., 2016]. To fill the gap between the most investigated *Thermus*, *Rhodothermus* and *Bacillus spp.*, the cytochrome *c* contents of membranes isolated from KF707 W.T. and oxidase mutant strains were determined using the SDS-PAGE-TMBZ staining gel technique [Laemmli, 1970; Thomas et al., 1976].

In a previous work, concerning KF707, a TMBZ gel of W.T. strain, grown in LB, was reported [Di Tomaso et al., 2002]; six bands were observed and they were attributed to several cytochrome *c* proteins, based on the comparison with the cytochrome *c* profile obtained in *R. capsulatus* and *R. sphaeroides* TMBZ gels [Hochkoeppler et al., 1995; Daldal et al., 2001].

After the KF707's genome sequencing and the analysis of the terminal oxidases gene cluster, the results previously observed resulted incorrect; this was suggested on the basis of proteins molecular weights.

In order to obtain a clear and detailed cytochrome *c*-type profile for KF707, new TMBZ gels were prepared with membrane fragments from cells of KF707 W.T. and oxidase mutant

strains, harvested at their stationary phase of growth ($OD_{600\text{ nm}}$ 0.7-0.9) in MSM with glucose or biphenyl [6 mM] as single carbon source.

As shown in Figure 3.3A, in membranes from glucose grown cells, seven TMBZ stained bands were found, while in biphenyl (Figure 3.3B), only five bands were present.

- The lowest band, at **17 kDa**, was present in KF707 W.T., in all mutant strains and in both carbon sources, which means that this protein was not attributable to any deleted oxidases. The molecular weight of this band was attributed to a di-haem cytochrome c_4 ; in KF707 there are three di-haem cytochrome c_4 (BAU71756-BAU75530-BAU75507) and their molecular weights are around 20-23 kDa.
- The two bands around **20-22 kDa**, in fragments from cells grown with glucose, were absent in *cbb3*-type oxidases mutants; in the same position, in Figure 3.3B, only one of these bands was observed. Based on the data previously obtained (the expression of Cbb₃2 oxidase during stationary phase of growth in biphenyl resulted almost absent) and on the molecular weight of the subunits containing cytochrome *c*-type domains, these two bands are attributable to subunits Cco01 and Cco02 (~22 kDa) of Cbb₃1 and Cbb₃2 oxidases.
- The band at **29 kDa**, similarly to the 17 kDa band was present in KF707 W.T., and in all mutant strains grown with both carbon sources; this band likely corresponds to the c_1 subunit (29 kDa) of *bc₁* complex.
- Around **34-35 kDa**, two bands were present in glucose, and only one (the highest) in biphenyl. These two lanes disappeared in mutants lacking *cbb3*-type oxidases and, as shown in Figure 3.3C, in membranes from cells grown with glucose, the highest band (35 kDa) being present in KFΔ*cco2* (lacking Cbb₃2 oxidase) mutant but not in KFΔ*cco1* (lacking Cbb₃1 oxidase); on the contrary, the 34 kDa band was not seen in KFΔ*cco2* strain but not in KFΔ*cco1*. With biphenyl, only the highest band was present in KF707 W.T. and KFΔ*cco2* mutant. Based on these considerations these two bands were attributed to CcoP1 and CcoP2 subunits (~40 kDa) of Cbb₃1 and Cbb₃2 oxidases, respectively.
- The band at **37 kDa**, was the most interesting since in a previous published work, this band was not found [Di Tomaso et al., 2002]. This band was absent in membranes from *caa3*-type oxidases mutant strains grown with both carbon

sources; in addition, this band was more intense with membranes from cells grown with biphenyl than with glucose. The dimension, the presence of this band in cells grown with biphenyl but not in $KF\Delta\text{cox1-2}$ mutants, suggested it corresponds to subunit II of the Caa_3 oxidase (42 kDa).

In order to uniquely assign a specific protein structure to each displayed band seen in TMBZ-gels, all of them were excised from the gels, purified with Zip-tip procedure and, finally, analyzed through Nano LC-MS/MS. This approach estimated the presence of more than hundred proteins for each band, but only one of them was identified as a protein containing a cytochrome *c*-type domain, recognized for the presence, in the sequence, of the CXXCH motif for the coordination of the haem *c*. As the Table 3.3 shows, in the 37 kDa bands from samples grown with glucose and/or biphenyl, several distinct peptides (8 and 15 respectively), belonging to CoxIIc subunit of Caa_3 oxidase, were identified. The table contains the amino acids coverage and the number of the peptide found for each protein; all these cytochrome *c* proteins were identified with more than one peptide and, in all cases, the coverage was identical or more than 30%. Taken together, these structural results strongly supported the earlier conclusion made on the role of a cytochrome *c* oxidase Caa_3 in biphenyl grown cells on KF707 based on the expression of the *coxI-II-III* gene cluster [Sandri et al., 2017].

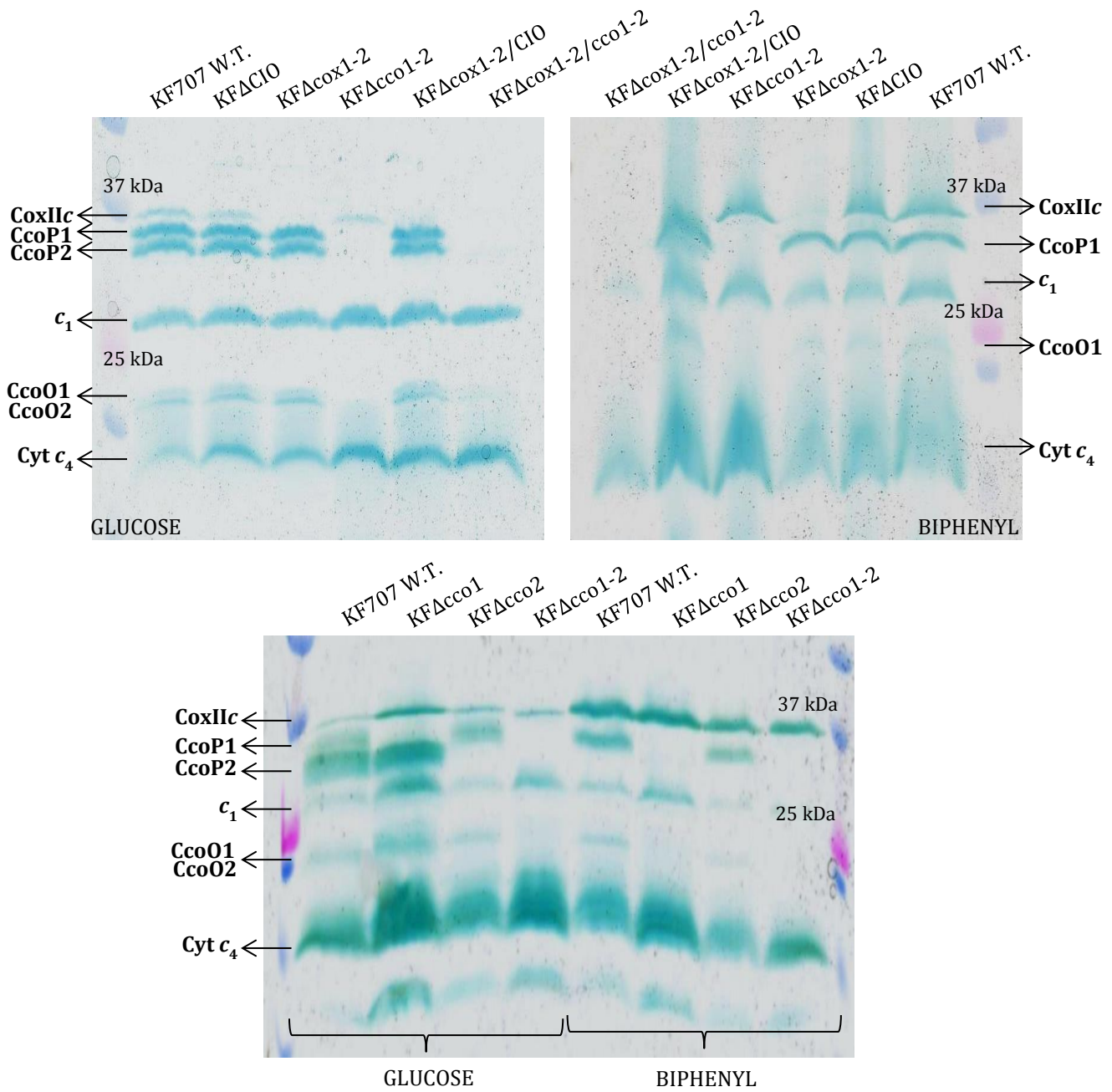


Figure 3.3: Cytochrome *c*-type detected in membranes of KF707 W.T. and mutant strains grown with glucose or biphenyl as carbon source until stationary phase (OD_{600 nm} 0.7-0.9). 200 μg of membrane fragments were analyzed by SDS-PAGE, and *c*-type cytochromes were revealed via their peroxidase activities using TMBZ staining.

Table 3.3: Nano LC-MS/MS analysis results from TMBZ bands extracted from gels realized with KF707 W.T. and mutant strains membrane fragments from cells grown in MSM medium with glucose or biphenyl [6 mM] as sole carbon source. The amino acids coverage, significant peptides, their modifications and XCorr are listed.

17 kDa	Accession	Description and % coverage			
	L8MT74	Cytochrome <i>c</i> ₄ OS= <i>Pseudomonas pseudoalcaligenes</i> KF707 = NBRC 110670 GN=ppKF707C_770 PE=3 SV=1 – [L8MT74_PSEPS] – NCBI Cyt <i>c</i> ₄ BAU71765 – 31.36%			
	Sequence		Modification	XCorr	
	DIEAVSSYIQLGH AAVcGAcHGPDGNSAAPNFPK TVLEmTGLLTNmSDQDmADLAA YFASQK		C4 – C7 M5 – M12 – M17	4.76 4.31 4.27	
22 kDa	Accession	Description and % coverage			
	L8MRV9	<i>cbb</i> ₃ -type cytochrome <i>c</i> oxidase subunit OS= <i>Pseudomonas pseudoalcaligenes</i> KF707 = NBRC 110670 GN=ppKF707_18660 PE=4 SV=1 – [L8MRV9_PSEPS] – NCBI CcoO1 BAU73558 – 44.39%			
	Sequence		Modification	XCorr	
	YGHYSVAGESVWDHPFLWGSK TEmDALVAYLQVLGTAIK mPSYPWLVENK TALELEGR GKTEmDALVAYLQVLGTAIK KLGVPYTD DDIAGAR LGVPYTD DDIAGAR YSDDWHR		M3 M1 M5	6.88 4.94 3.76 2.96 2.95 2.86 2.71 2.03	
	Accession		Description and % coverage		
	L8MLE9	<i>cbb</i> ₃ -type cytochrome <i>c</i> oxidase subunit OS= <i>Pseudomonas pseudoalcaligenes</i> KF707 = NBRC 110670 GN=ppKF707_18700 PE=4 SV=1 – [L8MLE9_PSEPS] – NCBI CcoO2 BAU73558 – 44.33%			
22 kDa	Sequence		Modification	XCorr	
	YGHYSVAGESVWDHPFLWGSK ALQTLGVPYSEDDVAGAQA AVK mPAYPWLVENTLDGKD TAAK TEmDALVAYLQVLGTA VK GKTEmDALVAYLQVLGTA VK mPAYPWLVENTLDGK YSDDWHR		M1 M3 M5 M1	6.88 5.44 5.12 4.62 4.37 3.07 2.03	
	Accession		Description and % coverage		
	L8M8C7	Ubiquinol cytochrome <i>c</i> oxidoreductase, cytochrome <i>c</i> ₁ subunit OS= <i>Pseudomonas pseudoalcaligenes</i> KF707 NBRC 110670 GN=ppKF707_9870 PE=4 SV=1 – [L8M8C7_PSEPS] – NCBI Cyt <i>c</i> ₁ BAU72675 – 37.07%			
	Sequence		Modification	XCorr	
	DLGIPEELmmENLVFTGAK IQNLVTF LAYSALPVK VFPNVGmPNVLVSLQGR TWFGAAPPDLTLVAR VRGNDWLYSYLR GNDWLYSYLR LTEAEFDEK		M9 – M10 M7	3.64 3.28 3.03 2.89 2.81 2.71 2.12	
29 kDa	Accession	Description and % coverage			
	L8M8C7	Ubiquinol cytochrome <i>c</i> oxidoreductase, cytochrome <i>c</i> ₁ subunit OS= <i>Pseudomonas pseudoalcaligenes</i> KF707 NBRC 110670 GN=ppKF707_9870 PE=4 SV=1 – [L8M8C7_PSEPS] – NCBI Cyt <i>c</i> ₁ BAU72675 – 37.07%			
	Sequence		Modification	XCorr	
	DLGIPEELmmENLVFTGAK IQNLVTF LAYSALPVK VFPNVGmPNVLVSLQGR TWFGAAPPDLTLVAR VRGNDWLYSYLR GNDWLYSYLR LTEAEFDEK		M9 – M10 M7	3.64 3.28 3.03 2.89 2.81 2.71 2.12	

34 kDa	Accession	Description and % coverage		
	L8MQP2	<i>cbb₃</i> -type cytochrome <i>c</i> oxidase subunit OS= <i>Pseudomonas pseudoalcaligenes</i> KF707 = NBRC 110670 GN=ppKF707C_18680 PE=3 SV=1 – [L8MQP2_PSEPS] – NCBI CcoP2 BAU73559 - 52.41%		
		Sequence	Modification	XCorr
		mAAmPAWGEILGDSGVR	M1 – M2	4.25
		VHLAAYVYSLSHK		3.69
		LPEGAQADLEAGK		3.65
		EVDKAEQQYGPIFAR		3.63
		QDLAGLKLPEGAQADLEAGK		3.39
		GLFPGYADGWTQVAQWQR		3.37
		NGQmPAQLEYLGEDK	M3	3.27
	GAmGFPNLTGDWR	M2	3.10	
	AEQQYGPIFAR		3.05	
	LPEGAQADLEAGKK		2.96	
	GPTDQmGHAFDGIEEYDNPLPK	M7	2.88	
	mAAMPAAWGEILGDSGVR	M1	2.77	
	WGGAPDAIR		2.58	
	YSAmSVEEVAK	M4	2.46	
	QDLAGLKLPEGAQADLEAGKK		2.35	
	YSAMSVEEVAKDPSAmK	M16	2.29	
35 kDa	Accession	Description and % coverage		
	L8MMN9	<i>cbb₃</i> -type cytochrome <i>c</i> oxidase subunit OS= <i>Pseudomonas pseudoalcaligenes</i> KF707 = NBRC 110670 GN=ppKF707C_18640 PE=3 SV=1 – [L8MMN9_PSEPS] – NCBI CcoP1 BAU73555 - 46.30%		
		Sequence	Modification	XCorr
		VHLAAYVYSLSQKPAEEGEAK	M5	5.69
		GTPAmGAPNLTHPSAFIYGSSFAQLQQTIR		4.68
		QGVmPAQENILGNDK	M4	3.13
		GAYGFPNLTNDWR		2.70
		QESTEETVGHSDGIEEYDNPLPK		2.58
		HGVmPAWGEVLGEQGVV	M4	2.46
		ADKQYGPIFAK		2.33
	YAAmPIEEVAKDPQALK	M4	2.31	
	QYGPIFAK		2.07	
37 kDa	Accession	Description and % coverage		
	L8MR96	Cytochrome <i>c</i> oxidase subunit OS= <i>Pseudomonas pseudoalcaligenes</i> KF707 = NBRC 110670 GN=ppKF707C_5503 PE=3 SV=1 – [L8MR96_PSEPS] – NCBI CoxII BAU71737 - 38.7%		
		Sequence	Modification	XCorr
		YLGdqEFFSNLATPSEQIHNK	M16	5.73
		ADHLNIVFHGKPGTsmAAFGK		5.43
		DEHYLLEVDQPLVVPVGTK		5.40
		ALTDKEWTLDELVAR		5.12
		ADHLNIVFHGKPGTsmAAFGK		4.79
		APKDEHYLLEVDQPLVVPVGTK		4.75
		KDAIPGFVNESWTR		4.17
	LKELTDKEWTLDELVAR		4.16	
	GQcTElcGKDHGFmPIVVEAK	C3 – C7 – M14	4.10	
	DHGFmPIVVEAK	M14	3.74	
	NAWGNNTGDmVTPK	M5	3.23	
	EVLALKQAESQ	M10	3.00	
	EWTLDDELVAR		2.96	
	GQcTElcGK		2.18	

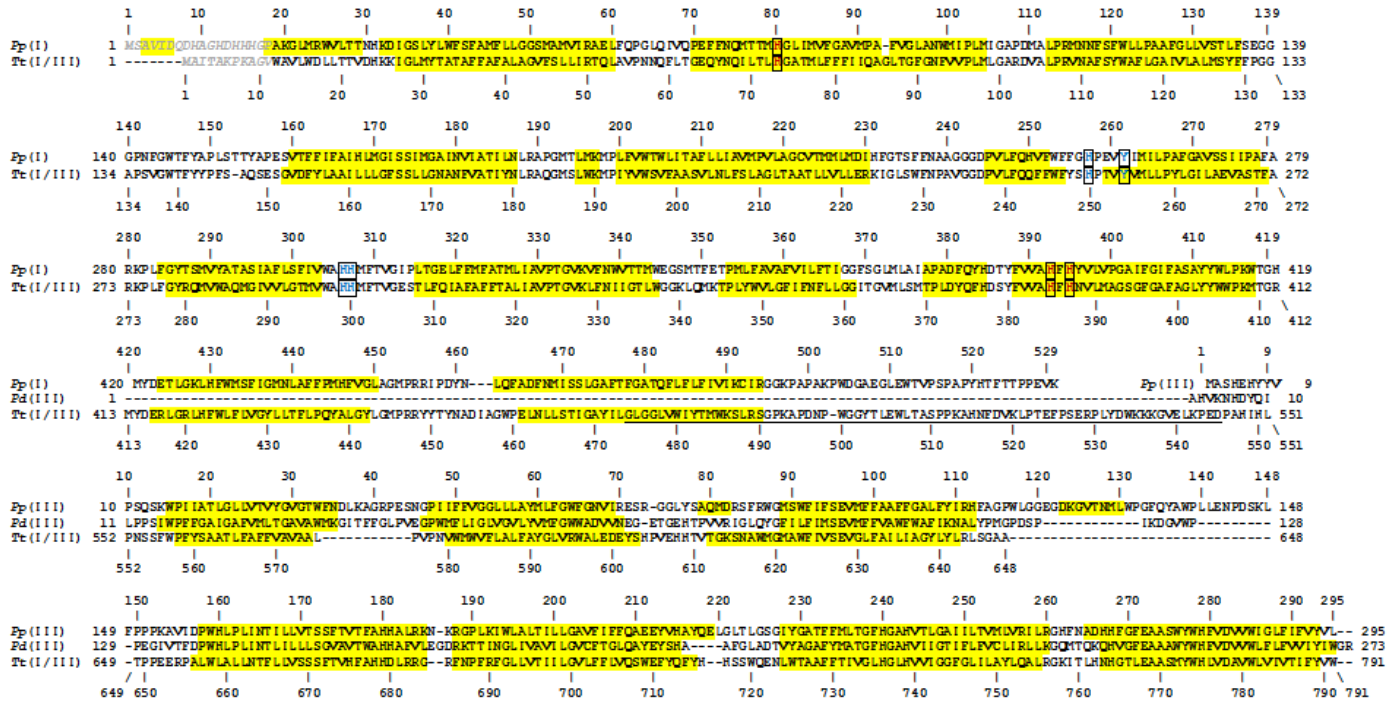
3.3.2 Caa₃ protein modeling

Following the demonstration by SDS-PAGE TMBZ staining and Nano LC-MS/MS that, the subunit II of KF707 Caa₃ oxidase contains a cytochrome *c* domain, a model structure of this protein, *Pp-caa₃*, based on the X-ray structure of *caa₃*-type cytochrome *c* oxidase from *T. thermophilus* (hereafter *Tt-caa₃*) [Lyons et al., 2012], was generated. *Pp-caa₃* consisted of three subunits, named SU I, IIC and III (Figure 3.4A). SU I (encoded by *coxI* gene) is composed by 12 transmembrane α -helices linked mainly by unstructured linkers and contains two haems *a_s* groups, located in the hydrophobic core of the domain, and one mononuclear copper center (named Cu_B) (Figure 3.4A and 3.4B). SU IIC is a fusion of canonical SU II and a cytochrome *c* domain, as observed in the case of homologous protein from *T. thermophilus* [Mather et al., 1991]. It is composed by two transmembrane α -helices in direct contact with SU I and a periplasmic domain consisting of a 7-strands antiparallel β -sheet fused with a typical cytochrome *c* subunit. SU IIC contains the haem *c* group with the Fe-ion bound to His282 and Met332, and the homobinuclear copper center (Cu_A) bound to His181, Cys216, Glu218, Cys220, His224 and Met227 (Figure 3.4A, B and C). Finally, SU III is composed by six transmembrane α -helices and is in direct contact with SU I.

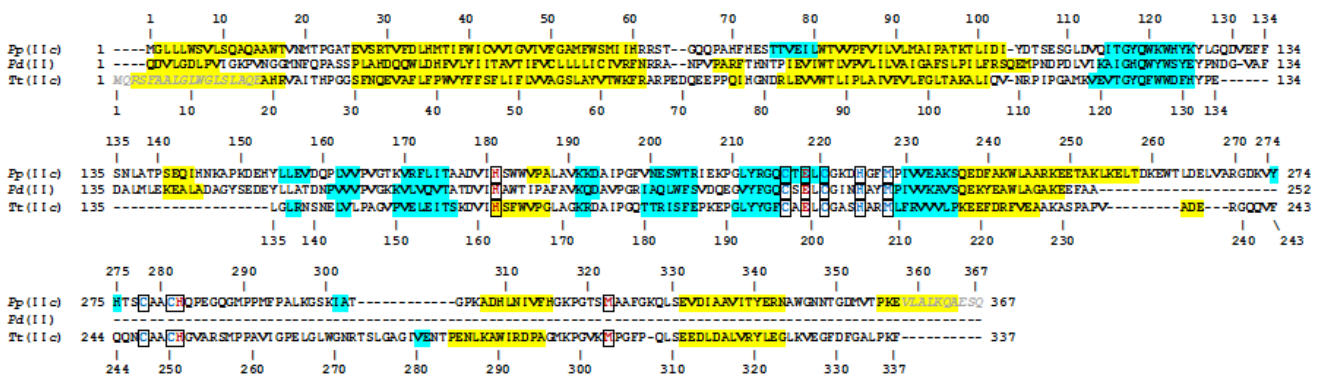
Alignment 3.1: Sequence alignment of *Pp-*caa*₃* SU I, IIc and III [*Pp*(I), *Pp*(IIc), and *Pp*(III), respectively] with the corresponding SU from *Par. denitrificans* (*Pd-*aa*₃*) and *T. thermophilus* (*Tt-*caa*₃*).

The colored secondary structure elements (α -helix, yellow; β -strand, cyan) are derived from the prediction performed by the PROMALS3D server. Iron and copper binding residues are bordered and colored in red and blue, respectively. Italicized gray residues were not modeled, due to the absence of a template for such regions. The linker between SU I and III in *Tt-*caa*₃* is underlined.

SU I/III Promals 3D alignment



SU II Promals 3D alignment



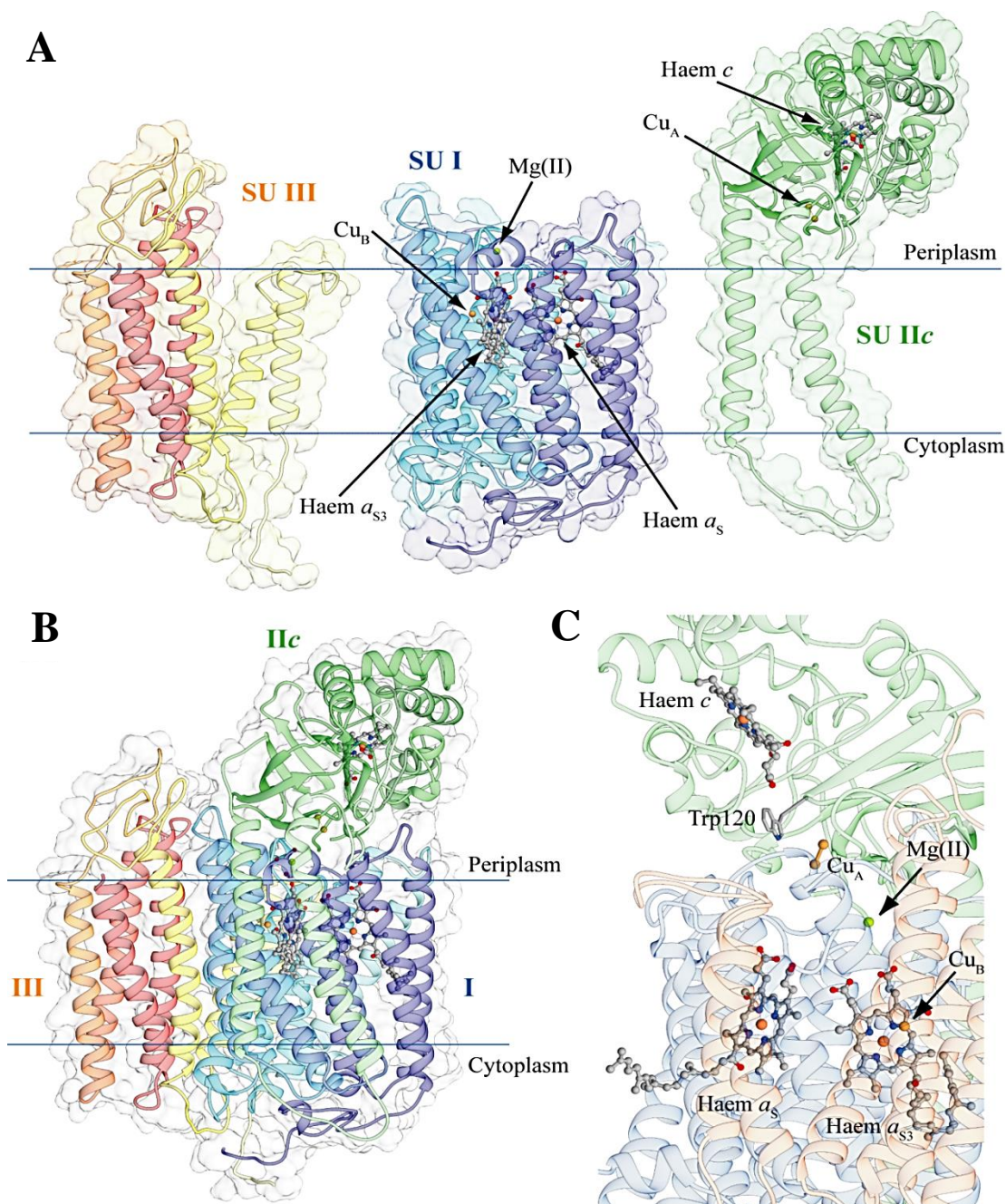


Figure 3.4. Ribbon representation of the Caa₃ oxidase homology model of KF707; SU I, SU IIc and SU III are shown as single entities (**A**) or with their organization (**B**) and their cofactor arrangements (**C**). The subunits are colored in light blue, yellow and light green in the proximity of the N-terminus, and in dark blue, dark red and dark green at the C-terminus of SU I, IIc and III, respectively. The haems are in balls and sticks with the iron and copper metal centers as orange and ochre spheres, respectively. The Mg (II) ion in SU I is shown as a green sphere. Residues involved in electron transport are reported as sticks, and colored accordingly to atom type.

The protein surface shows the typical charge distribution of a membrane protein (Figure 3.5), with a large hydrophobic region in the correspondence of the transmembrane region of SU I, II and III, twined with negatively and positively charged surfaces exposed to the aqueous environment of the periplasm and of the cytoplasm, respectively. The analysis, made with ConSurf 2016 [Ashkenazy et al., 2016], of the protein surface of the *Pp-caa₃* *Pp-caa₃* SU IIc outer-membrane region, revealed three conserved residues on a flat section located on the His282 side of the haem *c* group: Ala280, Gln283 and Phe293. Of these residues, only Ala280 is conserved in the *Tt-caa₃* sequence, suggesting a different way of interaction between the Caa₃ SU IIc and its soluble electron donor in the two species *T. thermophilus* and KF707 [Noor and Soulimane, 2012; Sandri et al., 2017].

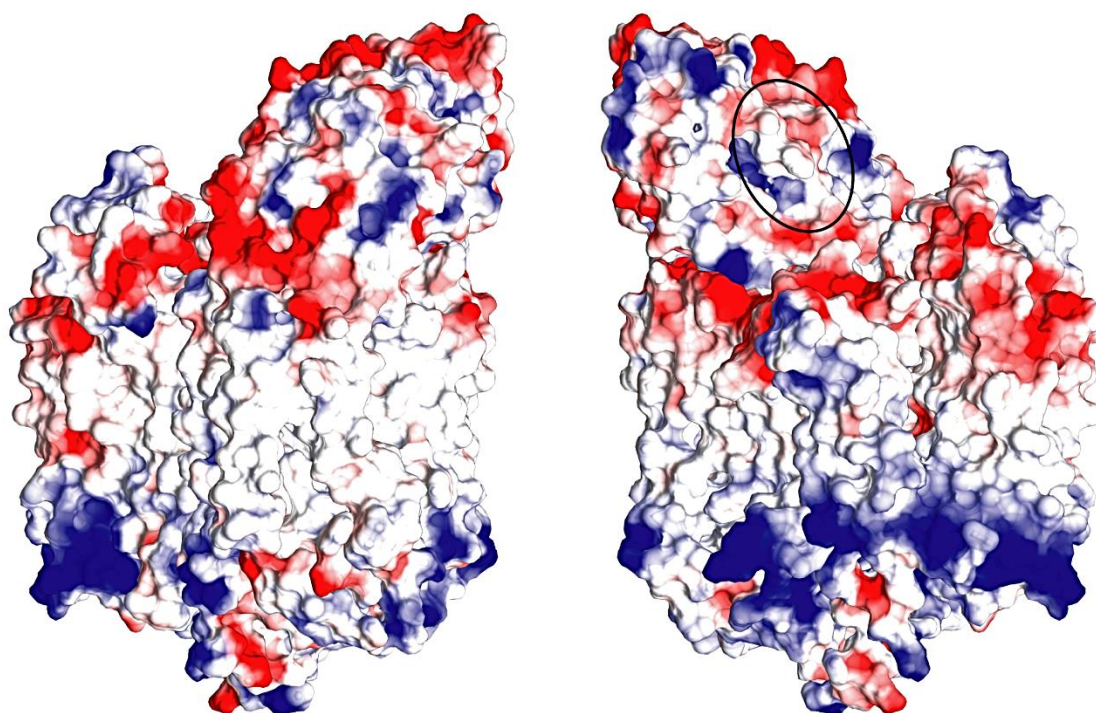


Figure 3.5: Solvent excluded surface of *Pp-cao₃* model structure colored according to the electrostatic potential contoured from -10.0 (intense red) to +10.0 kT/*e* (intense blue) (where *k* is the Boltzmann constant, *T* is the absolute temperature, and *e* is the electron charge). The black circle indicates the conserved region found on the His282 side of SU II haem *c* pocket. The surface on the right panel is rotated by 180° around the vertical axis respect to the surface in the left panel.

The electron transfer pathway observed in *Tt-caa₃* between the SU IIC haem *c* and the homobinuclear Cu_A center is conservatively mutated in the *Pp-caa₃* structure. Indeed, in *Tt-caa₃*, the electron transfer from the Cu_A binuclear center is proposed to proceed via the hydrogen bound His205 side chain of SU IIC to the amide carbonyl groups of Arg447 and Arg448 in SU I. Another hydrogen bond connects the peptide nitrogen of Arg448 to the haem porphyrin A attached propionate [Farver et al., 2006]. All of these residues are conserved in KF707 as His224 of SU IIC, Arg454 and Arg455 of SU I, suggesting that electron transfer from Cu_A to *aa₃* haem is similar in both *T. thermophilus* and KF707 species. Further, the *Tt-caa₃* Phe126 is mutated into Trp120 in KF707 *Pp-caa₃* with similar electron transfer properties, while the copper binding Cys224 (*Pp-caa₃* numbering) is conserved in both sequences.

A further distinctive feature of the Caa₃ oxidases is the presence of two proton channels located in SU I, named D- and K-pathways, respectively [Lyons et al., 2016]. These are conduits for the protons that are pumped across the membrane, and are required for chemical reduction of oxygen in the haem-Cu binuclear center (*a_{S3}*-Cu_B). In the *Tt-caa₃* structure, the D-pathway begins near to Asp103 and leads through a solvent-filled cavity to Tyr248 near SU I haem *a_{S3}*. In the *Pp-caa₃* model structure, most of the residues constituting the pathways are fully conserved or conservatively substituted (e.g., *Tt-caa₃* Tyr248 corresponds to *Pp-caa₃* Phe255) (Figure 3.6). However, a major difference is observed at the end of the D-pathway, in the proximity of haem *a_{S3}*, where *Tt-caa₃* Gln84, Ser249 and Thr252 have been substituted with Pro91, Gly256, and Glu259. Consequently, the so-called YS gateway observed in the *Tt-caa₃* structure [Lyons et al., 2012] is not present in that of *Pp-caa₃*. The K-pathway originates at *Tt-caa₃* with Glu84 of SU IIC and continues up to the binuclear copper center Cu_B via the cross-linked SU I/III His250-Tyr254, by means of Lys328. These residues are fully conserved in the *Pp-caa₃* model structure (SU IIC Glu78 and SU I His257-Tyr261 and Lys335) (Figure 3.6).

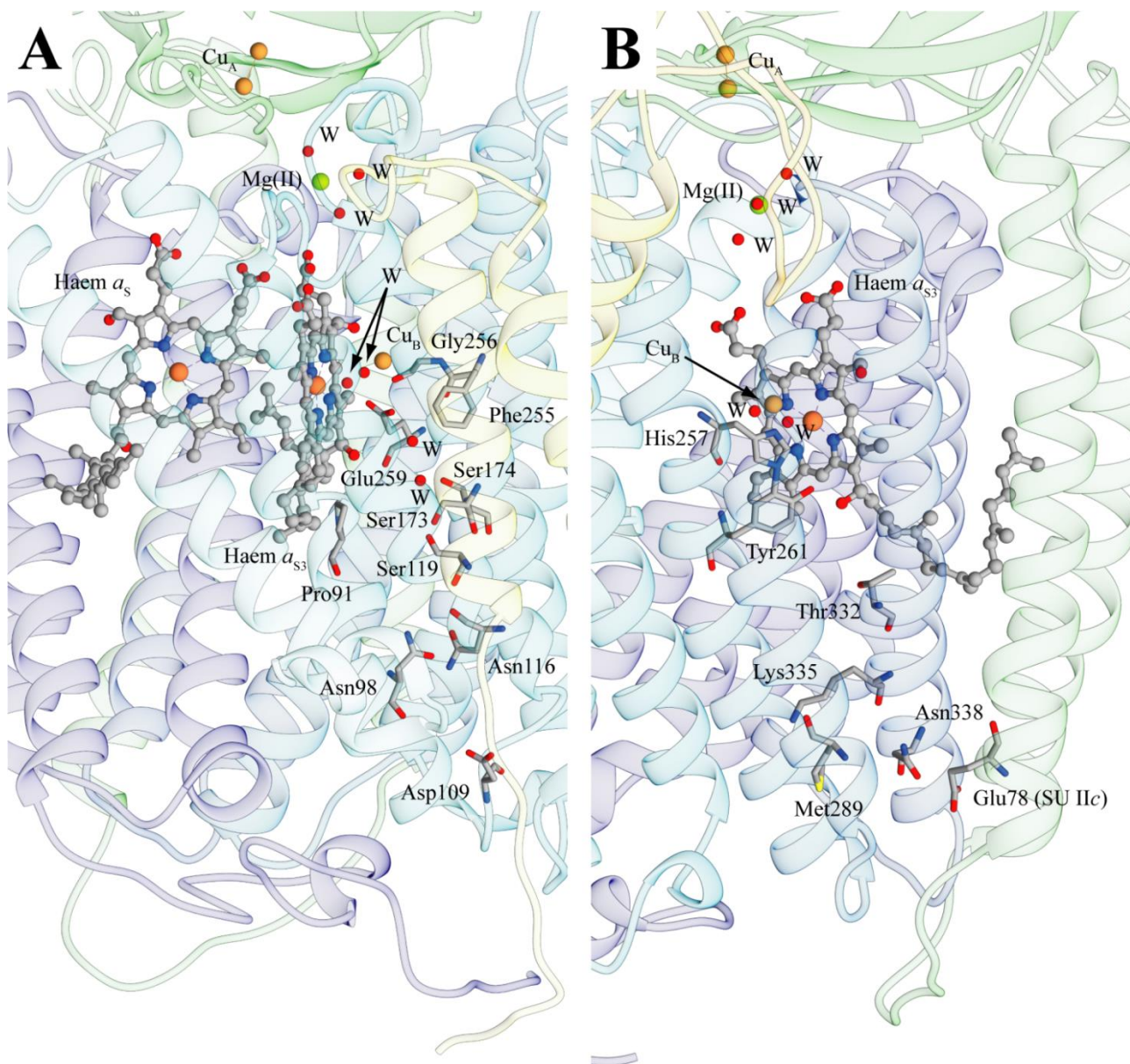


Figure 3.6: Proton D- and K-pathways (A and B, respectively) in the Caa₃ oxidase model structure of KF707. The protein backbone is reported as ribbons colored as in Figure 3.5. The haem groups are in balls and sticks with the iron and copper metal centers as orange and other spheres, respectively. The Mg (II) ion in SU I is reported as a green sphere, while water molecules (W) are depicted as red spheres. The residues mentioned in the text are in sticks colored accordingly to the atom type.

3.3.3 Cytochrome *c* oxidases electron donor

The KF707 genome, similarly to other species of γ -Proteobacteria but in contrast to *R. capsulatus* and *R. sphaeroides* in which the electron donor for cytochrome oxidases is the mono-haem cytochrome *c*₂, does not own a gene for cytochrome *c*₂; it derives that the electron donor(s) to the KF707 cytochrome oxidases belong(s) to the di-haem cytochrome *c*₄ annotated in KF707 genome.

This consideration is in line with the results obtained in Chapter 2, Table 2.7 where it was shown that horse heart cytochrome *c* (HH cyt *c*) is a poor electron donor to terminal oxidases. Indeed this activity, in either glucose or biphenyl, was 5-6 times lower than that measured with TMPD as electron donor, suggesting the low capacity of soluble HH cyt *c* to reduce KF707 respiratory oxidases, which are featured by *c*-type haems as catalytic subunits. This observation is in line with an early report, in which it was shown that HH cyt *c* was a poor substrate for the *cbb*₃-type oxidases activity of *V. cholerae*; in this latter species, the rate of oxygen reduction with HH cyt *c* was several fold lower than that with the soluble di-haem cytochrome *c*₄, which was identified as the physiological electron donor to the Cbb₃ oxidase [Chang et al., 2010].

Analysis of the KF707 annotated genome indicated the presence of three genes identified as cyt *c*₄ (BAU71765, BAU75530 and BAU75507) and of two genes identified as cyt *c*₅ (BAU77240 and BAU71764). Genes BAU71765 and BAU71764, coding for *c*₄ and *c*₅, respectively, are located in tandem on the same operon; these two genes have a high identity (85% and 74% respectively), with the *c*₄ (PA5490) and *c*₅ (PA5491) examined in *P. aeruginosa* PAO1 [Arai et al., 2014] and in *V. cholerae* [Chang et al., 2010]. On the contrary, the other putative cytochrome *c*₄ resulted to have a very low percentage identity (35% and 38%) compared to the *c*₄ electron donor found in PAO1. In addition, the cytochrome *c* profile obtained through TMBZ gels, showed the presence of only one soluble cytochrome *c* molecule, the di-haem *c*₄, identified through Nano LC-MS/MS analysis as the molecule encoded by BAU71765 gene (Figure 3.3; Table 3.3).

To investigate the role of the hypothetical electron donor for KF707 cytochrome oxidase enzymes, three different deletion mutant strains, obtained from the elimination of the genes BAU71765 and BAU71764 (cyt c_4 and cyt c_5), were constructed by Gene SOEing PCR method and conjugation.

Initially, the phenotype of these mutant strains, named $KF\Delta c_4$, $KF\Delta c_5$ and $KF\Delta c_4/c_5$, was analysed with the use of the NADI assay, on LB plates after 24 hours of growth at 30°C, and growth curves in LB or minimal salt medium, with the addition of glucose or biphenyl [6 mM]. As Figure 3.7A shows, the NADI test resulted partially negative (blue colour was less intense), in the case of cytochrome c_4 deletion ($KF\Delta c_4$ and $KF\Delta c_4/c_5$); on the contrary, $KF\Delta c_5$ did not show any difference as compared to the W.T. strain. It is also apparent by the growth curves courses, Figure 3.7B, that deletion of c_4 severely inhibited the growth rate of mutant strains such as $KF\Delta cox1-2/cco1-2$ (grey curve) while, the mutant lacking c_5 has the same growth profile of the W.T. strain. These preliminary results, taken together, suggest an involvement of the cytochrome c_4 , encoded by BAU71765, as a physiological electron donor to KF707 cytochrome c oxidases.

In addition, a TMBZ gel of membranes from KF707 W.T. and $KF\Delta c_4$ cells in their stationary growth phase was performed. As shown in Figure 3.3 (W.T. and $KF\Delta c_4$ mutant lanes) the 17 kDa bands, corresponding to cytochrome c_4 was not seen in $KF\Delta c_4$ while, all the other cytochrome c proteins were present. This latter result suggests that when cytochrome c_4 is deleted, there is no negative regulation in cytochrome oxidases promoter; these enzymes continue to be transcribed and translated, even at the stationary phase of growth.

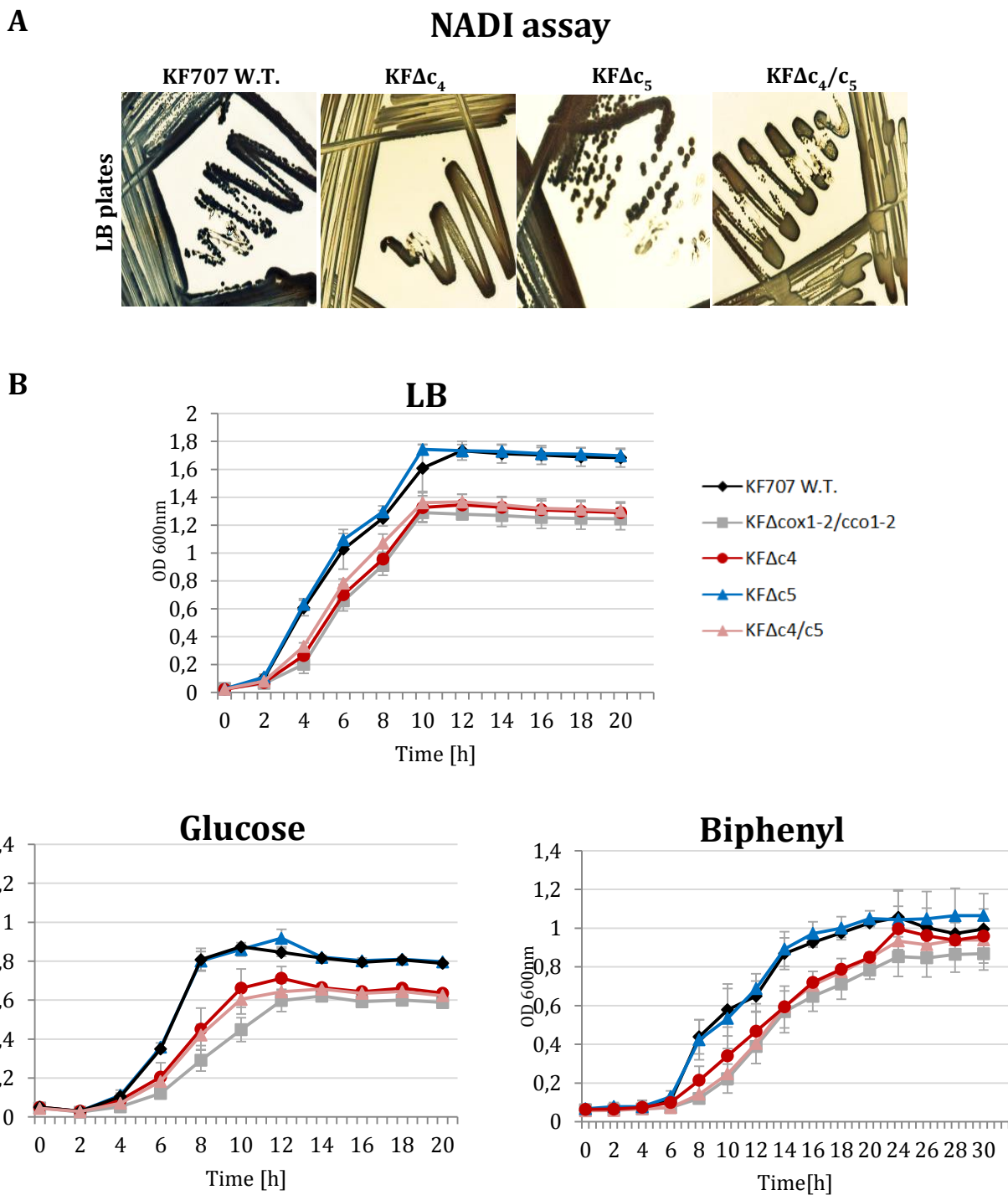


Figure 3.7: **A)** NADI assay and **B)** growth curves for KF707 W.T. and cytochrome *c* mutant strains. The assay was performed on LB plates, after an overnight growth. For growth curves, strains were grown in 50 mL of LB or MSM medium (with glucose or biphenyl [6 mM] as sole carbon source) in 250 mL flasks shaken at 130 rpm, the optical densities were evaluated at 600 nm every two hours and growths were stopped at stationary phase.

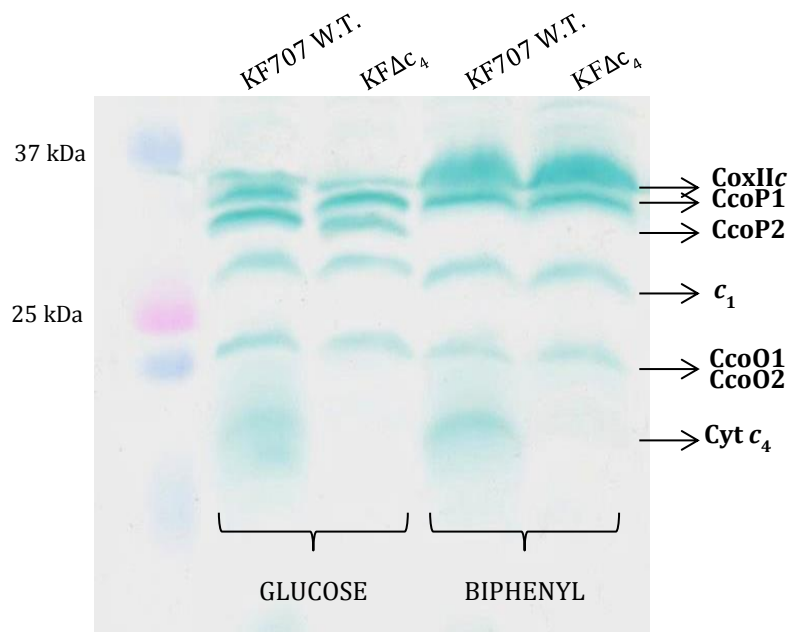


Figure 3.8: Cytochrome *c* type detected in membranes of KF707 W.T. and KFΔ_{c₄} strains, grown with glucose or biphenyl [6 mM] as carbon source until stationary phase (OD_{600 nm} 0.7-0.9). 200 μg of membrane fragments were analysed by SDS-PAGE and *c*-type cytochromes were revealed via their peroxidase activities using TMBZ staining.

In order to better verify that the main electrons transfer pathway is compromised due to the lack of cytochrome *c*₄, five KFΔ_{c₄} *lacZ* translational fusion strains were obtained using the protocol described in Chapter 2. With these strains, the promoters expression of the five different terminal oxidases was analysed at two different stages of growth, in cells grown with rich LB medium or in minimal salt medium with the addition of glucose [6 mM].

As shown in Figure 3.9, the expressions of the cytochrome *c* oxidases (Cbb₃₁, Cbb₃₂ and Caa₃) were the same in W.T. and in KFΔ_{c₄} mutant strains, with both carbon sources and phases of growth, and this confirms the results obtained with the TMBZ gel. All the cytochrome *c* oxidases are produced and their promoters regulation is not affected by the lack of cytochrome *c*₄. On the contrary, as far as concerns the CIO promoter expression, significant differences were observed in the case of KFΔ_{c₄} mutant. In all the cases analysed, the CIO oxidase was overexpressed as compared to the W.T. strain and in particular during exponential growth phase. These data suggest that the main electron transfer pathway, which contains the *bc*₁ complex and terminal cytochrome *c* oxidases, is affected by the lack of *c*₄.

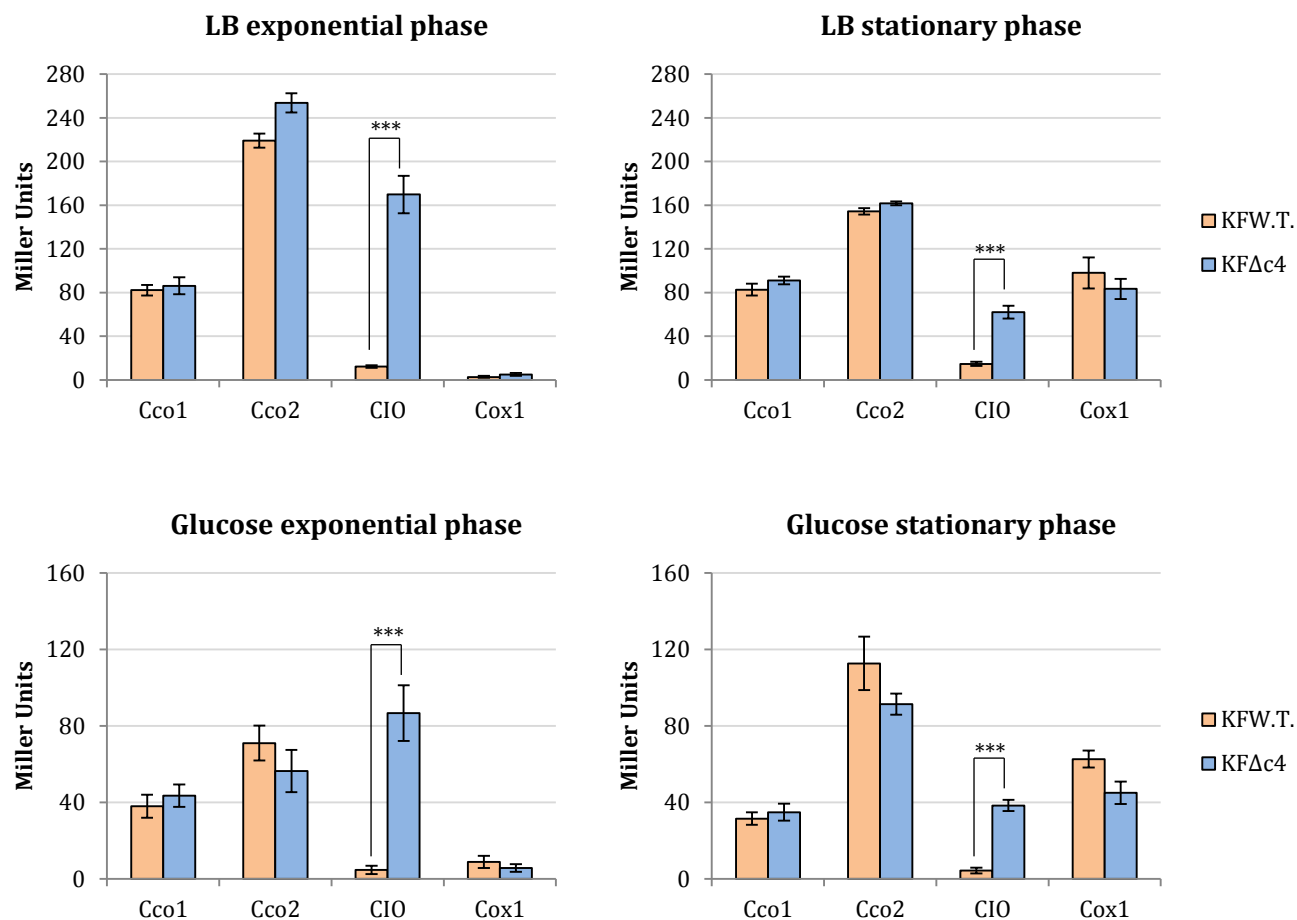


Figure 3.9: β -galactosidase activities measured in cell extracts derived from the KF707 W.T. and KF Δc_4 *lacZ* translational fusion strains, grown aerobically in LB or MSM medium with glucose [6 mM]. The assays were performed at two different stages of growth, exponential and stationary. Asterisks indicate that mean values are significantly different according to two samples *T*-test within pairs of strains (***) $p < 0.001$.

In order to confirm all the results obtained in this section and to establish the role of cytochrome *c*₄ as an electron donor to KF707 Caa₃ oxidases, the triple mutant KF Δc_4 /*cco1-2* was constructed. The rate of oxygen consumption initiated by addition of NADH (or ascorbate/TMPD) as electron donors was determined in membranes from this new mutant, KF Δc_4 and KF707 W.T. strain. The data (Table 3.4) showed that in both KF Δc_4 and KF Δc_4 /*cco1-2* membranes from cells growth either with glucose or biphenyl, NADH respiration was largely insensitive to 50 μ M of cyanide (this chemical is known to fully inhibit both *caa*₃- and *cbb*₃-type of cytochrome oxidases, as explained in Chapter 2). Thus, in

the absence of cytochrome c_4 , most of the NADH/oxygen consumption is sustained *via* the CIO oxidase activity. This latter activity was ~ 2 -3 fold higher than the equivalent activity found in KF707 W.T. membranes, but similar to that seen with KF Δ cco1-2 membranes. Most importantly, the ascorbate/TMPD-initiated oxygen consumption activity in KF Δ c_4 membranes was 70% and 80% less than that in KF707 W.Y. membranes from cells grown on glucose or biphenyl, respectively, supporting the crucial role of cytochromes c_4 in mediating TMPD oxidation *via* the terminal oxidases. Furthermore, considering that the Caa₃ oxidase was generally expressed in biphenyl-grown cells, the decrease in the ascorbate/TMPD activity seen by comparing membranes from biphenyl-grown KF Δ c_4 /cco1-2 with those from similarly grown KF Δ cco1-2, unequivocally demonstrated that cytochrome c_4 acts as a physiological electron donor also to KF707 Caa₃ oxidase.

Table 3.4: Respiratory activities in membranes from KF707 W.T. and oxidase mutant cells grown in glucose and/or in biphenyl, as sole carbon source, until the stationary phase.

Electron donors		NADH		ASCORBATE	
Additions		/	CN ⁻	TMPD	TMPD/CN ⁻
Strains					
GLUCOSE	KF W.T.	158 ± 9.0	31 ± 5.0	150 ± 15	10 ± 2.0
	KF Δ c_4	67 ± 2.0	55 ± 4.0	52 ± 2.0	4.5 ± 1.0
	KF Δ cco1-2	160 ± 8.0	114 ± 0.1	38 ± 5.0	8 ± 1.0
	KF Δ c_4 /cco1-2	85 ± 6.0	80 ± 5.0	10 ± 1.0	8 ± 1.0
BIPHENYL	KK W.T.	110 ± 3.0	10 ± 0.5	161 ± 13	8 ± 2.0
	KF Δ c_4	34 ± 2.0	31 ± 2.0	32 ± 2.0	3 ± 1.0
	KF Δ cco1-2	97 ± 8.0	27 ± 1.5	115 ± 11	5 ± 1.5
	KF Δ c_4 /cco1-2	28 ± 1.5	27 ± 1.5	15 ± 1.0	5.3 ± 1.0

Symbols and abbreviations used: N₃⁻, sodium azide [50 μM]; CN⁻, potassium cyanide [50 μM]; Cyt c, horse heart cytochrome c [50 μM]; TMPD, N,N,N',N'-tetramethyl-p-phenylene diamine [50 μM]. Rates, expressed as nmoles of O₂ consumed min⁻¹ mg of protein⁻¹, are the mean of at least two/three membrane preparations from independent cell cultures.

3.4 Discussion

Unlikely Eukaryotic (mammalian) respiratory systems where electrons are transferred to a single terminal cytochrome *c* oxidase of *aa*₃-type, most bacteria possess multiple terminal oxidases that differ in their proton pumping efficiencies and oxygen affinities, enabling energy transduction under various oxygen tensions [Poole and Cook, 2000]. Cytochrome *c* oxidases of *aa*₃-type have a low affinity for oxygen with a proton pumping stoichiometry close to 1 H⁺/e⁻, whereas oxidases of *cbb*₃-type show a high affinity for oxygen but with a H⁺/e⁻ ratio close to 0.5 [Han et al., 2011; Morris and Schmidt, 2013]. Because of the H⁺/e⁻ ratio, oxidases of *aa*₃-type are expected to be the major terminal oxidases expressed under aerobic (high O₂) conditions. For instance, in *R. sphaeroides* the *aa*₃-type oxidase is expressed when oxygen is abundant, while the *cbb*₃-type oxidase provides the ability to reduce oxygen below micromolar concentration [Baker et al., 1998]. However, the paradigm which predicts the expression of a specific terminal oxidase as a function of the relative oxygen tension in the growth medium, does not consider other parameters such as the amount and type of the carbon source available to cells and/or their optimal growth temperature, just to name a few. In *P. aeruginosa* PAO1 and *S. oneidensis* MR-1, under the same growth conditions, expression of putative genes encoding *aa*₃-type oxidases remained low under high oxygen tension, whereas those encoding *cbb*₃-type oxidases were high [Kawakami et al., 2010; Le Laz et al., 2014; Le Laz et al., 2016]. In particular, expression of the *aa*₃-type oxidase in *P. aeruginosa* PAO1, was found to be induced under nitrogen-, iron- and/or carbon-starvation [Kawakami et al., 2010; Arai 2011; Le Laz et al., 2016]. Especially the latter findings open up new perspectives in bioenergetics, as they suggest a tight metabolic control over the expression of the respiratory oxidases, irrespective of the O₂ tension available to cells. Moreover, it is known that the electron transport rate catalyzed by the respiratory chain depends on the capacity of soluble redox carriers to efficiently connect the membrane bound redox complexes to terminal oxidases [Sone et al., 2004]. Bacterial species evolved strategies, such as forming respiratory super-complexes, or fusing a *c*-type haem carrier to a terminal oxidase subunit, to overcome these rate limitations [Sone et al., 2004]. Examples of the latter kind were reported in the thermophiles *T. thermophilus* and *R. marinus* and the spore-forming *B. subtilis*, in which the subunit II of an *aa*₃-type oxidase contains an extra domain carrying a *c*-type haem [Mather et al., 1991;

Lauraeus et al., 1991; Lyons et al., 2016]. Even more complex is the situation in the facultative anaerobe *S. oneidensis* MR-1, in which the gene sequence of the C-terminal extension of the *aa₃*-type oxidases subunit II predicts the binding of two *c*-type haems [Le Laz., 2014]. Interestingly also this oxidase, named Ccaa₃, is expressed under nutrient-starved conditions as previously seen in *P. aeruginosa* PAO1 for the orthodox *aa₃*-type oxidase [Kawakami et al., 2010; Le Laz et al., 2016]. Unexpectedly, operons coding for *aa₃*-type oxidases with *c*-type domains were also reported in the anaerobe *D. vulgaris* [Lobo et al., 2008], and in the anoxygenic phototrophs *Rubrivivax gelatinosus* and *R. sphaeroides* [Zannoni et al., 2009; Hassani et al., 2010]. These observations, taken together, suggest that non-orthodox *aa₃*-type oxidases carrying additional *c*-type haems subunits (classified as Type A2 HCO) are more frequently encountered among the bacterial genera and habitats than initially thought [Sone et al., 2004]. Indeed, the earlier suggestion that the genome of KF707 contains a gene cluster coding for a Caa₃ oxidase which is expressed in cells grown on biphenyl [Sandri et al., 2017], extends the presence of a Type A2 cytochrome oxidase to a *Pseudomonas* species and also implies the existence of a tight metabolic control over the expression of the respiratory components. Here, using SDS-PAGE- TMBZ staining and tandem mass spectrometry analyses, we demonstrate for the first time that a protein band of 37 kDa corresponds to the *c*-type domain containing SU IIc of Caa₃ oxidase of KF707. As expected, the 37 kDa TMBZ stained band was absent from a mutant derivative of KF707 lacking the *coxI-II-III* gene cluster (KF707Δ*cox1-2*). Moreover, this SU IIc is more abundant in membranes from cells grown on biphenyl than those grown on glucose, in agreement with the previously determined promoter activities using *caa₃-lacZ* fusion constructs [Sandri et al., 2017].

In the light of these findings, the amino acid sequences and predicted structure of the *caa₃*-type oxidase of KF707 (*Pp-caa₃*) were compared with those from *T. thermophilus* (*Tt-caa₃*) (Alignment 3.1). A large part of the haem *c* pocket is conserved in the *Pp-caa₃* SU IIc, especially on the His282 side. On the other hand, the strand-loop-strand motif constituting the bottom of the haem *c* pocket of *Tt-caa₃* (corresponding to the residues 273-284 in *T. thermophilus* numbering) is not present in *Pp-caa₃*. This loss is compensated by a large insertion that is absent in *T. thermophilus* (residues 129-153 in the *Pp-caa₃* numeration),

and was modeled by using the structure of the aa_3 -type cytochrome *c* oxidase from *Par. denitrificans* (*Pd-aa₃*). Our structural model suggests that the haem *c* pocket in KF707 is a mix between the pockets observed in the *Tt-caa₃* and *Pd-aa₃* structures.

Comparing the homology model of *Pp-caa₃* with the structure of *Tt-caa₃*, we note that the electron transfer pathway seen between the SU I/c haem *c* and the homobinuclear center Cu_A of the latter is highly conserved in the former, except for a few conservative substitutions.

In *Tt-caa₃*, electron transfer from the Cu_A binuclear center is proposed to proceed via the hydrogen bound His205 side chain of SU I/c to the amide carbonyl groups of Arg447 and Arg448 in SU I. Another hydrogen bond connects the peptide nitrogen of Arg448 to the haem porphyrin A attached propionate [Farver et al., 2006]. All of these residues are conserved in KF707 as His224 of SU I/c, Arg454 and Arg455 of SU I, suggesting that electron transfer from Cu_A to *a*-type haems is similar in both *T. thermophilus* and KF707 species. Furthermore, the *Tt-caa₃* Phe126 is mutated into Trp120 in KF707 *Pp-caa₃* with similar electron transfer properties, while the copper binding Cys224 (*Pp-caa₃* numbering) is conserved in both sequences.

A further distinctive feature of the Caa₃ oxidases is the presence of two proton channels located in SU I, named D- and K-pathways, respectively [Lyons et al., 2016]. These are conduits for the protons that are pumped across the membrane, and are required for chemical reduction of oxygen in the haem-Cu binuclear center (a_{S3} -Cu_B). In the *Tt-caa₃* structure, the D-pathway begins near to Asp103 and leads through a solvent-filled cavity to Tyr248 near of SU I haem a_{S3} . In the *Pp-caa₃* model structure, most of the residues constituting the pathways are fully conserved or conservatively substituted (e.g. *Tt-caa₃* Tyr248 corresponds to *Pp-caa₃* Phe255) (Figure 3.6). However, a major difference is observed at the end of the D-pathway, in the proximity of haem a_{S3} , where *Tt-caa₃* Gln84, Ser249 and Thr252 have been substituted with Pro91, Gly256, and Glu259. Consequently, the so-called YS gateway observed in the *Tt-caa₃* structure [Lyons et al., 2012] is not present in that of *Pp-caa₃*. The K-pathway originates at *Tt-caa₃* with Glu84 of SU I/c and continues up to the binuclear copper center Cu_B via the cross-linked SU I/III His250-

Tyr254, by means of Lys328. These residues are fully conserved in the *Pp-caa₃* model structure (SU IIC Glu78 and SU I His257-Tyr261 and Lys335) (Figure 3.6).

Altogether, the above structural features confirm the gene sequence analysis that predicted some similarities between the *Tt-caa₃* and the *Pp-caa₃*, but also opened up a series of questions to be addressed in the near future.

Another aspect that requires further investigation in respect to the Caa₃ oxidase of KF707, concerns the proton pumping capacity. There are indeed differences at the end of the D-proton pathway in KF707 SU I in the proximity of haem *a*₃ with respect to the equivalent sequence in *T. thermophilus*, where *Tt-caa₃* Gln84, Ser249 and Thr252 have been substituted with Pro91, Gly256 and Glu259 in *Pp-caa₃*. This change leads to the lack in the *Pp-caa₃* structure of the YS gateway seen in the *Tt-caa₃* structure [Lyons et al., 2012], although it is hard to predict how this variation would affect the proton pumping stoichiometry of this enzyme. In this respect, we note that all attempts to obtain a KF707 multiple-oxidases mutant containing only the *caa₃*-type oxidase were unsuccessful [Sandri et al., 2017]. Similarly, a mutant of *P. aeruginosa* PAO1 (strain QXAa) that contained only the *aa₃*-type oxidase was unable to grow aerobically [Arai et al., 2014], unless it contained a suppressor mutation (strain QXAaS2) carrying a mutation in the two-component regulatory system RoxSR to regain the capacity to grow aerobically [Osamura et al., 2017]. Assuming that *P. aeruginosa* PAO1 and KF707 have similar regulatory mechanisms - which is likely - we are tempted to propose that the inability of the *caa₃*-type oxidase to sustain the aerobic growth of KF707 is unlikely to depend on its proton pumping efficiency.

An interesting aspect which deserves attention is that the protein surface of the *Pp-caa₃* SU IIC at its outer-membrane region shows three conserved residues (Ala280, Gln283 and Phe293) of which only one (Ala280) is conserved in *Tt-caa₃*. A possibility is that this difference might reflect the presence of different electron donors to the SU IIC of *T. thermophilus* versus that of KF707 Caa₃ oxidase. In the case of KF707, this Chapter showed for the first time in a *Pseudomonas* species that the 17 kDa di-haem *c₄* (BAU71765) functions as the main electron donor to the Caa₃ oxidase. In the case of *T. thermophilus* Caa₃ oxidase, although the multi-domain di-haem cytochrome *c₅₅₀* acts as an electron donor

[Robin et al., 2013], this subject remains a matter of controversy [Noor and Soulimane 2012]. In KF707, the electron donor(s) to cytochrome *c* oxidases is not firmly established, although the experiments conducted on the KF Δ *c*₄ mutant strain have shed some light on the role of the cytochrome *c*₄ (BAU71765) as donor to the terminal *cbb*₃ oxidases. Indeed, similarly to *P. aeruginosa* PAO1 in which the deletion of gene PA5490 coding for cyt *c*₄ slightly inhibits the cell growth [Arai et al., 2014] a partial negative NADI assay was observed in KF707, which suggests an involvement of *c*₄ in cytochrome *c* oxidases activities. An important consideration arises from the β -galactosidase assays (Figure 3.9) since the expression of the CIO promoter in KF Δ *c*₄ mutant is 10 times enhanced as compared to the W.T. strain during the exponential phase of growth and 4-5 times higher at the stationary phase. These important results indicate that the main electron transfer pathway, i.e. the one formed by the *bc*₁ complex and cytochrome *c* oxidases, is impaired and the reduced electron transport up-regulates the CIO promoter expression analogously to the effect seen by deleting the *Cbb*₃₁ oxidase [Sandri et al., 2017; Chapter 2]. Apparently, a decrease of the electron flow through the cytochrome *c* oxidases pathway causes a change in the oxidation-reduction state of the aerobic respiration chain leading to the overexpression of the CIO oxidase as seen by Comolli and Danohue [2002] by deleting the *bc*₁ complex.

In summary, although the role and function of the *Caa*₃ oxidase in KF707 necessitate further work to be fully understood, the present thesis Chapter presents biochemical and structural evidences that unequivocally establish the expression of a *caa*₃-type cytochrome *c* oxidase in KF707. In addition, we have shed some light on the role of the cytochrome *c*₄ (BAU71765) as donor to the terminal *caa*₃- and *cbb*₃-type oxidases.

Chapter 4

The role of the genes *relA* and *spoT* coding for the stringent response in *Pseudomonas pseudoalcaligenes* KF707

Background: The bacterial stringent response

Bacteria evolved several cellular regulatory mechanisms to respond and survive to external environmental changes. Many of these systems convert the external stimuli into variation of the cell concentration of specific molecules, named secondary-messengers (or alarmones), acting as pleiotropic regulators of key molecular targets [Hauryliuk et al., 2015]. In particular, there are three major nucleotide-based secondary-messengers: cyclic AMP, cyclic di-GMP and (p)ppGpp (guanosine pentaphosphate and/or guanosine tetraphosphate). The so called **stringent response** is one of the mechanisms which are activated in response to environmental changes. Specifically, it is induced when bacterial cells are subjected to particular types of stress such as heat shock, UV light or nutrient deprivation (amino acids, carbon, nitrogen, phosphate or fatty acids starvations). This system causes a slowdown or blockage of the bacterial normal growth to survive in the hostile environment [Cashel et al., 1996] and it is based on the control of the gene expression by the **alarmones (p)ppGpp**; these two molecules, ppGpp and pppGpp, are produced by the addition of a pyrophosphate to the 3'-OH position of GDP or GTP respectively [Chatterji and Ojha, 2001] (Figure 4.1). It has been shown that during the exponential growth phase, bacteria produce (p)ppGpp at a basal level, and they are continually synthesized and hydrolyzed by specific enzymes since, these molecules are the major modulators of the bacterial growth rate and fine-tuners of the general metabolism [Potrykus et al., 2011; Kriel et al., 2012; Gaca et al., 2013]. In case of stresses, alarmones start regulating the cellular metabolism by acting at two different levels: at the transcriptional level, as these secondary-messengers control the expression of genes involved in the amino acids biosynthesis [Potrykus and Cashel, 2008], and regulating the

nucleotide metabolism, as (p)ppGpp molecules bind directly the enzymes that are involved in the nucleotide biosynthesis and uptake [Gallant et al., 1971; Hochstadt-Ozer and Cashel, 1972]. Notably, both (p)ppGpp and stringent response mechanism play an important role in a wide variety of pathogenic cellular processes, such as for example: the virulence regulation [Dalebroux et al., 2010], the antibiotic resistance [Poole, 2012], the persistence [Maisonneuve and Gerdes, 2014] and the survival during host invasion.

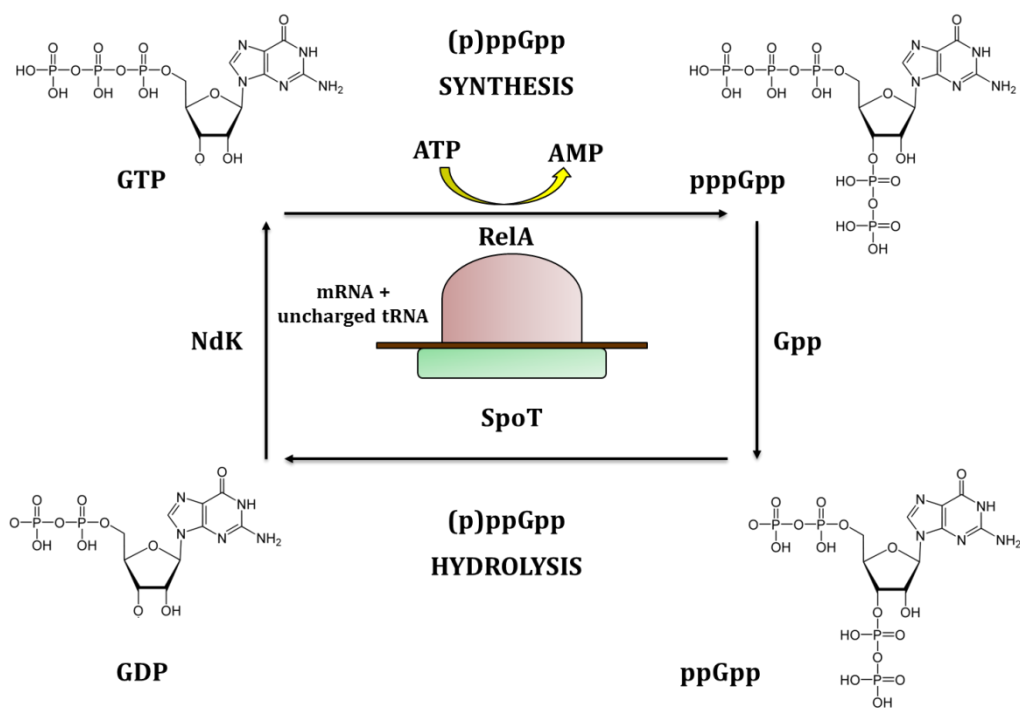


Figure 4.1: The (p)ppGpp metabolism, the long RSH proteins, RelA and SpoT, synthesize ppGpp from GTP and ppGpp from GDP, generating AMP as a by-product. Interconversion of ppGpp to ppGpp is catalyzed by ppGpp phosphatase (Gpp) and translational GTPases. SpoT catalyzes the degradation of ppGpp and ppGpp to form GTP and GDP, respectively. Interconversion of GDP to GTP is catalyzed by nucleoside diphosphate kinase (Ndk) [Hauryliuk et al., 2015].

The RelA/SpoT Homologue (RSHs protein)

The intracellular concentration of (p)ppGpp is regulated by different enzymes; the **RelA/SpoT homologue (RSH)** family has a key role in the synthesis of (p)ppGpp from ATP, GTP or GDP and in their hydrolysis to GTP or GDP [Potrykus and Cashel 2008; Atkinson et al., 2011] (Figure 4.1). The degradation of (p)ppGpp is also mediated by non-RSH enzymes

called Nudix hydrolases [Ooga et al., 2009; Ito et al., 2012], while the conversion of pppGpp to ppGpp is catalyzed by a pppGpp-5'-phosphohydrolase [Kanjee et al., 2012], or by other GTPase, such as the elongation factor G (EF-G) [Hamel and Cashel, 1973].

The RSH enzymes are highly conserved in bacteria and there are two types of them: the recently discovered “short proteins”, that have a single domain and the “long proteins”, which contain multiple domains [Atkinson et al., 2011]. The regulation and balance of activities carried out by members of RSH family is critical for bacteria. When the synthesis and hydrolysis activities of (p)ppGpp are equally active, a futile cycle of these secondary-messengers is catalyzed to maintain the proper functioning of the cell; a high synthesis of (p)ppGpp is a consequence of the stringent response activation [Mechold et al., 2013]. In Gram negative γ -Proteobacteria, such as *E. coli*, the stringent response is mediated by two multi-domain enzymes: RelA and SpoT [Hauryliuk et al., 2015] (Figure 4.1, 4.2 and 4.3). The **RelA** protein is associated with the 50S subunit of ribosomes and it has the ability to synthesize (p)ppGpp, as a response to amino acid starvation or heat shock [Gallant et al., 1977], due to the presence of the ribosomal site-A discharge [Jain et al., 2006]. Under amino acids starvation, cells accumulate deacylated tRNA that binds weakly the A-site of the ribosome; RelA protein, stimulated by the 3'-OH of the mRNA protruding from the ribosome, is directly activated. The activation of RelA resulted in the synthesis of (p)ppGpp alarmone (Figure 4.3) [Sprinzl et al., 1976; Potrykus and Cashel, 2008; Hauryliuk et al., 2015]. In contrast to cytosolic RelA, **SpoT** is a cytoplasmic protein, responsible for both the basal synthesis of (p)ppGpp during bacterial growth and the hydrolysis of alarmones under stress conditions. It has a dual function: it is a weak synthetize and strong hydrolyzes enzyme and responds to different starvation conditions such as fatty acids, iron, and carbon source [Magnusson et al., 2005; Wu and Xie, 2009]. The hydrolysis function of SpoT is extremely important for maintaining the correct (p)ppGpp concentration in the presence of RelA and, in *E. coli*, the disruption of *spoT* gene is lethal [Xiao et al., 1991].

Some bacteria possess a particular protein that is able to carry out, with the same efficiency, the synthesis and the hydrolysis of (p)ppGpp: it is called **Rel** enzyme and it is phylogenetically closer to the SpoT protein presents in γ -Proteobacteria [Wu and Xie, 2009].

The difference among the various systems that are present in microorganisms (single or double enzyme) is the result of a recent evolution; indeed, in some β and γ -Proteobacteria the presence of the two paralogues enzymes was found [Mittenhuber, 2001].

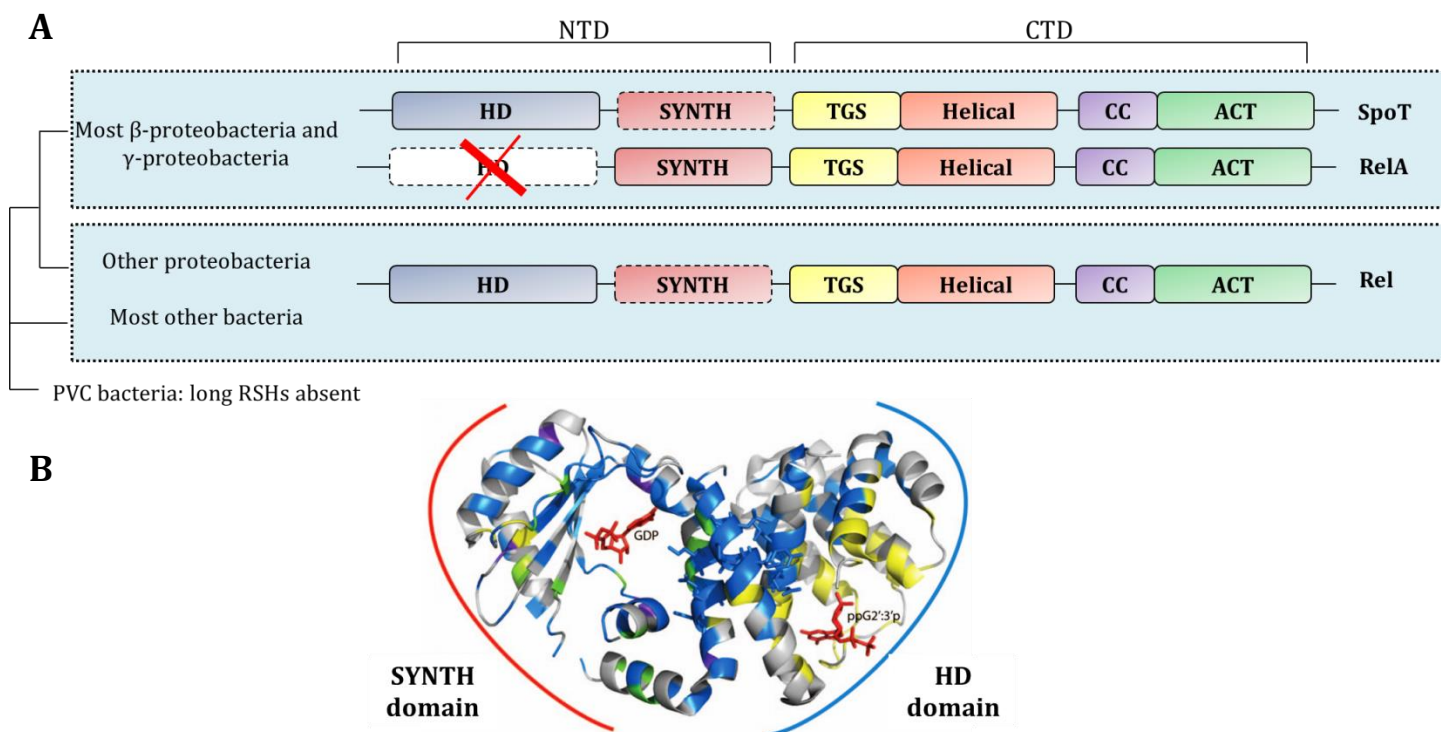


Figure 4.2: **A)** The domains of the SpoT, RelA and Rel proteins. The colored boxes, representing each domain, show their approximate location along the proteins, the dashed borders indicate domains with reduced or absent functional activity. In the case of SpoT, the synthesis (SYNTH) activity is weak, whereas hydrolysis (HD) activity is completely absent in RelA. The HD and the SYNTH domains comprise the amino-terminal domain (NTD), whereas the ThrRS GTPase and SpoT (TGS), helical, conserved cysteine (CC) and ACT domains together are comprised the carboxy-terminal domain (CTD). The phylogenetic tree summarizes the evolutionary relationship among bacteria that contain or lack long RSHs [Haurlyuk et al., 2015]. **B)** Structure of NTD of the Rel protein from *Streptococcus equisimilis*; the SYNTH and the HD domain are shown and it is possible to observe the GDP/GTP and the (p)ppGpp binding sites [Atkinson et al., 2011].

All the RSH proteins have the same six-domain structure which is divided into (Figure 4.2):

- ✓ The N-terminal region, that contains the fundamental (p)ppGpp hydrolysis and synthesis domains (**HD** and **SYNTH**).
- ✓ The C-terminal region, that contains the GTPase domain (TGS), a helical domain, the domain containing conserved cysteine (**CC**) and the aspartatokinase chorismate mutase and TyrA domain (**ACT**). These domains contribute to the RSH protein regulation [Atkinson et al., 2011],

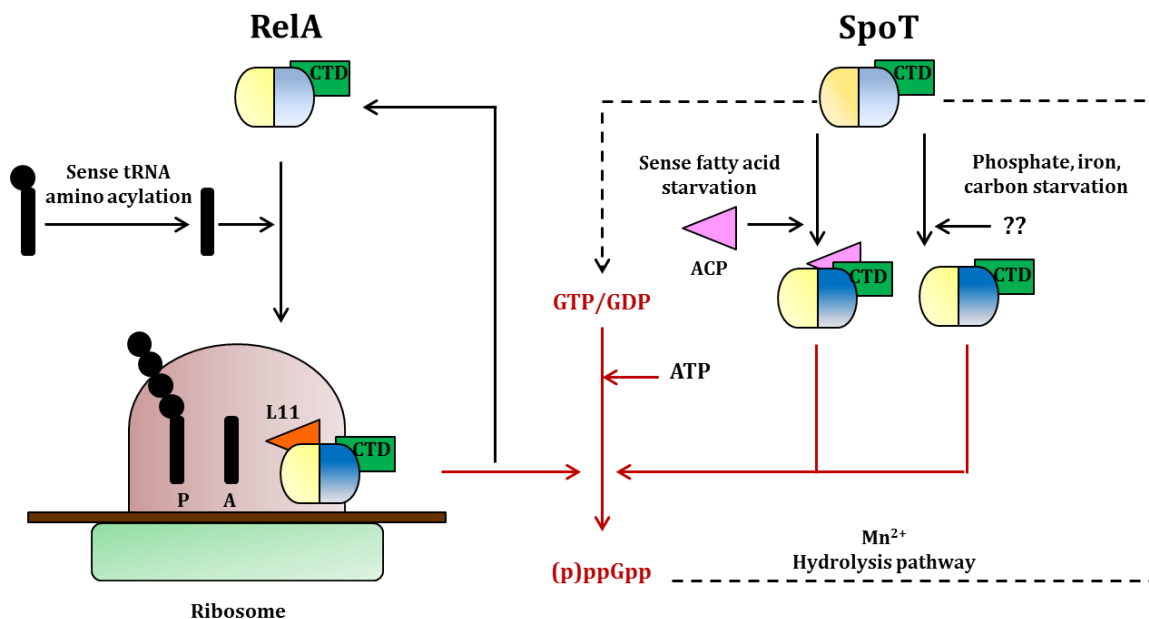


Figure 4.3: Roles of RelA and SpoT, the NTD hydrolase/synthase (yellow and blue) and the CTD (green) domains are shown. Activation of RelA requires: an uncharged tRNA, a translating ribosome with an empty A-site and L11 protein. Synthesis of (p)ppGpp from GTP or GDP involves pyrophosphoryl transfer from ATP and it is accompanied by release of RelA. SpoT regulation is divided in two ways. Acyl carrier protein (ACP) lacking fatty acids binds SpoT and the CTD region shifts the activity balance to synthesis. Other stress conditions provoke a similar shift of the activity balance by unknown mechanisms. Hydrolysis of (p)ppGpp regenerates GTP or GDP and requires Mn²⁺ [Potrykus and Cashel, 2008].

The SYNTH domain is necessary to synthesize (p)ppGpp and contains a binding site for GDP or GTP: furthermore, the synthesis reaction requires the presence of a Mg²⁺ in the catalytic site. The HD domain is designated for the hydrolysis of (p)ppGpp, and contains the typical amino acid motif His-Asp and a series of α -helices; its particular structure has a conformation that makes the bond with the (p)ppGpp molecules possible. SpoT-type hydrolases are usually pyrophosphatase Mn²⁺ dependent enzymes [Aravind and Koonin 1998; Hogg et al., 2004]. In bacteria that have only one RSH protein which performs both functions, this protein has both SYNTH and HD active domains; on the contrary, in the case of RelA, the HD domain is present but not functioning, while in SpoT enzymes they are both present but the HD domain has more activity than SYNTH domain [Aravind and Koonin, 1998; Atkinson et al., 2011].

In all these enzymes the C-terminal region contains a series of domains that bind particularly specific substrates and that participate in the regulation of the protein. The ACT domain regulates the synthetase activity in relation to the amino acids concentration. The TGS domain is involved in the response to the fatty acids starvation; ACP protein, a cofactor in the fatty acids and lipids metabolism, binds the TGS domain in SpoT enzyme [Battesti and Bouveret, 2006]. This binding is determined by the ratio of acetylated and non-acetylated ACP present in the cell and is also responsible for the (p)ppGpp accumulation during growth under stress conditions (Figure 4.3).

The role of (p)ppGpp in bacterial cells

Regulation of transcription

During stress conditions bacteria cells accumulate (p)ppGpp. This phenomenon causes changes in the **RNA polymerase** (RNAP) activity and in the global gene expression. The regulation of transcription, mediated by (p)ppGpp, can be activated in three different ways: i) direct inhibition of the ribosomal promoters, ii) direct activation of the amino acids biosynthesis promoters and iii) indirect activation by alternative σ factors [Potrykus and Cashel, 2008]. During amino acids starvation the transcription of rRNA and ribosomal gene promoters are inhibited by the alarmones; at the same time these molecules activate the genes for the amino acid biosynthesis [Potrykus and Cashel, 2008]. The transcription regulation of the genes by (p)ppGpp is closely related to RNAP; in fact, RNA polymerase is a direct target of the alarmones, that bind to it destabilizing the open complex RNAP-gene promoter [Chatterji and Ojha, 2001; Artsimovitch et al., 2004; Potrykus and Cashel, 2008]. In *E. coli*, it was shown that (p)ppGpp molecules exert their physiological effects by interacting directly with RNAP via **DskA**, that is a transcription factor and it is a DnaK suppressor; this molecule is essential to amplify the alarmones effects [Dalebroux and Swanson, 2012]. When (p)ppGpp and DskA bind the RNAP there is no physical interaction between them, because they are located at opposite sites of the polymerase: the binding of these three molecules is determined by the presence of Mg^{2+} ions. DskA protein is crucial in different mechanisms: it regulates cell division, it is involved in quorum sensing processes, it influences the expression of virulence factors [Wu and Xie, 2009]. DskA, associated with (p)ppGpp, causes opposite effects within the cell: it down-regulates the high expression of

stable RNAs (tRNA and rRNA) and of the genes involved in the cell division, while, it up-regulates the expression of the genes necessary for the stress responses [Magnusson et al., 2005]. (p)ppGpp and DskA are also responsible for the stimulation of the alternative σ -factor **RpoD** (also named σ^{70}). During the exponential phase of growth, RpoD interacts with the RNAP to initiate the transcription of genes that are essential for the synthesis of proteins, lipids and DNA. Throughout the stringent response, high concentration of (p)ppGpp inhibits RNAP to bind strongly the σ^{70} dependent gene promoters (such as tRNA and rRNA); consequently, RNAP is available to bind other alternative σ factors that are necessary to transcribe genes involved in the stress response [Dalebroux and Swanson, 2012]. **RpoS** (also named σ^S), it is one of the most active alternative σ factor, is crucial during stationary phase for stress resistance and for the expression of virulence factors, in different pathogenic bacteria [Gummeson et al., 2009; Battesti et al., 2011].

Effects on bacterial physiology

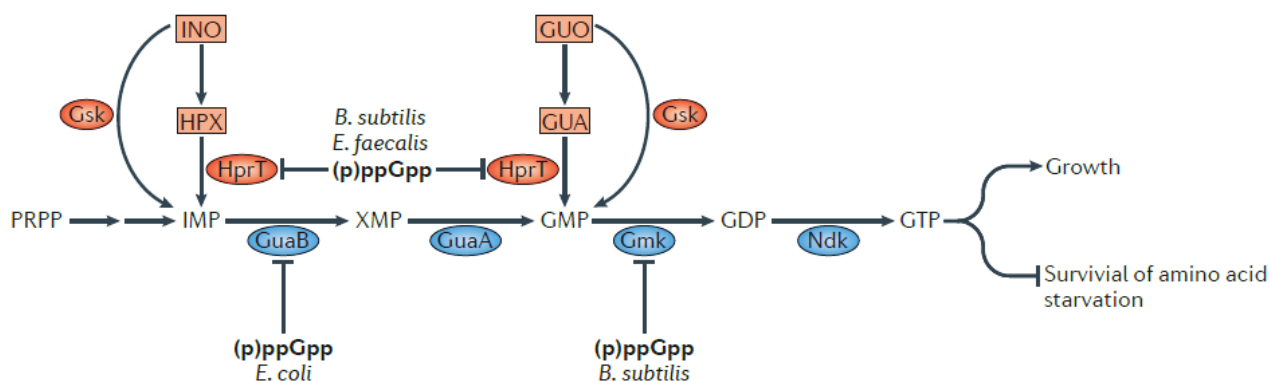


Figure 4.4: In *Escherichia coli*, the salvage pathway (red) utilizes either guanosine (GUO), guanine (GUA), inosine (INO) or hypoxanthine (HPX) as substrates. Guanosine kinase (Gsk) converts the nucleosides guanosine and inosine to GMP and inosine 5'-phosphate (IMP), respectively. The *de novo* pathway uses phosphoribosyl pyrophosphate (PRPP) as a starting compound for the multistep synthesis of IMP, which is further converted to GTP. The transformation is achieved in four steps: IMP is first converted into xanthosine 5'-phosphate (XMP) by IMP dehydrogenase (GuaB), and GMP synthase (GuaA) then converts XMP into GMP. GMP is transformed into the final product, GTP, via sequential rounds of phosphorylation: GMP kinase (Gmk) catalyses the conversion of GMP into GDP, which is then converted to GTP by nucleoside diphosphate kinase (Ndk).

The specific targets of guanosine tetraphosphate and guanosine pentaphosphate (collectively termed (p)ppGpp)-mediated control vary according to species and differ in *E. coli*, *B. subtilis* and *Enterococcus faecalis*. In *E. coli*, (p)ppGpp inhibits GuaB; in *B. subtilis* and *E. faecalis*, (p)ppGpp inhibits hypoxanthine phosphoribosyltransferase (HprT; the enzyme that catalyses the conversion of both hypoxanthine to IMP and guanine to GMP); in *B. subtilis*, (p)ppGpp also inhibits Gmk [Hauryliuk et al., 2015].

The alarmones play different roles in the bacterial physiology and they perform their mechanism at different levels.

(p)ppGpp also operate in regulating **GTP biosynthesis**; there are two different pathways for GTP production, the *de novo* pathway and the *salvage* pathway (Figure 4.4).

In the first case, phosphoribosyl pyrophosphate (PRPP) is used as a starting compound for the inosine-5'-phosphate (IMP) synthesis, then the pathway continues until the production of GTP; in the second case, the *salvage* pathway, the nucleotides are synthesized from intermediates (nucleobases and ribonucleobases) [Jensen et al., 2008; Hauryliuk et al., 2015]. In both cases, the (p)ppGpp play an important role; their importance in the nucleotide synthesis was first discovered in *E. coli* [Irr and Gallant, 1969] and subsequently it was found that they act at the level of IMP dehydrogenase (GuaB) [Pao and Dyess, 1981], while in *B. subtilis* (p)ppGpp are involved and in the regulation of GMP kinase (GmK) and HprT, which catalyzes the conversion of both hypoxanthine to IMP and guanine to GMP [Kriet et al., 2014]. In this latter bacterium, an overproduction of GTP was observed in mutants lacking genes encoding functional RSH enzymes; in addition, it was shown that in growth media containing guanosine, the GTP levels increased causing an imbalance of GTP metabolism, which leads to a decrease in survival during starvation [Kriet et al., 2014].

Several studies have shown the involvement of the stringent response in virulence, pathogenesis and persistence of pathogenic bacteria. For example, in *V. cholerae* the RelA deletion causes a down-regulation of its virulence [Haralalka et al., 2003], while in *Mycobacterium tuberculosis* it has been shown that, the absence of *relA* and/or *spoT* genes, prevents long-term survival within the host [Primm et al., 2000].

(p)ppGpp appear to be also involved in cell division and in the morphogenesis of bacterial colonies; in *Mycobacterium smegmatis*, knockout mutants of RSH proteins, determined a difference in the growth and size of the colonies, which was directly associated with the lack of alarmones production [Mathew et al., 2004; Dahl et al., 2005].

Finally, these nucleosides seem to also affect the antibiotics production; in fact, in *Streptomyces coelicolor* the overproduction of (p)ppGpp blocked the synthesis of antibiotics and secondary metabolites [Chakraborty and Bibb, 1997].

For all these reasons, (p)ppGpps are also named global regulators of bacterial cells since they are versatile molecules and secondary-messengers implicated in a variety of functions and in the regulations of the entire cellular metabolism (Figure 4.5).

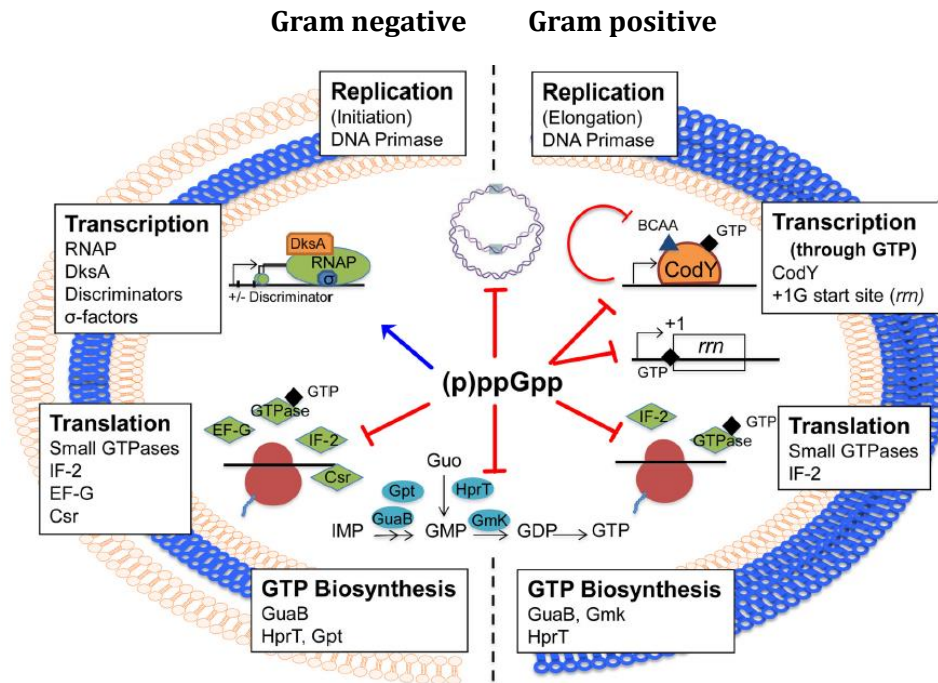


Figure 4.5: Main targets of (p)ppGpp in Gram negative (γ -Proteobacteria) and in Gram positive (*Firmicutes*). The regulatory nucleotides (p)ppGpp alter cellular metabolism in response to stress by directly binding to a variety of enzymes. The alarmones act, in both bacterial types, at different levels: during DNA replication, RNA transcription and translation and in GTP biosynthesis [Gaca et al., 2015].

4.1 Introduction

The bacterial stringent response has long been studied in the pathogenic bacterium *Pseudomonas aeruginosa* or in other *Pseudomonas* strains while, up to now, there are no report on the role of RSH proteins in *Pseudomonas pseudoalcaligenes* KF707. As previously described, γ -Proteobacteria such as *Pseudomonas spp.*, usually have two different proteins involved in the balance of (p)ppGpp: RelA, the foremost producer of the alarmones, and SpoT, the secondary producer and the sole responsible the degrading these signaling molecules [Vogt et al., 2011].

An initial study conducted on *P. aeruginosa* PAO1 demonstrated that in this human opportunistic pathogen, the complex **quorum sensing** circuit linked to the stationary σ factor RpoS, was required for cell density-dependent production of many secreted virulence factors. In particular, it was found that the overexpression of RelA protein activated RpoS and led to premature production of LasB, an extracellular virulence factor. In addition, it was observed that *lasR* and *rhlR* genes, involved in the regulation of two different quorum sensing systems, were prematurely activated by a stringent response mediated by RelA overexpression [van Dalden et al., 2001].

More recently, a series of studies on the role of the stringent response in *P. aeruginosa* **virulence** in a *Drosophila melanogaster* model system were published [Vogt et al., 2011]. It was shown that in *P. aeruginosa* RelA deleted mutant the virulence was attenuated. In a subsequent work, examining the role of SpoT, the construction of a *P. aeruginosa* RelA/SpoT double mutant strain, revealed that it was unable to establish a chronic infection in *D. melanogaster* and it was incapable of synthesizing the correct amount of virulence determinants like pyocyanin, elastase, protease and siderophores. In addition this mutant was defective in **swarming** and **twitching motility** and it was also less able to withstand stresses, such as oxidative stress and heat shock as compared to *P. aeruginosa* PAO1 W.T. strain [Vogt et al., 2011]. *P. aeruginosa* was also used as a model organism to better understand the relationship between the starvation response and the **antibiotic tolerance** in **biofilms**.

Usually, when nutrients are limited, bacteria become highly tolerant to antibiotics; in *P. aeruginosa* it was demonstrated that the antibiotic tolerance of nutrient-limited cultures and biofilm formation was mediated by active starvation responses. These protective mechanisms are controlled by the stringent response molecules and, it was discovered a link between the stringent response mediated tolerance and the reduction of oxidant stress levels in bacterial cells. Furthermore, the inactivation of stringent response mechanism sensitized biofilms production improving the efficiency of antibiotic treatment in experimental infections [Nguyen et al., 2011]. In addition, it was found that stringent response was required for optimal catalase activity and H₂O₂ tolerance during both planktonic and biofilms growth conditions [Khakimova et al., 2013].

It has recently been demonstrated that the ability of *Pseudomonas* sp. strain DF41 to inhibit the fungal pathogen *Sclerotinia sclerotiorum* is related with the stringent response mechanism. Indeed, it was discovered that a mutant lacking *relA* and/or *spoT*, exhibited increased antifungal activity. Subsequently, studies investigating the link between the stringent response and regulators of biocontrol, demonstrated that the *rpoS* transcription was reduced significantly in *relA/spoT* mutant strain [Manuel et al., 2011]. Similar results were reported in *Pseudomonas chlororaphis* PA23, where the deletion of the stringent response encoding genes also increased the inhibition of *S. sclerotiorum* and the production of pyrrolnitrin, lipase and protease [Manuel et al., 2012].

Interestingly (p)ppGpp alarmones seem to be required even for virulence, cells size control and survival for *P. syringae* on plants. In the *relA/spoT* mutant of this latter strain, the bacterial growth was significantly reduced and it was completely impaired to colonize bean leaves or roots. In addition, the lacking of the (p)ppGpp production resulted in loss of swarming motility, increased sensitivity to oxidative stress and antibiotic tolerance and the reduction of pyoverdine production [Chatnaparat et al., 2015].

Finally, in *P. putida* KT2440, a link between stringent response and the synthesis of medium-chain-length polyhydroxyalcanoates (**mcl-PHAs**), was discovered. mcl-PHAs are produced using various substrates, but, the molecular mechanisms for their synthesis in

response to environmental stimuli are still not clear. A stringent response mutant of *P. putida* KT2440, unable to produce (p)ppGpp, was analyzed and it resulted to be able to accumulate mcl-PHAs in both optimal and nitrogen limiting conditions; the starvation in this mutant strain, did not change the efficiency of the mcl-PHAs production [Mozejko-Ciesielska et al., 2017].

From the above reported results, it is apparent that the stringent response phenomenon in *Pseudomonas* spp., is extremely complex and it is associated with different mechanisms which are used by bacteria to cope with environmental changes. The ability of KF707 to use a large variety of compounds for growth, prompted to us to analyze whether the stringent response is involved in KF707 growth in the presence of specific carbon sources.

In this respect, it is noteworthy that an early investigation, conducted in 2009 before the completion of KF707 genome sequencing [Triscari-Barberi et al., 2012], led to the isolation of a mutant (named KF707 4.2) which was selected from a library obtained by random insertion of the mini-Tn5-*lacZ1* transposone. This mutant strain was unable to grow in a medium containing a mix of benzoic acid (BA) and 3-chlorobenzoic acid (3-CBA); on the contrary, the KF707 W.T strain grew in the presence of these two compounds. The amino acid sequence that was interrupted by the transposone, was found to be comprised between the SYNTH and the TGS domain in SpoT protein. Additional phenotype analysis conducted on this mutant strains, reported that it was unable to grow in the presence of 2,-3,-4-CBA+BA; however, when biphenyl was added in the growth medium, it recovered the ability to degrade these types of compounds. A Phenotype Microarray analysis of this mutant, detected a large reorganization in the metabolism of aromatics and nitrogenous carbon sources; finally, the detection of the (p)ppGpp production revealed that KF707 4.2 mutant had defects in the production of these alarmones when exposed to an inducer of the stringent response.

Taken together, these results, suggested an involvement of SpoT in the regulation of the metabolism of chlorinated compounds. As described in the General Introduction, the degradation of PCBs is a process that requires the presence of biphenyl (co-metabolism), and in this specific case it seems that the stringent response protein SpoT is involved in the

second part of the PCBs metabolic pathway, following biphenyl degradation. The involvement of the stringent response in the metabolism of chlorinated compounds has never been studied and this link could be an important clue to better understand KF707's ability to adapt to extreme environment contaminated by toxic compounds.

4.2 Materials and Method

4.2.1 Bacterial strains and plasmids

All strains and plasmids, used in this chapter, are listed in Table 4.1.

Table 4.1: Bacterial strains and plasmids.

Bacterial Strains	Relevant Genotype	Reference
<i>P. pseudoalcaligenes</i> KF707		
Wild type (W.T.)	Amp ^r	Furukawa and Miyazaki, 1986
KFΔrelA	Deletion of <i>relA</i> , Amp ^r	This study
KFΔrelA/spoT	Deletion of <i>relA</i> and <i>spoT</i> Amp ^r	This study
KFΔrelA/spoT <i>cox1Lac</i>	Deletion of <i>relA</i> and <i>spoT</i> , <i>coxII::lacZ</i> translational fusion, Amp ^r	This study
KFΔrelA/spoT <i>cco2Lac</i>	Deletion of <i>relA</i> and <i>spoT</i> , <i>ccoN2::lacZ</i> translational fusion, Amp ^r	This study
KFΔrelA/spoT + <i>relA</i>	Deletion of <i>relA</i> and <i>spoT</i> Amp ^r + pSEVA342- <i>relA</i>	This study
KFΔrelA/spoT + <i>spoT</i>	Deletion of <i>relA</i> and <i>spoT</i> Amp ^r + <i>spoT</i>	This study
KFΔrelA/spoT + <i>relA</i> + <i>spoT</i>	Deletion of <i>relA</i> and <i>spoT</i> Amp ^r + pSEVA342- <i>relA</i> + <i>spoT</i>	This study
<i>Escherichia coli</i>		
DH5α	<i>supE44, hsdR17, recA1, endA1, gyrA96, thi1, relA1</i>	Hanahan, 1983
HB101	Sm ^r , <i>recA, thi, pro, leu, hsdR</i>	Boyer and Roland-Dussoix, 1969
Plasmids	Relevant Genotype	Reference
pG19II	Gm ^r , <i>sacB, lacZ</i> , cloning vector and conjugative plasmid	Maseda et al., 2004
pSEVA342	Cm ^r , pRO1600/ColE1, <i>lacZα</i> -pUC19	Silva-Rocha et al., 2012
pG19IIΔrelA	Gm ^r , <i>sacB, lacZ</i> , carrying Δ <i>relA</i> deleted fragment	This study
pG19IIΔspoT	Gm ^r , <i>sacB, lacZ</i> , carrying Δ <i>spoT</i> deleted fragment	This study
pSEVA342- <i>relA</i>	Cm ^r , pSEVA342 carrying <i>relA</i> gene	This study
pG19II- <i>spoT</i>	Gm ^r , <i>sacB, lacZ</i> , carrying <i>spoT</i> gene	This study

4.2.2 KF707 deletion mutant and complemented strains for *relA* and *spoT* genes

Deletion mutant strains were obtained by using Gene SOEing PCR technique and conjugation protocol, as described in General Materials and Methods.

All the primers used for the deletion Δ constructs and for the amplification of *relA* and *spoT* genes, for the KF707 complementation strains, are listed in Table 4.2.

Table 4.2: Primers used for the construction of the deletion fragments (Δ) and for the amplifications of *relA* and *spoT* genes. The red nucleotides form the overlap region for the UP and DOWN deletion fragments union PCR, while the nucleotides that form the cutting site for the restriction enzymes are in bold.

Gene	Primer name	Sequence	Restriction enzyme
ΔrelA	FOR up	TAAAT TCTGCAGG TCTTCAGGCCGACCTG	<i>Pst</i> I
	REV up	AGTGTGTACTAACAGCGTAGT CCTTGCCTACCTTCCCTAC	
	FOR down	ACTACGCTGTTAGTACACACT TTGGCGCCGGAGCCTGCGAAGC	
	REV down	ACATGAT CTAGACT TCTCGGCGCGCTCCTC	<i>Xba</i> I
ΔspoT	FOR up	AT CACTGCAGACT TTCGTCAAGGGAAGCGTCG	<i>Pst</i> I
	REV up	TAGGAGTCAGTATGGAACAGT GATCTGTCTCCTTGCCGGCCT	
	FOR down	ACTGTTCATACTGACTCCTA GTA AACCAAGGAGTTCCC	
	REV down	GGTT GAATTCT GAAAGCGCATGGCGGGTTCCCT	<i>Eco</i> RI
<i>relA</i>	FOR	CAACAA AGCTT GGTACAGGTGAAGCG	<i>Hind</i> III
	REV	TCAGTTGGAT CCCTAGGCT GCGCGGTTACG	<i>Bam</i> HI
<i>spoT</i>	FOR	ATCGATA AGCTT GCCGAGCATAGACGCCTCGC	<i>Hind</i> III
	REV	ATATTAG GATCC TACGCGCGCACGCGGGTGAT	<i>Bam</i> HI

To restore the wild type genotype in KF Δ relA/*spoT* mutant strains, *relA* and *spoT* genes were reintroduced using pSEVA342 and pG19II vectors, respectively.

The two genes *relA* and *spoT* were amplified, using a High Fidelity Taq Polymerase (Thermo Fisher), provided with a proofreading activity in order to avoid errors during polymerization; the reagents were added according to the datasheet.

After the reactions, PCR products were purified with a Gel Extraction kit (QIAquick – QIAGEN), digested with specific restriction enzymes (listed in Table 4.2) and individually ligated into pSEVA342 and pG19II. The correct cloning was confirmed by plasmid DNA extraction, Colony PCR and DNA sequencing analysis. Finally, the conjugation protocol (General Materials and Methods) was performed by using KF Δ relA/*spoT* deletion mutant

strain, recombinant pSEVA342 and/or pG19II plasmids, and *E. coli* HB101 strain carrying the pRK2021 helper plasmid. Through this method, it was possible to reintroduce the wild type genes in the deleted mutant strain. At the end, through Colony PCR and DNA sequencing analysis, complementations were confirmed.

4.2.3 Growth of KF707 mutant strains with different carbon sources

The effect of the deletion of *relA* and *spot* genes was assessed by monitoring cells growth in liquid cultures and on plates, using LB or minimal salt medium (MSM) with the addition of a single carbon source [6 mM]. Several types of carbon sources were used, namely: pyruvate, succinate, fumarate, glucose, fructose, benzoate, *p*-hydroxybenzoate and biphenyl. When necessary, antibiotics were added to the growth medium at the following concentrations: kanamycin (Km), 50 µg/mL, gentamycin (Gm), 10 µg/mL, chloramphenicol (Cm), 25 µg/mL and ampicillin (Amp), 50 µg/mL.

For growth on plates of KF707 W.T., mutant and complemented strains, LB and MSM media were prepared as described in General Material and Methods, with the addition of 15 g/L of Agar (in the case of biphenyl, which is insoluble in water, few crystals of this compound were added on the lid of the plates and cells grew up by using the biphenyl vapors). To monitor cell growth, a single colony of bacterial strains was initially inoculated in 10 mL of LB medium and grown overnight; later on, cells were centrifuged and washed twice with 0.1 M Phosphate Buffer (pH 7.0) and, finally, 20 µL of 10⁻¹ and 10⁻² dilutions were spotted in the middle of the plates and cells were incubated at 30°C for one week.

For growth curves, in liquid media, KF707 W.T. and mutant strains were grown aerobically at 30°C and 130 rpm in 250 mL glass flasks containing 50 mL of LB or MSM supplemented with a single carbon source (pyruvate, succinate, fumarate, glucose, fructose, benzoate, *p*-hydroxybenzoate, and biphenyl); each carbon source was added to the sterile medium in order to have a final concentration of 6 mM.

A single colony of bacterial strains was first inoculated in 10 mL of LB medium and grown overnight; then cells were centrifuged, washed twice with 0.1 M Phosphate Buffer (pH 7.0), and inoculated (2%) on LB or MSM to obtain an initial OD_{600 nm} around 0.05. Growth curves were performed by monitoring the OD_{600 nm} values every two hours, until the stationary growth phase.

4.2.4 Growth of KF707 W.T. and mutant strains in the presence of a stringent response inducer

To observe the induction of the stringent response mechanism, an artificial compound, DL-serine hydroxymate (SHX), inducing a stringent response caused by serine amino acid starvation, was used [Tosa and Pizer 1971].

Cells of KF707 W.T. and KF Δ relA/spoT mutant were grown on 250 mL flasks containing 50 mL of LB medium, at 30°C and 130 rpm for two hours, and then they were subjected to a treatment with SHX [400 μ g/mL]. Subsequently, four hours after the SHX addition, KF707 W.T. and mutant strain were re-inoculated in 50 mL of LB, after two steps of washing with phosphate buffer in order to remove SHX. Then the growth rate of the new cultures were observed by monitoring the OD_{600 nm} values every hour; in parallel the OD_{600 nm} of the strains, grown in LB+SHX, were monitored.

4.2.5 (p)ppGpp detection analysis

(p)ppGpp levels were determined using a radiolabeling assay [Kasai et al., 2004], with the following modifications. KF707 W.T., KF Δ relA, KF Δ relA/spoT mutant and complemented strains were grown on LB medium or on MSM medium with 6 mM of different single carbon sources, at 30°C at 150 rpm, until they reached an OD_{600 nm} close to 0.6. Further to induce the stringent response, SHX [400 μ g/mL] was added and cells were incubated for one hour. In all experiments before the radioactive assay cells were washed twice with saline solution and 60 μ L of each preparation were used for the assay. Initially, all the samples were incubated for 15 minutes at 30°C with 3 μ L of 100 μ Ci/mL ³²P (Perkin Elmer). Subsequently, cells were centrifuged for 7 minutes at 13.000 rpm and the liquid was discarded after this step, nucleotides were extracted by adding 10 μ L of cold formic acid [1 M] to each sample; cells were then lysed by two freeze-thaw cycles on dry ice. All the samples were centrifuged for 10 minutes at 130 rpm.

Finally, 3 or 1.5 μ L of each sample were spotted on the bottom of a cellulose-polyethyleneimine thin-layer chromatography (TLC) plate and nucleotides were separated using KH₂PO₄ [1.5 M, pH 3.4] as solvent. The solvent was added to completely cover the bottom of the TLC plates and, after 45 minutes, the run was stopped.

TLC plates were then dried and exposed to a phosphor screen overnight; after 24 hours radioactivity was measured by using a radioactive scanner Fujifilm FLA3000.

4.2.6 KF707 W.T. and KF Δ relA/spoT mutant strain 2-DE analysis

Bacterial proteins extraction

To obtain the 2-DE proteome map of KF707 W.T. and KF Δ relA/spoT grown in the presence of benzoic acid [6 mM], cells were grown in 50 mL of MSM medium until the exponential phase of growth ($OD_{600\text{ nm}}$ between 0.45-0.6). Then, cultures were transferred into a sterile 50 mL falcon, centrifuged for 30 minutes at 4°C and 5.000 rpm and pellets were washed twice with 20 mL of Tris-HCl solution [25 mM, pH 7.5]. Finally, 2 mL of each cell preparation were transferred into 2 mL tubes, centrifuged for five minutes at 4°C and 5.000 rpm, the supernatants were discarded and pellets were frozen at -80°C.

Pellets were re-suspended in 350 μ L of lysis buffer (Urea [7 M], Thiourea [2 M], CHAPS [4% w/v], Na₂EDTA [5 mM], Tris [20 mM, pH 6.8]), containing Protease Inhibitors Cocktail (GE Healthcare Bio-Science AB, Sweden). Then, samples were incubated for 20 minutes, at room temperature, and then they were disrupted by sonication using Diagenode Bioruptor Nextgen (8 minutes at medium amplitude, with 30 seconds plus 30 seconds of pause on ice). Later on, samples were centrifuged for 10 minutes at 15°C and 13.000 rpm and supernatants were collected. Finally, they were treated with a clean-up step, by using ReadyPrep 2D Clean-up kit (Biorad, USA), according to the manufacturer's instructions. At the end of the protocols samples were suspended in buffer containing Urea [7 M], Thiourea [2 M], CHAPS [4% w/v], DTT [50 mM], Tris [20 mM, pH 6.8] and protein concentrations were measured by Bradford Quick Start™ reagent (Biorad, USA). Samples aliquots were stored at -80°C until used.

2-DE and image analysis

All 2-DE separation and image analysis were carried out using GE Healthcare devices and reagent, Iso Electric Focusing was performed using IPG strips (13 cm *pI* 3-10 non-linear or 13 cm *pI* 4-7 linear). The samples were diluted in 250 μ L of re-hydration buffer (Urea [7 M], Thiourea [2 M], CHAPS [4%], IPG buffer [1%], DeStreak™ reagent [1.2%] and Bromophenol

Blue in trace). After 24 hours, the isoelectrofocusing (IEF) was performed in the Ettan IPGphorIII at 15°C and with 50 μ A max, by using the following program:

- ✓ 500 V for five hours, gradient to 1.000 V for two hours, gradient incline to 8.000 V for three hours until 20.000 V/hrs total and finally a hold step at 500 V.

Subsequently, IPG strips were incubated, for 15 minutes, in Equilibration buffer (Urea [6 M], Glycerol [30% v/v], SDS [2% w/v] and Tris HCl [75 mM, pH 8.8]) containing DTT [130 mM] and then, in the same Equilibration buffer containing Iodoacetamide [135 mM] for 15 minutes. After, strips were sealed in place on top of Criterion Precasted Gels-Any kD (Biorad, USA), using agarose [1% w/v] in running buffer with a trace of bromophenol-blue. The second dimension was performed using Mini Protean tetra Cells (Biorad, USA), under constant current (30 mA/gel and 250 V max); gels were fixed in Methanol [40% v/v] and in Acetic acid [10% v/v] for two hours and stained overnight with Colloidal Coomassie Blue G solution and scanned with Pharos-FX system. Analysis of protein map was done by Proteomweaver™ software (Biorad, USA).

Samples preparation for mass spectrometry

The mass spectrometry analysis was performed using the most interesting spots, they were excised from gels and treated as suggested in Shevchenko et al., 2007. Briefly, spots were de-stained in ammonium bicarbonate in acetonitrile (ACN) [50 mM]: then, samples were reduced with DTT [10 mM] and alkylated with iodoacetamide [55 mM] in ammonium bicarbonate [100 mM]. After dehydration in ACN was completed and gel pieces were equilibrated, for two hours at 4°C, in A-Solution (ammonium bicarbonate [10 mM] and 10% ACN), containing 13 ng/ μ L of porcine trypsin for MS (Sigma-Aldrich), samples were incubated overnight at 37°C. The day after, samples were centrifuged and supernatants were harvested, gel pieces were covered by Extraction solution (5% formic acid in ACN). Finally, after 15 minutes of incubation, at 37°C, supernatants from this latter step were pooled into the corresponding supernatants of the previous step and dried up in SpeedVac (Savant™).

Mass spectrometry analysis

Dry peptides from each gel fraction were resuspended in 25 μL of a mixture of water: acetonitrile: formic acid 97:3:2, sonicated for 10 minutes at room temperature and centrifuged at 12,100 rpm for 10 minutes. Analysis were performed on an ESI-Q-TOF Accurate-Mass spectrometer (G6520A, Agilent Technologies, Santa Clara, CA, USA), controlled by MassHunter software (v. B.04.00) and interfaced with a CHIP-cube to an Agilent 1200 nano-pump. Two biological replicates were performed for each sample.

Chromatographic separation was performed on a chip (Agilent Technologies) with a 75 μm I.D., 43 mm, 300 \AA C18 column, prior to a desalting step through a 40 nL trap column. The injected sample (4 μL) was loaded onto the trap column with a 4 $\mu\text{L}/\text{min}$ 0.1% (v/v) formic acid (FA):acetonitrile (ACN) (98:2 v/v) phase flow. After 3 minutes, the precolumn was switched in-line with the nanoflow pump (450 nL/min, phase A: water:ACN:FA (96.9:3:0.1 v/v/v), phase B: ACN:water:FA 94.5:5:0.1 v/v/v), equilibrated in 2% (v/v) B. The peptides were eluted from the RP column through the following gradient: 2% for one minute, 2->24% B over a period of 24 minutes, 24-35% B in 3', 35->90% B in 0.1', then hold at 90% B for 6 minutes, and switched back to 2% B for column reconditioning, for a total runtime of 45 minutes. Ions were formed in a nano-ESI source, operated in positive mode, 1860 V capillary voltage, with the source gas heated at 350°C and at a 5 L/min flow. Fragmentor was set to 160 V, skimmer lens operated at 65 V. Centroided MS and MS² spectra were recorded from 300 to 1700 m/z and 50 to 1700 m/z, respectively, at scan rates of 6 and 3 Hz. The eight most intense multi-charged ions were selected for MS² nitrogen-promoted collision-induced dissociation. The collision energy was calculated according to the following expression: $CE_{(V)} = 3.6 \cdot \left(\frac{m/z}{100}\right) - 3$. A precursor active exclusion of 0.2 minutes was set up, and the detector operated at 2 GHz in extended dynamic range mode. Mass spectra were automatically recalibrated with two reference mass ions.

Protein identification

Raw data, converted from the vendor's data format into mascot generic format using MassHunter Qualitative Analysis (v. B.05.00), were searched against Swiss-Prot, Uniprot or TrEMBL for peptide sequences and C-RAP (<ftp://ftp.thegpm.org/fasta/cRAP>) for contaminants with MASCOT (Version 2.4, Matrix Science, London, UK). The following search parameters were used: 40 ppm precursor tolerance, 0.1 Da fragment mass error allowed, two missed cleavage allowed for trypsin, carbamidomethyl as a fixed modifier of cysteine residues and methionine oxidation as variable modification. The false discovery rate was estimated through an internal decoy database search; all results were filtered to have a FDR < 0.1.

4.2.7 Other analyses

All the experiments performed with the KF707 and deletion mutant strains, including growth curves, swarming assay, the construction of *lacZ*-containing strains and β -galactosidase assay, were conducted as previously described in Chapter 1 or Chapter 2.

4.3 Results

4.3.1 KF707 *relA* and *spoT* deleted mutant and complemented strains

The KF707 genome sequencing analysis revealed that, as many other *Pseudomonas* strains, KF707 owns two different protein for synthesis and hydrolysis of (p)ppGpp which are:

- the **GTP/GDP pyrophosphokinase RelA** (BAU76106 – 748 aa – 84 kDa – pI 7)
- the **GTP/GDP pyrophosphokinase/pyrophosphohydrolase SpoT** (BAU77268 – 702 aa – 79 kDa – pI 9).

KF707 deleted mutants for *relA* gene and double mutant for *relA/spoT* genes were obtained, by Gene SOEing PCR and conjugation protocols. In addition, the deletion of the single *spoT* gene was also tested, but, in this case, it was impossible to obtain the mutant since the deletion of *spoT* in KF707, was lethal. The same result has previously been observed in other bacteria, such as in *E. coli* [Xiao et al., 1991], *V. cholerae* [Oh et al., 2015], *P. aeruginosa* PAO1 [Vogt et al., 2011], *P. chlororaphis* PA23 [Manuel et al., 2012] and *Pseudomonas. sp.* strain DF41 [Manuel et al., 2011]; apparently, in a *relA+* background, the SpoT enzyme is required to maintain the correct (p)ppGpp balance [Potrykus and Cashel, 2008].

To restore the wild type genotype in KF707 single or double deletion mutant strains, pSEVA342 and pG19II were used. In the case of RelA protein, the *relA* gene was cloned into pSEVA432 and the plasmid was transferred by a conjugation protocol into KFΔ*relA* and/or KFΔ*relA/spoT* while, in the case of SpoT protein, *spoT* gene was cloned into pG19II and the genotype was completely restored by a double cross-over recombination. In both cases, the complementation was confirmed by PCR and DNA sequencing analysis.

4.3.2 KF707 W.T. and mutant strains growth on different carbon sources

The effect of the deletion of *relA* and *spoT* in KF707 was assessed by growth on plates and in liquid cultures, using MSM medium with the addition of single carbon sources [6 mM].

As reported in Table 4.3, growth on plates of KF707 W.T., KFΔ*relA* and KFΔ*relA/spoT* was monitored for a week, at three different serial dilution (10^{-1} , 10^{-2} and 10^{-3}) of the initial LB cultures. Results, show in Table 4.3, indicate that, in the case of LB medium and of media containing Krebs Cycle's intermediates as carbon sources (pyruvate, fumarate and succinate), W.T. and mutant strains were able to grow at the same level.

Some differences were found in the presence of sugars: KF707 W.T. and KF Δ relA mutant showed the same pattern of growth, while KF Δ relA/spoT mutant started its growth 12 hours later. Finally, the major differences between KF707 W.T. and double mutant strain were found when aromatic compounds were used as single carbon source. In all of these cases, the mutant growth started 24 or 48 hours later compared to that of the W.T. strain. The experiments were repeated at least three times with all the mutants and the conditions previously described.

Table 4.3: Media, strains and the time necessary (expressed in hours, hrs) for a complete growth on plates, are listed in this table. Plates were analyzed every 12 hours during an experimental time course of five days.

Medium	Strains		
	KF707 W.T.	KF Δ relA	KF Δ relA/spoT
LB	after 12 hrs	after 12 hrs	after 12 hrs
MSM - Pyruvate	after 12 hrs	after 12 hrs	after 12 hrs
MSM - Fumarate	after 12 hrs	after 12 hrs	after 12 hrs
MSM - Succinate	after 12 hrs	after 12 hrs	after 24 hrs
MSM - Glucose	after 12 hrs	after 12 hrs	after 24 hrs
MSM - Fructose	after 24 hrs	after 24 hrs	after 36 hrs
MSM - Benzoate	after 36 hrs	after 36 hrs	after 60 hrs
MSM - <i>p</i> -Hydroxybenzoate	after 36 hrs	after 36 hrs	after 60 hrs
MSM - Biphenyl	after 36 hrs	after 36 hrs	after 72 hrs

To better analyzed the mutants phenotype, growth curves, in MSM medium with different carbon sources [6 mM], were performed, OD_{600 nm} values were monitored every two hours until the stationary phase of growth. Curves were obtained for KF707 W.T., KF Δ relA and KF Δ relA/spoT mutant strains, and for KF Δ relA/spoT +spoT complemented strain (Figure 4.6).

In all the conditions tested, KF707 W.T. strain and KF Δ relA, had the same phenotype and their growth rate did not change (Figure 4.6, black and gray curves). The double mutant strain, KF Δ relA/spoT (Figure 4.6, blue curves), shows an optimal growth rate in the

presence of pyruvate and fumarate, whereas a lag phase was apparent with sugars, such as glucose and fructose; this lag being also present in cells grown on plates. Moreover, in the presence of aromatic carbon sources, such as benzoate and biphenyl, the lag seen before the exponential growth phase increased significantly.

On the other hand, following this initial consistent lag phase, which may be due to cell adaptation to grown on sugars or aromatic carbon sources, mutant cells begin to grow at the same rate of KF707 W.T. strain. This phenomenon is unusual and it suggests the involvement of an unknown mechanism, replacing the stringent response, or otherwise, the presence in KF707 genome of alternative genes that synthesize and hydrolyze the (p)ppGpp, similarly to SpoT. In this respect, many bacteria were reported to have alternative RSH proteins: *V. cholerae*, for example, has an additional small (p)ppGpp synthetase, named RelV, which lacks the N-terminal hydrolase domain [Oh et al., 2015].

These phenotypic results, obtained from growth analysis on plate or in liquid medium, suggest an involvement of the stringent response enzyme SpoT during growth in the presence of sugars or aromatic compounds; conversely, the lack of only RelA protein does not seem to produce any change of cell phenotypes. This effect is peculiar because the stringent response was reported to be associated with nutrient starvation [Xiao et al., 1991; Krol and Becker, 2011; Oh et al., 2015; Ancona et al., 2015] but not with the type of carbon source used to support bacterial growth.

To confirm the fundamental role of SpoT enzyme, KF Δ relA/spoT +spoT complemented strain growth curves (Figure 4.6, orange curves) were performed. Indeed, in cells where the *spoT* gene was restored, the wild type phenotype became evident and the lag phase disappeared with all the carbon sources tested.

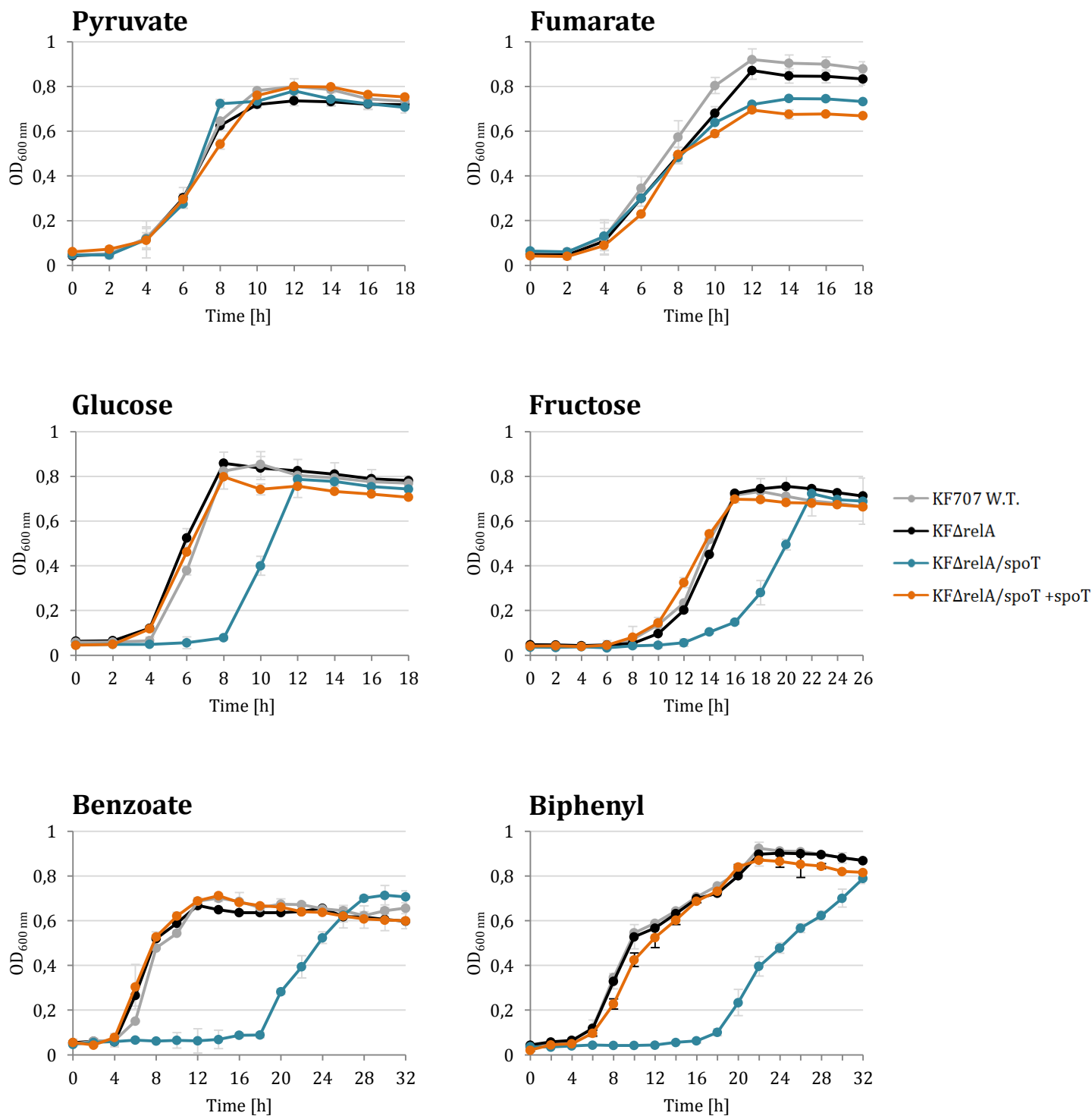


Figure 4.6: Growth curves of KF707 W.T., KFΔrelA and KFΔrelA/spoT deletion mutant strains and KFΔrelA/spoT +spoT complemented strain. Strains were grown in 50 mL of MSM medium in 250 mL flasks shaken at 130 rpm, with 6 mM of different single carbon sources. The optical densities were observed at 600 nm every two hours and growths were stopped at late-stationary phase.

4.3.3 Growth in the presence of stringent response inducer

To investigate the double mutant phenotype, an additional growth test was conducted on KF707 W.T. and KF Δ relA/spoT cultures in the presence of a stringent response inducer, serine hydroxymate (SHX) (Figure 4.7).

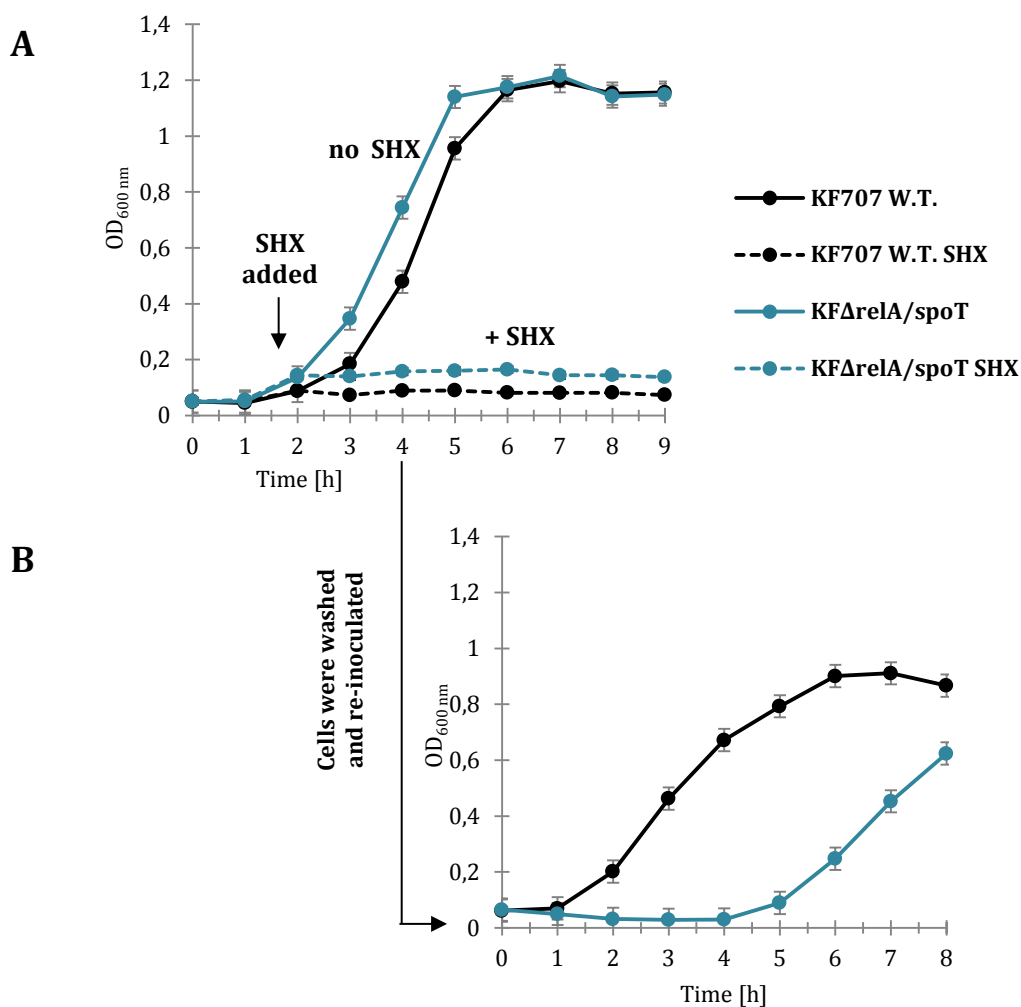


Figure 4.7: **A)** Growth curves of KF707 W.T. and KF Δ relA/spoT mutant strains, with and without SHX [10 mM] treatment. **B)** The two strains were re-inoculated, after four hours with SHX treatment, and growth were monitored.

As shown in Figure 4.7 A, following the addition of SHX [10 mM], after two hours of growth on LB medium, a stop of the cell growth in both strains tested was apparent. At time 4 hours, KF707 W.T. and double mutant cells were washed twice, with saline solution, in order to remove SHX, and they were re-inoculated in 50 mL of LB. The graph (Figure 4.7B)

shows that KF707 W.T., re-started growing, after one hour while, KF Δ relA/spoT showed a five hours lag phase before resuming its normal growth.

This result suggests the existence of an alternative mechanism, which acts in a way similar to the stringent response, to support KF Δ relA/spoT growth during amino acid starvation or other stress conditions.

4.3.4 (p)ppGpp detection analysis

The (p)ppGpp detection analysis was performed to test the possible involvement of the stringent response in the metabolism of sugars and aromatic compounds in KF707.

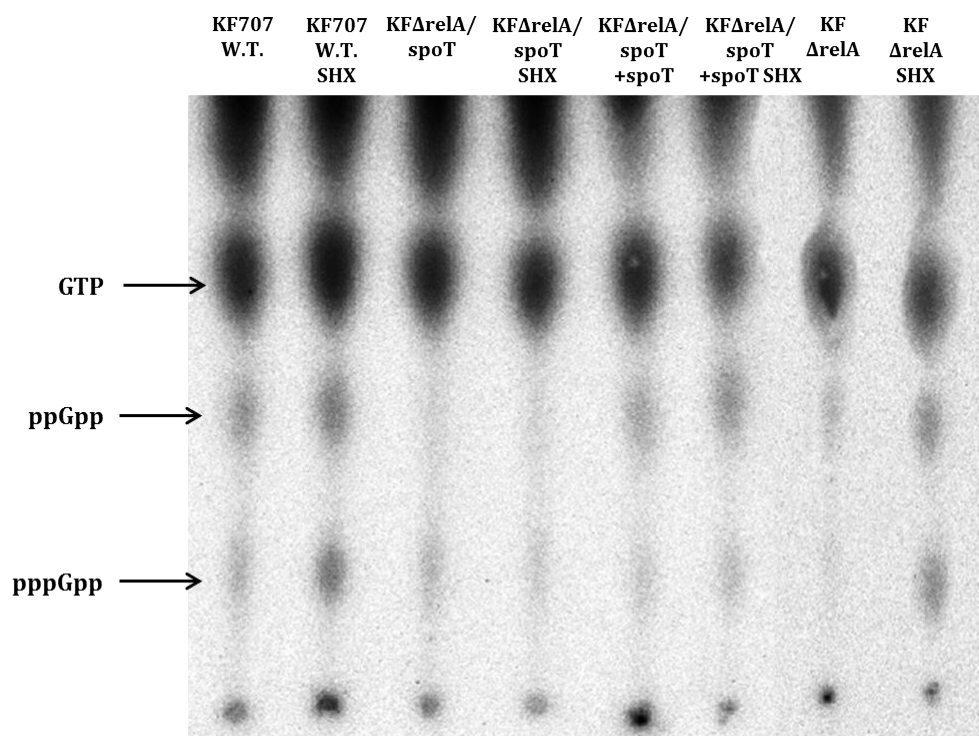


Figure 4.8: (p)ppGpp analysis in cells of KF707 W.T., deleted and complemented strains grown in 50 mL of LB with or without the induction of the stringent response with SHX [10 mM]. Cells were labelled with 32 P and nucleotides were extracted and separated by thin-layer chromatography.

An initial experiment was conducted to verify the production of alarmones in KF707 W.T., mutant strains and complemented strain, with a SHX [10 mM] treatment (Figure 4.8). The four strains were grown in 50 mL of LB medium until exponential phase ($OD_{600\text{ nm}} \sim 0.6$); then cells were treated with SHX for two hours and collected to perform the (p)ppGpp detection analysis, with radioactive 32 P (Paragraph 4.2.5).

Following the SHX treatment an increase of the (p)ppGpp production was detected in KF707 W.T. cells; the same result was obtained in the case of KF Δ relA while, the double mutant KF Δ relA/spoT did not show the production of the alarmones, with or without the stringent response inducer. Conversely, in the complemented mutant strain (KF Δ relA/spoT +spoT), the W.T. phenotype was partially restored. This results confirmed the correct deletion and complementation of the *spoT* gene, the role of the SHX in KF707 (as a stringent response inducer), and also suggested that the alternative mechanism explaining the KF707 *relA* and *spoT* deletion phenotypes, is not related with the production of (p)ppGpp. Apparently, the overcoming of the initial lag phase, after SHX treatment in KF Δ relA/spoT mutant, is likely to depends on other genes or proteins not related to the stringent response mechanism.

The (p)ppGpp analysis was also performed in cells grown in MSM medium with different single carbon sources.

In this set of experiments, KF707 W.T., KF Δ relA/spoT and complemented strain, were grown until the exponential phase ($OD_{600\text{ nm}} \sim 0.5$) in MSM medium with different single carbon sources [6 mM], before performing the (p)ppGpp detection analysis. The thin-layer chromatography obtained are shown in Figure 4.9. Panel A shows the (p)ppGpp production, in cells grown with Krebs Cycle's; unexpectedly, also with this type of carbon sources the alarmones were produced in KF707 W.T. and in complemented strain, while they were not present in *relA/spoT* double mutant strain. Similar results were also obtained for cells grown with sugars (glucose and fructose) and with benzoate. These data taken together suggested the involvement of the secondary-messengers (p)ppGpp during growth in MSM medium and not only in the case of sugars or aromatic compounds as carbon sources. Additionally, the absence of (p)ppGpp in KF Δ relA/spoT double mutant was interpreted to show the existence of an alternative mechanism allowing the bypass of the initial lag phase without the involvement of alarmones production. Further, in the double mutant strain the production of GTP and GDP was also reduced (Figure 4.9), so that the normal cycle for the production of these secondary-messengers is clearly affected by the lack of *relA* and *spoT* genes.

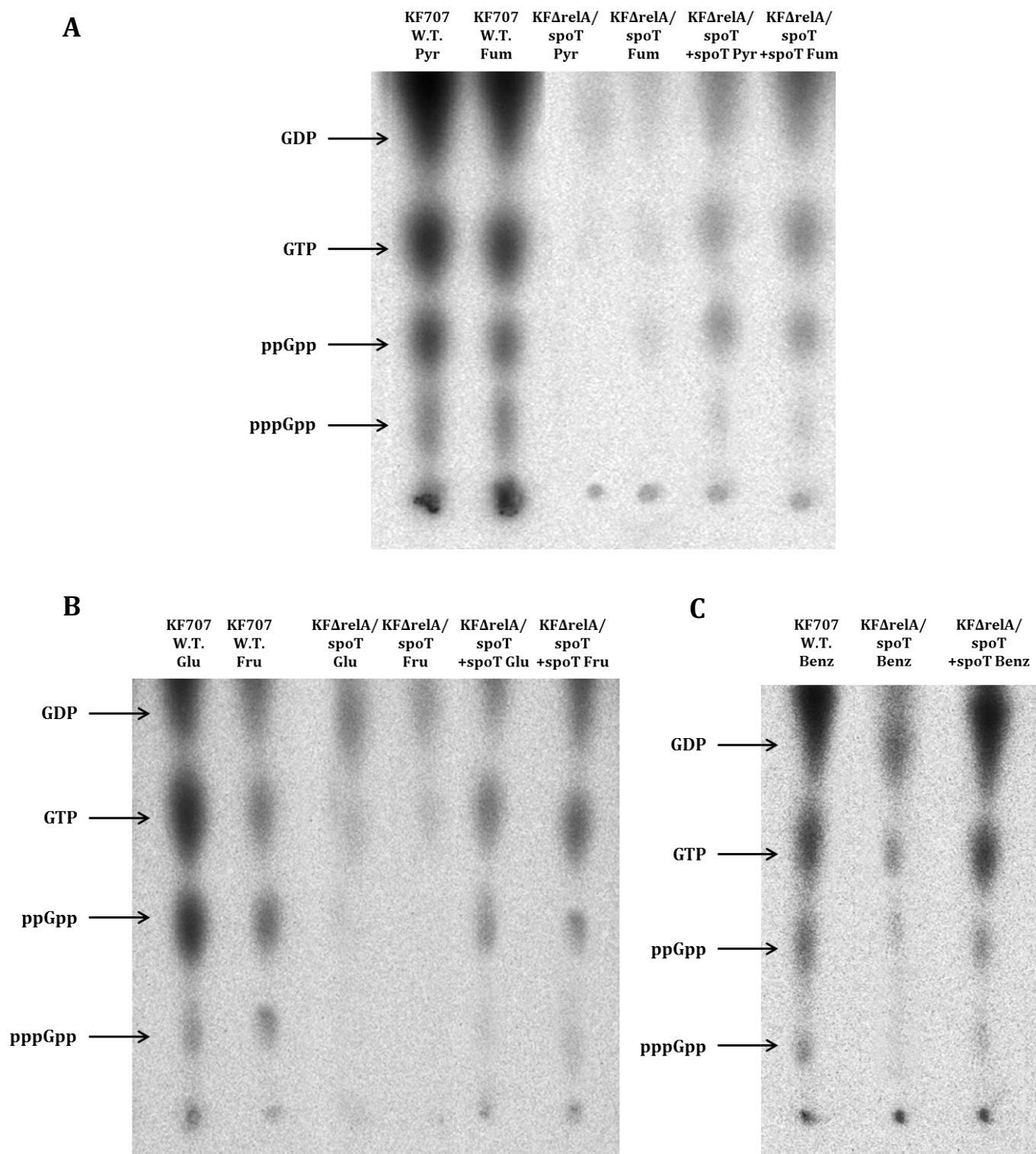


Figure 4.9: (p)ppGpp analysis in cells of KF707 W.T., deleted and complemented strains grown in 50 mL of MSM medium with different single carbon source [6 mM]: **A)** Krebs Cycle's compounds, pyruvate or fumarate; **B)** Sugars, glucose or fructose and **C)** Aromatic compound, benzoate. Cells were labelled with ^{32}P and nucleotides were extracted and separated by thin-layer chromatography.

4.3.5 KF707 W.T. and KF Δ relA/spoT mutant strain 2-DE analysis

To determine the existence of an alternative and/or compensatory mechanism which is activated during growth in MSM in the absence of the effective proteins of the stringent response, the KF707 proteome analysis was conducted. Experiments were performed in duplicate with KF707 W.T. and *relA/spoT* double mutant strain cells, grown in MSM with benzoate [6 mM] and harvested at their exponential phase ($OD_{600\text{ nm}}$ 0.4-0.6). The collected samples were processed for purification and extraction of proteins, as described in Materials and Methods 4.2.6. Protein quantification, performed by Bradford method, was the following: 6.02 and 6.55 $\mu\text{g}/\mu\text{L}$; 5.32 and 6.40 $\mu\text{g}/\mu\text{L}$ for KF707 W.T. and KF Δ relA/spoT, respectively.

For the proteome analysis, 2-DE was performed with two different type of IPG strips: initially the analysis was conducted with non-linear *pI* 3-10 strips, and 185 μg of proteins were charged for each sample; thereafter linear *pI* 4-7 strips were used and 220 μg of proteins were charged. We decided to use these type of strips, because previous studies on *P. aeruginosa* proteome, reported that the major part of the cytoplasmic proteins (77.5 %) fell in the *pI* range between 4 to 7 [Nouwens et al., 2000].

Following the first and the second dimension run, gels were stained overnight with Colloidal Coomassie Blu G solution and then the images were recorded by using Pharos-FX scan system. Once gels images were obtained, the protein maps from KF707 W.T. and double mutant strain were compared by Proteomweaver™ software.

Apparently the Figures 4.10 and 4.11 show that, in both of cases, differences in protein expression were observed; as predicted, most visible protein spots were concentrated in the acidic region of the gel [Lecoutere et al., 2012]. For the analysis of individual spots, the most expressed proteins or only those present in the double mutant strain (blue spots) were examined. What is noticeable is that, even using two different type of IPG strips, the area comprised between *pI* 4.5-5.5 and with a molecular weight between 30-70 kDa contains most of the proteins that appeared more expressed in KF Δ relA/spoT (Figure 4.10 and 4.11 red boxes).

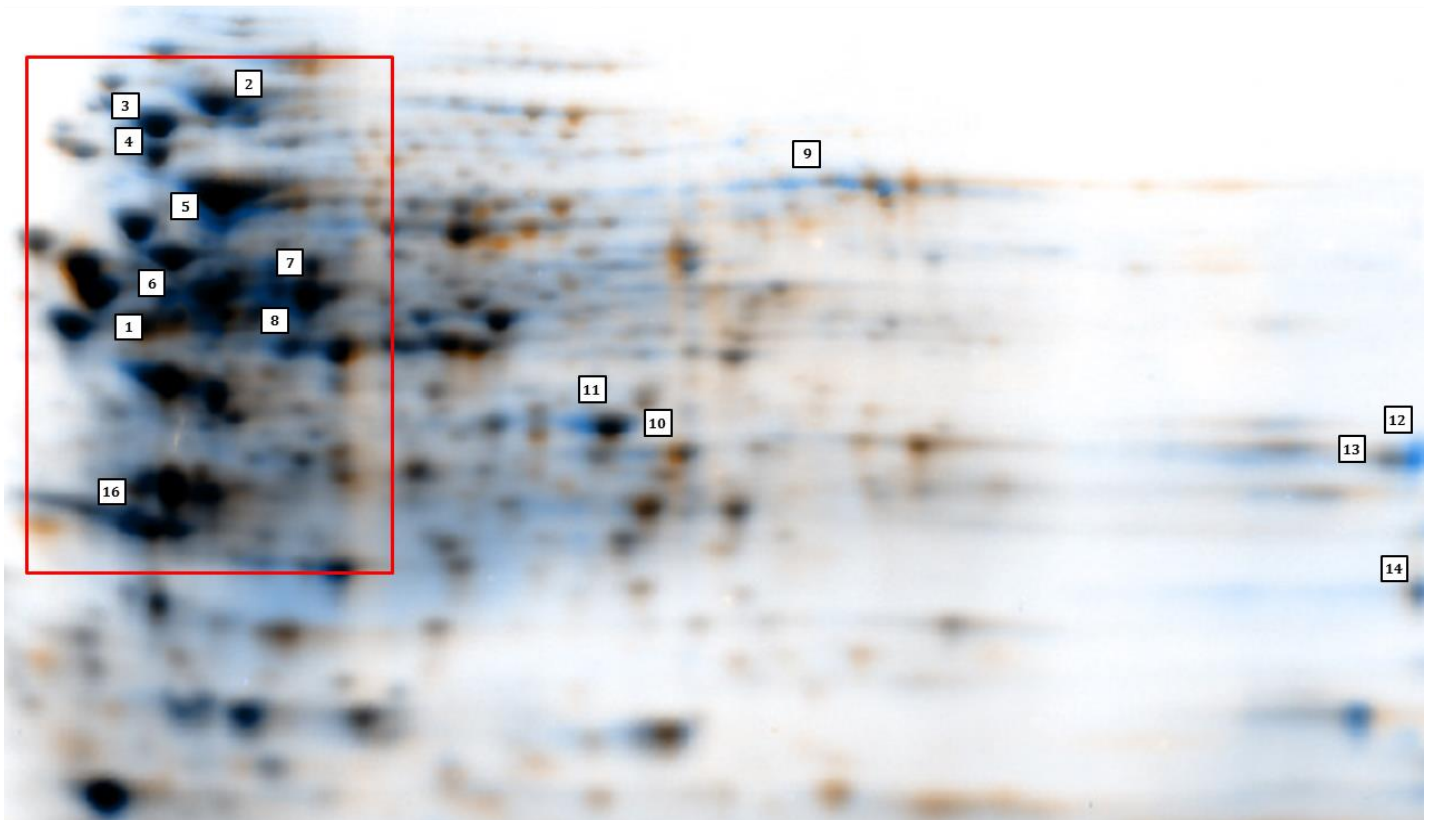
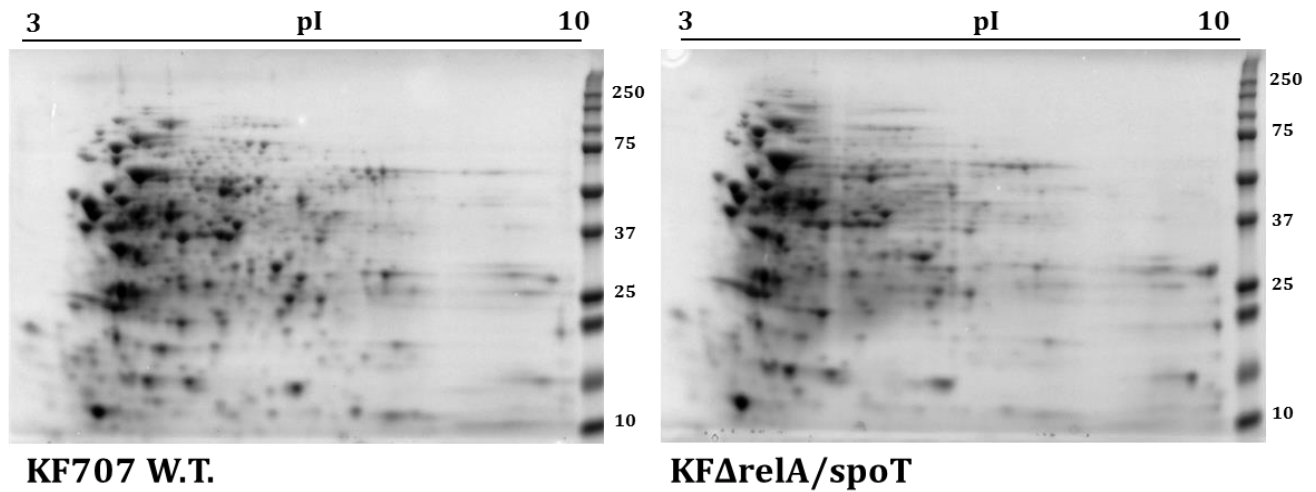


Figure 4.10: Two-dimensional electrophoresis (2-DE) map of KF707 W.T. (on the left) and KF Δ relA/spoT (on the right), grown in 50 mL of MSM medium with benzoate [6 mM] as sole carbon source. One dimension strips pI 3-10 (non linear) – 13 cm / Two dimension Gel Criterion TGX Any Kda. 185 μ g of protein were charged and gels were stained with Colloidal Coomassie. The gel comparison was performed with Proteomweaver™ software: the orange spots represent the KF707 W.T. proteome profile, the blue spots the KF Δ relA/spoT profile. Numbers indicate the most interesting spots, most or just expressed in the mutant strain, which were analyzed through Nano LC-MS/MS.

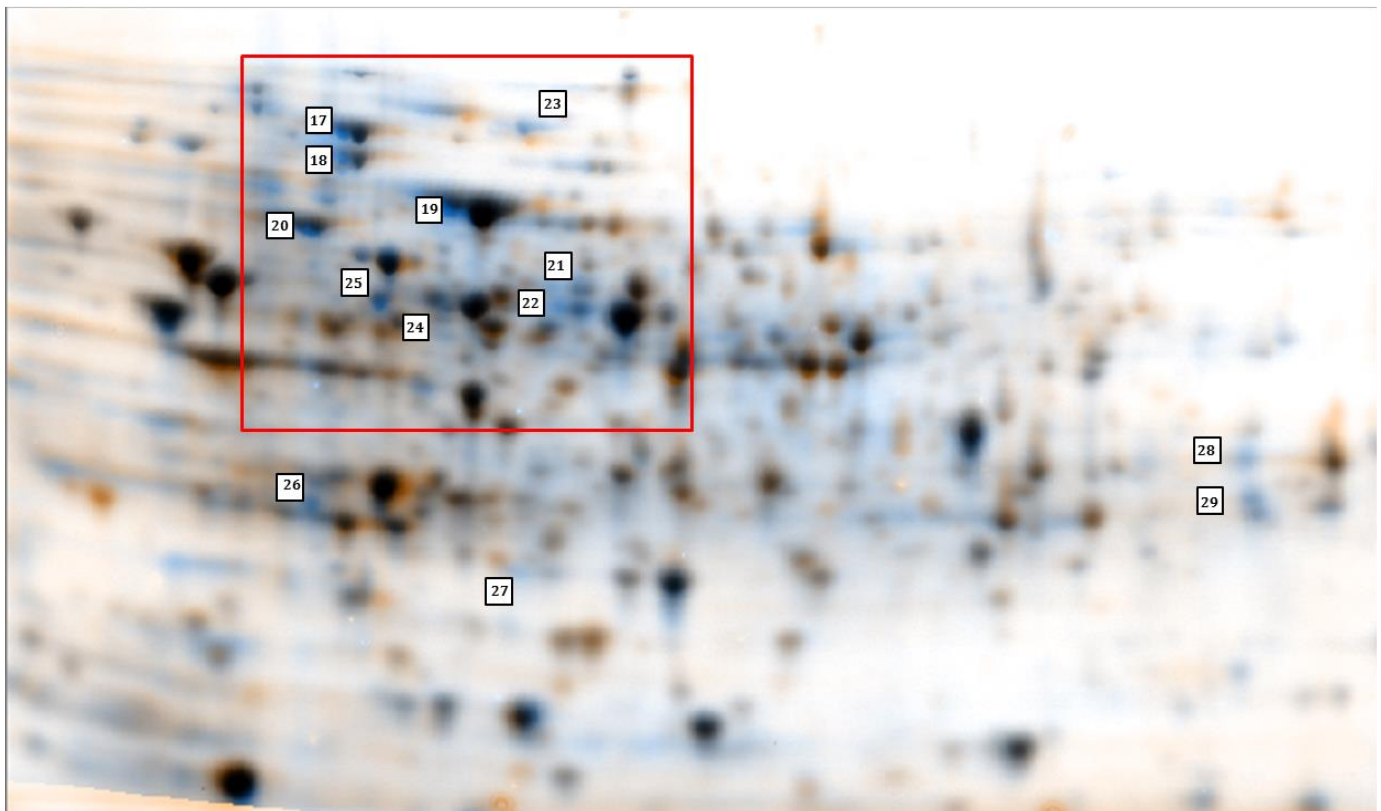
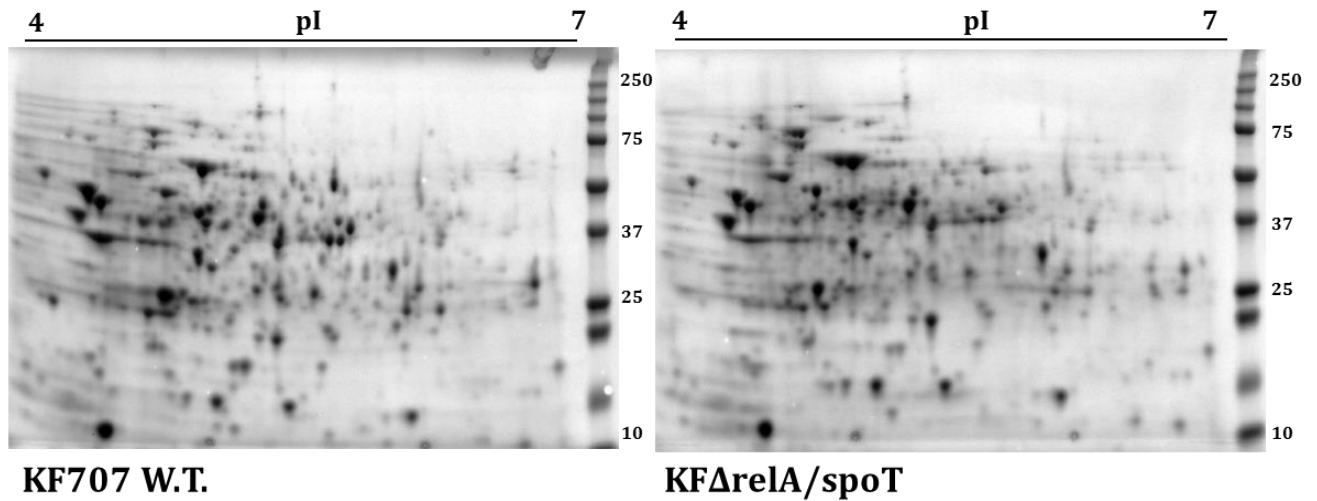


Figure 4.11: Two-dimensional electrophoresis (2-DE) map of KF707 W.T. (on the left) and KF Δ relA/spoT (on the right), grown in 50 mL of MSM medium with benzoate [6 mM] as sole carbon source. One dimension strips pI 4-7 (linear) – 13 cm / Two dimension Gel Criterion TGX Any Kda. 220 μ g of protein were charged and gels were stained with Colloidal Coomassie. The gel comparison was performed with Proteomweaver™ software: the orange spots represent the KF707 W.T. proteome profile, the blue spots the KF Δ relA/spoT profile. Numbers indicate the most interesting spots, most or just expressed in the mutant strain, which were analyzed through Nano LC-MS/MS.

All of these selected spots were excised from the gels, purified, digested with trypsin and analyzed with Nano LC-MS/MS, finally proteins were identified by searching the Swiss-Prot, Uniprot or TrEMBL databases using Mascot (Matrix Science, MA); the results are listed in Table 4.4.

Table 4.4: List of proteins most expressed in KFDrelA/spoT mutant strain 2-DE gels, identified through the comparison with KF707 W.T., analysis performed by using Proteomweaver™ software (Biorad, USA). The spots number are reported in the first column; samples between 1 to 16 were identified from pI 3-10 non linear gel while, samples between 16 to 29 were identified from pI 4-7 gel. In the table are shown: the UNIPROT code, the name of the protein, the number of the amino acids of the protein (aa), the predicted molecular weight (MW), the predicted isoelectric point (pI), the number of the amino acids sequences identified by Nano LC-MS/MS analysis (Id.) and the description of the function of the proteins. For some protein, that resulted situated in the same position (same MW and pI) of the two gels, only one spot was analyzed (the one obtained from the pI 4-7 gel), these information are listed in the last column.

Spot	UNIPROT	Protein	aa	MW	pI	Id.	Description	Note
1	L8MPJ5	Benzoate-specific porin	418	45.6	5.07	/	Porin OprD binds basic amino acids, dipeptides containing a basic residue and imipenem and related zwitterionic carbapenems	Based on spot 25
2	L8MLM0	Translation elongation factor G	709	78	5.01	/	Elongation factor G catalyzes the translocation step of protein synthesis in bacteria	Based on spot 23
3	L8MU64	Chaperone protein DnaK	638	68.4	4.84	/	Expression by stress conditions e.g. heat shock/ Acts as a chaperone	Based on spot 17
4	L8MDX9	30S ribosomal protein S1	559	48.4	4.88	/	Binds mRNA; thus facilitating recognition of the initiation point. It is needed to translate mRNA with a short Shine-Dalgarno (SD) purine-rich sequence.	Based on spot 18
5	L8MN66	Heat Shock Protein 60 kDa Chaperonin GroEL	546	56.7	5.06	/	Expression by stress conditions e.g. heat shock/ Prevents misfolding and promotes the refolding and proper assembly of unfolded polypeptides generated under stress conditions	Based on spot 19
6	L8MR18	ATP synthase subunit β	458	49.5	4.94	/	Produces ATP from ADP in the presence of a proton gradient across the membrane. The catalytic sites are hosted primarily by the beta subunits.	Based on spot 25
7	L8MLT9	Dihydrolipoyllysine-residue succinyltransferase component of 2-oxoglutarate dehydrogenase complex	408	42.8	5.38	/	The 2-oxoglutarate dehydrogenase complex catalyzes the overall conversion of 2-oxoglutarate to succinyl-CoA and CO ₂	Based on spot 21
8	L8M8P8	Translation elongation factor Tu	396	33.8	4.92	/	Elongation factor Tu promotes the GTP-dependent binding of aminoacyl-tRNA to the A-site of ribosomes during protein biosynthesis	Based on spot 22
9	L8MPG4	Quino(Hemo) protein alcohol dehydrogenase	594	64.6	8.11	10	2-chloroethanol cytochrome-c oxidoreductase activity / Ethanol dehydrogenase, a bacterial quinol protein	Based on LC-MS/MS
10	L8MTG3	Acetylglutamate kinase	301	31.8	5.89	8	Acetylglutamate kinase catalyzes the ATP-dependent phosphorylation of N-acetyl-L-glutamate to form N-acetyl-L-glutamate 5-phosphate, which is the second step of arginine biosynthesis	Based on LC-MS/MS
11	L8MQZ5	Succinyl-CoA ligase [ADP-forming] alpha chain	295	30.2	5.79	6	ADP-forming/GDP-forming succinate-CoA ligase subunit alpha is the coenzyme A and phosphate binding subunit of the succinyl-CoA synthetase that couples the hydrolysis of succinyl-CoA to the synthesis of ATP/GTP, as part of the citric acid cycle (TCA)	Based on LC-MS/MS

12	L8MA96	50S ribosomal protein L1	231	24.2	9.56	12	Binds directly to 23S rRNA. The L1 stalk is quite mobile in the ribosome, and is involved in E site tRNA release / Protein L1 is also a translational repressor protein, it controls the translation of the L11 operon by binding to its mRNA	Based on LC-MS/MS
13	L8MA96	50S ribosomal protein L1	231	24.3	9.57	15	Binds directly to 23S rRNA. The L1 stalk is quite mobile in the ribosome, and is involved in E site tRNA release / Protein L1 is also a translational repressor protein, it controls the translation of the L11 operon by binding to its mRNA	Based on LC-MS/MS
14	L8M8Q6	50S ribosomal protein L10	166	17.5	9.22	8	Part of the ribosomal stalk of the 50S ribosomal subunit. The N-terminus interacts with L11 and the large rRNA to form the base of the stalk. The C-terminus forms an elongated spine to which L12 dimers bind in a sequential fashion forming a multimeric L10(L12) _X complex	Based on LC-MS/MS
16	L8MRZ6	Heat Shock Protein GrpE	189	20.8	4.84	/	Participates actively in the response to hyperosmotic and heat shock by preventing the aggregation of stress-denatured proteins, in association with DnaK and GrpE. It is the nucleotide exchange factor for DnaK and may function as a thermosensor.	Based on spot 26
17	L8MU64	Chaperone protein DnaK	638	68.4	4.84	11	Expression by stress conditions e.g. heat shock/ Acts as a chaperone	Based on LC-MS/MS
18	L8MDX9	30S ribosomal protein S1	559	48.4	4.88	9	Binds mRNA; thus facilitating recognition of the initiation point. It is needed to translate mRNA with a short Shine-Dalgarno (SD) purine-rich sequence.	Based on LC-MS/MS
19	L8MN66	Heat Shock Protein 60 kDa Chaperonin GroEL	546	56.7	5.06	13	Expression by stress conditions e.g. heat shock/ Prevents misfolding and promotes the refolding and proper assembly of unfolded polypeptides generated under stress conditions	Based on LC-MS/MS
20	L8MN14	Cell division trigger factor	436	48.4	4.81	6	Involved in protein export. Acts as a chaperone by maintaining the newly synthesized protein in an open conformation. Functions as a peptidyl-prolyl cis-trans isomerase	Based on LC-MS/MS
21	L8MLT9	Dihydrolypoyllysine-residue succinyltransferase component of 2-oxoglutarate dehydrogenase complex	408	42.8	5.38	18	The 2-oxoglutarate dehydrogenase complex catalyzes the overall conversion of 2-oxoglutarate to succinyl-CoA and CO ₂	Based on LC-MS/MS
22	L8M8P8	Translation elongation factor Tu	396	33.8	4.92	21	Elongation factor Tu promotes the GTP-dependent binding of aminoacyl-tRNA to the A-site of ribosomes during protein biosynthesis	Based on LC-MS/MS
23	L8MLM0	Translation elongation factor G	709	78	5.01	5	Elongation factor G catalyzes the translocation step of protein synthesis in bacteria	Based on LC-MS/MS
24	L8MLN4	Phosphoglycerate kinase	387	40.3	5.08	19	Involved in carbohydrate degradation, in a sub-pathway that is part of the glycolysis pathway/ Catalyzes the transfer of the high-energy phosphate group of 1,3-bisphosphoglycerate to ADP, forming ATP and 3-phosphoglycerate	Based on LC-MS/MS
25	L8MPJ5	Benzoate-specific porin	418	45.6	5.07	30	Porin OprD binds basic amino acids, dipeptides containing a basic residue and imipenem and related zwitterionic carbapenems	Based on LC-MS/MS
	L8MR18	ATP synthase subunit β	458	49.5	4.94	24	Produces ATP from ADP in the presence of a proton gradient across the membrane. The catalytic sites are hosted primarily by the beta subunits.	Based on LC-MS/MS
26	L8MRZ6	Heat Shock Protein GrpE	189	20.8	4.84	13	Participates actively in the response to hyperosmotic and heat shock by preventing the aggregation of stress-denatured proteins, in association with DnaK and GrpE. It is the nucleotide exchange factor for DnaK and may function as a thermosensor.	Based on LC-MS/MS
27	L8MLA1	Benzoate 1,2-dioxygenase β subunit	162	19.4	5.20	10	Benzoate 1,2-dioxygenase beta subunit	Based on LC-MS/MS

28	L8MER9	2-hydroxy-6-oxo-6-phenylhexa-2,4-dienoate hydrolase	286	31.9	6.25	21	Biphenyl pathway / Catalyzes an unusual C-C bond hydrolysis of 2-hydroxy-6-oxo-6-phenylhexa-2,4-dienoic acid (HOPDA) to produce benzoic acid and 2-hydroxy-2,4-pentadienoic acid	Based on LC-MS/MS
	L8MRA8	Methionine ABC transporter substrate-binding protein	258	28	6.93	19	Methionine ABC transporter substrate-binding protein	Based on LC-MS/MS
29	L8MRL0	Phosphonate ABC transporter phosphate-binding periplasmic component	283	30.7	7.79	18	ABC transporter, phosphonate, periplasmic substrate-binding protein; this is a family of periplasmic proteins which are part of the transport system for alkylphosphonate uptake.	Based on LC-MS/MS

As the Table 4.4 displays, RelA/SpoT homologous were not detected by the proteome analysis, confirming the lack of the activation of the stringent response mediated by (p)ppGpp production in the double mutant KF Δ relA/spoT.

Proteins belonging to three main categories are shown in different colors in Table 4.4, namely: proteins related to the ATP synthesis (blue), factors and ribosome proteins necessary for the proteins biosynthesis (pink) and Heat Shock Proteins (HSP) (yellow). In addition, specific enzymes related to the aromatic compounds degradation pathways were found (green).

Proteins involved in the ATP synthesis are likely necessary for the production of new nucleotides since, the absence of RelA and SpoT, as shown in the previous paragraph, causes a depletion of the GTP/GDP pool. The overexpression of HSP is interesting in relation to its possible involvement in the stringent response mechanism [Santoro, 1999]. The dramatic up-regulation of HSP is usually associated to stress conditions and probably, in this specific case, the lack of the effectors of the stringent response leads to the overproduction of these molecules.

4.3.6 Additional experiments

A series of additional experiments (the preliminary results obtained will be shown in this section) were conducted to evaluate the involvement of the stringent response in the swarming motility and in the modulation of terminal oxidases in KF Δ relA/spoT double mutant strain. Stringent response is in fact, a mechanism involved in different cellular processes due to (p)ppGpp ability to act at the transcriptional level by regulating the activation and deactivation of genes.

Stringent response and swarming motility in KF707

The connection between stringent response and swarming motility in *Pseudomonas* strains, has been recently studied. In particular, in *P. aeruginosa* PAO1 the lack of *relA* and *spoT* genes determines a significant impairment in swarming and twitching motility as compared to the W.T. strain; the diameter of the swarming area was reduced in the double mutant strain [Vogt et al., 2011]. This effect is negative for *P. aeruginosa* PAO1 cells because their reduced motility affects negatively the potential pathogenicity of the strain [Vogt et al., 2011]. Also in *P. syringae* DC3000 Δ relA/spoT mutant strain the swarming motility was reduced, suggesting that (p)ppGpp is involved in the control of motility in this bacteria. One of the major consequences of this effect was the reduced virulence of the strain versus tomato plants [Chatnaparat et al., 2015, 1 and 2].

To investigate the role of *relA* and *spoT* genes in KF707 swarming motility, an assay was performed with W.T. and double mutant strains. The swarming media was prepared as previously described in Chapter 1, with glucose or sucrose as carbon sources; bacteria were inoculated in the middle of the plates following an overnight growth on 50 mL of LB, at 30°C and 130 rpm, and the swarming area diameter was measured after one week. As shown in Figure 4.12A and B, the swarming motility in the two strains displayed considerable differences. Indeed, with both carbon sources the diameter of the swarming area in KF Δ relA/spoT mutant strain was clearly larger than that of KF707 W.T. strain. This result was totally unexpected because the current literature reports that the lack of the gene involved in the stringent response inhibit the swarming bacteria capacity [Vogt et al., 2011; Chatnaparat et al., 2015, 1 and 2].

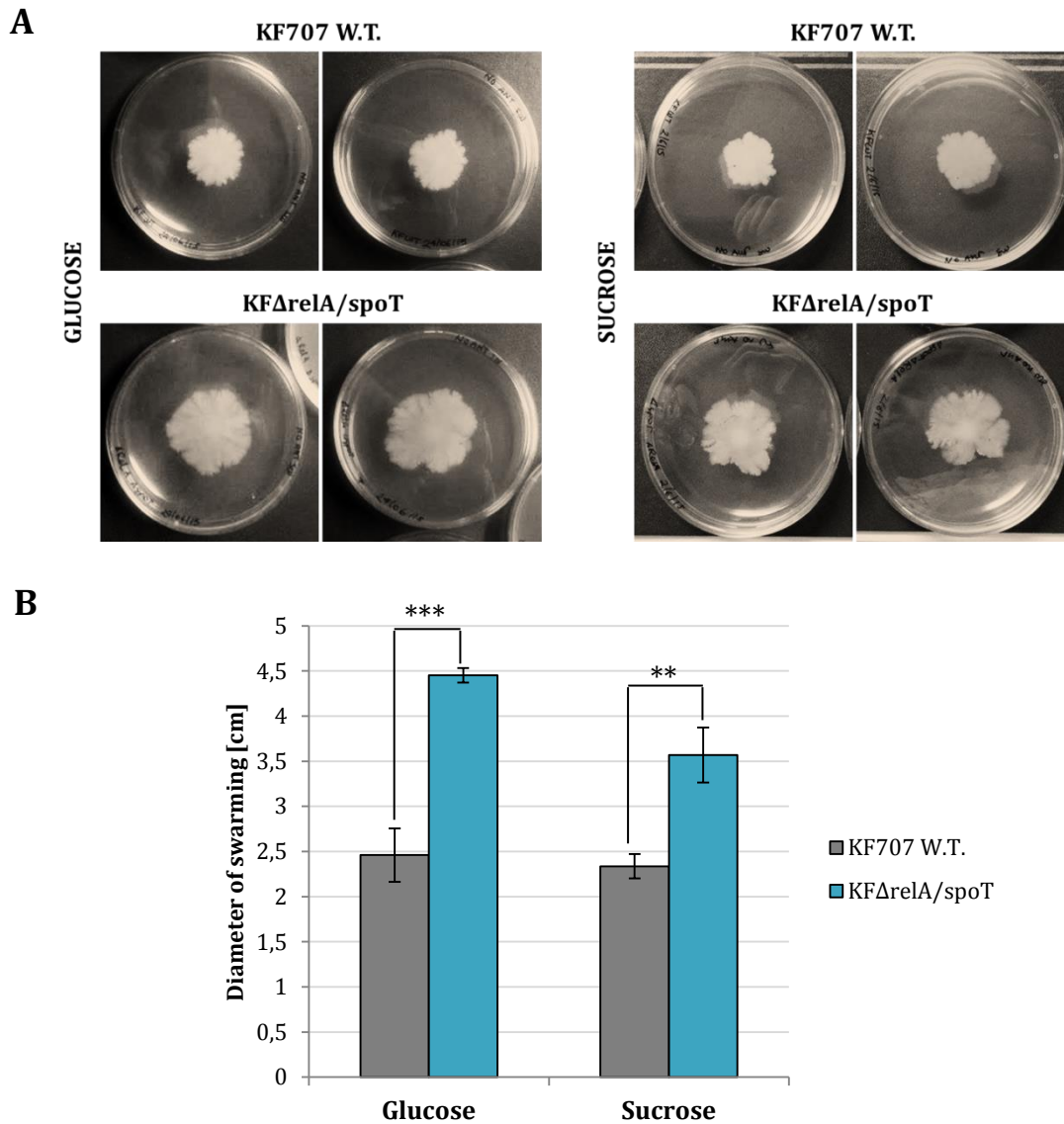


Figure 4.12: A) Swarming phenotypes of KF707 W.T. and KF Δ relA/spoT grown on swarming medium (agar 0.7% w/v) with glucose or sucrose as carbon source. The swarming areas were measured after one week incubation. **B)** The diameters of swarming areas and the standard deviations measured after one week are reported (growth on swarming medium agar [0.7% w/v], with glucose or sucrose as carbon source plates diameter 8.8 cm). The obtained results were verified by performing a two-sample *T*-test within pairs of strains. ** $p < 0.01$; *** $p < 0.001$. Results reflect three experimental replicates for each strain.

Stringent response and terminal oxidase promoters expression

Since the stringent response is a mechanism that primarily acts on the transcriptional level, activating or deactivating the transcription of specific genes, we thought to verify whether the expression and the modulation of KF707's respiratory terminal oxidases (previously shown, in Chapter 2 and 3, by us to be affected by growth carbon sources) varied in the absence of *relA* and *spoT* genes.

A relationship between these two mechanisms has never been demonstrated so far but, the involvement of transcriptional factors such as RpoS in both of these processes, is known.

The alternative sigma factor RpoS controls the synthesis of more than 100 genes, many of which are induced during stationary phase of growth [Patten et al., 2004; Lacour and Landini, 2004; Dong et al., 2008]. In *P. aeruginosa* PAO1, RpoS plays a significant role in *aa₃*-type cytochrome oxidases expression, it makes a minor contribution to the regulation of CIO and it does not have contribution to that of *cbb₃*-type [Cooper et al., 2003; Schuster et al., 2004; Kawakami et al., 2010]. In addition, RpoS is known to be necessary for survival under carbon starvation in *P. aeruginosa* [Jørgensen et al., 1999; Suh et al., 1999]; for these reasons the induction of *aa₃*-type oxidase, under nutrient starvation conditions, may be mainly the effect of the function of RpoS [Arai, 2011]. RpoS is also related to the stringent response as this molecule is correlated with the production of (p)ppGpp; when the concentration of these alarmones increases the level of RpoS also rises [Cashel et al., 1996; Gentry et al., 1993]. These secondary-messengers are implicated in transcriptional, translational and post-translational control of RpoS [Lange et al., 1995; Brown et al., 2002; Bougdour and Gottesman, 2007].

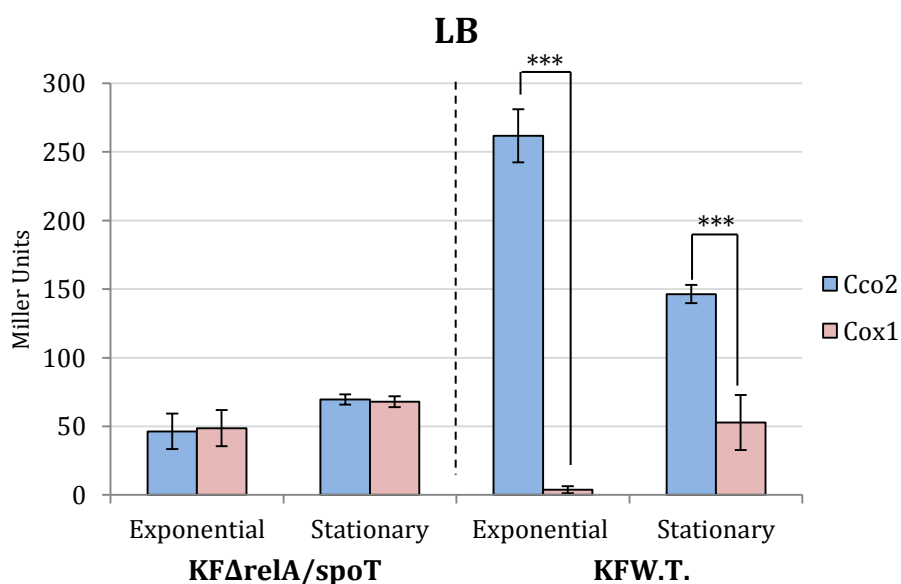
To analyze the existence of a connection between the stringent response and the modulation of the cytochrome oxidases expression, KF Δ relA/spoT-cox1Lac and KF Δ relA/spoT-cco2Lac *lacZ* translational fusion strains, were obtained, through the use of pUC18-mini-Tn7 (Chapter 2, Materials and Methods), and the expression of their promoters was evaluated by β -galactosidase assays. The assays were performed on LB and/or on MSM medium containing glucose or biphenyl [6 mM] as a single carbon source, at two different stages of growth, exponential (OD_{600 nm} 0.4-0.6) and stationary (OD_{600 nm} 0.7-0.9).

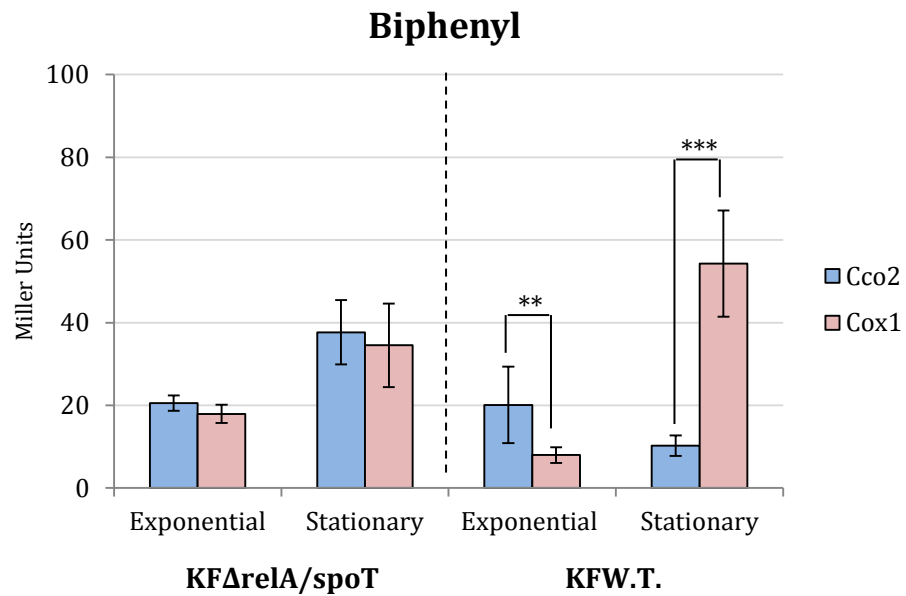
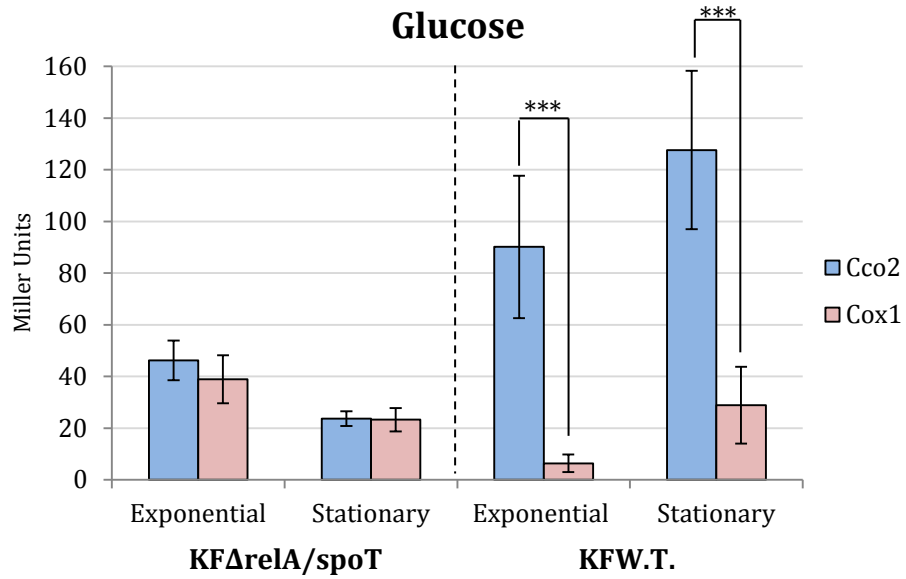
The results obtained with these two mutant strains were compared with the oxidases expression evaluated in KF707 W.T. strain.

As shown in Figure 4.13, the *Cbb32* and *Caa3* promoters activity was measured through β -galactosidase assay. Apparently, while KF707 W.T. cells show string differences in the expression of the oxidases as a function of the cell growth phase and media used in *KF Δ relA/spoT* mutant cells, the expression of the oxidase promoter was fully unaffected by metabolic parameters such as growth phase and carbon source.

These preliminary results, that needed to be repeated and further verified, suggest an involvement of the stringent response in the regulation of the oxidase expression in KF707 cells. The secondary-messengers (p)ppGpp, which regulate many cellular processes, probably play a role in the modulation of KF707 terminal oxidases, activating or deactivating the transcriptional regulators of these enzymes.

Figure 4.13: β -galactosidase activities measured in cell extracts derived from the KF707 W.T. and Δ relA/spoT translational fusion strains, grown aerobically in LB or MSM medium with glucose or biphenyl [6 mM]. The assays were performed at two different stages of growth, exponential and stationary. Asterisks indicate that mean values are significantly different according to two samples *T*-test within pairs of strains (** p <0.01 *** p <0.001).





4.4 Discussion

The stringent response is a global system that controls different cellular processes [Potrykus and Cashel, 2008]. In bacteria, this type of mechanism is activated in response to different stress conditions such as: heat shock, nutrient and amino acids starvation or pH changes. The effectors of the stringent response are the (p)ppGpp nucleotides, also named alarmones; these molecules act as secondary-messengers and respond by activating or deactivating a large number of genes [Hauryliuk et al., 2015].

In Proteobacteria, the proteins involved in the synthesis and hydrolysis of these molecules belong to the RelA/SpoT superfamily and usually *Pseudomonas* strains own two of these enzymes: RelA, that is specialized for (p)ppGpp synthesis and SpoT, which can hydrolyze and weakly synthesize the alarmones [Atkinson et al., 2011]. In *Pseudomonas* strains, it is known that the stringent response mechanism is involved in different processes such as: antibiotics tolerance [Nguyen et al., 2012], antifungal activity [Manuel et al., 2012], optimal catalase activity and hydrogen peroxide tolerance during growth [Khakimova et al., 2013], virulence and infection [Vogt et al., 2011; Chatnaparat et al., 2015], cell size control and survival on plants [Chatnaparat et al., 2015], nutrient limitation and biocide exposure [Greenway and England, 1999], quorum sensing and cell density [Van Delden et al., 2001].

In the genome of KF707 two genes coding respectively for RelA and SpoT proteins, were found (BAU76106 and BAU77268). Since the existence of a relationship between the stringent response and the carbon source used for growth has never been studied, we thought to construct KF707 deletion mutants, for *relA* and *spoT* genes, to examine their phenotypes when they grown in the presence of different carbon sources.

The first conclusion obtained in this present experimental work is that the absence of SpoT protein is lethal for KF707; this observation is not totally new, as in other bacteria species, such as *E. coli* and *Pseudomonas* strains [Potrykus and Chasel, 2008] it has been reported that the SpoT deletion destabilizes the balance between synthesis and hydrolysis of (p)ppGpp leading bacteria to death. In line with this, it was impossible to obtain the single mutant KF Δ spoT.

Analysis of the growth curves of $KF\Delta relA$ and $KF\Delta relA/spoT$ mutants indicated that the deletion of *relA* gene did not cause any alteration in the growth rate: on the contrary, when *spoT* was deleted in addition to *relA*, an evident impairment in the growth rate was observed with glucose, sucrose, benzoate and biphenyl, as carbon sources. In particular, with these compound an initial lag phase, lasting for 8-10 hours, was apparent. This phenomenon is unusual and it might suggest the presence, in KF707 cells, of a mechanism overcoming the stress response. Indeed, many bacterial strains possess in their genome alternative RSH proteins, named small RSH [Atkinson et al., 2011], which can be activated for example in the absence of RelA and/or SpoT. Unfortunately this possibility remains unsolved as we did not find homologues of these enzymes in the KF707 genome.

To get further insights into the response mechanism featuring $KF\Delta relA/spoT$ mutants, the KF707 growth recovery following the addition of the stringent response inductor, SHX, and the production of (p)ppGpp, were analyzed. In this respect it was observed that, after SHX addition to $KF\Delta relA/spoT$ mutant and W.T. cells the growth immediately stopped. Notably, when the inductor SHX was removed, the W.T. cells restarted their grow after one hour while the deletion mutant strain showed its characteristic lag (5-6 hours), before recovering its growth rate. This data supports the existence of an alternative stringent response mechanism although the analysis of (p)ppGpp production in $KF\Delta relA/spoT$, revealed that alarmones are not produced and the GTP/GDP pool decreased.

The proteome profile of the double mutant strain grown, until the exponential phase, on MSM with benzoate [6 mM] as sole carbon source, was analyzed and compared to that of the W.T. grown in the same conditions. Among the most expressed proteins in the double mutant strain, no RelA or SpoT homologues were found. However, three Heat Shock Proteins (HSP), molecules usually implicated in the heat shock response, have been identified [Santoro, 1999; Maleki et al., 2016]. Some of these molecules are chaperones (GrpE, DnaK, DnaJ or GroEL) while others are proteases, whose expression is usually controlled by transcriptional sigma factors [Richter et al., 2010]. Because in the double mutant strains $KF\Delta relA/spoT$, the putative genes that are activated during the stringent response were deleted, the overexpression of the genes coding for HSP, is probably required to respond to environmental changes and stress conditions.

Concerning the role of the stringent response in affecting the swarming motility of KF707, we have unexpectedly observed that cell motility is negatively affected by stringent response genes. Indeed, in *Pseudomonas* species, deletion of *relA* and *spoT* genes causes a decrease of the swarming motility [Vogt et al., 2011; Chatnaparat et al., 2015] whereas in KF707 these two genes mimic the negative effect of *cheA3* gene [Fedi et al., 2016; Chapter 1].

Finally, studying the expression of terminal cytochrome oxidases in KF Δ relA/spoT mutant strain it was observed that RelA and SpoT modulate the terminal oxidase promoters. This phenomenon has never been examined in detail and this observation open new perspectives as it suggest the participation of RelA, SpoT or (p)ppGpp in the control of KF707 respiration and in particular of the terminal oxidases [Potrykus and Cashel, 2008; Hauryliuk et al., 2015].

Since we are conscious that future experiments are necessary to complete and verify the results presented in this Chapter 4 a series of analysis have been planned to better understand the implication of RelA and SpoT genes in aromatic carbon metabolism, in the swarming motility and in the terminal oxidases modulation. Experiments, like Real-Time PCR, will be conducted to evaluate and to confirm the HSP overexpression in the double mutant KF Δ relA/spoT; the swarming phenotype, in mutant lacking *relA* and *spoT* will be further studied by using the KF707 complemented strains and/or other growth media conditions; finally the oxidase promotes expression will be completed by obtaining the *lacZ* translational fusion strains for Cbb₃₁, Ccaa₃ and CIO promoters along with Real-Time PCR test to verify the Cbb₃₁, Cbb₃₂, Caa₃ and CIO expressions.

General Conclusions

Prokaryotes are likely the most ancient and abundant form of life that has colonized the planet because they have been evolving to survive in harsh habitats environments, characterized by high temperatures, acidic or basic pHs conditions and/or contaminated by toxic organics and inorganics compounds. Microorganisms include pathogenic species to humans and plants but also species playing a fundamental role in biogeochemical cycles as individuals or in symbiotic associations with their hosts. Bacteria are also important for numerous human activities such as, for example: i) agriculture, ii) industrial manufacturing for the production of secondary metabolites like antibiotics, drugs and biosurfactants and iii) environmental technologies. This latter case comprises the so called bioremediation procedures that is the use of microorganisms to degrade or transform toxic compounds, an approach particularly important for the recovery/re-use of polluted sites. The efficiency of this approach depends not only on the ability of microorganisms to degrade pollutants, but also in their capacity to tolerate intermediate metabolites which are generated during the degradation of these compounds.

In this respect, *Pseudomonas pseudoalcaligenes* KF707, a Gram negative Proteobacterium that was isolated near a biphenyl manufacturing plant in Japan [Furukawa and Myazaki, 1986], is known as one of the most effective polychlorinated biphenyls (PCBs) degraders [Fedi et al., 2001]. Additionally, this bacterial strain can also tolerate the oxidative stress induced by toxic metal oxyanions such as tellurite (TeO_3^{2-}) and selenite (SeO_3^{2-}) [Di Tomaso et al., 2002; Zanaroli et al., 2002; Tremaroli *et al.*, 2007]. Finally, the KF707 genome analysis carried out after its complete sequencing in 2012 [Triscari-barberi et al., 2012], has highlighted the potential capacity of this bacterium to use as carbon and energy sources an extraordinary wide spectrum of aromatic compounds. These aspects, together, make KF707 a promising “microbial-cell tool” for environmental bioremediation procedures.

In this present PhD work, several aspects of KF707 metabolism have been studied for the first time. The results, a few of them requiring further verification, gave rise to an important set of biochemical and molecular clues useful for the KF707 application in environmental technologies.

- *The role of cheA genes in swarming and swimming motility*

Chemotaxis is regarded as a selective advantage for bacteria that colonize contaminated environments. It is a process allowing the migration of microorganisms (positive or negative) under the influence of a chemical gradient, leading the bacterium to find a chemically favorable niche to grow and survive in unfavorable environments. There are several examples where bacterial chemotaxis plays an essential role such as colonization of sites contaminated by xenobiotics, biofilm formation and invasion/pathogenic colonization of hosts [Grimm and Harwood, 1997; Pittman et al., 2001; Parales and Harwood, 2002; Stoodley, 2002]. KF707 chemotaxis presents one of these examples because the KF707 ability to form biofilms is essential for the colonization of contaminated sites and chemotaxis plays a crucial role in this mechanism [O'Toole and Kolter, 1998; Tremaroli et al., 2010; Tremaroli et al., 2011].

The genome of KF707 contains three *cheA* gene clusters - *cheA1*, *cheA2* and *cheA3* - predicted to be involved in the chemotaxis pathway, which were identified and annotated [Triscari-Barberi et al., 2012]. The experiments conducted and reported in Chapter 1, illustrate the peculiar role of *cheA* genes in the motility of KF707, namely: i) only the *cheA1* gene is involved in **swimming motility**, while *cheA2* and *cheA3* genes do not affect this type of movement; ii) the **swarming motility**, is strongly dependent on gene *cheA2* since its deletion determines the absence of this type of motility which is featured by cell colony ramifications on agar plates; iii) also *cheA1* gene deletion affects swarming motility while the lack of *cheA3*, when *cheA1* and *cheA2* genes are present, leads to an increase of the swarming motility as compared to KF707 W.T. Apparently, in KF707 the product of *cheA3* gene has a negative effect on the positive role of the other two gene clusters.

- *The modulation of the terminal respiratory oxidases in the presence of biphenyl*

In Prokaryotes, the respiratory electron transport chains differ from those present in Eukaryotes in that they are able to use multiple electron donors and acceptors to provide the metabolic flexibility to cope with highly variable the environmental niches [Hernandez and Newman, 2001]. In Chapter 2, the terminal oxidases of the respiratory electron transport chain of KF707 were characterized in terms of their response to different carbon sources. In the genome of KF707 were identified five terminal oxidases: two *caa₃*-type oxidases (*Caa₃* and *Ccaa₃*), two *cbb₃*-type (*Cbb₃1* and *Cbb₃2*) and one cyanide-insensitive quinol oxidase CIO. The results of Chapter 2 demonstrate that while the activity and the expression of both *cbb₃*-type oxidase were prevalent in glucose grown cells, as compared to the other oxidases, the activity and expression of the *caa₃*-type oxidase increased considerably only when biphenyl was used as carbon source; conversely, in biphenyl grown cells the expression of the *Cbb₃2* oxidase, was repressed. It was also found that the respiration activity and expression of the quinol oxidase CIO, was up-regulated in a *Cbb₃1* deletion strain as compared to KF707 W.T. The results, together, reveal that both function and expression of *cbb₃*- and *caa₃*-type oxidases in KF707 are modulated by biphenyl which is also the co-metabolite necessary for the activation of the PCBs degradation pathway.

In Chapter 3, by combining the peroxidase activity based haem-staining (SDS-PAGE-TMBZ) with tandem mass spectrometry analysis (Nano LC-MS/MS) of protein extracts from KF707 W.T. and respiratory mutant strains, we provided biochemical and structural evidence that KF707 overproduces a *Caa₃* oxidase, using cytochrome *c₄* as an electron donor, in cells grown with biphenyl as sole carbon source. To our knowledge, this is the first time that a cytochrome *c₄* *Caa₃* oxidase has been characterized in a *Pseudomonas* spp.

- *The role of *relA* and *spoT* genes in KF707 stringent response mechanism*

The stringent response mechanism is a sort of global genetic system that controls various bacterial processes in response to different stress conditions [Potrykus and Cashel, 2008]. In the genome of KF707, two genes coding for RelA and SpoT proteins and most likely involved in the stringent response mechanism, were found. The experiments conducted and reported in Chapter 4 show that while the deletion of *relA* does not affect the KF707 growth rate phenotype of cells grown on sugars and aromatic compounds, the lack of *spoT* determines a characteristic initial growth lag phase lasting for only of 8-10 hours. This phenomenon was further investigated by 2-DE and mass spectrometry analysis so conclude that the overcoming by KF707 cells of this lag phase was likely due to the expression of proteins similar to those involved in the Heat Shock Stress Response.

In bacteria the stringent response mechanism also affects cell motility while there are no indications in the literature of such an effect on respiratory chain components. In contrast with the reported literature, we unexpectedly observed that deletion of *relA/spoT* genes had a positive effect on the swarming ability of KF707 while, the expression of terminal cytochrome oxidases in KF Δ *relA/spoT* mutant strain was fully unaffected by the carbon source used for cell growth. These latter findings are of particular interest thus to deserve further investigation in the near future.

Bibliography

Abergel C., Nitschke W., Malarte G., Bruschi M., Claverie J.M. and Giudici-Orticoni M.T. The structure of *Acidithiobacillus ferrooxidans* *c*₄-cytochrome: a model for complex-induced electron transfer turning. (2003) *Structure*, Vol. 11, 547-555.

Abraham W.R., Nogales B., Golyshin P.N., Pieper D.H. and Timmis N.K. Polychlorinated biphenyl-degrading microbial communities in soils and sediments. (2002) *Current opinion in Microbiology*, Vol. 5, 246-253.

Abramowicz D.A. Aerobic and anaerobic biodegradation of PCBs: a review. (1990) *Critical Reviews in Biotechnology*, Vol. 10, 241-251.

Adler J. Chemotaxis in bacteria (1975) *Annual Review of Biochemistry*, 886.

Albury M.S., Elliott C. and Moore A.L. Towards a structural elucidation of the alternative oxidase in plants. (2009) *Physiologia Plantarum*, Vol. 137, 316-327.

Alm R.A. and Mattick J.S. Identification of a gene, *pilV*, required for type 4 fimbrial biogenesis in *Pseudomonas aeruginosa*, whose product possesses a pre-pilin-like leader sequence. (1995) *Molecular Microbiology*, Vol. 16, 485-496.

Alon U., Camarena L., Surette M.G., Aguera y Arcas B., Liu Y., Leibler S. and Stock J.B. Response regulator output in bacterial chemotaxis. (1998) *The EMBO Journal*, Vol. 17, 4238-4248.

Altshult S.F., Madden T.L., Schäffer A.A., Zhang H., Zhang Z., Miller W. and Lipman D.J. Gapped BLAST and PSI-BLAST: a new generation of protein database search programs. (1997) *Nucleic Acids Research*, Vol. 25, 3389-3402.

Alvarez-Ortega C. and Harwood C.S. Responses of *Pseudomonas aeruginosa* to low oxygen indicate that growth in the cystic fibrosis lung is by aerobic respiration. (2007) *Molecular Microbiology*, Vol. 65, 153-165.

Ancona V., Lee J.H., Chatnaparat T., Oh J., Hong J.I. and Zhao Y. The bacterial alarmone (p)ppGpp activates the Type III secretion system in *Erwinia amylovora*. (2015) *Journal of Bacteriology*, Vol. 197, 1433-1443.

Andersson D.I. and Hughes D. Gene amplification and adaptive evolution in bacteria. (2009) *Annual Review of Genetics*, Vol. 43, 167-195.

Anzai Y., Kim H., Park J.Y., Wakabayashi H. and Oyaizu H. Phylogenetic affiliation of the *Pseudomonas* based on 16s rRNA sequence. (2000) *International Journal of Systematic and Evolutionary Microbiology*, Vol. 50, 1563-1589.

Arai H., Roh J.H. and Kaplan R. Transcriptome dynamics during the transition from anaerobic photosynthesis to aerobic respiration in *Rhodobacter*. (2008) *Journal of Bacteriology*, Vol. 190, 286-299

- Arai H.** Regulation and function of versatile aerobic and anaerobic respiratory metabolism in *Pseudomonas aeruginosa*. (2011) *Frontiers in Microbiology*, Review, Vol. 2, 103.
- Arai H.**, Kawakami T., Osamura T., Hirai T., Sakai Y. and Ishii M. Enzymatic characterization and *in vivo* function of five terminal oxidases in *Pseudomonas aeruginosa*. (2014) *Journal of Bacteriology*, Vol. 196, 4206-4215.
- Aravind L. and Koonin E.V.** The HD domain defines a new superfamily of metal-dependent phosphohydrolases. (1998) *Trends in Biochemical Sciences*, Vol. 23, 469-472.
- Arras T.**, Schirawski J. and Unden G. Availability of O₂ as a substrate in the cytoplasm of bacteria under aerobic and microaerobic conditions. (1998) *Journal of Bacteriology*, Vol. 180, 2133-2136.
- Arslan E.**, Kannt A., Thöny-Meyer L. and Hennecke H. The symbiotically essential *cbb₃*-type oxidase of *Bradyrhizobium japonicum* is a proton pump. (2000) *FEBS*, Vol. 470, 7-10.
- Artsimovitch I.**, Patlen V., Sekine S., Vassylyeva M.N., Hosaka T., Ochi K., Yokoama S. and Vassylyev D.G. Structural basis for transcription regulation by alarmone ppGpp. (2004) *Cell*, Vol. 117, 299-301.
- Ashkenazy H.**, Abadi S., Martz E., Chay O., Mayrose I., Pupko T. and Ben-Tal N. ConSurf2016: an improved methodology to estimate and visualize evolutionary conservation in macromolecules. (2016) *Nucleic Acids Research*, Vol. 44, W344-W350.
- Atkinson G.C.**, Tenson T. and Hautylyuk V. The RelA/SpoT Homolog (RSH) superfamily: distribution and structural evolution of ppGpp synthetases and hydrolases across the tree of life. (2011) *PlosONE*, Vol. 6, e23479.
- Baker M.D.**, Wolanin P.M. and Stock J.B. Signal transduction in bacterial chemotaxis. (2006) *BioEssays*, Vol. 28, 9-22.
- Baker N.A.**, Sept D., Joseph S., Holst M.J. and McCammon J.A. Electrostatics of nanosystems: Application to microtubules and the ribosome. (2001) *PNAS*, Vol. 98, 10037-10041.
- Baker S.C.**, Ferguson S.J., Ludwig B., Page M.D., Richter O.M.H. and van Spanning R.J.M. Molecular genetics of the genus *Paracoccus*: metabolically versatile bacteria with bioenergetics flexibility. (1998) *Microbiology and Molecular Biology Reviews*, Vol. 62, 1046-1078.
- Battesti A. and Bouveret E.** Acyl carrier protein/SpoT interaction, the switch linking SpoT-dependent stress response to fatty acid metabolism. (2006) *Molecular Microbiology*, Vol. 62, 1048-1063.
- Battesti A.**, Majdalani N. and Gottesman S. The RpoS-mediated general stress response in *Escherichia coli*. (2011) *Annual Review of Microbiology*, Review, Vol. 65, 189-213.
- Bengtsson J.**, Tjalsma H., Rivolta C. and Hederstedt L. Subunit II of *Bacillus subtilis* cytochrome *c* oxidase is a lipoprotein. (1999) *Journal of Bacteriology*, Vol. 181, 685-688.
- Berg H.C.** Chemotaxis in bacteria. (1975) *Annual Review of Biophysics and Bioengineering*, 9050.
- Blat Y.**, Gillespie B., Bren A., Dahlquist F.W. and Eisenbach M. Regulation of phosphatase activity in bacterial chemotaxis. (1998) *Journal of Molecular Biology*, Vol. 284, 1191-1199.

Borisov V.B., Gennis R.B., Hemp J. and Verkhovsky M.I. The cytochrome *bd* respiratory oxygen reductase. (2011) *Biochimica et Biophysica Acta – Bioenergetics*, Review, Vol. 1807, 1398-1413.

Borja J., Taleon D.M., Auresenia J. and Gallardo S. Polychlorinated biphenyls and their biodegradation. (2005) *Process Biochemistry*, Review, Vol. 40, 1999-2013.

Bott M., Preisig O. and Hennecke H. Genes for a second terminal oxidase in *Bradyrhizobium japonicum*. (1992) *Archives of Microbiology*, Vo. 158, 335-343.

Bougdour A. and Gottesman S. ppGpp regulation of RpoS degradation via anti-adaptor protein IraP. (2007) *PNAS*, Vol. 104, 12896-12901.

Boyer H.W. and Roland-Dussoix D. A complementation analysis of the restriction and modification of DNA in *Escherichia coli*. (1969) *Journal of Molecular Biology*, Vol. 41, 459-472.

Bratlie M.S., Johansen J., Sherman B.T., Huang D.W., Lempicki R.A. and Drablos Finn. Gene duplications in prokaryotes can be associate with environmental adaptation. (2010) *BioMed Central Genomics*, 11:588.

Bratton M.R., Pressler M.A. and Hosler J.P. Suicide inactivation of cytochrome *c* oxidase: catalytic turnover in the absence of subunit II alters the active site. (1999) *Biochemistry*, Vol. 38, 16236-16245.

Bren A. and Eisenbach M. The N terminus of the flagellar switch protein, FliM, is the binding domain for the chemotactic response regulator CheY. (1998) *Journal of Molecular Biology*, Vol. 278, 507-514.

Brown L., Gentry D., Elliott T. and Cashel M. DskA affects ppGpp induction of RpoS at a translational level. (2002) *Journal of Bacteriology*, Vol. 184, 4455-4465.

Brzezinski P., Larsson G. and Adelroth P. Functional aspects of heme-copper terminal oxidases. (2004) *Advances in Photosynthesis and Respiration*, Vol. 15, 129-153.

Buschmann S., Warkentin E., Xie H., Langer J.D., Ermler U. and Michel H. The structure of *cbb₃* cytochrome oxidase provides insights into proton pumping. (2010) *Science*, Vol. 329, 327-330.

Cashel M., Gentry D.R., Hernandez V.J., Vinella D. The stringent response. (1996) Neidhardt F.C., Curtiss R. III, Ingraham J.L., Lin E.C.C., Low K.B., Magasanik B., Reznikoff W.S., Riley M., Schaechter M., Umberger H.E. (Eds.) *Escherichia coli and salmonella. Cellular and Molecular Biology*, second ed. American Society for Microbiology, Washington DC, pp. 1458–1496.

Cecchini G. Function and structure of Complex II of the respiratory chain. (2003) *Annual Review of Biochemistry*, Review, Vol. 72, 77-109.

Chakraborty R. and Bibb M. The ppGpp synthetase gene (*relA*) of *Streptomyces coelicolor* A3(2) plays a conditional role in antibiotic production and morphological differentiation. (1997) *Journal of Bacteriology*, Vol. 179, 5854-5861.

Chang H.Y., Ha Y., Pace L.A., Lin M.T., Lin Y.H. and Gennis R.B. The dihaem cytochrome *c₄* from *Vibrio cholera* is a natural electron donor to the respiratory *cbb₃* oxygen reductase. (2010) *Biochemistry*, Vol. 49, 7494-7503.

- Chatnaparat T.**, Li Z., Korban S.S. and Zhao Y. The bacterial alarmone (p)ppGpp is required for virulence and controls cell size and survival of *Pseudomonas syringae* on plants. (2015) *Environmental Microbiology*, Vol. 17, 4253-4270.
- Chatnaparat T.**, Li Z., Korban S.S. and Zhao Y. The stringent response mediated by (p)ppGpp is required for virulence of *Pseudomonas syringae* pv. *Tomato* and its survival on tomato. (2015) *Molecular Plant-Microbe Interactions*, Vol. 28, 776-789.
- Chatterji D. and Ohja A.K.** Revisiting the stringent response, ppGpp and starvation signaling. (2001) *Current Opinion in Microbiology*, Vol. 4, 160-165.
- Choi K.H. and Schweizer H.P.** mini-Tn7 insertion in bacteria in single *attTn7* sites: example *Pseudomonas aeruginosa*. (2006) *Nature Protocols*, Vol. 1, 153-161.
- Choi K.H.**, Gaynor J.B., White K.G., Lopez C., Bosio C.M., Karkhoff-Schweizer R.R. and Schweizer H.P. A Tn7-based broad-range bacterial cloning and expression system. (2005) *Nature Methods*, Vol. 2, 443-448.
- Comolli J. and Danohue T.J.** *Pseudomonas aeruginosa* RoxR, a response regulator related to *Rhodobacter sphaeroides* PrrA, activates expression of the cyanide-insensitive terminal oxidase. (2002) *Molecular Microbiology*, Vol. 45, 755-768.
- Comolli J. and Donohue T.J.** Differences in two *Pseudomonas aeruginosa* *cbb₃* cytochrome oxidases. (2004) *Molecular Microbiology*, Vol. 51, 1193-1203.
- Cooper M.**, Tavanka G.R. and Williams H.D. Regulation of expression of the cyanide-insensitive terminal oxidase in *Pseudomonas aeruginosa*. (2003) *Microbiology*, Vol. 149, 1275-1284.
- Cramer W.A. and Knaff D.R.** (1990) *Energy Transduction in Biological Membranes*, Springer.
- Crofts A.R.** The cytochrome *bc₁* complex: function in the context of structure. (2004) *Annual Review of Physiology*, Review, Vol. 66, 689-733.
- Cunningham L. and Williams H.D.** Isolation and characterization of mutants defective in the cyanide-insensitive respiratory pathway of *Pseudomonas aeruginosa*. (1995) *Journal of Bacteriology*, Vol. 177, 432-438.
- Cunningham L.**, Pitt M. and Williams H.D. The *cioAB* genes from *Pseudomonas aeruginosa* code for a novel cyanide-insensitive terminal oxidase related to the cytochrome *bd* quinol oxidases. (1997) *Molecular Microbiology*, Vol. 24, 579-591.
- D'mello R.**, Hills S. and Poole R.K. The cytochrome *bd* quinol oxidase in *Escherichia coli* has an extremely high oxygen affinity and two-oxygen binding haems: implications for regulation of activity *in vivo* by oxygen inhibition. (1996) *Microbiology*, Vol. 142, 755-763.
- Dahl J.L.**, Arora K., Boshoff H.L., Whiteford D.C., Pacheco S.A., Walsh O.J., Bonilla D.L., Davis W.B. and Garza A.G. The *relA* homolog of *Mycobacterium smegmatis* affects cell appearance, viability, and gene expression. (2005) *Journal of Bacteriology*, Vol. 187, 2439-2447.
- Daldal F.**, Mandaci S., Winterstein C., Myllykallio H., Duyck K. and Zannoni D. Mobile cytochrome *c₂* and membrane-anchored cytochrome *c_γ* are both efficient electron donors to the *cb₃*- and *aa₃*-type

cytochrome *c* oxidases during respiratory growth of *Rhodobacter sphaeroides*. (2001) *Journal of Bacteriology*, Vol. 183, 2013-2024.

Dalebroux Z.D., Svesson S.L., Gaynor E.C. and Swanson M.S. ppGpp conjures bacterial virulence. (2010) *Microbiology and Molecular Biology Review*, Review, Vol. 74, 171-199.

Dalebroux Z.D. and Swanson M.S. ppGpp: magic beyond RNA polymerase. (2012) *Nature Reviews Microbiology*, Review, Vol. 10, 203-212.

De Gier J.W.L., Schepper M., Rejinders W.N.M., van Dyck S.J., Slotboom D.J., Wame A., Saraste M., Krab K., Finel M., Stouthamer A.H., van Spanning R.J.M. and van der Oost J. Structural and functional analysis of *aa₃*-type cytochrome *c* oxidases of *Paracoccus denitrificans* reveals significant differences in proton-pump design. (1996) *Molecular Microbiology*, Vol. 20, 1247-1260.

Dehò G. and Galli E. *Biologia dei Microrganismi*. (2016).

Di Tomaso G., Fedi S., Carnevali M., Manegatti M., Taddei C. and Zannoni D. The membrane-bound respiratory chain of *Pseudomonas pseudoalcaligenes* KF707 cells grown in the presence or absence of potassium tellurite. (2002) *Microbiology*, Vol. 148, 1699-1708.

Dominguez-Cuevas P., Gonzales J.E., Marques S., Ramos J.L. and de Lorenzo V. Transcriptional tradeoff between metabolic and stress-response programs in *Pseudomonas putida* KT2440 cell exposes to toluene. (2006) *The Journal of Biological Chemistry*, Vol. 281, 11981-11991.

Dong T., Kirchhof M.G. and Schellhorn H.E. RpoS regulation of gene expression during exponential growth of *Escherichia coli* K12. (2008) *Molecular Genetics and Genomics*, Vol. 279, 267-277.

Edwards S.E., Loder C.S., Wu G., Corker H., Bainbridge B.W., Hill S. and Poole R.K. Mutation of cytochrome *bd* quinol oxidase results in reduced stationary phase survival, iron deprivation, metal toxicity and oxidative stress in *Azotobacter vinelandii*. (2000) *FEMS Microbiology Letters*, Vol. 185, 71-77.

Fain M.G. and Haddock J.D. Phenotypic and phylogenetic characterization of *Bukolderia* (*Pseudomonas*) sp. strain LB400. (2001) *Current Microbiology*, Vol. 42, 269-275.

Farver O., Grell E., Ludwig B., Michel H. and Pecht I. Rates and equilibrium of Cu_A to heme *a* electron transfer in *Paracoccus denitrificans* cytochrome *c* oxidase. (2006) *Biophysical Journal*, Vol. 90, 2131-2137.

Fava F., Bertin L., Fedi S. and Zannoni D. Metyl- β -cyclodextrin-enhanced solubilization and aerobic biodegradation of polychlorinated-biphenyls in two aged-contaminated soils. (2002) *Bioengineering*, Vol. 81, 381-390.

Fedi S., Carnevali M., Fava F., Andracchio A., Zappoli S. and Zannoni D. Polychlorinated biphenyl degradation activities and hybridization analysis of fifteen aerobic strains isolated from PCB-contaminated site. (2001) *Research Microbiology*, Vol. 152, 583-592.

Fedi S., Triscari-Barberi T., Nappi M.R., Sandri F., Booth S., Turner R.J., Attimonelli M., Cappelletti M. and Zannoni D. The role of *cheA* genes in swarming and swimming motility of *Pseudomonas pseudoalcaligenes* KF707. (2016) *Microbes and Environments*, Vol.31, 169-172.

- Ferguson-Miller S. and Babcock G.T.** Heme/Copper terminal oxidases. (1996) *Chemical Reviews*, Review, Vol. 96, 2889-2908.
- Figurski D.H. and Helinski D.R.** Replication of an origin-containing derivative of plasmid RK2 dependent on a plasmid function provided in *trans*. (1979) *PNAS*, Vol. 76, 1648-1652.
- Frangipani E.,** Slaveykova V.I., Reimann C. and Haas D. Adaptation of aerobically growing *Pseudomonas aeruginosa* to copper starvation. (2008) *Journal of Bacteriology*, Vol. 190, 6707-6717.
- Fujihara H.,** Yoshida H., Matsunaga T., Goto M. and Furukawa K. Cross-regulation of biphenyl- and salicylate-catabolic genes by two regulatory systems in *Pseudomonas pseudoalcaligenes* KF707. (2006) *Journal of Bacteriology*, Vol. 188, 4690-4697.
- Furukawa K. and Fujihara H.** Microbial degradation of polychlorinated biphenyls: biochemical and molecular features. (2008) *Journal of Bioscience and Bioengineering*, Review, Vol. 105, 433-449.
- Furukawa K. and Miyazaki T.** Cloning of a gene cluster encoding biphenyl and chlorobiphenyl degradation in *Pseudomonas pseudoalcaligenes*. (1986) *Journal of Bacteriology*, Vol. 156, 392-398.
- Furukawa K.,** Hirose J. and Suyama A. Gene components responsible for discrete substrate in the metabolism of biphenyl (*bph* operon). (1993) *Journal of Bacteriology*, Vol. 175, 5224-5232.
- Gabel C. and Maier R.J.** Oxygen-dependent transcriptional regulation of cytochrome *aa₃* in *Bradyrhizobium japonicum*. (1993) *Journal of Bacteriology*, Vol. 175, 128-132.
- Gaca A.O.,** Colomer-Winter C. and Lemos J.A. Many means to a common end: the intricacies of (p)ppGpp metabolism and its control of bacterial homeostasis. (2015) *Journal of Bacteriology*, Vol. 197, 1146-1156.
- Gaca A.O.,** Kaifasz J.K., Miller J.H., Liu K., Wand J.D., Abranches and Lemos J.A. Basal levels of (p)ppGpp in *Enterococcus faecalis*: the magic beyond the stringent response. (2013) *mBio*, Vol. 4, e00646-13.
- Gallant J., Irr J. and Cashel M.** The mechanism of amino acid control of guanylate and adenylate biosynthesis. (1971) *Journal of Biological Chemistry*, Vol. 246, 5812-5816.
- Gallant J.,** Palmer L. and Pao C.C. Anomalous synthesis of ppGpp in growing cells. (1977) *Cell*, Vol. 11, 181-185.
- Gao R. and Stock A.M.** Biological insight from structures of two-component proteins. (2009) *Annual Review of Microbiology*, Vol 63, 133-154.
- Gennis R.B. and Stewart V.** *Escherichia coli* and *Salmonella*: cellular and molecular biology. (1996) *Respiration*, ASM Press, 217-261.
- Grimm A.C. and Harwood C.S.** Chemotaxis of *Pseudomonas* spp. to the polyaromatic hydrocarbon naphthalene. (1997) *Applied and Environmental Microbiology*, Vol. 63, 4111-4115.
- Griswold I.J.,** Zhou H., Matison M., Swanson R.V., McIntosh L.P. et al. The solution structure and interaction of CheW from *Thermotoga maritima*. (2002) *Nature Structural Biology*, Vol. 9, 121-125.

- Gummesson L.**, Magnusson U., Lovmar M., Kvint K., Persson O., Ballesteros M., Farewell A. and Nystrom T. Increased RNA polymerase availability directs resources towards growth at the expense of maintenance. (2009) *The EMBO Journal*, Vol. 28, 2209-2219.
- Hamel E. and Cashel M.** Role of guanine nucleotides in protein synthesis. Elongation factor G and guanosine 5'-triphosphate, 3'-diphosphate. (1973) *PNAS*, Vol. 70, 3250-3254.
- Han H.**, Hemp J., Pace L.A., Ouyang H., Ganesan K., Rho J.H., Daldal F., Blanke S.R. and Genis R.B. Adaptation of aerobic respiration to low O₂ environments. (2011) *PNAS*, Vol. 108, 14109-14114.
- Hanahan D.** Studies on transformation of *Escherichia coli* with plasmid. (1983) *Journal of Molecular Biology*, Vol. 166, 557-580.
- Haralalka S., Nandi S. and Bhadra R.K.** Mutation in the *relA* gene of *Vibrio cholerae* affects in vitro and in vivo expression virulence factors. (2003) *Journal of Bacteriology*, Vol. 185, 4672-4682.
- Harrenga A. and Michel H.** The cytochrome *c* oxidase from *Paracoccus denitrificans* does not change the metal center ligation upon reduction. (1999) *Journal of Biological Chemistry*, Vol. 274, 33296-33299.
- Harshey R.M.** Bacterial motility on a surface many ways to a common goal. (2003) *Annual Review of Microbiology*, Vol. 57, 249-273.
- Hassani B.K.**, Steunou A.S., Liotenberg S., Reiss-Husson F., Astier C. and Ouchane S. Adaptation to oxygen: role of terminal oxidases in photosynthesis initiation in the purple photosynthetic bacterium, *Rubrivivax Gelatinosus*. (2010) *Journal of Biological Chemistry*, Vol. 285, 19891-19899.
- Hauryliuk V.**, Atkinson G.C., Murakami K.S., Tenson T. and Gerdes K. Recent functional insights into the role of (p)ppGpp in bacteria physiology. (2015) *Nature, Review*, Vol. 13, 298-309.
- Heitmann D. and Einsle O.** Structure and biochemical characterization of DHC₂, a novel diheme cytochrome *c* from *Geobacter sulfurreducens*. (2005) *Biochemistry*, Vol. 44, 12411-12419.
- Hernandez M.E. and Newman D.K.** Extracellular electron transfer. (2001) *Cellular and Molecular Life Science, Review*, Vol. 58, 1562-1571.
- Hoang T.T.**, Karkhoff-Shweizer R.R., Kutchma A.J. and Schweizer H.P. A broad-host-range Flp-FRT recombination system for site-specific excision of chromosomally-located DNA sequences: application for isolation of unmarked *Pseudomonas aeruginosa* mutants. (1998) *Gene*, Vol. 212, 77-86.
- Hochkoepler A.**, Jenney Jr F.E., Lang S.E., Zannoni D. and Daldal F. Membrane-associated cytochrome *c_y* of *Rhodobacter sphaeroides* is an electron carrier from the cytochrome *bc₁* complex to the cytochrome *c* oxidase during respiration.
- Hochstadt-Ozer J. and Cashel M.** The regulation of purine utilization in bacteria. V. Inhibition of purine phosphoribosyltransferase activities and purine uptake in isolated membrane vesicles by guanosine tetraphosphate. (1972) *Journal of Biological Chemistry*, Vol. 247, 7067-7072.
- Hofer B.**, Eltis L.D., Dowling D.N. and Timmis K.N. Genetic analysis of a *Pseudomonas* locus encoding a pathway for biphenyl/polychlorinated-biphenyl degradation. (1993) *Gene*, Vol. 130, 47-55.

- Hogg T.**, Mechold U., Malke H., Cashel M. and Hilgenfeld R. Conformational antagonism between opposing active sites in a bifunctional RelA/SpoT homolog modulates (p)ppGpp metabolism during the stringent response. (2004) *Cell*, Vol. 117, 57-68.
- Hosler J.P.** The influence of subunit III of cytochrome *c* oxidase on the D-pathway, the proton exit pathway and mechanism-based inactivation in subunit I. (2004) *Biochimica et Biophysica Acta – Bioenergetics*, Review, Vol. 1655, 332-339.
- Irr J. and Gallant J.** The control of ribonucleic acid synthesis in *Escherichia coli*: stringent control of energy metabolism. (1969) *Journal of Biological Chemistry*, Vol. 244, 2233-2239.
- Ito D.**, Kato T., Maruta T., Tamoi M., Yoshimura K. And Shigeoka S. Enzymatic and molecular characterization of *Arabidopsis* ppGpp pyrophosphohydrolase AtNUDX26. (2012) *Bioscience Biotechnology and Biochemistry*, Vol. 76, 2236-2241.
- Iwata S.**, Ostermeier C., Ludwig B. and Michel H. Structure at 2.8-Angstrom resolution of cytochrome-*c*-oxidase from *Paracoccus denitrificans*. (1995) *Nature*, Vol. 376, 660-669.
- Izumi K.**, Aramaki M., Kimura T., Naito Y., Udaka T., Uchikawa M., et al. Identification of a prosencephalic-specific enhancer of *SALL1*: comparative genomic approach using the chick embryo. (2007) *Pediatric Research*, Vol. 61, 660-665.
- Jackson R.J.**, Elvers K.T., Lee L.J., Gidley M.D., Wainwright L.M., Lightfoot J., Park S.F. and Poole R.K. Oxygen reactivity of both respiratory oxidases in *Campylobacter jejuni*: the *cydAB* genes encode a cyanide-resistant, low-affinity oxidase that is not of the cytochrome *bd* type. (2007) *Journal of bacteriology*, Vol. 189, 1604-1615.
- Jain V.**, Kumar M. and Chatterji D. ppGpp: stringent response and survival. (2006) *Journal of Microbiology*, Vol. 44, 1-10.
- Jensen K.F.**, Dandnell G., Hove-Jensen B. and Willemoes M. in *EcoSal – Escherichia coli* and *Salmonella*: Cellular and molecular biology. Chapter 3.6.2 (ASM Science, 2008).
- Jiménez J.I.**, Minambres B., Garcia J.L. and Diaz E. Genomic analysis of the aromatic catabolic pathways from *Pseudomonas putida* KT2440. (2002) *Environmental Microbiology*, Vol. 12, 824-841.
- Jo T. and Cheng J.** Improving protein fold recognition by random forest. (2014) *BMC Bioinformatics*, Vol. 14, S14.
- Jørgensen F.**, Bally M., Chapon-Herve V., Michel G., Lazdunski A. and Williams P. RpoS-dependent stress tolerance in *Pseudomonas aeruginosa*. (1999) *Microbiology*, Vol. 145, 835-844.
- Junemann S.** Cytochrome *bd* terminal oxidase. (1997) *Biochimica et Biophysica Acta*, Vol. 1321, 107-127.
- Kahlon R.S.** *Pseudomonas*: molecular and applied biology. (2016).
- Kanjee U.**, Ogata K. and Walid A.H. Direct binding targets of the stringent response alarmone (p)ppGpp. (2012) *Molecular Microbiology*, Vol. 85, 1029-1043.

- Kannt A.**, Soulimane T., Buse G., Becker A., Bamberg E. and Michel H. Electrical current generation and proton pumping catalyzed by the *ba₃*-type cytochrome *c* oxidase from *Thermus thermophilus*. (1998) *FEBS*, Vol. 343, 17-22.
- Kato J.**, Kim H.E., Takiguchi N., Kuroda A. and Ohtake H. *Pseudomonas aeruginosa* as a model microorganism for investigation of chemotactic behaviors in ecosystem. (2008) *Journal of Bioscience and Bioengineering*, Vol. 106, 1-7.
- Kawakami T.**, Kuroki M., Ishii M., Igarashi Y. and Arai H. Differential expression of multiple terminal oxidases for aerobic respiration in *Pseudomonas aeruginosa*. (2010) *Environmental Microbiology*, Vol. 12, 1399-1412.
- Kearns D.B.** A field guide to bacterial swarming motility. (2010) *Nature*, Review, Vol. 8, 634-644.
- Kenney L.J.** How important is the phosphatase activity of sensor kinases? (2010) *Current Opinion in Microbiology*, Vol. 13, 168-176.
- Khakimova M.**, Ahlgren H.G., Harrison J.J., English A.M. and Nguyen D. The stringent response controls catalases in *Pseudomonas aeruginosa* and is required for hydrogen peroxide and antibiotic tolerance. (2013) *Journal of Bacteriology*, Vol. 195, 2011-2020.
- Khan A.A.**, Whang R.F., Nawaz M.S. and Cerniglia C.E. Nucleotide sequence of the gene encoding *cis*-biphenyl dihydrodiol dehydrogenase (*bphB*) and the expression of an active recombinant His-tagged *bphB* gene product from a PCB degrading bacterium, *Pseudomonas putida* OU83. (1997) *FEMS Microbiology Letter*, Vol. 154, 317-324.
- Kita A.**, Takiguchi N. and Kato J. Cloning and characterization of *sigA* and *sigB* genes from *Rhodococcus opacus* strain B4: involvement of *sigB* in organic solvent tolerance. (2009) *Journal of Environmental Biotechnology*, Vol. 9, 43-50.
- Klamt S.**, Grammel H., Starube R., Ghosh R. and Gilles E.D. Modelling the electron transport chain of purple non-sulfur bacteria. (2008) *Molecular System Biology*, Vol. 4, 156.
- Koch H.G.**, Winterstein C., Saribas A.S., Alben J.O. and Daldal F. Roles of the *ccoGHIS* gene products in the biogenesis of the *ccb₃*-type cytochrome *c* oxidase. (2000) *Journal of Molecular Biology*, Vol. 297, 49-65.
- Koepke J.**, Olkhova E., Angere H., Müller H., Peng G. and Michel H. High resolution crystal structure of *Paracoccus denitrificans* cytochrome *c* oxidase: new insights into the active site and the proton transfer pathways. (2009) *Biochimica and Biophysica Acta – Bioenergetics*, Vol. 1787, 636-645.
- Kriel A.**, Bittner A.N., Kim S.H., Tehranchi A.K., Zou W.Y., Rendon S., Chen R., Tu B.P. and Wang J.D. Direct regulation of GTP homeostasis by (p)ppGpp. a critical component of viability and stress resistance. (2014) *Molecular Cell*, Vol. 48, 231-241.
- Krogh A.**, Brown M., Mian S., Sjölander K. and Haussler D. Hidden Markov models in computational biology: applications to protein modeling. (1994) *Journal of Molecular Biology*, Vol. 235, 1501-1531.
- Krol E. and Becker A.** ppGpp in *Sinorhizobium meliloti*: biosynthesis in to sudden nutritional downshift and modulation of the transcriptome. (2011) *Molecular Microbiology*, Vol. 81, 1233-1245.

- Krooneman J.**, Moore E.R.B., van Velzen J.C.L., Prins R.A., Forney L.J. and Gottshal J.C. Competition for oxygen and 3-chlorobenzoate between two aerobic bacteria using different degradation pathways. (1998) *FEMS Microbiology Ecology*, Vol. 126, 171-179.
- Lacour S. and Landini P.** σ^S -dependent gene expression at the onset of stationary phase in *Escherichia coli*: function of σ^S -dependent genes and identification of their promoter sequences. (2004) *Journal of Bacteriology*, Vol. 186, 7186-7195.
- Laemmli U.K.** Cleavage of structural proteins during the assembly of the head of bacteriophage T4. (1970) *Nature*, Vol. 227, 680-685.
- Lange R.**, Fischer D. and Hengg-Aronis R. Identification of transcriptional start sites and the role of ppGpp in the expression of *rpoS*, the structural gene for the sigma S subunit of RNA polymerase in *Escherichia coli*. (1995) *Journal of Bacteriology*, Vol. 177, 4676-4680.
- Laskowski R.A.**, MacArthur M.W., Moss D.S. and Thornton J.M. PROCHECK: a program to check the stereochemical quality of protein structures. (1993) *Journal of Applied Crystallography*, Vol. 26, 283-291.
- Lauffenburger D.A.** Quantitative studies of bacterial chemotaxis and microbial population dynamics. (1991) *Microbial Ecology*, Vol. 22, 175-178.
- Lauraeus M.**, Haltia T., Saraste M. and Wikstrom M. *Bacillus subtilis* expresses two kinds of haem-A-containing terminal oxidases. (1991) *The FEBS Journal*, Vol. 197, 699-705.
- Le Laz S.**, Kpebe A., Bauzan M., Lignon S., Rousset M. and Brgna M. Expression of terminal oxidases under nutrient-starved conditions in *Shewanella oneidensis*: detection of A-type cytochrome c oxidase. (2016) *Science Reports*, Vol. 6, 19726.
- Le Laz S.**, Kpebe A., Bauzan M., Lignon S., Rousset M. and Brugna M. A biochemical approach to study the role of the terminal oxidases in aerobic respiration of *Shewanella oneidensis* MR-1. (2014) *PLoSone*, Vol. 9, e86343.
- Lecoutere E.**, Verleyen P., Haenen S., Vandersteegen K., Noben J.P., Robben J., Schoofs L., Ceyskens P.J., Volckaert and Lavigne R, A theoretical and experimental proteome map of *Pseudomonas aeruginosa* PA01. (2012) *Microbiology Open*, Vol. 1, 161-181.
- Leedjarv A.**, Vask A., Virta M. and Kahru A. Analysis of bioavailable phenols from natural samples by recombinant luminescent bacterial sensors. (2006) *Chemosphere*, Vol. 64, 1910-1919.
- Levit M.N. and Stock J.B.** Receptor methylation controls the magnitude of stimulus-response coupling in bacterial chemotaxis. (2002) *Journal of Biological Chemistry*, Vol. 277, 36760-36765.
- Li J.**, Swanson R.V., Simon M.I. and Weis R.M. Response regulators CheB and CheY exhibit competitive binding to the kinase CheA. (1995) *Biochemistry*, Vol. 34, 14626-14636.
- Lobo S.A.**, Almeida C.C., Carita J.N., Teixeira M. and Saraiva L.M. The haem-copper oxygen reductase of *Desulfuvibrio vulgaris* contains a dihaem cytochrome c in subunit II. (2008) *Biochimica et Biophysica Acta*, Vol. 1777, 1528-1534.

- Lomize M.A.**, Pogozeva I.D., Joo H., Mosberg H.I. and Lomize A.L. OPM database and PPM web server: resources for positioning of proteins in membranes. (2012) *Nucleic Acids Research*, Vol. 40, D370-D376.
- Lowry O.H.**, Rosebrough N.J., Farr A.L. and Randall R.J. Protein measurement with the folin phenol reagent. (1951) *The Journal of Biological Chemistry*, 265-275.
- Luo Y.**, Zhao K., Baker A.E., Kuchma S.L., Coggan K.A., Wolfgang M.C., Wong G.C.L. and O'Toole G.A. A hierarchical cascade of second messengers regulates *Pseudomonas aeruginosa* surface behaviors. (2015) *MBio*, Vol. 6, e02456-14.
- Lyons J.A.**, Aragao D., Slattery O., Pislakov A.V., Soulimane T. and Caffrey M. Structural insights into electron transfer in *caa3*-type cytochrome oxidase. (2012) *Nature*, Vol. 487, 514-518.
- Lyons J.A.**, Hilbers F. and Caffrey M. Structure and function of bacterial cytochrome *c* oxidases. (2016) *Energy Transduction, and Signaling, Advances in Photosynthesis and Respiration*, Springer, Chapter 16.
- Mackova M.**, Vrchotova B., Francova K., Sylvestre M., Tomaniova M., Lovecka P., Demnerova K. And Macek T. Biotransformation of PCBs by plants and bacteria e consequences of plant-microbe interactions. (2007) *European Journal of Soil Biology*, Vol. 43, 233-241.
- Madigan M.T.**, Martiniko J.M., Bender K.S., Buckley D.H. and Sthal D.A. Brock biology of microorganisms. (2015).
- Magnusson L.U.**, Farewell A. and Nystrom T. ppGpp: a global regulator in *Escherichia coli*. (2005) *Trends in Microbiology*, Review, Vo. 13, 236-242.
- Maisonneuve E. and Gerdes K.** Molecular mechanisms underlying bacterial persistence. (2012) *Cell*, Vol. 157, 539-548.
- Manuel J.**, Berry C., Selin C., Fernando W.G.D. and de Kievit T. Repression of the antifungal activity of *Pseudomonas* sp. strain DF41 by the stringent response. (2011) *Applied and Environmental Biology*, Vol. 77, 5635-5642.
- Manuel J.**, Selin C., Fernando W.G.D. and de Kievit T. Stringent response mutants of *Pseudomonas chlororaphis* PA23 exhibit enhanced antifungal activity against *Sclerotinia sclerotiorum* *in vitro*. (2012) *Microbiology*, Vol. 158, 207-216.
- Marrs B. and Gest H.** Genetic mutations affecting the respiratory electron-transport system of the photosynthetic bacterium *Rhodopseudomonas capsulata*. (1973) *Journal of Bacteriology*, Vol. 114, 1045-1051.
- Maseda H.**, Sawada I., Saito K., Uchiyama K., Nake T. and Nomura N. Enhancement of the *mexAB-oprM* efflux pump expression by a quorum-sensing auto inducer and its cancellation but a regulator, MexT, of the *mexEF-oprN* efflux pump operon in *Pseudomonas aeruginosa*. (2004) *Antimicrobial Agents and Chemotherapy*, Vol. 48, 1320-1328.

Mather M.W., Springer P. and Fee J.A. Cytochrome oxidase gene from *Thermus thermophilus*. Nucleotide sequence and analysis of the deduced primary structure of subunit IIc of cyt *caa*₃. (1991) *Journal of Biological Chemistry*, Vol. 266, 5025-5035.

Matheron R. and Caumette P. Structure and functions of microorganisms: production and use of material and energy. (2011) *Environmental Microbiology: Fundamentals and Applications: Microbial Ecology*, Springer, Chapter 3.

Mathew R., Ojha A.K., Karande A.A. and Chatterji D. Deletion of the *rel* gene in *Mycobacterium smegmatis* reduces its stationary phase survival without altering the cell-surface associated properties. (2004) *Current Science*, Vol. 86, 149-153.

Matsushita K., Yamada M., Shinagawa E., Adachi O. and Ameyana M. Membrane-bound respiratory chain of *Pseudomonas aeruginosa* grown aerobically. A KCN-insensitive alternate oxidase chain and its energetics. (1983) *Journal of Biochemistry*, Vol. 93, 1137-1144.

Mattick H. Type IV pili and twitching motility. (2002) *Annual Review of Microbiology*, Vol. 56, 289-314.

Mechold U., Potrykus K., Murphy H., Murakami K.S. and Cashel M. Differential regulation by ppGpp versus pppGpp in *Escherichia coli*. (2013) *Nuclei Acids Research*, Vol. 41, 6175-6189.

Miller M.J. and Gennis R.B. The purification and characterization of the cytochrome *d* terminal oxidase complex of the *Escherichia coli* aerobic respiratory chain. (1983) *Journal of Biological Chemistry*, Vol. 258, 9159-9165.

Mills D.A. and Hosler J.P. Slow proton transfer through the pathways for pumped protons in cytochrome *c* oxidase induces suicide inactivation of the enzyme. (2005) *Biochemistry*, Vol. 44, 4656-4666.

Mittenhuber G. Comparative genomics and evolution of genes encoding bacterial (p)ppGpp synthetases/hydrolases (the Rel, RelA and SpoT proteins). (2001) *Journal of Molecular Microbiology and Biotechnology*, Vol. 3, 585-600.

Morris R.L. and Schmidt T.M. Shallow breathing: bacterial life at low O₂. (2013) *Nature Reviews Microbiology*, Vol. 11, pa. 205-212.

Mouncey N.J. and Kaplan S. Oxygen regulation of the *ccoN* gene encoding a component of the Cbb₃ oxidase in *Rhodobacter sphaeroides* 2.4.1T: involvement of the FnrL protein. (1998) *Journal of Bacteriology*, Vol. 180, 2228-2231.

Mozejko-Ciesielska J., Dabrowska D., Szalewska-Palas A. and Ciesielski S. Medium-chain-length polyhydroxyalkanoate synthesis by *Pseudomonas putida* KT2440 *relA/spoT* mutant: bioprocess characterization and transcriptome analysis. (2017) *AmB Express*, DOI 10.1186/s13568-017-0396-z.

Nelson K.E., Welnel C., Dodson R.J., Hilbert H., Martins dos Santos V.A., Foutus D.E., et al. Complete genome sequence comparative analysis of the metabolically versatile *Pseudomonas putida* KT2440. (2002) *Environmental Microbiology*, Vol. 4, 799-808.

- Nguyen D.**, Joshi-Datar A., Lepine F., Bauerle E., Olakanmi O., Beer K., McKay G., Siehnel R., Schafhauser J., Wang Y., Britigan B.E. and Singh P.K. Active starvation responses mediate antibiotic tolerance in biofilms and nutrient-limited bacteria. (2011) *Science*, Vol. 334, 982-986.
- Nikel P.I.**, Chavarrias M., Fuhrer T., Sauer U. and de Lorenzo V. *Pseudomonas putida* KT2440 strain metabolizes glucose through a cycle formed by enzymes of the Entner-Doudoroff, Embden-Meyerhof-Parnas and pentose phosphate pathways. (2015) *The Journal of Biological Chemistry*, Vol. 290, 25920-25932.
- Noor M.R. and Soulimane T.** Bioenergetics at extreme temperature: *Thermus thermophilus* *ba*₃- and *caa*₃-type cytochrome *c* oxidases. (2012) *Biochimica and Biophysica Acta – Bioenergetics*, Vol. 1817, 638-649.
- Nordlund I.**, Powlowski J., Hagstrom A. and Shingler V, Conservation of regulatory and structural genes for a multi-component phenol hydrolase within phenol-catabolizing bacteria that utilize a *meta*-cleavage pathway. (1993) *Journal of Bacteriology*, Vol. 139, 2695-2703.
- O'Toole G.A. and Kolter R.** Initiation of biofilm formation in *Pseudomonas fluorescens* WCS365 proceeds via multiple, convergent signaling pathways: a genetic analysis. (1998) *Molecular Microbiology*, Vol. 28, 449-461.
- Oh Y.T.**, Lee K.M., Bari W., Raskin D.M. and Yoon S.S. (p)ppGpp, a small nucleotide regulator, directs the metabolic fate of glucose in *Vibrio cholera*. (2015) *Journal of Biological Chemistry*, Vol. 290, 13178-13190.
- Ohtsubo Y.**, Maruyama F., Mitsui H., Nagata Y. And Tsuda M. Complete genome sequence of *Acidovorax* sp. strain KKS102, a polychlorinated-biphenyl degrader. (2012) *Journal of Bacteriology*, Vol. 194, 6970-6971.
- Okumura H.**, Nishiyama S., Sasaki A., Homma M. and Kawagishi I. Chemotactic adaptation is altered by changes in the carboxy-terminal sequence conserved among the major methyl-accepting chemoreceptors. (1998) *Journal of Bacteriology*, Vol. 180, 1862-1868.
- Ooga T.**, Ohashi Y., Kuramitsu S., Koyama Y., Tomita M., Soga T. and Masui R. Degradation of ppGpp by Nudix pyrophosphatase modulates the transition of growth phase in the bacterium *Thermus thermophilus*. (2009) *Journal of Biological Chemistry*, Vol. 284, 15549-15556.
- Osamura T.**, Kawakami T., Kido R., Ishii M. and Arai H. Specific expression and function of the A-type cytochrome oxidase under starvation conditions in *Pseudomonas aeruginosa*. (2017) *PLoSone*, Vol. 12, e0177957.
- Oura H.**, Tashiro Y., Toyofuku M., Ueda K., Kiyokama T., Ito S., et al. Inhibition of *Pseudomonas aeruginosa* swarming motility by 1-naphthol and other bicyclic compounds bearing hydroxyl groups. (2015) *Applied and Environmental Microbiology*, Vol. 81, 2808-2818.
- Paliwal V.**, Raju S. C., Midak A., Phale P.S. and Porohit H.J. *Pseudomonas putida* CSV86: a candidate genome for genetic bioaugmentation. (2014) *PLoSone*, Vol. 9, e84000.
- Pao C.C. and Dyess B.T.** Effect of unusual guanosine nucleotides on the activities of some *Escherichia coli* cellular enzymes. (1981) *Biochimica and Biophysica Acta*, Vol. 677, 358-362.

- Parales R.E. and Harwood C.S.** Bacterial chemotaxis to pollutants and plant-derived aromatic molecules. (2002) *Current Opinion in Microbiology*, Vol. 5, 266-273.
- Parkinson J.S.**, Hazelbauer G.L. and Falke J.J. Signaling and sensory adaptation in *Escherichia coli* chemoreceptors: 2015 update. (2015) *Trends in Microbiology*, Vol. 23, 257-266.
- Patten C.L.**, Kirchhof M.G., Schertzberg M.R., Morton R.A. and Schellhorn H.E. Microarray analysis of RpoS-mediated gene expression in *Escherichia coli* K-12. (2004) *Molecular Genetics and Genome*, Vol. 272, 580-591.
- Pei J.**, Kim B.H. and Grishin N.V. PROMALS 3D: a tool for multiple protein sequence and structure alignment. (2008) *Nucleic Acids Research*, Vol. 36, 2295-2300.
- Pereira M.M.**, Carita J.N. and Teixeira M. Membrane-bound electron transfer chain of the thermohalophilic bacterium *Rhodothermus marinus*: characterization of the iron-sulfur centers from the dehydrogenases and investigation of the high-potential iron-sulfur protein function by in vitro reconstitution of the respiratory chain. (1999) *Biochemistry*, Vol. 38, 1276-1283.
- Pereira M.M.**, Santana M. and Teixeira M. A novel scenario for the evolution of haem/copper oxygen reductases. (2001) *Biochimica et Biophysica Acta*, Review, Vol. 1505, 185-208.
- Pereira M.M.**, Sousa F.L., Verissimo A.F. and Teixeira M. Looking for the minimum common denominator in haem/copper oxygen reductases: towards a unified catalytic mechanism. (2008) *Biochimica et Biophysica Acta*, Review, Vol. 1777, 929-934.
- Pettersen E.F.**, Goddard T.D., Huang C.C., Couch G.S., Greenblatt D.M., Meng E.C. and Ferr T.E. UCSF Chimera – a visualization system for exploratory research and analysis. (2004) *The Journal of Computational Chemistry*, Vol. 25, 1605-1612.
- Pieper D.H.** Aerobic degradation of polychlorinated biphenyls. (2005) *Application of Microbiology and Biotechnology*, Review, Vol. 67, 170-191.
- Pitcher R.S. and Watmough N.J.** The bacterial cytochrome *cbb₃* oxidases. (2004) *Biochimica et Biophysica Acta – Bioenergetics*, Review, Vol. 1655, 388-399.
- Pittman M.S.**, Goodwin M. and Kelly D.J. Chemotaxis in the human gastric pathogen *Helicobacter pylori*: different roles for CheW and the three CheV paralogues, and evidence for CheV2 phosphorylation. (2001) *Microbiology*, Vol. 147, 2493-2504.
- Poggio S.**, Abreu-Goodger C., Fabela S., Osorio A., Dreyfus G., Vinuesa P. and Camarena L. A complete set of flagellar genes acquired by horizontal transfer coexist with the endogenous flagellar system in *Rhodobacter sphaeroides*. (2007) *Journal of Bacteriology*, Vol. 189, 3208-3216.
- Poole K.** Bacterial stress responses as determinants of antimicrobial resistance. (2012) *Journal of Antimicrobial Chemotherapy*, Vol. 67, 2069-2089.
- Poole R.K. and Cook G.M.** Redundancy of aerobic respiratory chains in bacteria? Routes, reasons and regulation. (2000) *Advances in Microbial Physiology*, Vol. 43, 165-224.
- Porter S.L. and Armitage J.P.** Phosphotransfer in *Rhodobacter sphaeroides* chemotaxis. (2002) *Journal of Molecular Biology*, Vol. 324, 35-45.

Potrykus K. and Cashel M. (p)ppGpp: still magical? (2008) *Annual Review of Microbiology*, Review, Vol. 62, 35-51.

Potrykus K., Murphy H., Philippe N. and Cashel M. ppGpp is the major source of growth rate control in *E. coli*. (2011) *Environmental Microbiology*, Vol. 13, 563-575.

Preisig O., Zufferey R. and Hennecke H. The *Bradyrhizobium japonicum* fixGHIS genes are required for the formation of the high-affinity *cbb₃*-type cytochrome oxidase. (1996-1) *Archives of Microbiology*, Vo. 165, 297-305.

Preisig O., Zufferey R., Thony-Meyer L., Appleby C.A. and Hennecke H. A high-affinity *cbb₃*-type cytochrome oxidase terminates the symbiosis-specific respiratory chain of *Bradyrhizobium japonicum*. (1996-2) *Journal of Bacteriology*, Vol. 178, 1532-1538.

Primm T.P., Andersen S.J., Mizrahi V., Avabock D., Rubin H. and Barry C.E. The stringent response of *Mycobacterium tuberculosis* is required for long-term survival. (2000) *Journal of Bacteriology*, Vol. 199, 4889-4898.

Raffalt A.C., Schmidt L., Christensen H.E.M., Chi Q. and Ulstrup J. Electron transfer patterns of the di-heme protein cytochrome *c₄* from *pseudomonas stutzeri*. (2009) *Journal of Inorganic Biochemistry*, Vol. 103, 717-722.

Richardson D.J. Bacterial respiration: a flexible process for a changing environment. (2000) *Microbiology*, Vol. 146, 551-571.

Robin S., Arese M., Forte E., Sarti P., Kolaj-Robin O., Giuffrè A. and Soulimane T. Functional dissection of the multi-domain di-heme cytochrome *c₅₅₀* from *Thermus thermophilus*. (2013) *PLoSone*, Vol. 8, e55129.

Rodrigues J.L.M., Kachel C.A., Aiello M.R., Quensen J.F., Maltseva O.V., Tsoi T.V. and Tiedje J.M. Degradation of Aroclor 1242 dechlorination products in sediments by *Burkholderia xenovorans* LB400 (ohb) and *Rhodococcus* sp. Strain RHA1 (*fcc*). (2006) *Applied and Environmental Microbiology*, Vol. 72, 2476-2482.

Rojo F. Carbon catabolite repression in *Pseudomonas*: optimizing metabolic versatility and interaction with the environment. (2010) *FEMS Microbiology*, Review, Vol. 34, 658-684.

Roy C. and Lancaster D. Succinate:quinone oxidoreductases: an overview. (2002) *Biochimica et Biophysica Acta – Bioenergetics*, Vol. 1553, 1-6.

Safarian S., Rajendran C., Muller H., Preu J., Langer J.D. Ovchinnikov S., Hirose T., Kusumoto T., Sakamoto J. and Michel H. Structure of a *bd* oxidase indicates similar mechanisms for membrane integrated oxygen reductases. (2016) *Science*, 352, 583-586.

Sali A. and Blundell T.L. Comparative protein modelling by satisfaction of spatial restraints. (1993) *Journal of Molecular Biology*, Vol. 234, 779-815.

Sambrook J., Fritsch E.F. and Maniatis T. Molecular cloning: a laboratory manual. 1989.

- Sandri F.**, Fedi S., Cappelletti M., Calabrese F.M., Turner R.J. and Zannoni D. Biphenyl modulates the expression and function of respiratory oxidases in the polychlorinated-biphenyls degrader *Pseudomonas pseudoalcaligenes* KF707. (2017) *Frontiers in Microbiology*, Vol. 8 – 1223.
- Santoro G.** Heat shock factors and the control of the stress response. (1999) *Biochemical Pharmacology*, Vol. 59, 55-63.
- Schuster M.**, Hawkins A.C., Harwood C.S. and Greenberg E.P. The *Pseudomonas aeruginosa* RpoS regulon and its relationship to quorum sensing. (2004) *Molecular Microbiology*, Vol. 51, 973-985.
- Sevilla E.**, Alvarez-Ortega C., Krell T. and Rojo F. The *Pseudomonas putida* HskA hybrid sensor kinase responds to redox signals and contributed to the adaptation of the electron transport chain composition in response to oxygen availability. (2013-2) *Environmental Microbiology*, Vol. 5, 825-834.
- Sevilla E.**, Silva-Jiménez, Duque E., Krell T. and Rojo F. The *Pseudomonas putida* HskA hybrid sensor kinase controls the composition of the electron transport chain. (2013-1) *Environmental Microbiology*, Vol. 5, 291-300.
- Shen M. and Sali A.** Statistical potential for assessment and prediction of protein structures. (2006) *Protein Science*, Vol. 15, 2507-2524.
- Shevchenko A.**, Tomas H., Havli J., Olsen J.V. and Mann M. In-gel digestion for mass spectrometric characterization of proteins and proteomes. (2006) *Nature Protocols*, Vol. 1, 2856-2860.
- Shi L.**, Sohaskey C.D., Kana B.D., Dawest S., North R.J., Mizrahi V. and Gennaro M.L. Changes in energy metabolism of *Mycobacterium tuberculosis* in mouse lung and under *in vitro* conditions affecting aerobic respiration. (2005) *PNAS*, Vol. 102, 15629-15634.
- Shimada S.**, Shinzawa-Itoh K., Baba J., Aoe S., Shimada A., Yamashita E., Kang J., Tateno M., Yoshikawa S. and Tsukihara T. Complex structure of cytochrome *c* oxidase reveals a novel protein-protein interaction mode. (2017) *The EMBO Journal*, Vol. 36.
- Shingler V.**, Powlowski J. and Marklund U. Nucleotide sequence and functional analysis of the complete phenol/3,4-dimethylphenol catabolic pathway of *Pseudomonas* sp. Strain CF600. (1992) *Journal of Bacteriology*, Vol. 174, 711-724.
- Siletsky S.A.**, Rapport F., Poole R.K. and Borisov V.B. Evidence for fast electron transfer between the high-spin haems in cytochrome *bd-I* from *Escherichia coli*. (2016) *PLoSone*, Vol. 11, e0155186.
- Silva-Rocha R.**, Martinez-Garcia E., Calles B., Chavarria M., Arce-Rodriguez A., de las Heras A., et al. The standard eutopean vector architecture (SEVA): a coherent platform for the analysis and deployment of complex prokaryotic phenotypes. (2012) *Nucleic Acids Research*, Vol. 41, D666-D675.
- Silversmith R.E.**, Levin M.D., Schilling E. and Bourret R.B. Kinetic characterization of catalysis by the chemotaxis phosphate CheZ. MODULATION OF ACTIVITY BY THE PHOSPHOSYLATED CheY SUBSTRATE. (2008) *The Journal of Biological Chemistry*, Vol. 283, 756-765.

- Söding J.**, Biegert A. and Lupas A.N. The HHpred interactive server for protein homology detection and structure prediction. (2005) *Nucleic Acids Research*, Vol. 33, W244-W248.
- Sone N.**, Hagerhall C. and Sakamoto J. (2004) *Respiration in Archea and Bacteria-Diversity of Prokaryotic Respiratory Systems*, 35-62.
- Sourjik V. and Wingreen N.S.** Responding to chemical gradients: bacterial chemotaxis. (2012) *Current Opinion in Cell Biology*, Vol. 24, 262-268.
- Sourjik V. and Berg H.C.** Receptor sensitivity in bacterial chemotaxis. (2002) *PNAS*, Vol. 99, 123-127.
- Sousa F.L.**, Alves R.J., Ribeiro M.A., Pereira-Leal J.B., Teixeira M. and Pereira M.M. The superfamily of heme-copper oxygen reductases: types and evolutionary consideration. (2012) *Biochimica et Biophysica Acta – Bioenergetics*, Vol. 1817, 629-637.
- Spiers A.J.**, Burckling A. and Rainey P.B. The causes of *Pseudomonas* diversity. (2000) *Microbiology*, Mini review, Vol. 146, 2345-2350.
- Sprinzi M.**, Wagner T., Lorenz S. and Erdmann V.A. Regions of tRNA important for binding to the ribosomal A and P sites. (1976) *Biochemistry*, Vol. 15, 3031-3039.
- Stelmack P.L.**, Gray M.R. and Pickard M.A. Bacterial adhesion to soil contaminants in the presence of surfactants. (1999) *Applied and Environmental Microbiology*, Vol. 65, 163-168.
- Stock A.M. and Stock J.B.** Purification and characterization of the CheZ protein of bacterial chemotaxis. (1987) *Journal of Bacteriology*, Vol. 169, 3301-3311.
- Stock J. and Levit M.** Signal transduction: hair brains in bacterial chemotaxis. (2000) *Current Biology*, Vol. 10, R11-R14.
- Stoodley L.H. and Stoodley P.** Development regulation of microbial biofilms. (2002) *Current Opinion in Microbiology*, Vol. 13, 228-233.
- Stover C.K.**, Pham X.Q., Erwin A.L., Mizoguchi S.D., Warrenner P., Hickey M.J., et al. Complete genome sequence of *Pseudomonas aeruginosa* PAO1, an opportunistic pathogen. (2000) *Nature*, Vol. 406, 959-964.
- Suh S.J.**, Silo-Suh L., Woods D.E., Hassett D.J., West S.E.H. and Ohman D.E. Effect of *rpoS* mutation on the stress response and expression of virulence factors in *Pseudomonas aeruginosa*. (1999) *Journal of Bacteriology*, Vol. 181, 3890-3897.
- Swem D.L. and Bauer C.E.** Coordination of ubiquinol oxidase and cytochrome Cbb₃ oxidase expression by multiple regulators in *Rhodobacter capsulatus*. (2002) *Journal of Bacteriology*, Vol. 184, 2815-2820.
- Sylvestre M. and Sandossi M.** Selection of enhanced PCB-degrading bacterial strains for bioremediation: consideration of branching pathways. (1994) *Biological Degradation and Remediation of Toxic Chemicals*.

Taira K., Hirose J., Hayashidall S. and Furukawa K. Analysis of *bph* operon from the polychlorinated biphenyl-degrader strain of *Pseudomonas pseudoalcaligenes* KF707. (1992) *The Journal of Biological Chemistry*, Vol. 267, 4844-4853.

Thomas P.E., Ryan D. and Levin W. An improved staining procedure for the detection of the peroxidase activity of cytochrome *P*-450 on sodium dodecyl sulfate polyacrylamide gels. (1976) *Analytical Biochemistry*, Vol.75, 168-176.

Thompson J.D., Higgins D.G. and Gibson T.J. CLUSTAL W: improving the sensitivity of progressive multiple sequence alignment through sequence weighting, position-specific gap penalties and weight matrix choice. (1994) *Nucleic Acid Research*, Vol. 22, 4673-4680.

Toledo-Cuevas M., Barquera B., Gennis R.B., Wikström M. and García-Horsman J.A. The *ccb₃*-type cytochrome *c* oxidase from *Rhodobacter sphaeroides*, a proton-pumping heme copper oxidase. (1998) *Biochimica and Biophysica Acta – Bioenergetics*, Vol. 1365, 421-434.

Tosa T. and Pizer L.I. Biochemical bases for the antimetabolite action of L-serine hydroxamate. (1971) *Journal of Bacteriology*, Vol. 106, 972-982.

Tremaroli V., Fedi S., Tamburini S., Viti C., Tatti E., Ceri H., Turner R.J. and Zannoni D. A histidine-kinase *cheA* gene of *Pseudomonas pseudoalcaligenes* KF707 not only has a key role in chemotaxis but also in affects biofilm formation and cell metabolism. (2011) *Biofouling*, Vol. 27, 33-46.

Tremaroli V., Fedi S., Turner R.J., Ceri H. and Zannoni D. *Pseudomonas pseudoalcaligenes* KF707 upon biofilm formation on a polystyrene surface acquire a strong antibiotic resistance with minor changes in their tolerance to metal cations and metalloid oxyanions. (2008) *Archives of Microbiology*, Vol. 190, 29-39.

Tremaroli V., Vacchi-Suzzi C., Fedi S., Ceri H., Zannoni D. and Turner R.J. Tolerance of *Pseudomonas pseudoalcaligenes* KF707 to metals, polychlobiphenyls and chlorobenzoates: effects on chemotaxis-, biofilm- and planktonic-grown cells. (2010) *FEMS Microbiology Ecology*, Vol. 74, 291-301.

Triscari-Barberi T., Simone D., Calabrese F.M., Attimonelli M., Hahn K.R., Amoako K.K., Turner R.J., Fedi S. and Zannoni D. Genome sequence of the polychlorinated-biphenyl degrader *Pseudomonas pseudoalcaligenes* KF707. (2012) *Journal of Bacteriology*, Vol. 194, 4426-4427.

Trumpower B.L. The protonmotive Q cycle. (1990) *The Journal of Biological Chemistry*, Minireview, Vol. 265, 11409-11412.

Tsang N., Macnab R. and Koshland D.E. Common mechanism for repellents and attractants in bacterial chemotaxis. (1973) *Science*, Vol. 181, 60-63.

Udaondo Z., Molina L., Daniels, Gomez M.J., Matilla A., Roca A., Fernández M., Duque E., Segura. And Luis Juan. Metabolic potential of the organic-solvent tolerant *Pseudomonas putida* DOT-T1E deduced from its annotated genome. (2013) *Microbial Biotechnology*, Vol. 6, 598-611.

Ugidos A., Morales G., Rial E., Williams H.D. and Rojo F. The coordinate regulation of multiple terminal oxidases by the *Pseudomonas putida* ANR global regulator. (2008) *Environmental Microbiology*, Vol. 10, 1690-1702.

- Van Delden C.**, Comte R. and Bally A.M. Stringent response activates quorum sensing and modulates cell density-dependent gene expression in *Pseudomonas aeruginosa*. (2001) *Journal of Bacteriology*, Vol. 183, 5376-5384.
- Vasil M.L.** How we learnt about iron acquisition in *Pseudomonas aeruginosa*: a series of very fortunate events. (2007) *Biometals*, Vol. 20, 587-601.
- Verissimo A.F. and Daldal F.** Cytochrome *c* biogenesis System I: an intricate process catalyzed by a maturase supercomplex? (2014) *Biochimica and Biophysica Acta – Bioenergetics*, Vol. 1837, 989-998.
- Verkhovsky M.I.**, Jasaitis A., Verkhovskaya M.L., Morgan J.E. and Wikstrom M. Proton translocation by cytochrome *c* oxidase. (1999) *Nature*, Vol. 400, 480-483.
- Vogt S.L.**, Green C., Stevens K.M., Day B., Erickson D.L., Woods D.E. and Storey D.G. The stringent response is essential for *Pseudomonas aeruginosa* virulence in the rat lung agar bead and *Drosophila melanogaster* feeding models of infection. (2011) *Infection and Immunity*, Vol. 79, 4094-4104.
- Wadhams G.H. and Armitage J.P.** Making sense of it all: bacterial chemotaxis. (2004) *Nature*, Review, Vol. 5, 1024-1037.
- Wang H. and Matsumura P.** Characterization of the CheA/CheZ complex: a specific interaction resulting in enhanced dephosphorylating activity on CheY-phosphate. (1996) *Molecular Microbiology*, Vol. 19, 695-703.
- Watanabe T.**, Fujihara H. and Furukawa K. Characterization of the second LysR-Type regulator in the biphenyl-catabolic gene cluster of *Pseudomonas pseudoalcaligenes* KF707. (2003) *Journal of Bacteriology*, Vol. 185, 3575-3582.
- Watanabe T.**, Inoue R., Kimura N. and Furukawa K. Versatile of biphenyl catabolic *bph* operon in *Pseudomonas pseudoalcaligenes* KF707. (2000) *The Journal of Biological Chemistry*, Vol. 275, 31016-31023.
- Wessner D.R.**, Dupont C. and Charles T.C. *Microbiology*. (2015).
- West A.H. and Stock A.M.** Histidine kinases and response regulator proteins in two-component signaling systems. (2001) *TRENDS in Biochemical Sciences*, Vol. 26, 369-376.
- Whitchurch C.B.**, Leech A.J., Young M.D., Kennedy M.D., Sargent D., Bertrand J.L., et al. Characterization of a complex chemosensory signal transduction system which controls twitching motility in *Pseudomonas aeruginosa*. (2004) *Molecular Microbiology*, Vol. 52, 873-893.
- Winstedt L. and von Wachenfeldt C.** Terminal oxidases of *Bacillus subtilis* strain 168: one quinol oxidase, cytochrome *aa₃* or cytochrome *bd*, is required for aerobic growth. (2000) *Journal of Bacteriology*, Vol. 182, 6557-6564.
- Wu J. and Xie J.** Magic spot: (p)ppGpp. (2009) *Journal of Cellular Physiology*, Vol. 220, 297-302.
- Xiao H.**, Kalman M., Ikebara K., Zemel S., Glaser G. and Cashel M. Residual guanosine 3',5'-bispyrophosphate synthetic activity of *relA* null mutants can be eliminated by *spoT* null mutations. (1991) *Journal of Biological Chemistry*, Vol. 266, 5980-5990.

Yeh J.I., Biemann H.P., Privè G.G., Pandit J., Khosland D.E. and Kim S.H. High-resolution structures of the ligand binding domain of the wild-type bacterial aspartate receptor. (1996) *Journal of Molecular Biology*, Vol. 262, 186-201.

Zannoni D. and Moore A.L. Measurement of the redox state of the ubiquinone pool in *Rhodobacter capsulatus* membrane fragments. (1990) *FEBS Letters*, Vol. 271, 123-127.

Zannoni D., Schoepp-Cothenet B. and Hosl J. Respiration and respiratory complexes. (2009) *The Purple Phototropic Bacteria*, 537-561.

Zhu K., Shen Q., Ulrich M. and Zheng M. Human monocyte-derived dendritic cells expressing both chemotactic cytokines IL-8, MCP-1, RANTES and their receptors, and their selective migration to these chemokines. (2000) *Chinese Medical Journal*, Vol 113, 1124-1128.